NOTCH SIGNALING IS ESSENTIAL TO MODULATE INTRAHEPATIC BILE DUCT STRUCTURE

By

Erin E. Sparks

Dissertation

Submitted to the Faculty of the

Graduate School of Vanderbilt University

in partial fulfillment of the requirements

for the degree of

DOCTOR OF PHILOSOPHY

in

Cell and Developmental Biology

May, 2011

Nashville, Tennessee

Approved:

Dr. Stacey Huppert

Dr. James Goldenring

Dr. Kathy Gould

Dr. Guoqiang Gu

Dr. Mark Magnuson

ACKNOWLEDGEMENTS

When I interviewed with the Interdisciplinary Graduate Program at Vanderbilt, I opened a fortune out of a fortune cookie that said, “Your present plans are going to succeed.” What the fortune forgot to mention was that success only comes with the help and support of many people. First and foremost, I would like to thank my mentor, Stacey Huppert; the dedication and love that Stacey has for science is absolutely contagious. She has always pushed me to be more and do more, which has allowed to me accomplish things I never dreamed of. I am grateful that Stacey has let me explore some of my less conventional ideas, and given me the freedom to grow as a scientist. The opportunities that Stacey has allowed me to have, with traveling to meetings and visiting other laboratories, have been invaluable to my success. On a personal note, Stacey has been a mentor and a friend. Her willingness to include me into her family, taking me in after a flood left me homeless and answering 2 am phone calls, are just a few of the things that Stacey has done to make my time in graduate school a wonderful one. I am blessed to call her a friend and a mentor.

I would also like to thank the members of my thesis committee, Dr. Jim Goldenring, Dr. Kathy Gould, Dr. Guoqiang Gu and Dr. Mark Magnuson for their continual support and encouragement. I can honestly say that I have enjoyed all of my committee meetings and receiving input and suggestions. I would not be here today if it were not for your guidance.

I would be remiss to not acknowledge the people who have made the science possible. First, I would like to thank the members of the Huppert lab, Kari Huppert, Charles Vanderpool and Teagan Walter. Kari, thank you for being the “lab mom” and working so hard to keep us in line. Thank you for the many vent sessions, for providing moral support and always giving us a good laugh with Chase stories. Also, thank you for your scientific

support and teaching me so much molecular biology. To Charlie and Teagan, thank you for always making the Huppert lab a fun and productive place to work.

Many investigators at Vanderbilt and elsewhere have provided support and guidance to me in the completion of this dissertation. At Vanderbilt, I'd like to thank Dr. Mark Magnuson for not only providing equipment with which to complete my research, but having an open door policy and teaching me to become a better writer. I'd also like to thank Dr. Mark deCaestecker and Dr. Guoqiang Gu for scientific support and help with my post-doctoral fellowship interviews. Dr. M. Kay Washington, has been an invaluable asset to my dissertation research in providing pathological assessment of my numerous mouse models. Dr. Bill Russell taught me to perform a 70% partial hepatectomy surgery, and has been a wonderful conduit into the world of the liver. Dr. Sandy Zinkel has provided unending support to help me establish immune studies within our lab. Dr. Dan Perrien and Dr. Todd Peterson were invaluable in the development of microCT analyses. Dr. Sam Wells has been a lot of fun to work with, as we played with different fluorescent resin conditions and microscopy techniques. To investigators outside of Vanderbilt, I must first thank Dr. Rafi Kopan at WashU for welcoming me into his scientific family, allowing me to present in his lab and providing letters of recommendation for post-doctoral fellowships. Dr. Mario Strazzabosco at Yale University has become a wonderful colleague and I am grateful for his many Skype chats and allowing me to travel to his lab to learn cholangiocyte isolations. Dr. Nancy Spinner at Penn has been a wonderful asset as we try to correlate our findings with Alagille syndrome. Further I am grateful for collaboration with Dr. David Rudnick at WashU, Dr. Grace Guo at the University of Kansas Medical Center and Dr. Alessandra Warren at the University of Sydney.

Last, but certainly not least, I'd like to thank my family and friends. To my parents, Gary and Janet, thank you for instilling in me to pursue my dreams and that I can do anything I set my mind to. I could not have done this if it was not for your love and support always. Thank you

for never getting sick of me calling and always keeping me grounded. To my brother Bryan, thank you for your love and support. I am proud to call you my brother. To the rest of my wonderful and extended family, thank you for the numerous phone calls, love and encouragement. I wouldn't be who I am without you. To April, Billy, Lindsay and Robin thank you for being wonderful supportive friends. Lindsay, thank you for being my senior graduate student and helping me with so much. Finally, I would like to thank Jon, the love of my life and my best friend. Thank you for always encouraging me and being proud of me. Thank you for the numerous late nights that you spent in lab so I didn't have to be alone. Thank you for everything, your love and support mean the world to me.

TABLE OF CONTENTS

LIST OF TABLES

LIST OF FIGURES

CHAPTER I

INTRODUCTION

The liver is the largest gland in the body, and second largest organ (preceded only by the skin). Proper liver function to regulate physiological processes, such as detoxification, metabolism (glycogen storage, decomposition of red blood cells, protein synthesis, and hormone production), and digestion, is indispensible to support life in vertebrates. Indeed, liver disease is the 4th leading cause of death among middle-aged adults in the United States, and ranks 12th in death rate for all ages (Courtesy of the Center for Disease Control). Liver disease includes a wide-range of disorders from drug or alcohol-induced damage to genetic disorders, infection and cancer. In the United States, the leading cause of liver-related death is due to cirrhosis of the liver. Conversely, in low-income nations, cirrhosis of the liver ranks as the 16th overall cause of death, and liver cancer is the 19th (Courtesy of the World Health Organization). An additional, yet less prevalent type of liver disease is hepatobiliary disease with estimates of the prevalence ranging from 1:500 to 1:2500 for cholestatic hepatobiliary disease. (Mushtaq et al., 1999). Our understanding of how liver development proceeds and liver disease initiates and progresses is limited. In this dissertation, I will use a model of a genetic hepatobiliary disease to help elucidate how proper development contributes to normal function and initiation of disease. I will first summarize what is currently known and the questions that remain with regards to liver development and hepatobiliary disease.

Hepatobiliary Disease

Hepatobiliary diseases are a subset of liver diseases that include a highly heterogenous group of diseases of the hepatocytes and biliary system, which can be caused by a variety of insults. Grossly, hepatobiliary disease can be divided into two major categories, acute and chronic. Sub-categories of liver disease include viral hepatitis, inflammatory liver disease, alcoholic liver disease and cholangiopathies. Often the same insults can lead to acute or chronic depending on the dose and length of exposure (Carton et al., 2007).

Cholangiopathies

A specific sub-type of hepatobiliary diseases are termed cholangiopathies, and refer to any disorder that affects the cholangiocytes (bile duct epithelial cells). This disease classification includes both acute and chronic disorders that affect both adult and pediatric populations. Cholangiopathies share a number of pathological characteristics, including inflammation, cholestasis, fibrosis, and apoptosis (Strazzabosco et al., 2005). However, three subcategories of cholangiopathies have been defined: 1. genetic or inherited disorders, 2. immune-mediated disorders, 3. idiopathic, drug-induced, ischemic and malignant disorders. All currently identified cholangiopathies and their associated phenotypes are listed in Table 1.1. The specific pathogenesis of most cholangiopathies remains largely unknown, however all cholangiopathies progress to ductopenia, defined as the loss of >50% of intrahepatic bile ducts (Bogert and LaRusso, 2007). Further, the diagnosis of a cholangiopathy is a strong indicator for the progression to liver transplant, accounting for 10-20% of total transplants in adult, and ~80% in pediatric (Strazzabosco et al., 2005).

Subcategory	Disease	Pathology/Pathogenesis
Genetic and Inherited	Alagille Syndrome (AGS)	JAGGED1 – Bile duct paucity
	Cystic Fibrosis (CF)	CFTR – Ductal cholestasis; focal biliary cirrhosis
	Progressive Familial Intrahepatic Cholestasis – Type 3 (PFIC-3)	MDR3 – Ductular reaction; early fibrosis
	Autosomal Dominant Polycystic Kidney Disease (ADPKD) **	PDK1 & PDK2 – Ductal plate malformations; biliary microhamartomas; cysts
	Autosomal Recessive Polycystic Kidney Disease (ARPKD) **	PKHD1 – Ductal plate malformations; biliary microhamartomas; cysts
	Autosomal Dominant Polycystic Liver Disease (ADPLD) **	PRKCSH & SEC63 – Ductal plate malformations; biliary microhamartomas; cysts
	Caroli's Syndrome **	PKHD1 (some cases) – Ductal plate malformations; cystic dilation of intrahepatic bile ducts
	Congenital Hepatic Fibrosis (CHF) **	MPI – Ductal plate malformations; biliary microhamartomas, fibrous stroma
Immune-mediated	Primary Biliary Cirrhosis (PBC)	Immune response towards cholangiocytes; biliary cirrhosis; end-stage liver disease
	Primary Sclerosing Cholangitis (PSC)	Immune-mediated association with Inflammatory Bowel Disease; recurrent cholangitis, biliary cirrhosis, cholangiocarcinoma
	Autoimmune cholangitis (AMA-negative PBC)	Immune response towards cholangiocytes; ductopenia
	Acute allograft rejection	Alloimmune T cell-mediated damage of bile duct epithelium
	Chronic allograft rejection	Ductopenic cholestatic syndrome; allograft failure
	Graft-versus-host disease (GVHD)	Ductopenia;cirrhosis
Idiopathic, Drug-Induced, Ischemic and Malignant	Biliary atresia (BA)	Embronic (10-20%) – ductal plate malformations; Perinatal (80-90%) – immune mediated bile duct destruction
	Sarcoidosis	(Rare liver involvement) Granulomatous cholangitis; ductopenia
	Idiopathic adulthood ductopenia	Ductopenia of unknown causes
	Drug-induced cholangitis	Variable from mild cholestasis to chronic cholestasis to ductopenia
	Ischemic	Segmental strictures to impair bile flow
	Malignant cholangiocarcinoma	Chronic biliary inflammation; bile duct lithiasis; fibropolycystic diseases; PSC

Table 1.1 Cholangiopathies. Cholangiopathies are diseases that affect the cholangiocytes, or bile duct epithelia. Three different disease sub-categories have been defined: genetic and inherited, immune-mediated, and idiopathic, drug-induced, ischemic and malignant. These sub-categories and the cholangiopathies that belong to these categories are listed in this table along with the pathological findings associated. For genetic and inherited diseases, the known gene mutation is underlined. ** - Diseases that are also classified as ciliopathies.

A major clinical finding of cholangiopathies is the presence of cholestasis. Cholestasis is the general term for loss or reduction of bile flow. The origin of cholestasis in cholangiopathies varies from loss of bile ducts to obstruction of the intra- or extra-hepatic bile ducts. Cholestasis is the dominant clinical concern in cholangiopathies, as cholestasis may initiate or worsen the progression of disease (Strazzabosco, 1997). Cholestasis is initially suspected when alkaline phosphate (ALP) is elevated. ALP is an enzyme that catalyzes the hydrolysis of phosphate esters at an alkaline pH, however it's function has little to do with cholestasis. ALP is expressed in all tissues of the body, but is concentrated in the liver and bone. In the liver, ALP expression is highest in bile canaliculi, the channel by which bile drains from hepatocytes into the biliary system. It is proposed that obstruction or damage of the bile ducts leads to the release of ALP into the blood stream (Lindor and Talwalker, 2008). Current therapy for cholestasis ranges from surgical intervention to administration of bile acid binding resins or secondary bile acids (Strazzabosco et al., 2005). Bile acid binding resins, such as cholestyramine were originally described as a treatment for xanthomas. Xanthomas are deposits of cholesterol-rich material in the skin, which results in severe pruritus or itching and is often associated with cholestatic liver disease (Visintine et al., 1961). Thus cholestyramine treats the symptoms of cholestasis, but does not address the root cause. Conversely, administration of a secondary bile acid, ursodeoxycholic acid (UDCA) is the only FDA-approved medical treatment for a specific cholangiopathy, Primary Biliary Cirrhosis (PBC). PBC is a disease in which immune cells attack cholangiocytes resulting in biliary cirrhosis (Table 1.1). While a treatment has been identified, approximately one-third of PBC patients do not respond to UDCA treatment and still require liver transplant (Nguyen et al., 2010). Further, the mode of action of UDCA is still unclear; some studies have demonstrated that UDCA stimulates hepatocyte transporters and thus hepatocyte function (Trauner et al., 2005). While some cholangiopathies have cholestasis as a result of improper hepatocyte function, others are due to the lack of bile ducts. Thus if the latter were

indeed the mode of UDCA action, it would seem an ineffective treatment option for cholestasis due to a lack of bile ducts. Understanding the mechanisms involved in the initiation and progression of cholangiopathies is critical for future therapeutics, which would circumvent the need for liver transplant.

A Genetic Cholangiopathy: Alagille Syndrome

Genetic or inherited cholangiopathies are among the more rare types of cholangiopathies. However, understanding how the liver develops, and how development is disrupted in these genetic disorders, will further understanding of cholangiopathies as a whole. In particular, Alagille syndrome (AGS; OMIM: 118450 and 610205) is a pleiotropic developmental disorder affecting, among other things, the liver intrahepatic bile ducts (IHBDs). The diagnosis of AGS is based on the paucity of IHBDs, and three to five other major features: chronic cholestasis, cardiac disease, skeletal abnormalities, ocular abnormalities, and characteristic craniofacial features (Alagille, 1996). Over 96% of AGS patients present with chronic cholestasis, which is attributed to the paucity of bile ducts (Emerick et al., 1999).

Mutations in the Notch signaling pathway are highly causative of AGS, with greater than 94% of patients having a mutation in JAGGED1, a ligand of the Notch pathway, and an additional two families, with mutations in NOTCH2, a receptor of the Notch pathway (McDaniell et al., 2006; Warthen et al., 2006). Despite a well-characterized genetic link, the pathogenesis of AGS is very poorly understood. Indeed, the mechanism by which bile duct paucity arises in AGS individuals remains unknown; whether paucity is a result of improper development, an inability to maintain ductal structures or a lack of post-natal branching and elongation remains to be determined (Emerick et al., 1999; Libbrecht et al., 2005). Further, there is no discernable correlation between the specific genetic mutation and clinical

phenotype (Krantz et al., 1998; Kamath et al., 2009). At this juncture, there are no molecular or pathological predictors to intimate the outcome of AGS patients.

The heterogeneous clinical course is highlighted by the following examples. First, cholestasis in AGS patients generally worsens until school age, and then in a subset of patients cholestasis stabilizes or resolves (Lykavieris et al., 2001). The features that distinguish patients who will stabilize or resolve the cholestasis have not been identified. Another example is a subset of patients who fail to excrete a biliary tracer upon hepatobiliary scintigraphy (Emerick et al., 1999). These patients are often misdiagnosed as biliary atresia patients. Biliary atresia is an idiopathic cholangiopathy characterized by the immune-mediate destruction of bile ducts, and mainly affects extrahepatic bile ducts (Table 1.1). The diagnosis of biliary atresia results in patients undergoing a hepatoportoenterostomy (Kasai procedure or Roux-en-Y procedure), a procedure that replaces the extrahepatic common bile duct with a segment of intestine to bypass blockage. Kaye and colleagues determined that AGS patients, who underwent a Kasai procedure after improper diagnosis, had more severe liver disease and thus progressed to liver transplant more often than AGS patient who did not undergo a Kasai procedure (Kaye et al., 2010). The authors suggest that the Kasai procedure itself was detrimental to liver function and resulted in liver failure, however it remains unclear whether these patients would have progressed to liver failure, regardless of the surgery, as a result of biliary obstruction. The last example of AGS clinical heterogeneity is that only 21-31% of AGS patients proceed to liver transplant, which is usually due to complications of chronic cholestasis (Kamath et al., 2010), however what makes these patients unique is unknown. Thus determining how a genetic mutation can lead to variable clinical outcomes is critical for patient stratification and future therapeutics of not only Alagille syndrome, but also cholangiopathies as a whole. To understand how developmental processes go awry in human diseases, it is important to first understand how liver architecture is normally acquired.

Hepatic Microarchitecture

In mammals, as specifically described here in mice, the liver is composed of seven lobes and contributes to approximately 5% of the body weight. The basic structural unit of the liver is the liver lobule (Figure 1.1). The lobule is composed of cords of hepatocytes radiating away from portal veins towards a central vein. Sinusoidal endothelial cells line the cords of hepatocytes, generating a capillary network from the afferent portal vein to the efferent central vein. The lobule is roughly hexagonal, with a central vein in the center, and portal veins at the six corners. Portal veins contribute to a microstructural feature called a portal triad. In addition to the portal vein, this triad contains an IHBD and a hepatic artery.

The IHBD acts as a conduit to mediate the transport of bile from the liver into the gallbladder for storage or into the duodenum for aid in digestion. Hepatocytes, which produce the bile, secrete bile into channels on their apical surface called canaliculi (Figure 1.2). Bile drains through the canaliculi into the canals of Hering, which are classically defined as lined by hepatocytes on one side, and cholangiocytes on the other. The canals of Hering represent the transition between the hepatocyte canaliculi and ductal system. After bile passage through the canals of Hering, bile enters the ductal system where it proceeds through an intricate IHBD network (Figure 1.2). Proper development of this microarchitecture is critical for liver function and homeostasis, however there are still gaps in the field of liver biology as it relates to the molecular, temporal and spatial cues required to generate hepatic microarchitecture. An overview of our current understanding of mammalian liver development, as studied in mice, is described below.

Murine Liver Development

The liver primordium is first identifiable at embryonic day (E) 8.5-9.0 in mice. The ventral foregut endoderm responds to mesenchymal signals to initiate the liver gene

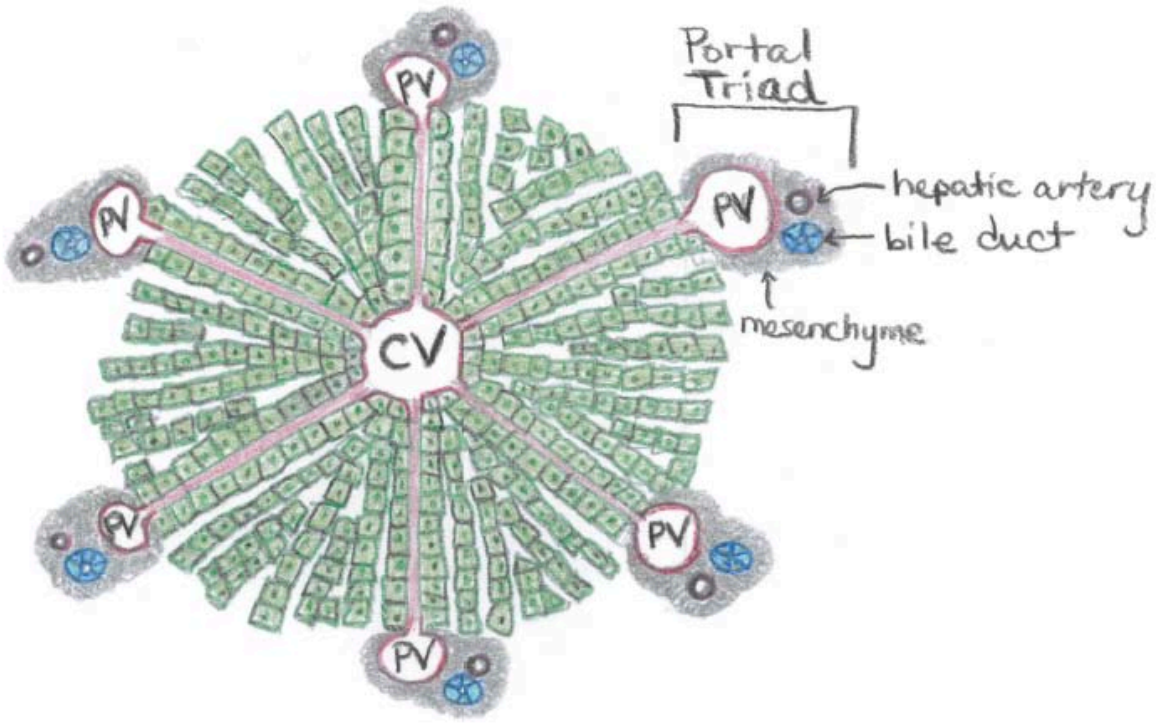

Figure 1.1 The hepatic lobule. The hepatic lobule is roughly hexagonal, with portal veins at the apexes and a central vein in the middle. Blood flow proceeds from the afferent portal veins through the hepatic sinusoids and to the efferent central vein. The portal vein a component of a microanatomical feature called the portal triad, consisting of a portal vein, a bile duct and a hepatic artery. Vessels – red, Hepatocytes – green, Bile Ducts – blue, Hepatic Artery – dark red, Mesenchyme – grey. CV – Central Vein, PV – Portal Vein.

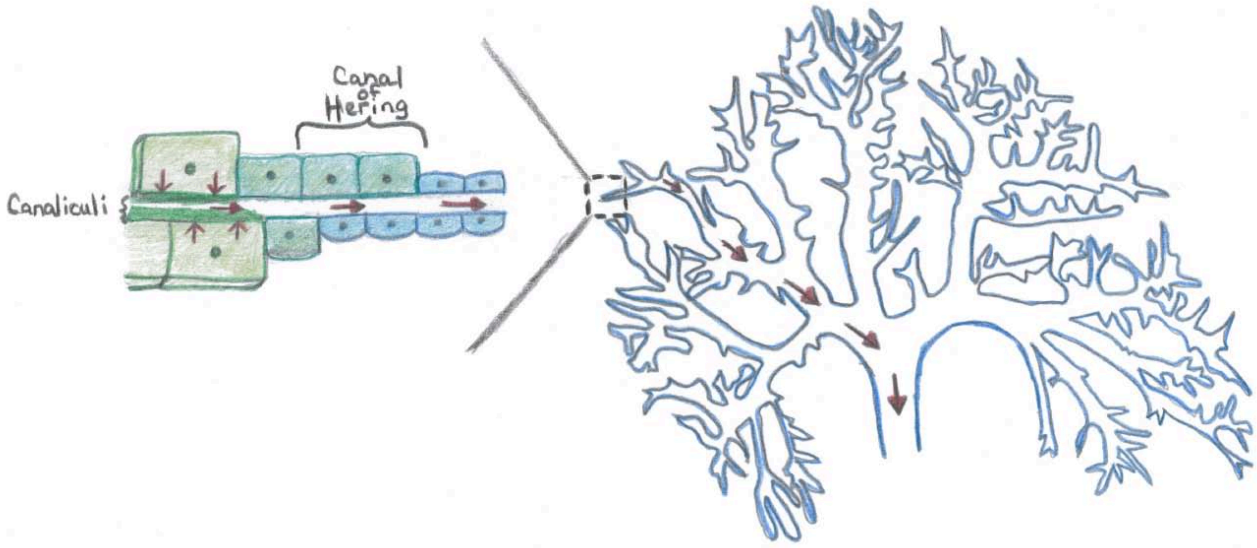

Figure 1.2 Bile conduits. Bile, produced by the hepatocytes, is first excreted into a canalicular space, then flows through the canaliculi into the canals of Hering, which are surrounded on one side by small hepatocytes, and on the other by cholangiocytes. Bile then enters into the intrahepatic bile ducts at the smallest branches, and continues to be transported out into the extrahepatic bile ducts. Red arrows indicate bile flow. Hepatocytes – green, Small Hepatocytes – blue-green, Cholangiocytes – blue.

regulatory network and formation of the liver diverticulum. The precise tissue source of these cues, whether septum transversum mesenchyme (STM), cardiac mesoderm, lateral plate mesoderm or vascular precursors, remains to be elucidated. It is however, well established that Fibroblast Growth Factor (FGF) and Bone Morphogenetic Protein (BMP) are required inductive cues, though the specific ligands and receptors involved are unclear (Reviewed in (Tremblay, 2010)). The liver diverticulum is composed of bi-potential progenitor cells termed hepatoblasts. Around E9.5, hepatoblasts delaminate, with the assistance of matrix metalloproteases, and migrate in cords into the surrounding STM. I will highlight cell lineages that orchestrate and define the hepatic microarchitecture.

Vascular Lineage

In the adult liver, the major blood vessels are the aforementioned portal vein, central vein, hepatic sinusoidal capillaries and hepatic artery. The precise patterning of these vessels is equally important for proper liver development and homeostasis as epithelial development. The majority of our understanding of hepatic vascular development is extrapolated from anatomical human studies of cadavers, however even then our understanding is limited.

The first vessels to form during development are the sinusoidal capillaries, which arise via angiogenesis of existing vessels in the STM during hepatoblast migration. In the adult, one major afferent vessel, the portal vein, transports blood from the intestine, pancreas and spleen into the liver. On the contrary, during development, two major afferent vessels, the umbilical vein and vitelline vein feed the liver. Segments of the vitelline vein form the portal vein, but it does not become the major afferent vessel until the umbilical vein collapses, which is after birth in humans. One major efferent vessel, the central vein, exists in the adult and egresses via the caudal (inferior) vena cava. Developmentally, the vitelline vein participates in the formation of the central vein. Whether murine afferent vessel

development occurs in a similar manner remains to be investigated. My thesis work describes a mouse model in which the number of portal veins per millimeter of tissue is reduced as a result of deleting Notch signaling within the hepatoblast population (Please refer to Chapter IV, Figure 4.11). This result suggests that the liver epithelial cell lineages is required to provide cues for venous remodeling. Further support of this hypothesis is a study by Masyuk et al., in which the authors fed α-Naphthylisothiocyanate (ANIT), a drug that induces cholangiocyte proliferation with chronic administration, to rats. In this study, the portal vein branching increases in concert with increased biliary branches (Masyuk et al., 2003). The molecular cues involved in a potential feedback loop between the biliary and portal vein system have yet to be elucidated.

The fourth and final vascular system within the liver is the hepatic artery, which develops substantially later in development than the venous and capillary systems. The hepatic artery originates from the celiac artery and it thought to respond to cues from ductal epithelium. In particular, one study showed that human and mouse cholangiocytes express angiogenic growth factors consistent with a model of hepatic artery recruitment. Further, this group and others used a mouse model in which bile ducts do not form properly and demonstrated that arterial development is also disrupted (Clotman et al., 2003; Fabris et al., 2008). Despite this seminal study, further experiments are needed to define the mechanisms of arterial recruitment by biliary epithelial cells and migration of endothelial cells to form the hepatic artery.

Hematopoietic Lineage

During mammalian development, the liver serves as the major hematopoietic organ beginning shortly after hepatoblast migration into the STM. Hematopoietic precursor cells first arise in the yolk salk and aorta-gonad-mesenepheros region where they are maintained until E11 (Moore and Metcalf, 1970). Beginning at E11, hematopoietic precursors appear

within the fetal liver and increase exponentially; the homing cues required for this transition have not been identified. For approximately the next 6 days of development the liver remains the primary hematopoietic organ (Ema and Nakauchi, 2000). While hematopoiesis continues in the liver until after birth, at E16 hematopoietic stem cells (HSCs) begin to take up residence in the spleen and bone marrow, the major sites of adult hematopoiesis. The homing and colonization of HSCs from the liver to the spleen and bone marrow is not well understood. Originally it was thought that HSCs, responding to a homing cue, left the fetal liver and homed to the sites of adult hematopoiesis. Yet work from Christensen et al. demonstrated that fetal HSCs are constitutively found in the circulation, and the seeding of the spleen and bone marrow is a gradual process (Christensen et al., 2004). These results suggest a progressive transition that involves homing and niche factor establishment within the spleen and bone marrow to define the adult HSC niche, and loss of fetal liver HSC niche factors. However, while the factors that establish and maintain the adult HSC niche have been investigated, it is currently unknown what maintains an HSC niche in the fetal liver and how these signals are lost during development. One *in vitro* study suggests that Wnt signaling within the fetal microenvironment maintains actively cycling HSCs, while Notch signaling within the adult microenvironment maintains quiescent HSCs, but this model remains to be substantiated (Martin and Bhatia, 2005). The contribution of HSCs to the formation and maintenance of hepatic microarchitecture is not well understood. On the other hand, it has been hypothesized that proper hepatic microarchitecture is required to define a HSC niche and improper liver epithelial development would disrupt embryonic hematopoiesis.

Mesenchymal Lineage

Mesenchymal cells termed hepatic stellate cells are found within the space of Disse between hepatocytes and the sinusoidal endothelial cells. The role of stellate cells in normal

and diseased liver has been well described (Friedman, 2008). Specifically, stellate cells have been suggested to facilitate bile duct development in humans (Libbrecht et al., 2002), although a mechanism has not been proposed. Vitamin A storage is an important function of stellate cells in quiescent liver (Hendriks et al., 1985). Further, stellate cells have been defined as an important mediator of the immune response by amplifying chemokines that recruit immune cells (Maher, 2001). Upon liver injury, stellate cells are activated into a myofibroblastic cell, which proliferates and contributes to fibrosis (Friedman, 2008).

The origin of the hepatic stellate cell had remained a mystery for many years. Originally it was proposed that stellate cells were of neural crest origin due to the expression of both mesenchymal and neural markers (GFAP, nestin, N-cam, NGF, BDNF, etc) (Geerts, 2001). However, lineage tracing studies using Wnt1-Cre, which is expressed in neural crest cells, and ROSA26 reporter mice, demonstrated that the neural crest is not the origin of hepatic stellate cells (Cassiman et al., 2006). Instead, a recent study using lineage tracing demonstrated that the origin of the hepatic stellate cells is mesodermal (Asahina et al., 2009). Thus, hepatic stellate cells are a unique and highly diverse population of cells within the liver that contribute to the hepatic microarchitecture. However, the breadth of their function and diversity remains to be fully understood.

Epithelial Lineage

Bi-potential hepatoblast progenitor cells have the potential to become either hepatocytes or cholangiocytes. Hepatocytes represent the preponderant population of the liver at approximately 70% of total liver cells in mice, while cholangiocytes represent only approximately 3% (Si-Tayeb et al., 2010). Hepatoblast cell fate decisions occur in a subset of cells adjacent to the portal vein in a wave from the hilum, or base of the liver, to the periphery. Whether all hepatoblasts are competent to become cholangiocytes remains controversial. Work from my thesis using a mouse model which constitutively activates

Notch signaling in hepatoblasts, resulting in excess cholangiocyte differentiation, suggests a zone of competence in proximity to the portal vein possibly due to unique inductive cues residing within that environment (Please see Chapter III, Discussion: *Notch signaling acts permissively with the hepatoblast population for cholangiocyte specification*). In contrast, another study, using an inducible system to constitutively activate Notch in adult hepatocytes suggests that all cells remain competent to become biliary cells (Zong et al., 2009). However, the authors of the later study define adult as post-natal (P) 4, when naïve hepatoblasts are still present and do not provide a global view to address where in the lobule the induced cholangiocytes are located. Thus their results remain controversial and a definitive answer as to the spatial and temporal cues regulating hepatoblast competence remains to be determined. Regardless, this decision of the bi-potential hepatoblast to become a cholangiocyte is the initiation of the process of biliary epithelial morphogenesis (Figure 1.3).

In contrast to other epithelial branching organs, such as the lung, the epithelial liver primordium and the bile duct network does not form via morphogenesis of a single epithelial sheet. Instead, the liver diverticulum delaminates, as described earlier, and the biliary epithelium begins to form by the differentiation of hepatoblasts into cholangiocytes directly adjacent to the portal vein. The sleeve of differentiating cells up-regulates cytokeratin19 to form a “ductal plate” surrounding the portal vein (Figure 1.3). In humans, a series of cytokeratins have been identified to mark the lineage restriction of hepatoblasts into the cholangiocyte cell fate (Crawford, 2002), however a lack of cross-reacting antibodies has prevented the translation of this information into murine models. Early mouse cholangiocytes are reactive to a pan-cytokeratin antibody, which recognizes a wide range of cytokeratins (56-64 kD molecular weight), and cytokeratin19. Unfortunately, cytokeratin19 is expressed early in the ductal plate and remains on throughout the lineage restriction. Thus,

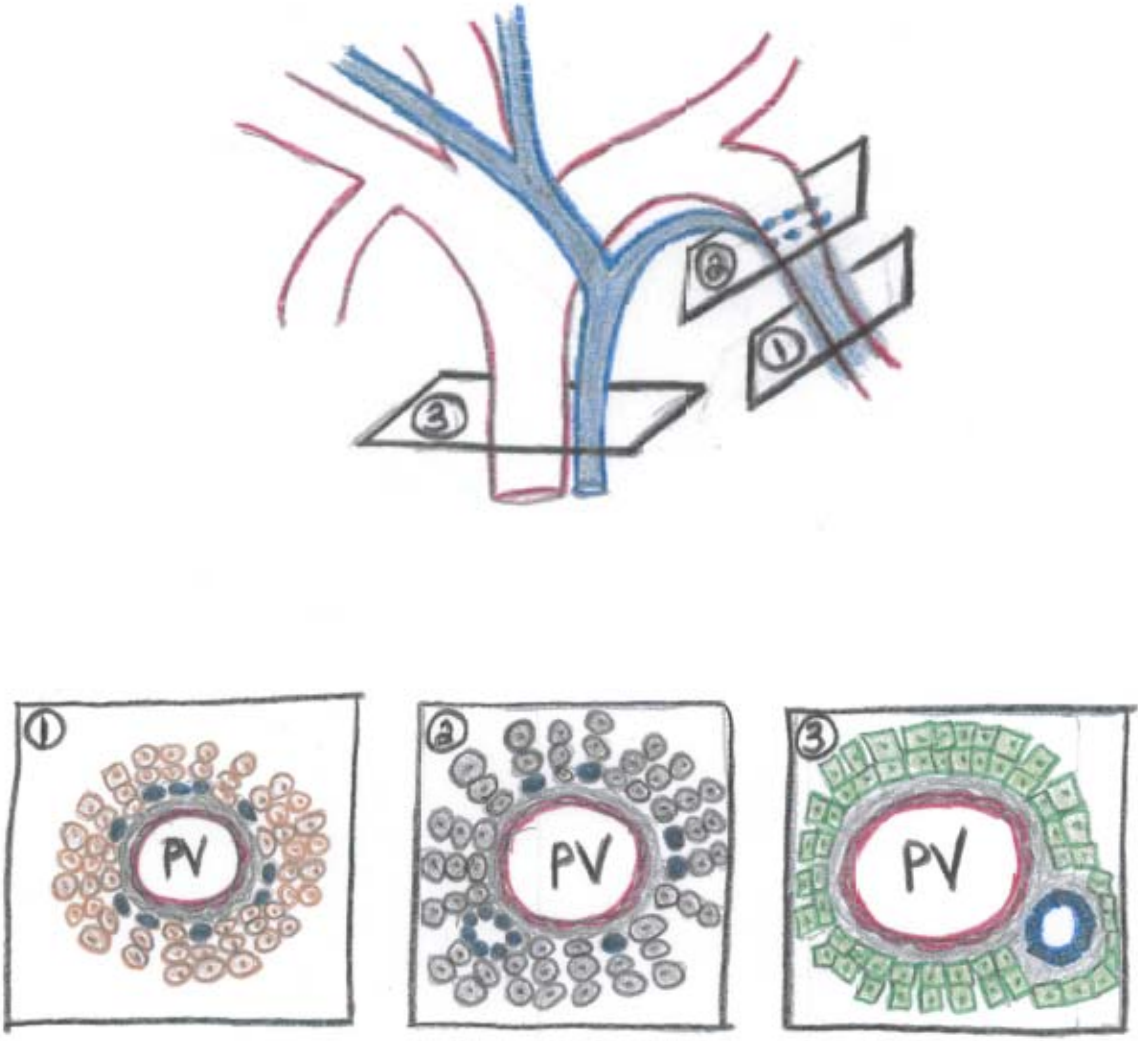

Figure 1.3 Bile duct morphogenesis. Bile duct development occurs in a wave from the hilum, or base of the lobe, towards the periphery tracking along the portal vein. The process of morphogenesis begins when (1) a ductal plate, composed of cells that up-regulate cytokeratin, is specified from hepatoblasts directly adjacent to the portal vein mesenchyme. Subsequently, (2) a subset of ductal plate cells form a luminal duct, and (3) the ductal plate cells not contributing to the bile duct regress, thus leaving the mature structure of a bile duct associated with a portal vein. Portal Vein/Endothelial Cells – red, Bile Ducts/Cholangiocytes – blue, Mesenchyme – grey, Early Hepatoblasts – light brown, Late Hepatoblasts – dark brown, Hepatocytes – green. PV – Portal Vein.

a lack of specific cholangiocyte markers in mouse has made it impossible to define the maturity and heterogeneity of early cholangiocytes. Subsequent to ductal plate formation, cholangiocytes at focal points within the ductal plate remodel to form a luminal ductal structure (Figure 1.3). What dictates the initial focal location of duct formation is not clear; however it is well established that hilar regions form first, with differentiation and remodeling occurring in a temporal fashion towards the periphery. Further, there is controversy within the field as to whether the luminal structure forms due to migration of cells from the ductal plate or a second wave of differentiation. *In vitro* evidence from Tanimizu et al., using collagen sandwich cultures of mouse hepatoblasts, demonstrated that a single epithelial sheet contained cells that delaminated and migrated to form luminal structures (Tanimizu et al., 2009). In contrast, a recent *in vivo* study of the expression of an early ductal marker, Sox9, suggests a model of transient asymmetry in which hepatoblasts nearest the portal vein differentiate foremost, followed by a second wave of differentiation of the remaining hepatoblasts (Antoniou et al., 2009). However, without the establishment of live cell imaging in mouse liver, neither model has yet to be conclusively demonstrated *in vivo*.

Cells of the ductal plate that do not contribute to the mature bile ducts undergo "regression". However, the mechanism of regression remains to be determined. The unincorporated cytokeratin19-positive cells are hypothesized to undergo apoptosis or de-differentiate to become hepatocytes. One study suggests that, in human development, these cells undergo apoptosis (Terada and Nakanuma, 1995), however I have been unable to demonstrate apoptosis in regressing ductal plate cells in the mouse, suggesting a de-differentiation program is more likely. Whether regression occurs differentially in human and mouse development remains to be definitely shown.

An additional consideration is that the adult biliary network is heterogeneous with regards to type of epithelium, whether cuboidal or columnar, normal function and response to injury (Glaser et al., 2009). While specific differences in cholangiocyte function will be

discussed later in this Introduction (Please refer to Adult Cholangiocytes: *Cholangiocyte Heterogeneity*), it is important to consider that it is currently unknown how hilar (branches originating at the hilum) and peripheral (branches originating from hilar branches) ducts are differentiated during development, and whether regionally different ducts arise by the same or different mechanisms. Currently, all models are based on the earliest duct formation, which originates at the hilar region. Therefore, it remains to be definitively described whether branches of the IHBD that form subsequent to and originate from hilar ducts form by the remodeling of a ductal plate, or a different mechanism. Additionally, while the basic morphology of biliary morphogenesis for hilar ducts has been elucidated, our understanding of the molecular cues, which initiate differentiation and remodeling, is in its infancy.

Molecular Cues for Bile Duct Development

Identification of signaling pathways that regulate cholangiocyte lineage restriction and morphogenesis has been limited. The two pathways that have been irrefutably identified to be required for biliary development are TGF-beta and Notch signaling. Interestingly, only Notch signaling has been linked to a human disease state (Please refer to *Hepatobiliary Disease: Alagille Syndrome*).

1. Overview of Transforming Growth Factor (TGF)-beta Signaling

The Transforming Growth Factor (TGF)-beta superfamily consists of sub-categories of signaling factors: TGF-beta, bone morphogenic proteins (BMPs), activin, nodal, myostatin and anti-Muellerian hormone (AMH). All ligands signal through a heterodimeric serine/threonine kinase receptor complex. Ligands bind the type II receptors (5 different types), which initiates association with the type I receptors (7 different types) and phosphorylation of the serine and threonine residues. Receptor activation then leads to a variety of downstream signals, with the canonical pathway signaling via Smads. TGF-beta,

activin, nodal and myostatin signal via receptors that phosphorylate Smad2 and 3, whereas BMP and AMH signal via receptors that phosphorylate Smad1, 5 and 8. Upon Smad phosphorylation, a common Smad, Smad4, associates with the complex to facilitate gene transcription (Massague and Gomis, 2006).

1A. TBF-beta in Cholangiocyte Development

The role of TGF-beta in *in vivo* cholangiocyte specification has been inferred by analysis of hepatocyte nuclear factor (HNF)-6 (part of the Onecut transcription factor family of proteins, OC1) knockout mice. HNF6 is highly expressed in biliary epithelial cells at the onset of the hepatoblast cell fate decision, and thus provided a potential target as an important transcription factor for biliary development (Clotman et al., 2002). Indeed, global knockout of HNF6 results in an excess of cytokeratin-positive biliary structures, which were identified as hybrid cells expressing markers of both cholangiocytes and hepatocytes (Clotman et al., 2002; Clotman et al., 2005). The global knockout of HNF6 phenocopies a liver-specific knockout of HNF1beta (Coffinier et al., 2002), therefore the authors investigated the possibility that loss of HNF6 reduced HNF1beta expression. By semi-quantitative reverse transcriptase PCR analysis, the authors demonstrated that HNF6 knockout mice had a reduction in HNF1beta transcript levels, and further that HNF6 bound the HNF1beta promoter by chromatin IP (ChIP) (Clotman et al., 2002).

The same group of investigators went on to determine that some redundancy exists within the Onecut transcription factors, and that global deletion of both HNF6 and OC2 resulted in a more severe expansion of the hybrid cells (Clotman et al., 2005). Interestingly, the authors demonstrated, when HNF6 knockout and HNF6/OC2 double knockout mice were crossed to a mouse line expressing a TGF-beta responsive promoter (12-Smad binding sites upstream of EGFP), that both knockout mice had an expansion in the domain of TGF-beta responsive cells (Clotman et al., 2005). It had been previously shown that TGF-

beta promotes the differentiation of cultured hepatoblasts into cholangiocytes (Isfort et al., 1997), thus the expansion of TGF-beta in HNF6 knockout and HNF6/OC2 double knockout would explain an increase in hybrid cells. Together these results suggest that HNF6 and OC2 are required to restrict the TGF-beta gradient required for biliary differentiation.

These studies suggest a direct role for HNF6 in the hepatoblast and/or early cholangiocyte cell fate decision. Therefore our laboratory undertook a project to test the cell autonomous requirement of HNF6 in liver development by deleting HNF6 specifically within the hepatoblast population. Surprisingly, we can detect no defects in the liver-specific HNF6 knockout (Vanderpool et al., In Preparation). These results suggest that while HNF6 is highly expressed in biliary epithelial cells (Clotman et al., 2002), it is not essential within this intrahepatic compartment. Instead the effects described in the global knockout suggest that the extrahepatic defects (i.e. an absent gallbladder and abnormal distended extrahepatic ducts) lead to secondary intrahepatic defects that resolve in 25% of HNF6 global null mice (Clotman et al., 2002). Interestingly though, when we cross our liver-specific HNF6 knockout with a liver-specific Notch signaling-deficient mouse, we find that loss of HNF6 exacerbates the cholestatic phenotype of the Notch deficient mice (Vanderpool et al., In Preparation). Thus suggesting in the background of cholestasis, HNF6 can synergize with Notch signaling to promote liver disease. In normal development, HNF6 protein is expressed exclusively in the liver epithelial lineage. However, it remains unknown what cells produce the TGF-beta to initiate a gradient and how this gradient is regulated. The mechanism by which HNF6 restricts the TGF-beta signal is not clear, however one study suggested that in the absence of HNF6, TGF-beta receptor type II expression is increased (Plumb-Rudewiez et al., 2004). Thus much work remains to elucidate the mechanisms by which TGF-beta and HNF6 contribute to biliary specification and morphogenesis.

2. Notch Signaling

Notch signaling is an evolutionarily conserved intercellular signaling pathway required for cell specification, lineage commitment and maintenance of stem and progenitor cells both during development and in adults (Chiba, 2006). Notch ligands, which are present on the cell surface, bind Notch receptors on the surface of an adjacent cell. Ligand and receptor interaction initiates a series of proteolytic cleavages (Figure 1.4). First, the receptor is cleaved in the extracellular domain by ADAM10 (a disintegrin and metalloprotease domain), a member of the ADAM family of metalloproteases (Bozkulak and Weinmaster, 2009; van Tetering et al., 2009). Directly following the ADAM10-mediated cleavage, the receptor is cleaved intramembranously by gamma-secretase, which releases the intracellular domain of the receptor (Notch Intracellular Domain – NICD) (De Strooper et al., 1999). Upon release from the membrane, the NICD translocates to the nucleus where it interacts with a common DNA-binding partner, recombination signal binding protein for immunoglobulin kappa J (RBP-J).

In the absence of the NICD, RBP-J acts as a co-repressor of gene transcription, however upon NICD association, RBP-J becomes a co-activator. In RBP-J's transcriptional repressive function, it has been shown to bind to promoter regions and perturb the interaction between the transcription factors TFIIA and TFIID (Olave et al., 1998). Further RBP-J has been shown to bind to other co-repressors such as SMRT (silencing mediator for retinoid and thyroid receptor) and MINT (Msx2-interacting nuclear target protein), which recruit histone deacetylases (Tanigaki and Honjo, 2010). Upon NICD translocation into the nucleus, the NICD binds RBP-J, displacing the co-repressor complex, and actively recruits co-activators, Matermind, PCAF and GCN5 to initiate gene transcription (Tanigaki and Honjo, 2010).

In mammals there are two families of canonical Notch ligands (JAG1 and 2, Delta-like-1, 3, and 4) which signal through four canonical Notch receptors (Notch1-4). Previously

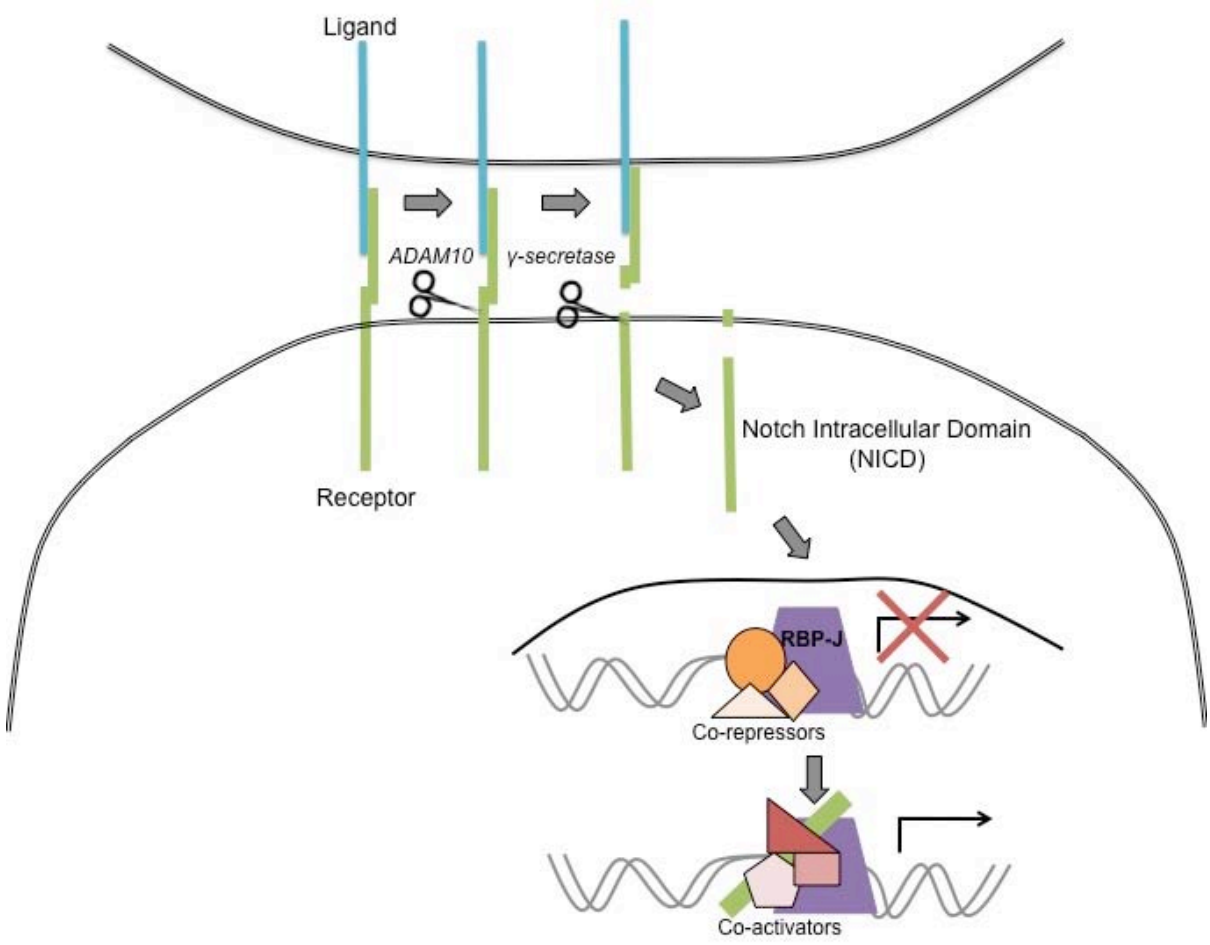

Figure 1.4 Notch signaling pathway. Notch signaling is initiated when a Ligand, present on the cell surface, interacts with a Receptor on the cell surface of an adjacent cell. Upon Ligand engagement, ADAM10 mediates cleavage of the extracellular portion of the Receptor. This cleavage allows for a second, gamma-secretase-dependent cleavage to occur intramembranously. These cleavages release the Notch Intracellular Domain (NICD) to translocate to the nucleus. In the nucleus, the NICD binds a common DNA-binding partner, RBP-J, displaces co-repressor proteins and recruits co-activators to facilitate gene transcription.

it has been shown that both Notch1 and Notch2 are essential for embryonic development, since mice with global loss of either receptor die embryonically (Swiatek et al., 1994; Conlon et al., 1995; Hamada et al., 1999). In contrast, Notch3 and Notch4 are dispensable for development as mice lacking these receptors are viable (Krebs et al., 2000; Krebs et al., 2003). However, in the absence of Notch1 or Notch2, Notch3 and Notch4 exhibit various degrees of redundant function (Pan et al., 2004).

Dysregulation of Notch signaling is intimately related to AGS, a disorder highlighted by paucity of bile ducts, thus revealing a role for Notch signaling in bile duct regulation. As mentioned earlier in this Introduction, it is unclear as to how Notch signaling contributes to bile duct paucity in AGS patients; whether by improper development, inability to maintain ductal structures or a lack of post-natal branching and elongation (Please refer to Hepatobiliary Disease: Alagille Syndrome). Since Notch signaling is classically required developmentally for binary cell fate decisions, it was initially hypothesized that Notch signaling is required within the hepatoblast to mediate the bi-potential cell fate decision to become a cholangiocyte or hepatocyte.

2A. Notch Signaling in Cholangiocyte Development: the Signal-Sending Cell

A number of mouse models have been generated to address this hypothesis. In an attempt to mimic the AGS clinical situation, Xue et al., generated mice homozygous and heterozygous for a targeted null mutation of the JAG1 gene (Xue et al., 1999). Mice homozygous for the Jag1 null mutation are embryonic lethal at E10 due to vascular defects. In contrast, mice that are heterozygous for the Jag1 null mutation, as observed in AGS patients, survive normally but exhibit mild eye defects (Xue et al., 1999). Thus this mouse model was not useful in understanding the role of Notch signaling in biliary development.

The next model generated was that of a hypomorphic allele of the Notch2 gene (McCright et al., 2001). Alternative splicing of the Notch2 mutant allele ($Notch2^{del1}$) leads to

the production of two different in-frame shifts, which remove one or two of the extracellular EGF repeats required for ligand binding. Homozoygous Notch2^{del1} mice demonstrate kidney glomerular development defects, heart and eye vascular abnormalities, as AGS, however still do not recapitulate the bile duct paucity observed in AGS patients (McCright et al., 2001).

The first mouse model to recapitulate a majority of the defects observed in AGS patients was described in 2002 by generating mice double heterozygous for the Jag1 null mutation and the Notch2 hypomorphic allele (McCright et al., 2002). The double heterozygous mice demonstrate jaundice, growth retardation, IHBD paucity, kidney, heart and eye defects. However, the skeletal and craniofacial malformations observed in AGS patients are not represented in the mouse model (McCright et al., 2002). The partial recapitulation of AGS by a double heterozygous mouse emphasizes the importance of the threshold of Notch activity required in an organ and cellular specific context, and suggests an explanation for the variable phenotype of AGS patients.

While the aforementioned studies provided the groundwork for a mouse model of AGS, the next important goal became determining the cell types in which Notch intracellular signaling was required (signal receiving versus signal sending cell). The localization of Notch ligands and receptors during liver development and in the adult in human and mouse studies, as assessed by immunohistochemistry or immunofluoresecence, revealed conflicting results (Table 1.2).

Initial investigations focused on the role of Jag1 in biliary development. Loomes et al. determined that conditional deletion of Jag1 within the hepatoblast had no affect on liver development. Indeed, mice only exhibited bile duct paucity when placed on the background of a Jag1 null allele (Loomes et al., 2007). Therefore, Jag1 is not required in the liver epithelial compartment for proper biliary development. Based on immunohistochemical

Ligands	Species	Ductal Plate	Bile Duct	Hepatic Artery	Portal Vein	Hepatocyte	Other	Study
Jagged1	**Human**	Yes (Dev)	Yes (Dev)	No	No	No		(Louis et al., 1999)
		No	No	Yes (Dev)	Yes (Dev)	No		(Crosnier et al., 2000)
				Yes (Dev)	Yes (Dev)	No		(Jones et al., 2000)
		Yes (Dev)		No	Yes (Dev)	No		(Loomes et al., 2002)
			Yes (Ad)	Yes (Ad)	Yes (Ad)	Yes (Ad)		(Nijjar et al., 2002)
		Yes (Dev)	Yes (Ad)	Yes (Dev, Ad)	Yes (Dev, Ad)	Yes (Dev, Ad)		(Flynn et al., 2004)
	Mouse	Yes (Dev)	No	Yes (Dev)	Yes (Dev)	Yes (Dev)		(Loomes et al., 2002)
			No	Yes (Dev)	Yes (Dev)	No	Mesenchymal (Dev)	(McCright et al., 2002)
		No	No	Yes (Dev)	Yes (Dev)	No	Mesenchymal (Dev)	(Kodama et al., 2004)
		No	No	Yes (Dev)	Yes (Dev)	No		(Tanimizu and Miyajima, 2004)
		No	Yes (Dev)	Yes (Dev)	Yes (Dev)	No	Mesenchymal (Dev)	(Hofmann et al., 2010)

Ligands	Species	Ductal Plate	Bile Duct	Hepatic Artery	Portal Vein	Hepatocyte	Other	Study
Notch1	**Human**		Yes (Ad)	No	No	No	SEC (Ad)	(Nijjar et al., 2001)
			Yes (Ad)	Yes (Ad)	No	Yes (Ad)		(Flynn et al., 2004)
	Mouse	No	No	No	No	Yes (Dev)		(Loomes et al., 2002)
Notch2	**Human**		Yes (Ad)	Yes (Ad)	Yes (Ad)	Yes (Ad)	SEC (Ad)	(Nijjar et al., 2001)
			Yes (Ad)	Yes (Ad)	No	Yes (Ad)		(Flynn et al., 2004)
	Mouse	No	No	No	No	Yes (Dev)		(Loomes et al., 2002)
			No	No	No	No		(McCright et al., 2002)
		No	Yes (Dev)	No	No	No		(Kodama et al., 2004)
		Yes (Dev)		No	No	Yes (Dev)		(Tanimizu and Miyajima, 2004)
Notch3	**Human**		Yes (Ad)	Yes (Ad)	Yes (Ad)	Yes (Ad)		(Nijjar et al., 2001)
		No		Yes (Ad)	Yes (Ad)	Yes (Ad)	Mesenchymal (Ad)	(Flynn et al., 2004)
	Mouse	Yes (Dev)	No	Yes (Dev)	Yes (Dev)	No		(Loomes et al., 2002)
Notch4	**Human**		No	Yes (Ad)	No	No		(Nijjar et al., 2001)
			No	Yes (Ad)	No	No		(Flynn et al., 2004)
	Mouse	No	No	No	No	Yes (Dev)		(Loomes et al., 2002)

Table 1.2 Immunohistochemical expression of Notch pathway components in liver. This table summarizes currently published work which has suggested the cells, both developmentally and in the adult, that express different components of the Notch pathway (Ligands and Receptors). This data includes only immunohistochemical identification in tissue section in both human and mouse studies. Developmental studies are identified by **Dev**. Adult studies are identified by **Ad**. SEC – Sinusoidal Endothelial Cells.

analysis, Jag1 was consistently expressed in both the portal vein endothelium and mesenchyme (Table 1.2). A recent study examining the necessity of Jag1 within specific cell lineages demonstrated that the requirement of Jag1 resides within the portal vein mesenchyme (Hofmann et al., 2010). Hofmann et al. demonstrated that an endothelial-mediated deletion of Jag1 had no effect on bile duct morphogenesis. In contrast, a smooth-muscle-actin-mediated deletion of Jag1 recapitulated bile duct paucity as observed in AGS patients (Hofmann et al., 2010). These results are consistent with the mode of Notch action signaling between adjacent cells, as the portal hepatoblasts abut mesenchyme, not endothelium. Thus the signal-sending cell (expressing ligand) is considered to be the portal vein mesenchyme and the signal-receiving cell (expressing receptor), the hepatoblasts adjacent to the portal vein.

2B. Notch Signaling in Cholangiocyte Development: the Signal-Receiving Cell

The majority of research investigating the role of Notch signaling in bile duct development has focused on the cell autonomous requirement of Notch signaling within the liver epithelium. At this point, it is important to make note of a deficiency of Cre lines with which to mediate deletion in the liver epithelium. For the purpose of my studies, I have utilized an Albumin-Cre transgene (Alb-Cre) (Postic and Magnuson, 2000). While this Cre line was originally reported to mediate deletion of the glucokinase locus at 6 weeks with 90% efficiency in a C57/Bl6 background, as assessed by Southern blot, it has since been revealed that in a CD1 background Alb-Cre is expressed much earlier within the hepatoblast (Please refer to Appendix A for more information). Other Cre lines used to mediate hepatoblast deletion are: the albumin-enhancer and promoter plus alpha-fetoprotein-enhancer driven Cre (Alfp-Cre; (Kellendonk et al., 2000)) and Forkhead box A3 driven Cre (FoxA3-Cre; (Lee et al., 2005)). Unfortunately, none of these Cre lines mediates gene deletion before the initial specification and diverticulum formation. Indeed, the earliest

documented Cre line is the FoxA3-Cre, and it has been reported to mediate recombination of the Rosa26 Reporter (R26R) in 81% of liver epithelial cells at E15.5 (Zong et al., 2009). Despite subtle differences in timing of deletion, little difference is observed in the resulting phenotype using Alb-Cre, FoxA3-Cre or Alfp-Cre, as assayed by cytokeratin-positive ductal morphology.

The first study to investigate the cell-autonomous requirement of Notch signaling was Lozier and colleagues who used Alb-Cre to mediate deletion of a Notch2 floxed allele (Lozier et al., 2008). In parallel with this study, our laboratory was also examining the requirement of Notch2 in liver epithelial cells (Please refer to Chapter III, Results: *Modulating Notch Signaling within the Hepatoblast Lineage Alters IHBD Development*). Both my work and that of Lozier et al. determined that liver-specific loss of the Notch2 receptor results in the presence of un-remodeled cholangiocytes in peripheral liver tissue (Lozier et al., 2008). This phenotype is reminiscent of AGS patient biopsies.

While Notch2 is generally considered the primary receptor in the liver, it remains possible that the other receptors may partially compensate in the absence of Notch2. Therefore, Geisler et al., investigated the ductal defects as a consequence of Alb-Cre-mediated deletion of Notch1 and Notch2 (Geisler et al., 2008). In concert with this study, our laboratory was also examining the liver-specific requirement of Notch1 and Notch2 (Please refer to Chapter III, Results: *Modulating Notch Signaling within the Hepatoblast Lineage Alters IHBD Development*). Both my work and that of Geisler et al. demonstrate that the loss of Notch1 and Notch2 is morphologically indistinguishable from that of Notch2 liver-specific knockout mice, and also displayed un-remodeled cytokeratin-positive cells in the periphery (Geisler et al., 2008). However, as these conclusions were drawn from observations in tissue section and the number of cytokeratin-positive cells not quantified, this does not preclude the possibility that the Notch2 liver-specific knockout and the Notch1/Notch2 liver-specific double knockout have subtle but differential effects on the intact three-dimensional

(3D) biliary architecture. Indeed this is the case, as I have adapted a method of resin casting to reveal the 3D structure of the biliary system, and the Notch1/Notch2 liver-specific double knockout has more severe paucity of peripheral branch density than the Notch2 liver-specific knockout alone (Please refer to Chapter III, Figure 3.10). Thus these results suggest that in the absence of Notch2, a level of compensation from other Notch receptors can occur.

While the major Notch receptors are considered to be the Notch1 and Notch2 receptors, it is possible that in the absence of these receptors, the minor Notch receptors, Notch3 and Notch4, may compensate. Therefore to remove all signaling from Notch receptors, our laboratory and the Stanger laboratory independently examined the liver-specific deletion of RBP-J, the common DNA binding partner for all four Notch receptors (Zong et al., 2009). Two caveats are noted regarding the use of RBP-J to delete Notch signaling; first in the absence of the NICD, RBP-J acts as a co-repressor, therefore loss of RBP-J has the potential to lead to de-repression of target genes. While de-repression upon loss of RBP-J is a possibility as demonstrated by a recent study in embryonic stem cell cultures (Meier-Stiegen et al., 2010), to date, no study has demonstrated that de-repression occurs *in vivo*. In fact, a recent study demonstrated that loss of RBP-J alone was not sufficient to mediate de-repression in developing thymocytes (Chari et al., 2010). The second caveat of note is that RBP-J has been proposed to have Notch-independent functions. This phenomenon has been described for the pancreas and spinal cord, in which RBP-J interacts with Ptf1a, a transcription factor expressed only in these two tissues (Obata et al., 2001; Hori et al., 2008). However, a Notch-independent role for RBP-J other than by Ptf1a interaction has not been described in mammals.

Therefore, our laboratory and others examined the effect of liver-specific deletion of RBP-J on bile duct development (Please refer to Chapter III, Results: *Modulating Notch Signaling within the Hepatoblast Lineage Alters IHBD Development*). Utilizing a FoxA3-

mediated deletion of RBP-J, Zong et al. demonstrated a reduction in the number of cells specified within the ductal plate (Zong et al., 2009). Interestingly, despite using FoxA3-mediated gene deletion, there are still cells specified and ducts formed, albeit fewer. My results using Alb-Cre mediated deletion of RBP-J demonstrate similar results; fewer cells specified in the ductal plate and fewer ducts formed. Using resin casting to visualize the effects on the 3D architecture as a consequence of deleting RBP-J demonstrates a drastic reduction in peripheral branch density (Please refer to Chapter III, Figure 3.10). Thus, loss of RBP-J reveals a more severe phenotype than loss of both the Notch1 and Notch2 receptors. The differential phenotypes with the liver-specific loss of RBP-J versus the liver-specific loss of the Notch1 and Notch2 receptors further suggests that the threshold of Notch activity will be important to define the histopathology in AGS patients. These results suggest either a Notch-independent role of RBP-J, de-repression of gene targets or compensation by the Notch3 and/or Notch4 receptors in the absence of Notch1 and Notch2. Thus we examined the transcript levels of each of the Notch receptors in the Notch2, Notch1/Notch2 and RBP-J loss-of-function mice. Interestingly, in the Notch1/Notch2 double knockout, there is a significant increase in the transcription of the Notch3 and Notch4 receptors at P15, suggesting the possibility of receptor compensation (Sparks et al., 2010). Further in the RBP-J loss-of-function mice, there is an increase in the transcription of all four receptors, suggesting a futile attempt to compensate for the lack of Notch signaling.

Together studies of the cell-autonomous requirement of Notch signaling in the liver epithelium have suggested a threshold requirement for Notch signaling in bile duct development (Figure 1.7). Thus in the absence of all Notch signaling (loss of RBP-J), fewer ductal cells are specified during development. However, when signaling is removed via deletion of only two of the receptors (loss of Notch1 and Notch2), hepatoblasts specify the correct number of ductal cells, but they cannot remodel properly. It is intriguing to note that in the absence of all Notch signaling, some ductal cells are still specified. This observation

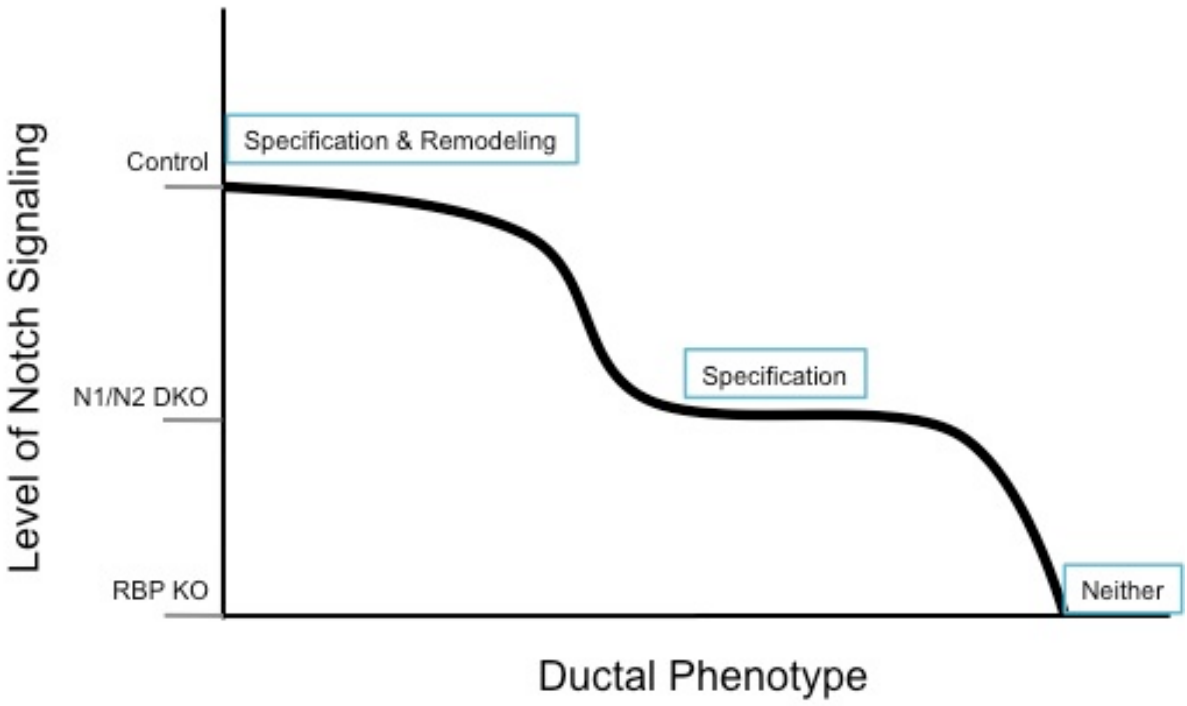

Figure 1.5 A threshold requirement for Notch signaling in bile duct development. This graph represents the threshold requirement of Notch signaling during bile duct development. The Y-axis represents the level of Notch signaling, whereas the X-axis represents the ductal phenotype. In the presence of complete Notch signaling, specification and remodeling occur normally, however when signaling from two of the receptors is lost, only specification occurs and remodeling is deficient. Finally, when all Notch signaling is lost, via deletion of the common DNA-binding partner, both specification and remodeling are deficient.

leads to speculations as to whether Notch signaling acts permissively or instructively within the hepatoblast population. The specification of fewer ductal plate cells can be attributed to Notch signaling acting permissively, or to gene deletion occurring in a mosaic fashion during the process of the initial cell fate decision of the hepatoblast. As discussed earlier in this introduction, the Cre lines available for liver-specific deletion affect hepatoblasts at E15.5 at the earliest, and the initial hepatoblast cell fate decision occurs as early as E13 as observed by ductal plate formation. However, identical phenotypes in RBP-J knockout mice regardless of the timing of Cre deletion, suggests that this does not affect the amount of cells specified. Therefore, I hypothesize that Notch signaling is acting permissively within the hepatoblast to influence cholangiocyte cell fate decisions. Support of this hypothesis comes from an *in vitro* study where the NICD was expressed in cultured hepatoblasts (Tanimizu and Miyajima, 2004). Under these conditions, the expression of the NICD is not sufficient to drive the cholangiocyte fate in hepatoblasts. However, when hepatoblasts expressing the NICD were cultured on Matrigel containing growth factor stimulants, cholangiocyte markers were up-regulated (Tanimizu and Miyajima, 2004), thus suggesting that Notch maintains cells with the competency to become cholangiocytes, but additional cues are required to instruct the cell fate.

The instructive or permissive role of Notch signaling in the hepatoblast population was further investigated *in vivo* using mouse models that constitutively express the NICD upon recombination of a STOP cassette in the ROSA26 locus (Murtaugh et al., 2003; Tchorz et al., 2009). Our laboratory has investigated the consequence of chronic Notch1 ICD expression, via Alb-Cre-mediated recombination (NICD), on biliary development. NICD mice have an increase in the number of specified and remodeled biliary cells, suggesting Notch1 is both necessary and sufficient for bile duct development (Please refer to Chapter III, Results: *Modulating Notch Signaling within the Hepatoblast Lineage Alters IHBD Development*). However, the excess biliary cells are restricted to zones, which trace along

the tracts of the portal vein system (Please refer to Chapter III, Figure 3.7). These results support a permissive role for Notch signaling in biliary development, in which Notch maintains a competency zone of hepatoblasts with the potential to become cholangiocytes. Interestingly, when the Notch2 ICD (N2ICD) is expressed via Alb-Cre-mediated recombination, an excess of biliary cells are also specified and remodelled, but are restricted to regions directly adjacent to the portal vein (Tchorz et al., 2009), indicating the limited potential of Notch2 versus Notch1 in the ability to maintain hepatoblast competence. Unfortunately, the authors used the lectin *Dolichos biflorus* agglutinin (DBA) as a marker of ductal cells, which I have shown to be specific to hilar ducts (Please refer to Chapter III, Figure 3.8). Thus the precise effect of N2ICD expression on peripheral ducts remains to be fully understood. Zong and colleagues proposed a contrasting interpretation although they used a similar study. In their approach, they use the inducible Cre-mediated expression of the NICD within the liver epithelial population by Alb-CreER to make the assessment whether the expression of the NICD in mature hepatocytes can induce biliary transdifferentiation (Zong et al., 2009). The authors interpret the observation of excess cholangiocytes to suggest that Notch signaling acts instructively to specify the cholangiocyte cell fate in adult liver epithelia. However, some weaknesses in this experimental approach are the assumption that P4 is an adult and no naïve hepatoblasts remain. Also the authors do not examine if there is regional specificity of this potential transdifferentiation, which could be attributed to the known hilar to peripheral maturation of bile ducts. Thus the role of Notch signaling as an instructive or permissive cue in hepatoblast specification into cholangiocytes remains to be definitely determined, however the majority of evidence at this junction points towards a permissive role.

The cell-autonomous role of Notch signaling in hepatoblast specification has been extensively studied, however the precise requirement and regulation of signaling remains largely a mystery. In addition, the post-natal consequence of improper liver development

has not been extensively studied in a genetically defined model. The work described within this dissertation begins to address this question. The proper function of adult cholangiocytes is crucial for proper liver function, thus understanding how developmental modulations affect the adult function is critical for the generation of future therapeutics aimed to restore cholangiocyte function in cholangiopathies.

Adult Cholangiocytes

Cholangiocyte Function

Cholangiocytes provide not only the structure of the IHBD, but also provide many important physiological functions to maintain normal metabolic homeostasis. Cholangiocytes provide a conduit for bile to flow out of the liver, however the IHBD is not just a passive channel. Instead cholangiocytes modify the fluidity and alkalinity of bile, produced by hepatocytes, through coordinated secretory and absorptive processes. While cholangiocytes contribute to only a small percentage of total liver cells (~3%), their ability to effectively modulate bile production is evidenced by the fact that cholangiocytes contribute up to 30% of the bile volume in humans (Nathanson and Boyer, 1991). Cholangiocytes regulate bile volume by the secretion of osmolites such as Cl^- and HCO_3^-, generating an osmotic gradient which drives water secretion into the luminal space (Roberts et al., 1994). While the function of cholangiocytes is generalized as the regulation of bile composition, the heterogeneity of the biliary epithelium, with respect to function and response to injury, has recently come to light (Glaser et al., 2004; Glaser et al., 2009).

Cholangiocyte Heterogeneity

Three categories of heterogeneity have been defined: morphological, secretory and proliferative. Morphological heterogeneity is defined by the size of cholangiocytes and the

type of epithelium they generate. For example, cholangiocytes that compose the hilar ducts are larger (mean cell size in mouse = 13.24±0.17μm), columnar and contribute to ducts >15 μm in diameter; in contrast, peripheral cholangiocytes are smaller (mean cell size in mouse = 8.84±0.08 μm), cuboidal and contribute to ducts <15 μm in diameter (Glaser et al., 2009).

Cholangiocyte secretory function is regulated by homone-responsive Ca^{2+}- or cyclic adenosine 3',5'-monophosphate (cAMP)-dependent events. However, only large cholangiocytes express the receptors and transporters required for ductal secretion, thus suggesting a secretory heterogeneity within the biliary system exists as well (Glaser et al., 2004; Glaser et al., 2009). The functional role of small cholangiocytes in normal biliary homeostasis is unknown at this juncture. Further, it remains unclear whether all large cholangiocytes are equivalent in their ability to regulate ductal secretions, or another level of heterogeneity exists within the broader population.

The final category of cholangiocyte heterogeneity was determined based on the ability of individual cell populations to respond to injury. Normal cholangiocytes are mitotically dormant, however in response to injury a limited range of cholangiocytes are able to respond by proliferating. Specifically, after bile duct ligation (BDL), a procedure used to model cholestatic liver disease, large bile ducts proliferate, whereas small bile ducts do not. Similarly, small bile ducts are resistant to carbon tetracholoride (CCL_4)-induced damage, whereas large bile ducts lose their proliferative and secretory capacity. Interestingly, upon loss of large bile duct function, the small bile ducts begin to express the receptors and transporters required for ductal secretion (Kanno et al., 2000). The proliferation and functional quiescence of small bile ducts, and their ability to compensate for lost function in the large bile ducts has led to the hypothesis that small cholangiocytes represent the liver stem cell population (Alpini et al., 2002).

Cholangiocyte Cilia

As with most cells in the body (one exception being hepatocytes), cholangiocytes have a primary cilium located on their apical cell surface. While cholangiocyte cilia were described as early as 1963 (Grisham, 1963), the functional significance of the primary cilium was not appreciated until recently. Cholangiocyte cilia are now recognized as vital sensory organelles that detect changes in bile flow, composition and osmolality (Masyuk et al., 2008). The importance of the primary cilia is highlighted by a number of cholangiopathies that arise due to defects in ciliogenesis (ciliopathies; Table 1.1). As with a heterogeneous cholangiocyte population, the length of primary cilia is also heterogeneous. Large bile ducts have longer cilia than small bile ducts (approximately two times) (Huang et al., 2006). Thus, cilia length has been proposed to correlate with the functional heterogeneity of biliary epithelium.

Liver Regeneration

With the high prevalence of liver disease in the United States, understanding the mechanisms involved in liver regeneration is important for the development of new therapeutic options. The ability of the liver to regenerate after injury has intrigued researchers for centuries. It is generally accepted that two modes of liver regeneration occur: 1. proliferation of normally quiescent hepatocytes and 2. activation of a quiescent liver progenitor cell. Despite conjecture that a quiescent progenitor cell resides within the biliary epithelium, few studies have investigated the role of cholangiocytes in liver regeneration.

Partial Hepatectomy

Liver regeneration, as classically described, is not achieved by the traditional mechanism of appendage replacement; instead when a portion of the liver is removed (i.e.

one or more lobes), the remaining lobes undergo a compensatory proliferation to recover the mass. The typical experiment to study liver regeneration is the 70% partial hepatectomy (PHx). Pioneering work, outlining the major physiological alterations after PHx in rats, was performed by Nancy Bucher (Bucher and Glinos, 1950; Bucher et al., 1951; Bucher, 1963; Bucher, 1967; Bucher et al., 1969; Bucher et al., 1977). More recently, genetic knockouts in mouse models have allowed a better understanding of the signaling pathways involved in regeneration.

The main cellular source of regeneration after PHx is proliferation of normally quiescent hepatocytes. Hepatocyte proliferation peaks at approximately 24 hours post-PHx in rat (approximately 36 hours for mice, (Miliutina, 1989)), with each hepatocyte undergoing one or two mitotic divisions to restore hepatic mass after 70% PHx (Stocker and Heine, 1971). The cues that trigger hepatocyte proliferation and thus liver regeneration remain controversial. While many factors involved in hepatocyte replication have been shown to be up-regulated after PHx, knockout of any one of these is not sufficient to prevent liver regeneration, suggesting a redundancy within the signaling pathways (Michalopoulos, 2007). Of further interest is that, while hepatic mass is recovered within five to seven days, the cues that regulate the precise control to stop growth remain a mystery (Michalopoulos, 2007).

The majority of studies on liver regeneration have focused on the role of the hepatocyte, with cholangiocytes remaining largely ignored. In recent reviews, it is stated the proliferation of non-hepatocyte cells occurs approximately 24 hours after hepatocyte proliferation (i.e. 48 hours in the rat) (Michalopoulos and DeFrances, 1997). Interestingly, the reference cited, and the only study to investigate cholangiocyte proliferation post-PHx to my knowledge, states that proliferation is occurring between 20 and 24 hours post-PHx in the rat (Grisham, 1962). Thus suggesting that hepatocyte and cholangiocyte proliferation is occurring simultaneously. The source of this discrepancy in the timing of cholangiocyte

proliferation is not understood. Further, the time course of cholangiocyte proliferation after PHx in mice has not be determined. In Appendix E, I begin to investigate the mechanism of ductal regeneration after PHx and provide initial evidence that the ductal system expands in concert with the growth of the remaining lobes.

While many studies have investigated the role of individual signaling pathways and transcription factors on liver regeneration following PHx, to date no single factor can prevent the initiation or termination of liver regeneration (Riehle et al., 2011). A further unexplored question is what regulates the seemingly infinite regenerative ability of the liver. For example, a landmark study demonstrated that liver still regenerates after twelve successive surgeries on the same animal (Stocker et al., 1973). Further, it was shown more recently that cultured hepatocytes can undergo at least 80 doublings (Overturf et al., 1997). Thus, understanding the regenerative capacity of the liver and the factors that regulate each stage is critical for the next steps in liver therapeutics.

Liver Progenitor Cells

Under normal circumstances, liver regeneration occurs via proliferation of hepatocytes. However, in the instance where hepatocytes are prevented from replicating, a facultative cell population arises in the vicinity of the portal vein, called “oval cells”, so termed based on their ovular shape (Farber, 1956). Experimental models of oval cell proliferation are achieved by the administration of hepatotoxic drugs. The origin and potential of oval cells has been the focus of many studies in recent years, however many key questions remain unanswered.

As oval cells are considered a transit amplifying population of cells, the question remains as to where the originating progenitor cell resides. Further, it is unknown whether a true progenitor cell exists in a latent form maintained from embryonic development, or if the plasticity of differentiated liver cells allows a mature cell type to dedifferentiate and act as a

stem cell. The origin of the oval cell has been purported to be many different cell types. Specifically, the functional heterogeneity of the ductal epithelium, as discussed early (Please refer to Adult Cholangiocytes: *Cholangiocyte Heterogeneity*) has lead to the hypothesis that small bile duct cells act as liver progenitors (Alpini et al., 2002). Thus far the most defining work to determine the origin of oval cells was published by Kuwahara and colleagues (Kuwahara et al., 2008). In this study, the authors used sub-lethal doses of acetaminophen in conjunction with label-retaining cell assays to define up to four potential protenitor cell niches. Specifically, label-retaining cells were found in the canals of Hering, intralobular bile ducts, periductular mononuclear cells and peribiliary hepatocytes (Kuwahara et al., 2008). Work from our laboratory using a cytokeratin19-CreER mouse to lineage label cytokeratin19-positive cells prior to injury and trace cells after induction of an oval cell response as a result of feeding 3,5-diethoxycarbonyl-1,4-dihydrocollidine (DDC), suggests that oval cells do not arise from a cytokeratin19-positive population (Teagan Walter, unpublished observations). Thus, these lineage-tracing results rule out cytokeratin19-positive cells as a potential source of progenitor cells. It remains possible that multiple progenitor cell sites exists within the liver, and that activation of the individual compartments may vary based on the type of injury, however this has not been investigated.

A second line of investigation is the contribution of oval cells to recovering cell populations during and after liver injury. Initially, it was shown that oval cells in culture had the potential to up-regulate markers of cholangiocytes and hepatocytes, thus suggesting the bi-potential nature of oval cells (Germain et al., 1988; Lazaro et al., 1998). The gold-standard experiment to test the ability of oval cells to repopulate the liver *in vivo* was provided by Wang and colleagues (Grisham, 1962). In this study, the authors utilize a unique model of liver failure, the tyrosinema model, fumarylacetoacetate hydrolase (Fah)-deficient mice (Grompe et al., 1993). With continuous administration of 2-(2-nitro-4-trifluoromethylbenzoyl)-1,3-cyclohexanedione (NTBC), Fah-deficient mice survive normally,

however upon withdrawal of NTBC, Fah-deficient mice undergo mass hepatic failure via hepatocyte death (Grompe et al., 1995); thus these mice are ideal for addressing the reconstitution potential of various cell types. In the aforementioned study, a heterogeneous population of DDC-responsive oval cells were transplanted into Fah-deficient mice after withdrawal of NTBC to determine their repopulation potential *in vivo*. Indeed, the oval cells were able to repopulate and rescue the Fah-deficient metabolic liver failure (Wang et al., 2003). Using the same Fah-deficient mice, in the same study the authors went on to demonstrate that oval cells do not arise from hepatocytes or bone marrow stem cells (Wang et al., 2003).

Despite the description of oval cells over 55 years ago, our understanding of their origin and how they contribute to alleviating liver disease remains poorly characterized. Further, the effect DDC has on the biliary architecture has not been investigated. Therefore in Appendix E, I begin to investigate the structural alterations induced by DDC treatment and discuss the discrepancies between cholestatic liver disease and drug-induced oval cell production. The identification of liver progenitor cells has very important clinical implications, and could provide an alternative therapy for the treatment of cholestatic liver disease; however much work remains to determine whether a liver progenitor cell exists or plasticity of differentiated cells contributes to this atypical liver regeneration.

Aims of the Dissertation

In my dissertation, I aim to first address the requirement of different levels of Notch signaling in bile duct development and describe the three-dimensional bile duct structure (Please refer to Chapter III). Next, I will investigate the hypothesis that Notch signaling is required for the post-natal maintenance of biliary structure (Please refer to Chapter IV). In the investigation of this hypothesis, I have revealed a previously unappreciated phenotype of progressive post-natal obstruction of the IHBD. The mechanisms contributing to this

obstruction and the acute requirement of Notch signaling in the adult are investigated in Chapter V. Thus, this dissertation will address the requirement of proper biliary development in the progression of cholestatic liver disease.

CHAPTER II

MATERIALS AND METHODS

Mouse Lines

CD1 mice carrying the *Albumin-Cre* transgene (*Alb-Cre*) (Postic and Magnuson, 2000) or the *Cytokeratin19-CreER* knockin allele (*K19-CreERT2*) (Means et al., 2008) were crossed with the conditional deletion allele for Notch1 (*Notch1*$^{flox/flox}$) (Pan et al., 2004), Notch2 (*Notch2*$^{flox/flox}$) (McCright et al., 2006), RBP-J (*RBP-J*$^{flox/flox}$) (Han et al., 2002), the conditional activation allele for Notch1 (*ROSA26*^{Notch1}) (Murtaugh et al., 2003), and the ROSA26 reporter allele (R26R) expressing LacZ (Soriano, 1999) or enhanced yellow fluorescent protein (EYFP) (Srinivas et al., 2001). Further crosses were performed to obtain homozygous genotypes. Control genotypes are: *Alb-Cre, K19-CreER, Notch1*$^{flox/flox}$*;Notch2*$^{flox/flox}$*, Notch1* $^{flox/+}$*;Notch2*$^{flox/+}$*, Notch1*$^{flox/flox}$*;Notch2*$^{flox/+}$*, RBP-J*$^{flox/flox}$*, and ROSA26*^{Notch}. Genotyping was performed by polymerase chain reaction (PCR) analysis using previously published primer pairs. All breeding and experimental procedures were done with prior approval by the Vanderbilt Institutional Animal Care and Use Committee. Infection with *Helicobacter hepaticus* was ruled out by testing fecal samples for bacterial DNA by PCR.

Serum Chemistry

Peripheral blood was collected post-mortem via a cardiac stick. Blood was centrifuged at 13,200 RPM for 5 minutes in a tabletop centrifuge to separate the serum. Serum was transferred into a new tube and sample analysis was completed within 7 days of collection. Alanine aminotransferase (ALT), total bilirubin (TB) and alkaline phosphatase

(ALP) were measured using colorimetric endpoint assays as per the manufacturer's protocol (Teco Diagnostics).

Bile Acid Isolation and Analysis

Bile acids were isolated from four different pools: the liver, gallbladder, serum and feces. Mice were fasted for 4 hours, with continual collection of feces. Upon sacrifice, blood was drawn via a cardiac stick, and set aside. Mice were weighed and the abdomen opened. The gallbladder was excised by first tying a ligature on the cystic duct just below to the gallbladder. The gallbladder was removed, and broken apart using #5 forceps in a tube to release the bile. Forceps were rinsed with methanol to maximize collection. The liver was extracted, and 110-115 mg from the center slice of the left lobe was maintained for analysis. Remaining fecal matter in the distal colon was removed and added to the previously collected feces. Internal standards (IS) for ultra performance liquid chromatography-tandem mass spectrometry (UPLC-MS/MS) analysis were: 40 µg/ml glycochenodeoxycholic-2,2,4,4-d4 acid (d4-G-CDCA) and 20 µg/ml chenodeoxycholic-2,2,4,4-d4 acid (d4-CDCA) (C/D/N Isotopes, Inc.).

For the extraction of liver bile acids, 20 µl of IS was added to tubes (one for each sample), and kept on ice. The liver sample was transferred into a dounce homogenizer with 5 volumes of water (i.e. 500 µl for 100 mg and 550 µl for 110 mg). Liver was homogenized until clear and transferred into the 15 ml tubes with IS. Samples were vortexed and allowed to equilibrate for 5-10 min. For extraction, 3 ml of 5% ammonia hydroxide in acetonitrile was added to the samples, and vortexed immediately. Samples were then allowed to shake at room temperature for 1 hour, and then centrifuged at 12,000 x g for 15 min. The supernatant was retained and set aside. The pellet was resuspended in 1.5 ml of methanol, vortexed and allowed to shake for an additional 20 min, and then centrifuged at 12,000 x g for 20 min. The supernatants were combined and dried under a vacuum. Samples were reconstituted in 200

µl of 50% methanol, votexed and filtered through a 0.2 µm filter, by centrifuging at 12,000 g for 10 min. Samples were stored at -20ºC until analysis.

For the extraction of gallbladder bile acids, 50 µl of IS was added to the tubes with the collected gallbladder bile. Samples were vortexed and centrifuged at 15,000 x g for 10 min. The supernatant was retained and set aside. The pellet was reconstituted in 2 ml of methanol, vortexed and allowed to shake for 30 min, and then centrifuged at 15,000 x g for 10 min. The supernatant was retained and set aside. The pellet was reconstituted with another 2 ml of methanol, vortexed and then centrifuged at 15,000 x g for 10 min. Supernatants were combined and dried under a vacuum. Samples were reconstituted in 500 µl of 50% methanol and stored at -20ºC until analysis.

For the extraction of serum bile acids, the collected blood was spun at 13,200 RPM for 5 min in a tabletop centrifuge. Serum was retained, and 100 µl was added to 5 µl of IS. Samples were vortexed, and equilibrated at room temperature for 5 min. After equilibration, 1 ml of methanol was added to the samples, they were vortexed and allowed to equilibrate again for 10 min at room temperature. Samples were vortexed, and centrifuged at 12,000 x g for 10 min. The supernatant was retained and set aside. The pellet was resuspended in 300 µl of methanol, allowed to shake for 30 min at room temperature, and then centrifuged at 12,000 x g for 10 min. Supernatants were combined and dried under a vacuum. Samples were reconstituted in 50 µl of 50% methanol and stored at -20ºC until analysis.

For the extraction of fecal bile acids, feces was allowed to dry at room temperature, and then ground in liquid nitrogen. Ground feces was weighed out to between 49-51 mg. Feces was placed in a tube and 20 µl of IS and 2 ml of methanol was added. Samples were vortexed, allowed to shake for 30 min at room temperature, and centrifuged at 12,000 x g for 10 min. The supernatant was retained and set aside. The pellet was resuspended in 2 ml of methanol, vortexed and allowed to shake for 30 min at room temperature. Samples were centrifuged at 12,000 x g for 10 min. Supernatants were combined and dried under a

vacuum. Samples were reconstituted in 200 µl of 50% methanol and stored at -20ºC until analysis.

UPLC-MS/MS analysis was performed at the University of Kansas Medical Center using techniques previously described (Zhang and Klaassen, 2010). A Waters ACQUITY ultra performance LC system was used for bile acid quantification. Chromatographic separations were performed on an ACQUITY UPLC BEH C18 column (1.7 µm, 100 x 2.1 mm I.D.) heated to 45ºC in the column compartment, using a gradient elution of mobile phase A (10 mM ammonium acetate in 20% acetonitrile) and mobile phase B (10 mM ammonium acetate in 80% acetonitrile). The injection volume was 7.5 µl and the flow rate set at 0.4 ml/min. The sample manager system temperature was maintained at 4ºC. The mass spectrometer was a Waters Quattro Premier XE triple quadrupole instrument with an ESI source. The entire LC-MS system was controlled by MassLynx 4.1 software. All bile acids were detected in the negative mode. The capillary, extractor, and RF voltages were set at 3 kV, 4 V and 0 V, respectively.

Bile acid stock solutions were diluted with 50% methanol and spiked with 10 µl of IS to construct standard curves between 5 and 50,000 ng/ml. The assignment of target BAs in the UPLC profile was conducted by comparing their retention behavior and molecular mass spectra with the available bile acid reference standards. Quantification was performed via peak area rations (analyte versus IS) by linear-weighted ($1/x^2$) least squares calibration curves within a range of working standard conditions.

Immunohistochemistry and Immunofluorescence

Liver tissue was fixed at 4°C overnight in 4% paraformaldehyde. Tissue for frozen embedding was equilibrated in 30% sucrose, embedded in optimal cutting temperature compound (OCT), and sectioned at 10 µm. Tissue for paraffin embedding was processed by dehydration through alcohol and xylene, followed by paraffin infusion. Paraffin-embedded

tissue was sectioned at 6 μm, de-paraffinized, rehydrated, and subjected to antigen retrieval (antibody specifics in Table 2.1). For both frozen- and paraffin-embedded tissue, sections were incubated with primary antibody overnight at 4°C in 1% bovine serum albumin (BSA) in phosphate buffered saline (PBS) or 1% BSA, 0.2% nonfat dry milk, and 0.3% Triton X-100 (Table 2.1). Sections were then incubated overnight at 4°C in the appropriate secondary antibody in 1% BSA or 1% BSA, 0.2% nonfat dry milk, and 0.3% Triton-X 100 in PBS (Table 2.2). For immunohistochemical analysis, slides were incubated with R.T.U. Vectastain Elite Universal ABC kit for peroxidase or alkaline phosphatase, and developed with the substrate DAB and/or Vector Red. Slides were counterstained with Hematoxylin and Eosin or Mayer's hematoxylin using standard histology techniques (Carson, 1990). For immunofluorescence, slides were incubated in bis-benzamide for DNA identification. Images were acquired using a Zeiss Axioplan2 microscope and QImaging RETIGA EXi camera.

Histology

Identification of sulfated acid and acid mucins was achieved by staining with alcian blue pH 1.0 and 2.5 respective, using standard histological techniques (Carson, 1990). Sirius red staining was achieved by deparaffinization, incubation in sirus red (Newcomer Supply) for 1 hour, followed by two quick washes in acidified water (0.5% glacial acetic acid). Slides were then counterstained with methyl green for 5 min (stock is 5%, use at 0.5% in 0.1M sodium acetate buffer, pH 4.2), and washed in acidified water. Water was completely removed before placing the slides in three changes of 100% ethanol, clearing in xylene and mounting.

Antibody	Company	Species	Concentration	Antigen Retrieval
Pan-cytokeratin	Dako	Rabbit	1:200 (no amp) 1:2000 (amp)	100 mM Tris, pH 10, ON, 60ºC, or Pro K, 5'
Cytokeratin19 (Troma III)	Developmental Studies Hybridoma Bank (DSHB)	Rat	1:100 (no amp) 1:1000 (amp)	100 mM Tris, pH 10, ON, 60ºC, or Pro K, 5', RT
DBA-biotin	Vector	n/a	1:100	Pro K, 5', RT
BrdU	Abcam	Rat	1:400 (amp)	2N HCl, 20', 37ºC, + Boric acid/Borate buffer, 1', RT, + trypsin solution, 3', 37ºC + Pro K, 5', RT
Beta-catenin	Sigma	Rabbit	1:500 (amp)	100 mM Tris, pH 10, ON at 60ºC
Arl13b	From Tamara Kaspary	Rabbit	1:500 (no amp)	Citrate Buffer, microwave, 10'
Apoptag	Chemicon	n/a	n/a	as per manufacturer's instructions

Table 2.1 Primary antibodies. Primary antibodies used within this dissertation and the conditions under which they were used. Pro K – Proteinase K (Dako).

Antibody	Company	Concentration
Anti-rabbit-biotin	Jackson Immunoresearch	1:1000
Anti-rat-biotin	Jackson Immunoresearch	1:1000
Avidin-Cy2	Jackson Immunoresearch	1:300
Avidin-Cy3	Jackson Immunoresearch	1:300
Anti-rat-Cy2	Jackson Immunoresearch	1:300
Anti-rabbit-Cy3	Jackson Immunoresearch	1:300

Table 2.2 Secondary antibodies. Secondary antibodies used within this dissertation and the conditions under which they were used.

ARIOL Analysis

The percent of cytokeratin19-positive area was determined with the ARIOL SL-50 automated image analysis system (Applied Imaging). Cell surface cytokeratin19 staining was processed and classified as positive or negative based on user-trained thresholds that evaluate color and intensity of staining. Three different mice were analyzed from each genotype (control, RBP KO and NICD) per time point. Total cytokeratin19-positive area in fields from hilar or peripheral regions was normalized to total nuclear area for analysis.

Bile Ducts per Portal Vein and Portal Veins per millimeter Calculations

Mice of each genotype (control and RBP KO) were stained with cytokeratin19. A total of nine cross-sections from the left or medial lobe for each mouse were analyzed for independent cytokeratin19-positive luminal structures per portal vein in the periphery. A portal vein is defined as having a bile duct associated. The number of portal veins per millimeter was calculated by dividing the number of portal veins by the total peripheral tissue area as calculated by ImageJ software (Abramoff et al., 2004).

Proliferation Analysis

BrdU (5-bromo-2-deoxyuridine) was injected at 100 mg/kg body weight at 1 hour prior to sacrifice at P15. For proliferation analysis at P30, P60, P90 and P120 BrdU was administered at 1mg/ml in the drinking water for 4 days prior to sacrifice. Tissue sections from at least 2 different mice were examined for the number of BrdU and pan-cytokeratin double-positive cells at the hilum and periphery. At least 200 pan-cytokeratin-positive cells were counted from each region per mouse. The proliferation index was calculated by dividing the number of double-positive cells by the number of pan-cytokeratin-positive cells.

CFDA Dye Injections and Analysis

CFDA (Carboxyfluorescein diacetate succinimidyl ester; Vybrant CFDA SE Cell Tracer Kit, Invitrogen) was reconstituted in 90µl of DMSO (10mM stock solution), as per the manufacturer's instructions. Aliquots were kept at -20ºC and used within two weeks. For injection, 10 µl of the CFDA stock was added to 1 ml of PBS immediately prior to injection. The PBS/CFDA mixture was injected into either the common bile duct or portal vein. After injection, liver was left in the body for 1 hour at room temperature to facilitate dye uptake by cells. Tissue was fixed overnight in 4% paraformaldehyde and paraffin processed as usual.

For both analyses involving CFDA, paraffin sections were stained with cytokeratin19 using a Cy3 secondary. Dual fluorescence was used to determine either the number of portal veins with bile ducts associated for portal vein injections or the number of double-positive bile ducts for bile duct injections. For the portal vein analysis, total dye-labeled vessels were also counted and the data represented as a ratio of portal veins with bile ducts associated to total portal veins.

Resin Casts

Resin Injection

Mice were sacrificed and the common bile duct was isolated and cannulated above the pancreas using stretched polyethylene-10 tubing. Cannulae were secured in the common bile duct by a ligature of 5.0 silk. PBS was manually flushed through the common bile duct to ensure proper cannulation. Liquid Mercox II resin (1ml; Ladd Industries) was mixed with 0.1 g of catalyst. Resin mixture was injected by manual, retrograde perfusion into the common bile duct until resistance was met. At this point, the cannula was removed and the common bile duct was ligated. Liver tissue was then either macerated or fixed for clearing.

Maceration

For maceration, the whole liver was resected from the abdominal cavity and floated in warm tap water for 10-30 minutes to allow the resin to cure. Then individual lobes were separated and placed in 15% potassium hydroxide overnight at room temperature to macerate the tissue. The following day, casts were rinsed with water and allowed to dry.

Clearing

For clearing, the whole liver was resected from the abdominal cavity and floated in 4% paraformaldehyde overnight at 4°C. After fixation, individual lobes were separated and transferred into 50% methanol in PBS for 4-12 hours at room temperature on a rocker. Lobes were then transferred to 100% methanol for an additional 4-12 hours at room temperature on a rocker. After equilibration in 100% methanol, lobes were incubated with a 1:2 benzyl alcohol/benzyl benzoate (BABB) solution overnight at room temperature on a rocker.

Nile Red

Nile red (BioReagent grade, Sigma) was dissolved at 1 mg/ml in acetone to generate a stock solution. Nile red was used at 0.05 mg/ml in resin (50 µl nile red stock + 1 ml resin) for analysis. Resin was mixed with the nile red solution before addition of catalyst to ensure good miscibility.

Imaging

Macerated and cleared resin casts were imaged using a Leica MZ 16 FA stereoscope and QImaging RETIGA 4000R camera. Cleared resin casts were imaged in a solution of BABB to reduce glare. Nile red resin surface images were obtained using an

Axiophot/TE300 and MicroMax CCD camera. Cleared nile red resin cast images were obtained by acquiring a z-stack using a Nikon AZ100 and Nikon DS-QiMC black and white/DS-Ri1 color camera. Nile red fluorescence was visualized under all filters, but imaged under a Green/Red filter.

MicroCT

Scanning

Whole left lobe corrosion casts were scanned by microCT (model μCT40; Scanco Medical AG). Resin casts from control, RBP KO and NICD mice at P60, P90 and P120 were analyzed. Images were acquired with a 20 μm voxel size at 45 kV, 114 μA, 500 projections per 180º rotation, 300 ms integration, and 2X frame averaging to reduce noise. An optimized density threshold and Gaussian noise filter were applied to the 3D stack of images to segment the resin cast from air and generate a 3D reconstruction of the entire IHBD network. Analysis of ductal architecture was performed with the manufacturer's software. The methods used to calculate the structural properties of the IHBD have been used to study analogous properties of trabecular bone (Muller, 2009).

Volume and Thickness Determination

Total resin cast volume was calculated directly from the 3D reconstructions using total segmented voxel volume. Branch thickness was calculated by direct thickness determination, as described previously (Hildebrand and Rüegsegger, 1997). Briefly, a sphere is fitted within each point of the cast reconstruction, the diameter of the sphere is recorded, and the mean of all spheres represents the mean branch thickness. Use of distance ridge calculation allows for inclusion of local neighboring voxels; although this

method does not eliminate redundant points, it ensures that all points are included in the analysis. This calculation has no structural assumption.

Segment Determination

The total number of segments, independent of the total analyzed volume, was calculated using the plate-model of Parfitt (Parfitt et al., 1983) to provide segment number per total analyzed volume ($1/mm^3$). The total number of segments was determined by multiplying the segment number per total analyzed volume by the total cast volume (mm^3).

Main Branches

The determination of resin cast main branch patterning, and diameter of main branches was calculated visually by removing smaller diameter branches from the 3D reconstruction image. Control casts at P60, P90 and P120 were initially examined to determine a branch thickness that consistently incorporated the main branches, and a main branch pattern was defined from these reconstructions. Subsequently, these parameters were applied to RBP KO and NICD casts at P60, P90 and P120.

RNA Preparation and Quantitative RT-PCR

Total RNA was isolated using TRIZOL and a Turbo DNA-Free kit. Total RNA (2.5 µg) was used in complementary DNA synthesis using the SuperScript III First-Strand kit. Quantiative real-time PCR was carried out using the ABI Prism 7900. Liver X receptor (LxR), farnesoid X receptor (FxR), multi-drug resistance-2 (MDR2), multi-drug resistance protein-2 (MRP2), multi-drug resistance protein-3 (MRP3), bile salt export pump (BSEP), Cholesterol 7 alpha-hydroxylase (Cyp7a1) and organic anion transporting polypeptide-1 (OatP1) messenger RNA was measured from three independent samples per genotype run in triplicate. Primer sequences are provided in Table 2.3.

Gene	Forward (5' to 3')	Reverse (5' to 3')
MRP3	GCA GCA GAA CCA AGC ATC AAG	GAC CGA CTC CTC ACC TGG
MDR2	GCA GCG AGA AAC GGA ACA G	GGT TGC TGA TGC TGC CTA GTT
MRP2	GGA TGG TGA CTG TGG GCT GAT	GGC TGT TCT CCC TTC TCA TGG
FxR	CGC TGA GAT GCT GAT GTC TTG	CCA TCA CTG CAC ATC CCA GAT
Cyp7a1	CAG GGA GAT GCT CTG TGT TCA	AGG CAT ACA TCC CTT CCG TGA
LxR	CTG GTG AGC CTC CGT ACT TTG	TCA GTC TGC TCC ACC CGT G
OatP1	CAG TCT TAC GA GTG TGC TCC AGA T	ATG AGG AAT ACT GCC TCT GAA GTG
BSEP	CTG CCA AGG ATG CTA ATG CA	CGA TGG CTA CCC TTT GCT TCT
GAPDH	GAC ACC CAC TCC TCC ACC TTT G	GTC CAC CAC CCT GTT GCT GTA G

Table 2.3 Primers for quantitative RT-PCR. Primers used within this dissertation are described.

Statistical Analysis

Data was subject to either a two-tailed Student's *t*-test or a one-way ANOVA with Dunnett's post-test or Tukey's multiple comparison post-test compared to control mice. A *P*-value of less than 0.05 was considered statistically significant.

CHAPTER III

THE ROLE OF NOTCH SIGNALING IN THE REGULATION OF INTRAHEPATIC BILE DUCT SPECIFICATION AND REMODELING

Introduction

In humans, mutations in the Notch pathway are causative of Alagille syndrome (AGS) (McDaniell et al., 2006; Warthen et al., 2006). AGS is a pleiotropic autosomal dominant disorder that is primarily characterized by neonatal jaundice, cholestasis and paucity of intrahepatic bile ducts (IHBDs). However, the underlying requirement for Notch signaling in liver development and in the adult is not well understood. For example, it remains controversial as to whether Notch regulates changes in cell fate decisions, proliferative status and/or maintenance of biliary structures. It is also not well understood how two-dimensional alterations in bile duct formation correlate to three-dimensional architecture changes.

To analyze the cell-autonomous requirement of Notch signaling in the formation and patterning of the mouse biliary system, I used mouse models that modulate levels of Notch signaling specifically within the hepatoblast. Further, I have adapted a resin casting method that allows visualization of the 3D architecture. With this approach, I have demonstrated a dose-dependent requirement for Notch signaling in the establishment of peripheral branches, suggesting a level of receptor redundancy. Further, constitutive activation of the Notch pathway results in an excess of biliary branches, indicating that Notch is both necessary and sufficient for biliary morphogenesis.

Results

Modulating Notch Signaling within the Hepatoblast Lineage Alters IHBD Development

To define the cell autonomous role of Notch signaling within early hepatoblast cell fate decisions, I used mouse models to modulate levels of Notch signaling within the hepatoblast lineage. Three mouse models were utilized to attain varying degrees of Notch loss: 1. *Alb-Cre;Notch2*$^{flox/flox}$ (N2 KO), 2. *Alb-Cre;Notch1*$^{flox/flox}$ (N1 KO), 3. *Alb-Cre;Notch1*$^{flox/flox}$*;Notch2*$^{flox/flox}$ (N1/N2 DKO), and 4. *Alb-Cre;RBP-J*$^{flox/flox}$ (RBP KO). Notch gain of function was achieved by utilizing *Alb-Cre;ROSA26*^{Notch1} (NICD). To assess the affect each of these models has on bile duct development, liver tissues were examined histologically and immunohistochemically from embryonic day 16 (E16) to post-natal day 30 (P30).

Bile duct development occurs in a temporal fashion beginning at the hilum and progressing to the periphery of liver lobes. In the adult, the columnar epithelium composing hilar ducts has been shown to be functionally distinct from the cuboidal epithelium composing peripheral ducts (Glaser et al., 2009). Therefore, for the purposes of these studies, I distinguish between hilar and peripheral regions (Figure 3.1).

As Notch2 was originally described as the predominant Notch receptor in the liver, both in humans and in mouse models (McCright et al., 2002; McDaniell et al., 2006), I first examined the histology of bile ducts in N2 KO liver sections. Consistent with a concurrent publication (Lozier et al., 2008), I observed that ductal plates are able to form in N2 KO (Figure 3.2). However at P3, the structures are irregular, with cytokeratin-positive cells that are not closely associated with the portal vein (Figure 3.2 D-E). However, by P15, clear differences are observed in peripheral bile ducts. An abundance of un-remodeled,

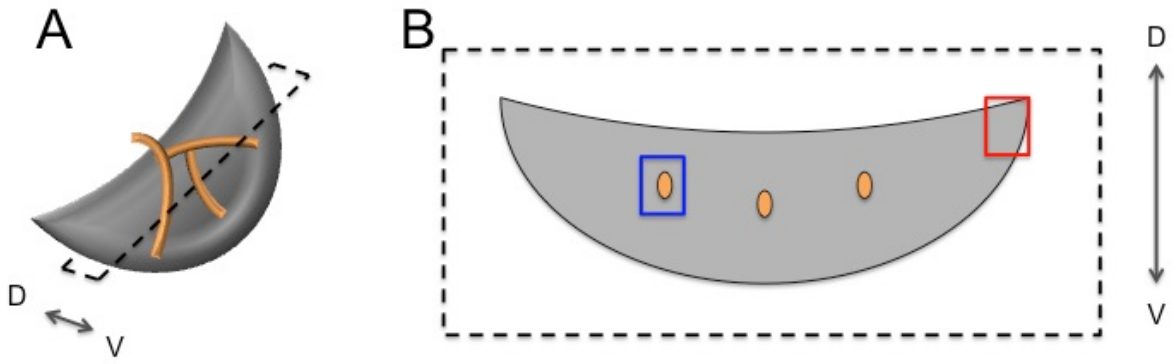

Figure 3.1 Hilum and periphery distinction. This schematic demonstrates how the hilar and peripheral ducts were consistently defined within the tissue section. (A) Left lobe of the mouse liver, with the hilar bile ducts running through (orange). The lobe was cut along the plane indicated by the dotted line for embedding and sectioning. (B) A section through the left lobe reveals the hilar bile ducts within the tissue section. The blue box indicates a hilar duct, and the red box indicates a representative region where peripheral ducts were analyzed. D – dorsal, V- ventral.

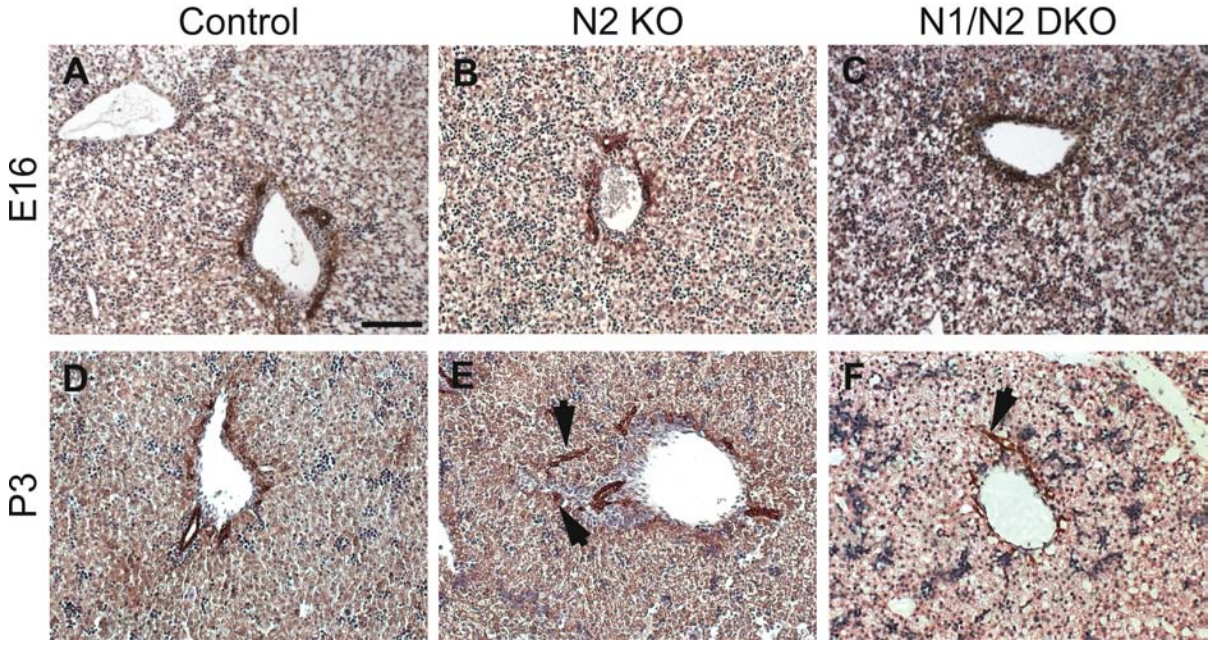

Figure 3.2 Hepatoblast-specific deletion of Notch1 and Notch2 does not disrupt ductal plate formation. Paraffin-embedded sections from control (A,D), N2 KO (B,E) and N1/N2 DKO (C,F) tissue, at E16 and P3 was stained for pan-cytokeratin to mark ductal plate formation and counterstained with hematoxylin and eosin. (A-C) Control, N2 KO and N1/N2 DKO livers have indistinguishable ductal plate formation at E16. (D-F) At P3, the N2 and N1/N2 DKO liver demonstrate normal ductal plate remodeling, with excess ductal plate remnants visible (arrows). Scale bar = 100 μm.

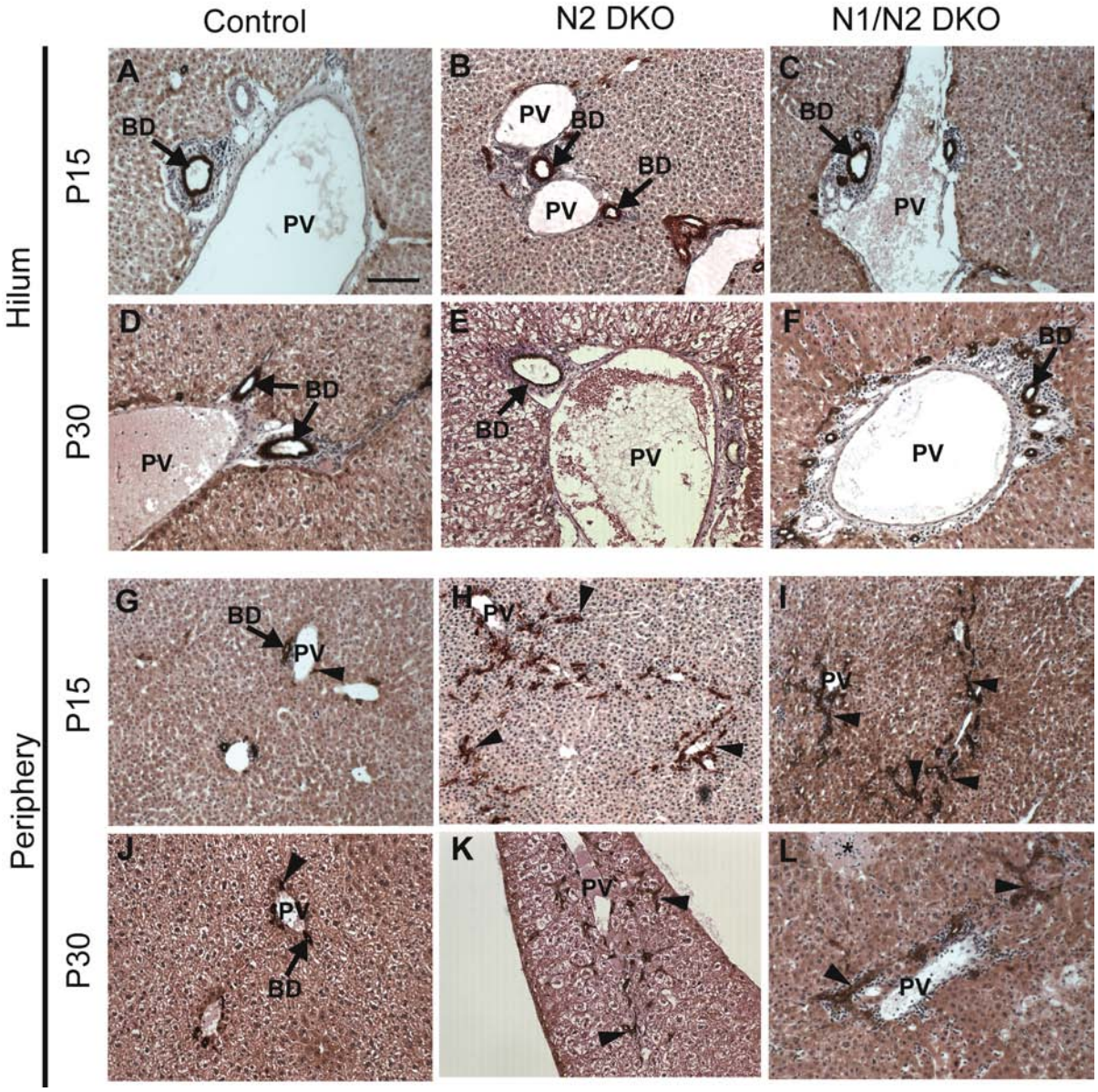

Figure 3.3 Morphologic defects of pan-cytokeratin-positive cells in hilar and peripheral liver tissue with hepatoblast-specific deletion of Notch1 and Notch2. Paraffin-embedded sections from control (A,D,G,J), N2 KO (B,E,H,K) and N1/N2 DKO (C,F,I,L) at P15 and p30 were stained for pan-cytokeratin to mark cholangiocytes and counterstained with hematoxylin and eosin. (A-F) Hilar ducts appear grossly normal in all genotypes at P15 and P30. (G-L) Peripheral bile ducts are un-remodeled in the N2 KO and N1/N2 DKO when compared with control. Un-remodeled cytokeratin-positive cells are observed at P15 and P30. Arrowheads – un-resolved ductal plate remnants. Asterisk – necrosis. PV – portal vein, BD – bile duct. Scale bar = 100 μm.

cytokeratin-positive ductal cells are noted specifically at the periphery (Figure 3.3 H,K). My work and that of others indicates that conditional loss of Notch2 via Alb-Cre deletion, results in failure of bile duct morphogenesis, but did not affect hepatoblast specification as indicated by indistinguishable ductal plate formation at E16 (Figure 3.2 B-C) (Lozier et al., 2008).

Despite the idea that Notch2 is the predominant receptor in liver, evidence that the Notch1 and Notch3 receptors are also expressed in liver, specifically in the bile ducts, has been demonstrated (Table 1.2). As the function of Notch3 is dispensable for life, I investigated the possibility that the Notch1 receptor can compensate in the absence of Notch2. When only the Notch1 receptor is lost within the hepatoblast populations (N1 KO), biliary development is morphologically indistinguishable from control tissue (data communicated by Melanie Brown). In N1/N2 DKO liver tissue, ductal plate formation was morphologically indistinguishable from the N2 KO (Figure 3.2 B-C, E-F). Further N1/N2 DKO liver demonstrated similar un-remodeled, cytokeratin-positive ductal cells at the periphery (Figure 3.2 E-F), which also persist until P30 (Figure 3.3 I,L). In N2 KO and N1N2 DKO livers at P30, there is a wave of hepatic necrosis observed, however the significance of this remains to be understood (Figure 3.4 B and data not shown). In contrast to the observed peripheral defects, analysis of hilar bile ducts revealed normal ductal morphology with mild inflammation (Figure 3.3 F). My work and that of Geisler et al. concluded that bile duct morphology changes N2 KO and N1/N2 DKO were qualitatively indistinguishable from each other in two-dimensional (2D) analysis (Geisler et al., 2008).

At this juncture, my results and those of others suggest that Notch signaling is required for bile duct morphogenesis, but not specification. However, two caveats are noted with this conclusion: The first is that signaling from the Notch3 and/or Notch4 receptor is still possible. The second is that my examination of *Alb-Cre*-mediated gene deletion suggests recombination of floxed alleles is occurring between E14 and E16. Thus deletion is occurring at or after the initial hepatoblast cell fate decision, and therefore these mouse

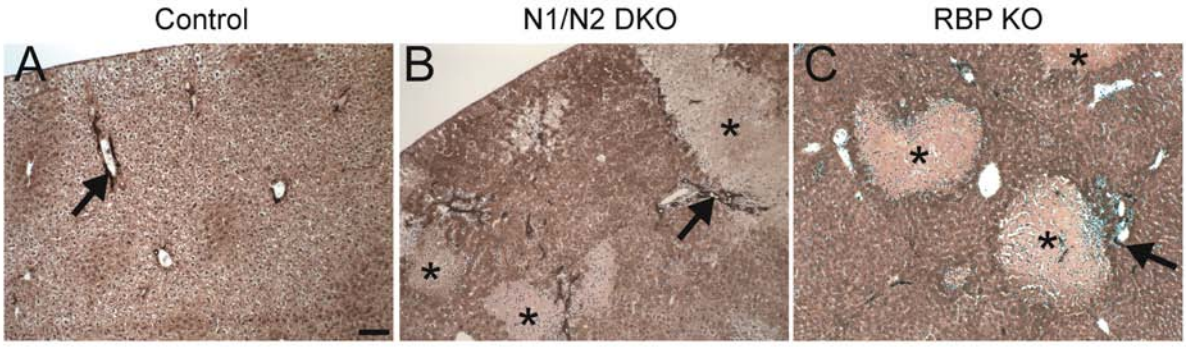

Figure 3.4 Focal regions of necrosis are observed in N1/N2 DKO and RBP KO mice at P30. Paraffin-embedded sections from the left lob of P30 control (A), N1/N2 DKO (B) and RBP KO (C) mice were immunostained with pan-cytokeratin, and counterstained with hematoxylin and eosin. Images were obtained from the periphery as indicated in Figure 3.1. Arrows – pan-cytokeratin-positive cells. Asterisk – necrotic tissue. Scale bar = 100 μm.

models may only be affecting ducts that are formed later in development, i.e. peripheral ducts (Please refer to Appendix A).

To investigate the possibility that the Notch3 and/or Notch4 receptors can compensate in the absence of Notch1 and Notch2, I used a mouse model that deletes RBP-J, the common DNA-binding partner required for all four canonical Notch receptors to signal (RBP KO). In RBP KO peripheral liver tissue, ductal plates are able to form (Figure 3.5B). My observations suggest a reduction in the number of cells specified (Figure 3.5E), which is consistent with the data of Zong et al., using a FoxA3-Cre mediated deletion of RBP (Zong et al., 2009). Surprisingly, the reduction in cells within the ductal plate leads to the formation of patent ductal structures, albeit fewer, without the un-remodeled cytokeratin-positive ductal cells as observed in the N2 KO and N1/N2 DKO (Figure 3.5H,K). At P30, RBP KO livers also exhibit a wave of hepatocyte necrosis (Figure 3.4C), thus suggesting this is a common mechanism in mouse models of hepatobiliary disease. Similar to the N1N2 DKO results, hilar ducts in RBP KO demonstrated normal ductal morphology with mild inflammation (Figure 3.6 H,K). The different peripheral phenotypes between N1N2 DKO and RBP KO suggest a role for the Notch3 and/or Notch4 receptors in the absence of Notch1 and Notch2. To investigate this hypothesis, our laboratory investigated the mRNA expression of all four receptors in the various loss-of-function mouse models at P15. These results confirmed an increase in the Notch3 and Notch4 receptor mRNA in the N1/N2 DKO liver (data courtesy of Kari Huppert, (Sparks et al., 2010)).

Thus loss-of-function studies demonstrate a threshold requirement for Notch signaling in bile duct development. Subsequent to ductal plate establishment, Notch1 and Notch2 are necessary for bile duct morphogenesis, but Notch3 and Notch4 are sufficient to maintain the un-remodeled cytokeratin-positive cells. Further reduction of Notch signaling via loss of RBP-J results in ductal plate defects and fewer cytokeratin-positive cells.

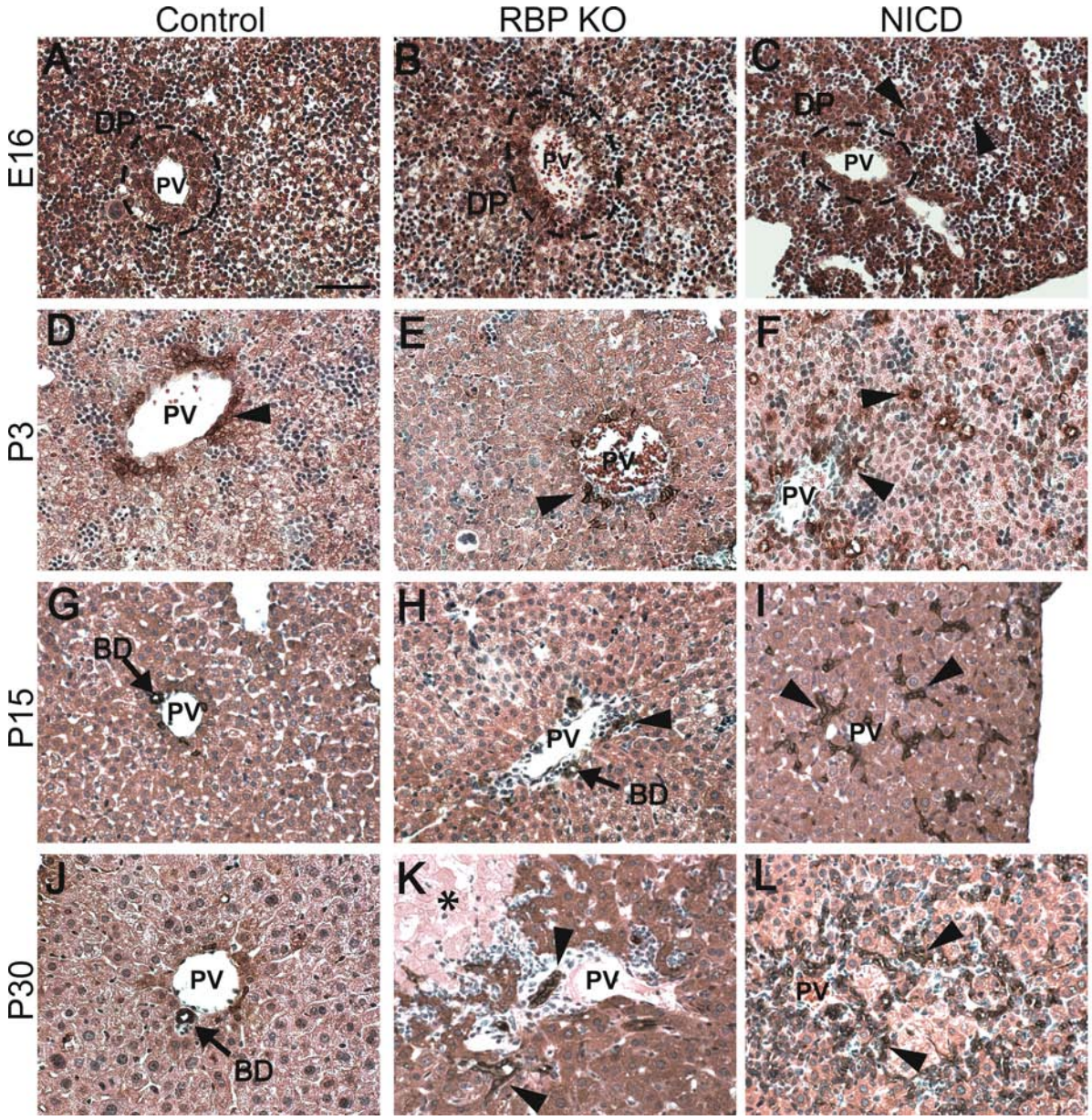

Figure 3.5 Morphological defects in pan-cytokeratin-positive cells in peripheral liver tissue with Hepatoblast-Specific Deletion of RBP-J or Activation of Notch1. Paraffin-embedded sections from control (A,D,G,J), RBP KO (B,E,H,K) and NICD (C,F,I,L) tissue over a developmental time course was immunostained for pan-cytokeratin to mark cholangiocytes and counterstained with hematoxylin and eosin. Images were obtained from the periphery as indicated in Figure 3.1. (A,B) At E16, control and RBP KO liver appear grossly identical with pan-cytokeratin-positive cells contributing to a ductal plate. (D,E) At P3, it becomes difficult to locate pan-cytokeratin-positive bile ducts in RBP KO mice. (G,H,J,K) Fewer bile ducts are observed in RBP KO mice compared to control mice at P15 and P30. (C) At E16, NICD mice appear to have cords of pan-cytokeratin-positive cells radiating from the ductal plate. (F) By P3, these cells have begun to form tubules within the parenchyma. (I,L) The excess pan-cytokeratin-positive cells are maintained at P15 and P30. Arrowheads – ectopic pan-cytokeratin-positive cells. PV – portal vein, DP – ductal plate, BD – bile duct. Scale bar = 100 μm.

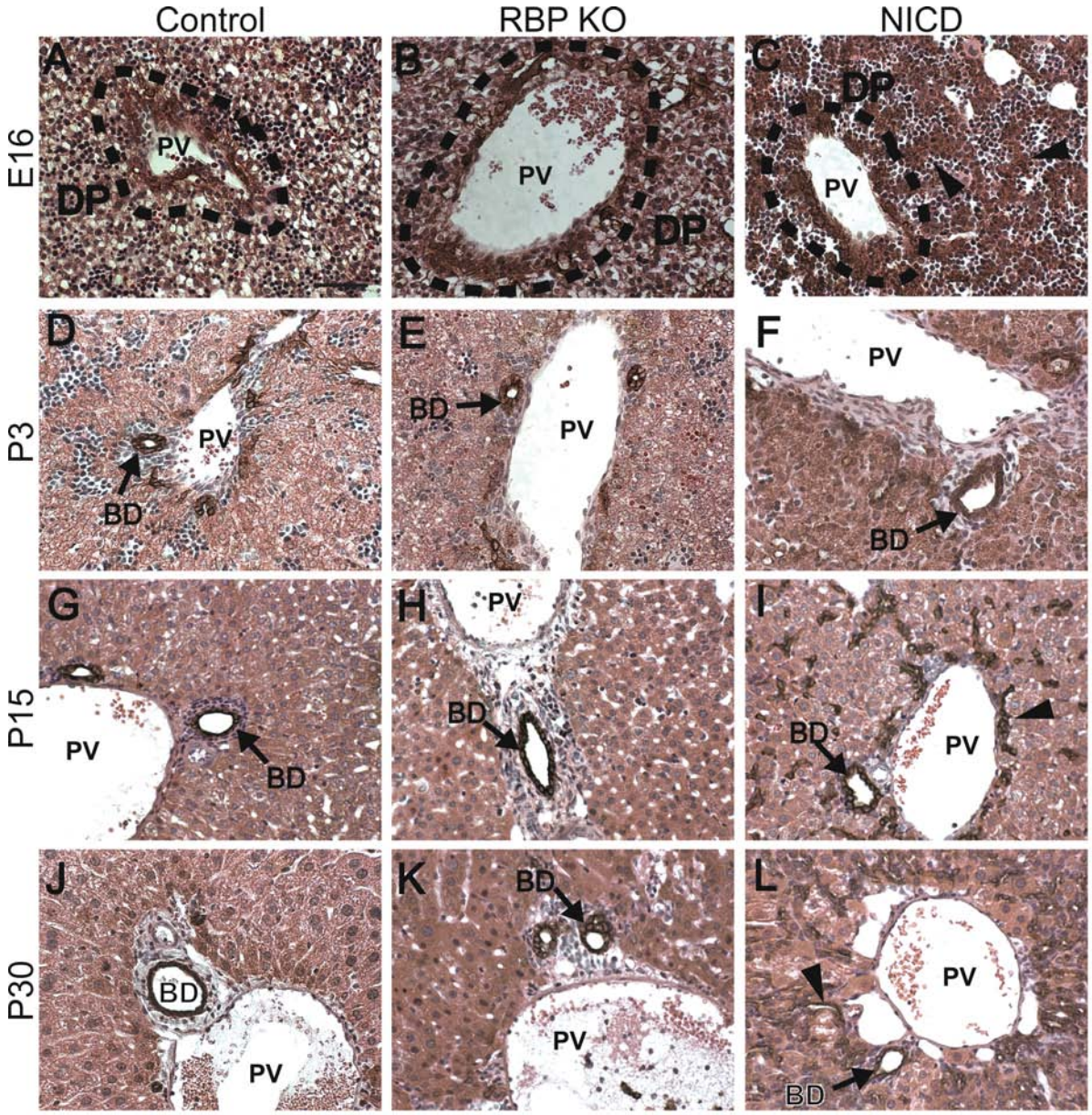

Figure 3.6 Morphological defects in pan-cytokeratin-positive cells in hilar liver tissue with hepatoblast-specific deletion of RBP-J or activation of Notch1. Paraffin-embedded sections from control (A,D,G,J), RBP KO (B,E,H,K) and NICD (C,F,I,L) tissue over a developmental time course was immunostained for pan-cytokeratin to mark cholangiocytes and counterstained with hematoxylin and eosin. Images were obtained from the hilum as indicated in Figure 3.1. (A-F) At E16 and P3, each genotype appears grossly identical, although NICD mice (C,F) have an increase in portal vein associated pan-cytokeratin-positive cells at this time. (I) By P15, an excess of pan-cytokeratin-positive cells is apparent in the parenchyma of NICD mice, which persists at P30 (L). Conversely, in the hilum of RBP KO mice, at P15 (H) and P30 (K), there is mild to moderate inflammation and bile ducts appear tortuous and distorted. Arrowheads – un-resolved ductal plate remnants. PV- portal vein, DP – ductal plate, BD – bile duct. Scale bar = 100 μm.

However, morphological defects are limited to peripheral ducts, therefore suggesting that either gene deletion by Alb-Cre does not affect early hepatoblast decisions and thus hilar development, or Notch is differentially required for the development of peripheral versus hilar ducts. Since I am able to show that *Alb-Cre* has at least been expressed in the majority of hilar ducts (Please refer to Appendix A), I postulate that Notch is differentially required.

To determine if Notch signaling is sufficient to induce cholangiocyte cell fate, I activated Notch signaling within the hepatoblast lineage by constitutive expression of the Notch1 intracellular domain (NICD mouse). In both peripheral and hilar regions, ductal plates form normally, but with extra cytokeratin-positive cells present within the portal veins-associated parenchyma (Figure 3.5-3.6 C,F,I,L, arrowheads). These excess cytokeratin-positive cells persist throughout development and results in an increase in patent bile ducts (Figure 3.5-3.6 C,F,I,L). Therefore, Notch signaling is sufficient although not necessary to promote biliary specification and morphogenesis. Interestingly, Notch1, independent of Notch2, is sufficient to induce cholangiocyte differentiation, further supporting a role of Notch1 in bile duct development.

To understand the long-term consequences of improper bile duct development, and whether the phenotypes could be attributed to a developmental delay, I examined P120 liver tissue. In both the N2 KO and N1/N2 DKO, the peripheral un-remodeled cells, which were present at P15, are maintained within the parenchyma (Figure 3.7 G-H). Further, the RBP KO mice demonstrate fewer bile ducts in the periphery as a consequence of the reduction in cytokeratin-positive cells contributing to the ductal plate (Figure 3.7 I). In the N2 KO, N1/N2 DKO and RBP KO hilar regions patent bile ducts are maintained and morphologically indistinguishable from control (Figure 3.6 A-D, arrows). Additionally, in NICD liver tissues, the excess cytokeratin-positive cells are maintained and appear to be zonal (Figure 3.7 E,J).

An important question remains as to the maturity status of the cholangiocytes in each of the aforementioned mouse models. Unfortunately, there is a deficit of markers to detail

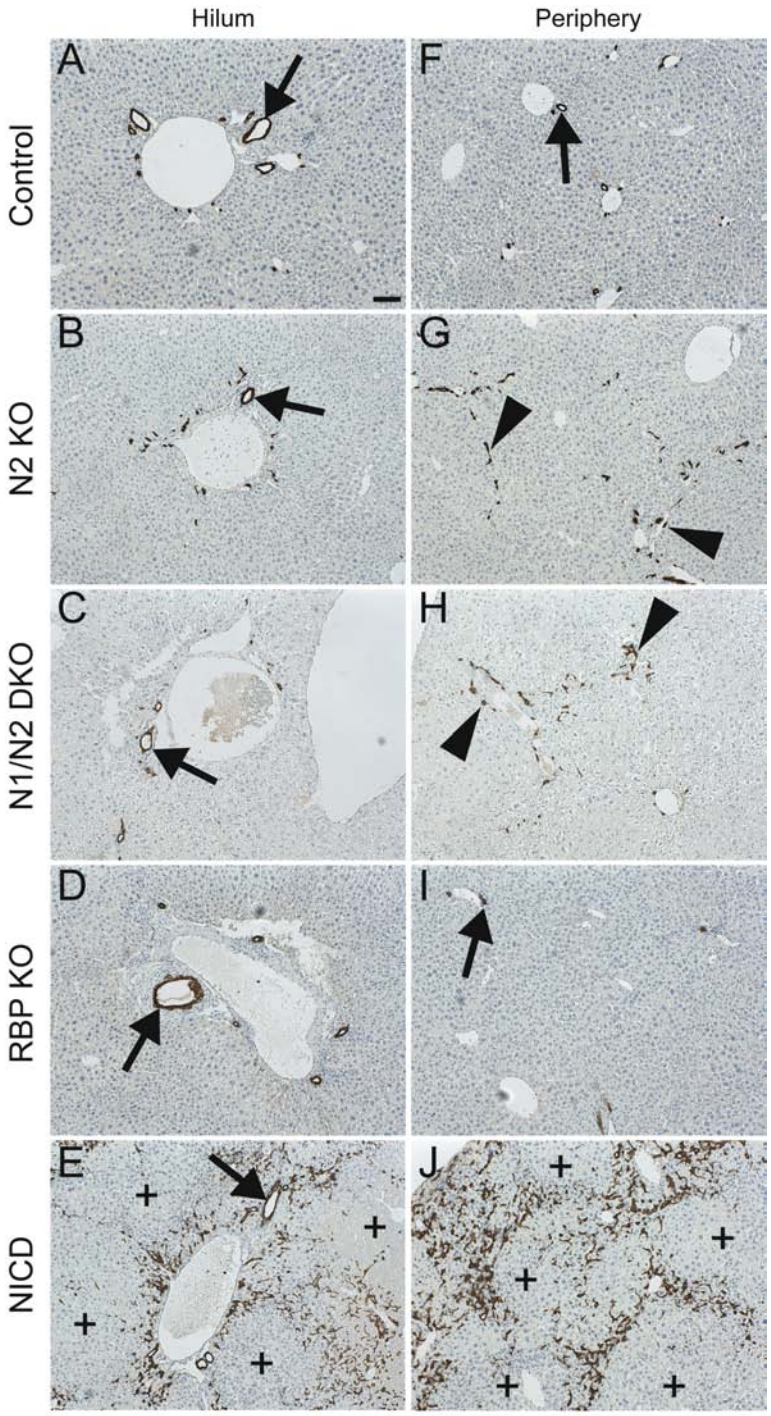

Figure 3.7 Alterations in cytokeratin19-positive cholangiocytes at P120 as a consequence of chronic modulations of Notch signaling. Paraffin-embedded sections from control (A,F), N2 KO (B,G), N1/N2 DKO (C,H), RBP KO (D,I), and NICD (E,J) tissue was immunostained for cytokeratin19 to mark cholangiocytes and counterstained with Mayer's hematoxylin. (A-E) Images obtained at the hilum. (F-J) Images obtained from the periphery. Arrows – bile ducts. Arrowheads – cytokeratin19-positive cells that have not formed patent bile ducts. Plus signs – regions void of cytokeratin19-positive cells. Scale bar = 100 μm.

the lineage restriction of cholangiocytes during development and to mark the heterogeneity of cholangiocytes within a patent bile duct. One marker purported to mark a more mature cholangiocyte, albeit with "patchy distribution", is the lectin *Dolichos biflorus* agglutinin (DBA) (Shiojiri and Nagai, 1992). We were surprised to find that in control mice, the patchy distribution resulted from DBA marking only hilar ducts (Figure 3.8 A,F,A',F'). Thus, DBA expression may not mark more mature ducts, but instead mark hilar ducts, further supporting the differential roles of hilar versus peripheral ducts in normal function. When we analyzed DBA binding in the N2 KO, N1/N2 DKO and RBP KO mice, we found that these genetic manipulations only affected the non-DBA-positive set of peripheral ducts (Figure 3.8 B-D, G-I, B'-D', G'-I'). Further, in NICD mice, we found that all of the excess cytokeratin-positive cells were not DBA-positive (Figure 3.8 E, J, E', J'); therefore suggesting again we are only affecting peripheral cholangiocyte development.

Excess Cytokeratin-Positive Cells are Not Due to Changes in Proliferation

It was previously proposed that the un-remodeled cytokeratin-positive cells observed in the N2 KO and N1/N2 DKO, as well as in AGS patients, are a consequence of bile duct proliferation (Loomes et al., 2007). To investigate this possibility, I analyzed the incorporation of 5-bromo-2-deoxyuridine (BrdU), a thymidine analogue, into newly synthesized DNA. Mice were administered BrdU via the drinking water at P26 and sacrificed at P30 for analysis. In control mice, 15.4% of peripheral cytokeratin-positive cells proliferate over a 4-day period (Figure 3.9, A,F,L; Table 3.1). N2 KO, N1/N2 KO and RBP KO mice demonstrated no significant difference in the amount of hilar or peripheral proliferation at this time, thus suggesting that proliferation does not play a role in the un-remodeled cytokeratin-positive cells (Figure 3.9, B-D,G-I,L; Table 3.1). Proliferation at P15 after a 1-hour pulse of BrdU was assessed, but again no differences were detected (Figure

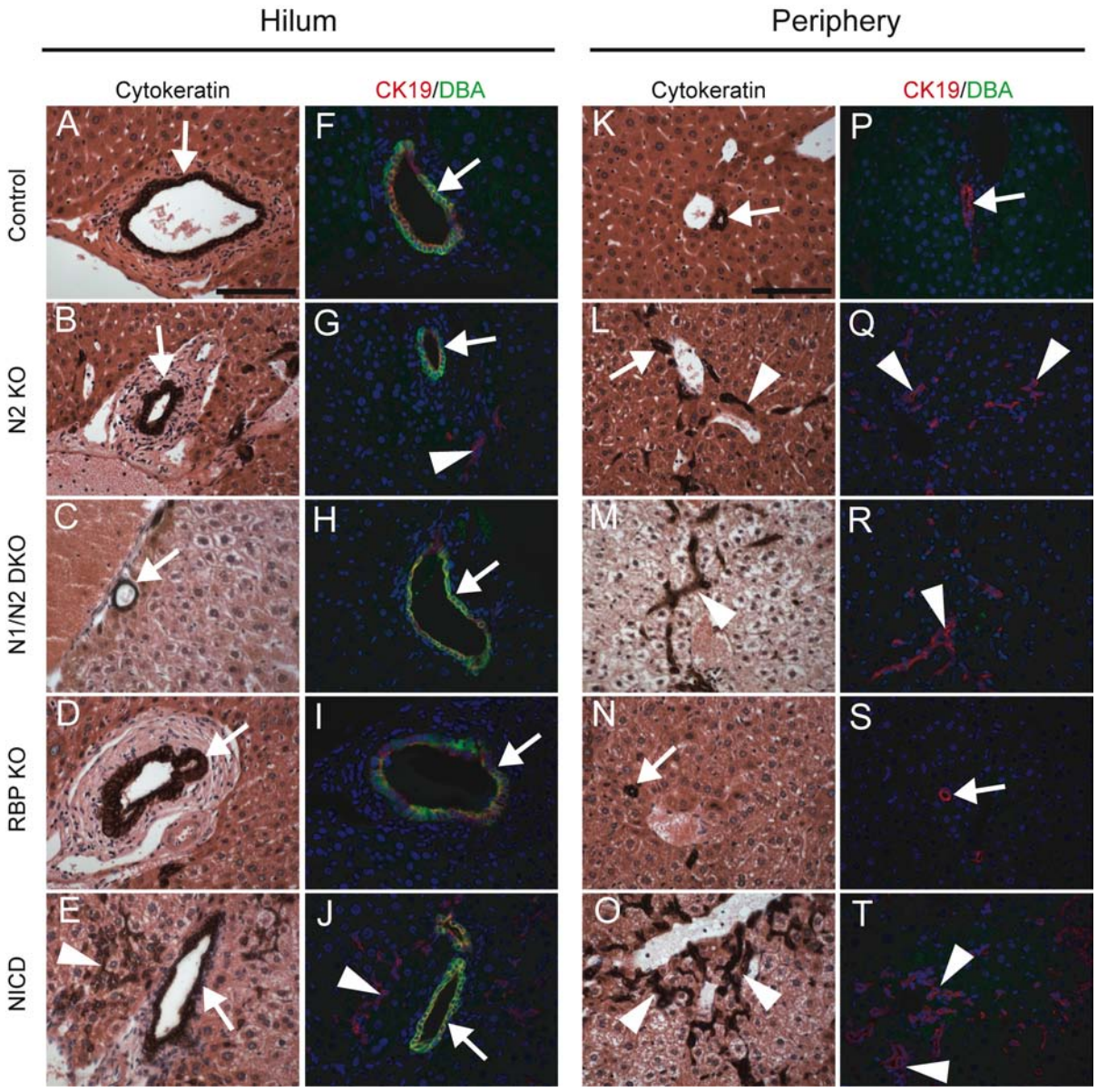

Figure 3.8 Modulations of Notch signaling only affect peripheral, non-DBA-positive, cholangiocytes. Paraffin-embedded sections from P120 control (A,F), N2 KO (B,G), N1/N2 DKO (C,H), RBP KO (D,I) and NICD (E,J) tissue was immunostained for cytokeratin19 to visualize all bile ducts and counterstained with hematoxylin and eosin (A-E). An additional slide was stained for cytokeratin19, the lectin *Dolichos biflorus* agglutinin (DBA), and bis-benzamide to mark DNA (F-J, Cytokeratin19 – red, DBA – green, bis-benzamide - blue). Hilar images (A-J) demonstrate that the majority of cells composing hilar ducts are double positive for DBA and cytokeratin19. All cytokeratin19-positive cells in hilar regions that are not incorporated into a ductal structure are DBA-negative. Peripheral images (A'-J') demonstrate that all peripheral ducts regardless of genotype are cytokeratin19-positive and DBA-negative. Specifically, all excess ductal cells in NICD mice are not DBA-positive. Arrows – bile ducts. Arrowheads –un-remodeled ductal cells. Scale bar = 100 μm.

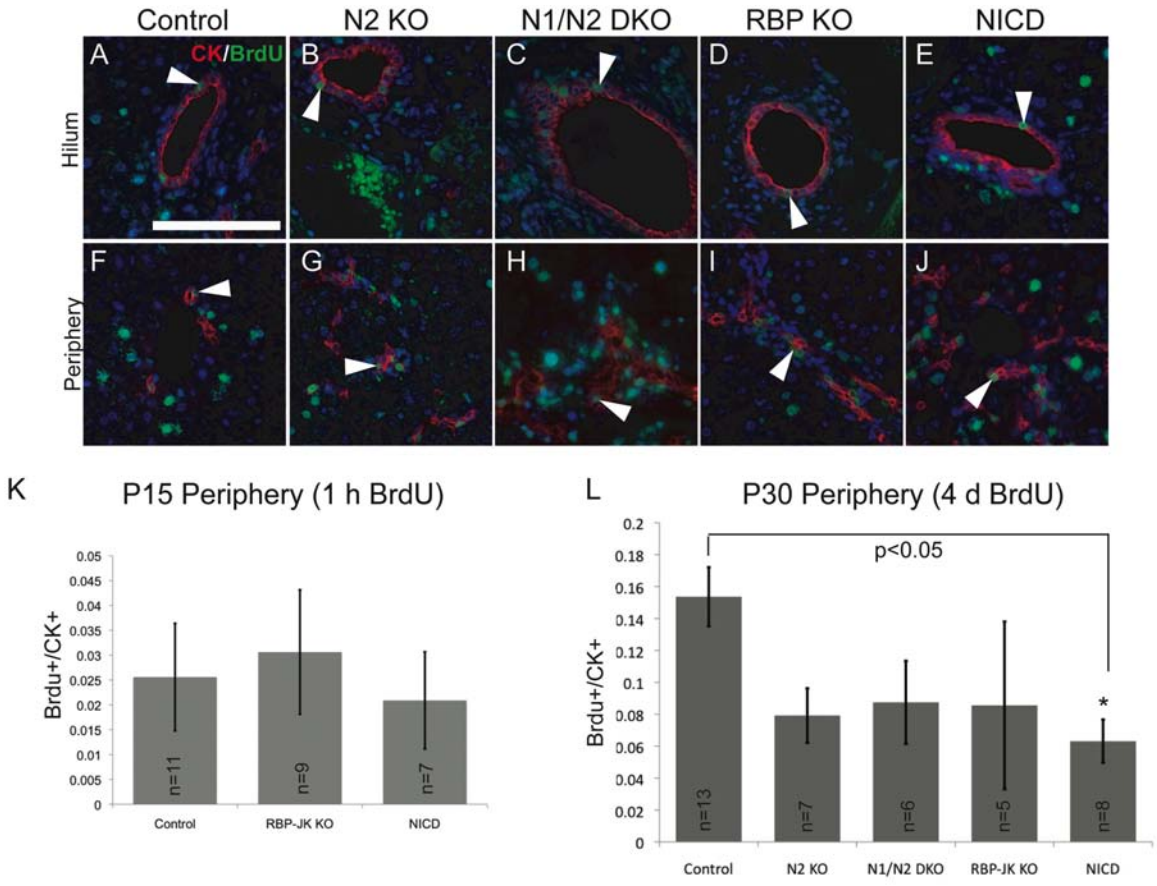

Figure 3.9 BrdU incorporation indicates that modulations in Notch signaling do not affect the proliferation index of cholangiocytes. (A-J) Representative sections from P30 mice labeled for 4 days with BrdU administered via drinking water. Paraffin-embedded sections were stained for pan-cytokeratin to mark cholangiocytes, BrdU to mark DNA replication and bis-benzamide to mark DNA. The pan-cytokeratin-positive cells and double-positive pan-cytokeratin and BrdU cells were counted from regions at the hilum (A-E) and periphery (F-J). (K-L) Ratio of double positive to total pan-cytokeratin-positive cells, absolute numbers in Table 1. (K) Peripheral analysis of P15 mice with 1-hour BrdU pulse. (L) Peripheral analysis of P26 administered BrdU for 4 days and sacrificed at P30. NICD mice have a significantly decreased percent proliferation as compared to control. Percent proliferation was calculated per region analyzed and averaged. Statistical analysis was performed using a one-way ANOVA with Dunnett's post-test. Arrowheads – double positive cells. Error bars – standard error of the mean. *$p \leq 0.05$. Scale bar = 100 μm.

P15 with one hour BrdU pulse

		Hilar			Peripheral			TOTALS	
N	Genotype	Regions analyzed	Total wsCK	%	Regions analyzed	Total wsCK	%	Total wsCK	%
2	Control	7	306	2.1	11	222	2.6	528	2.3
2	RBP KO	4	305	3.1	9	203	3.1	508	3.1
3	NICD	7	677	2.7	7	986	2.1	1663	2.4

P30 with four day BrdU label

		Hilar			Peripheral			TOTALS	
N	Genotype	Regions analyzed	Total wsCK	%	Regions analyzed	Total wsCK	%	Total wsCK	%
2	Control	5	209	6.8	13	296	15.4	505	11.1
2	N2 KO	7	284	17.4	7	305	7.9	589	12.7
2	N1/N2 DKO	4	265	5.7	6	338	8.8	603	7.2
2	RBP KO	5	243	4.7	5	210	8.6	453	6.6
2	NICD	8	356	6.1	8	509	6.3	865	6.3

Table 3.1 Proliferation of pan-cytokeratin-positive cells at P15 and P30. BrdU was either injected 1-hour prior to sacrifice (P15, top) or administered in the drinking water, 4 days prior to sacrifice (P30, bottom). N equals the number of mice analyzed by double-immunofluorescence of paraffin sections for pan-cytokeratin and BrdU. Regions of analysis were as identified in Figure 3.1, and total indicates the combination of hilum and periphery. The number of fields counted at 40x is indicated as “Regions analyzed”. The number of double-positive BrdU/pan-cytokeratin cells was divided by the total number of pan-cytokeratin-positive cells for each region to obtain the percent proliferation. These regional percentages were averaged to obtain a mean proliferation index (%).

3.9, K; Table 3.1). Interestingly, a significant decrease in cytokeratin-positive cell proliferation was observed at P30 in NICD mice (Figure 3.9, E,J,L; Table 3.1). Reduced cholangiocyte proliferation suggests, not only that the excess cytokeratin-positive cells arise due to increased specification, not proliferation, but also that the increased cholangiocytes compensate for the extra ductal mass by being less proliferative.

Notch Signaling Dosage Regulates Three-Dimensional IHBD Architecture

Thus far, histological studies have given insight as to how Notch signaling regulates bile duct specification and remodeling, however it has not allowed interpretation as to what is functionally connected within the 3D architecture of the IHBD. It remains possible that the variable histological phenotypes result in indistinguishable 3D structures, however analysis of liver function suggests this is not the case (Table 3.2). While histological analysis of N2 KO and N1/N2 DKO livers has not allowed me to distinguish a morphological difference, liver function tests suggest that N1/N2 DKO have more severe liver damage. Further, liver function tests in RBP KO mice suggest the most severe damage, consistent with the idea that lack of bile ducts is the most severe phenotype. Conversely, NICD mice have improved, but not statistically significant, liver function. Therefore, I hypothesized that the three-dimensional IHBD architecture would support the severity observed in liver function tests.

To date, three-dimensional imaging of the mouse liver has been limited due to the size and density of the organ. To resolve the three-dimensional architecture of the IHBD, I utilized a method of resin casting via retrograde injection into the common bile duct. Left lobe resin casts from control mice at P120 reveal an intricate branched structure, with fine resolution (Figure 3.10 A). In N2 KO resin casts, there is a minimal loss of peripheral branch density, but the majority of branches have formed (Figure 3.10 B). As predicted, N1 KO

Genotype	n	ALT	n	TB	n	ALP
Control	40	57.5 ± 5.5	37	1.2 ± 0.1	29	8.421±1.197
N2 KO	17	75.1 ± 14.4	15	1.0 ± 0.2	7	21.90±10.55
N1N2 DKO	13	95.5 ± 14.3 *	12	2.2 ± 0.6	6	35.68±14.89
RBP KO	24	123.6 ± 14.4 **	17	2.1 ± 0.9	23	34.90±7.038 **
NICD	27	47.3 ± 3.2	23	0.9 ± 0.1	7	34.09±8.744

Table 3.2 Serum chemistry analysis. Serum was obtained from 2-month old to 4-month old mice of the indicated genotypes and analyzed for alanine aminotransferase (ALT), total bilirubin (TB), and alkaline phosphatase (ALP). Values are mean (IU/L) ± standard error of the mean. P values are calculated by a one-way ANOVA with Dunnett's post-test comparing to control mice. Control values are pooled from littermate controls from all genetic backgrounds. *$p \leq 0.05$, **$p \leq 0.01$.

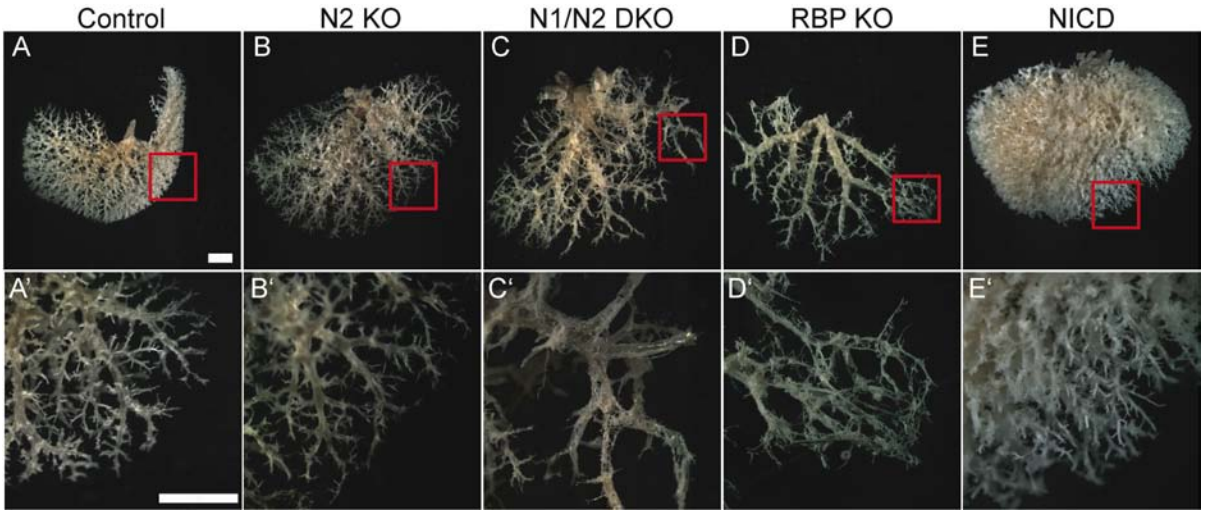

Figure 3.10 Three-dimensional resin casting of the biliary system reveals a role for Notch signaling in determining IHBD density. (A-E) Representative images of the ventral surface of left lobe resin casts are shown with red squares to designate the area in A'-E' at P120. (A,A') Control mice, 10 full casts from four different familial crosses were analyzed. (B,B') N2 KO, six full casts from three different familial crosses were analyzed. (C,C') N1/N2 DKO cats, three full casts from three different familial crosses were analyzed. (D,D') RBP KO, six full casts from three different familial crosses were analyzed. (E,E') NICD, five full casts from four different familial crosses were analyzed. Loss of Notch signaling reveals dose-dependent loss of branch density, whereas activation of Notch signaling reveals an increase in branch density. Scale bar = 2 mm.

resin casts are indistinguishable from control (data communicated by Melanie Brown). However, in N1/N2 DKO resin casts, there is a more dramatic reduction in peripheral branch density (Figure 3.10 C), thus further confirming that the N1/N2 DKO is a more severe phenotype than N2 KO alone. The most severe of all is the RBP KO resin cast, which displays the greatest paucity of peripheral branches (Figure 3.10 D). Conversely, activation of Notch signaling results in an excess of formed branches (Figure 3.10 E).

Discussion

There is a threshold requirement for Notch signaling at multiple stages during IHBD development

Modulating the levels of Notch deficiency within the hepatoblast leads to a variety of histological phenotypes. Specifically, loss of the Notch2 receptor (N2 KO) or the Notch1 and Notch2 receptors (N1/N2 DKO) results in un-remodeled cytokeratin-positive cells at the periphery (Figure 3.3), which are maintained until P120 (Figure 3.7). These cells could be due to a failure of ductal plate regression, or a proliferation of cholangiocytes, both options resulting in too many cholangiocytes, which are not incorporated into a duct. Investigation of the proliferation index in N2 KO and N1/N2 DKO cholangiocytes demonstrate no change from control at the hilum or periphery (Figure 3.9, Table 3.1). Thus my results suggest that the un-remodeled cytokeratin-positive cells can either not receive cues to regress or are unable to remodel into ductal structures. Further reduction of Notch activity via loss of RBP (RPB KO) result in fewer cells contributing to the ductal plate, (Figure 3.5) which results in a post-natal reduction in the number of bile ducts formed (Figure 3.7). Taken together, these results suggest that Notch activity is required at different levels for the specification of cholangiocytes and IHBD remodeling.

On the contrary, the constitutive activation of Notch signaling (NICD) results in an excess number of specified cholangiocytes (Figure 3.5), which remodel and are continuous with the ductal system (Figure 3.10). Surprisingly, the constitutive activation of Notch1, as demonstrated here, is able to maintain an excess of ductal cells until P120 (Figure 3.7), whereas a separate study, which constitutively activated Notch2 within the hepatoblasts demonstrated that Notch2 promotes ductal morphogenesis, but is not sufficient to maintain ductal structures outside the immediate portal environment (Tchorz et al., 2009). Thus we

suggest that while Notch1 maybe dispensable for normal biliary development, it may be critical to maintain tubular structures post-natally.

Notch signaling affects peripheral, but not hilar duct development

In this study, I was careful to define hilar and peripheral duct development and architecture (Figure 3.1) due to functional differences previously described (Glaser et al., 2009). My results demonstrate that modulations in Notch signaling only affect the peripheral ducts. The differential affects could be due to either different mechanisms that determine the formation of hilar or peripheral branches, or it may be due to the timing of Alb-Cre mediated recombination. Although I can demonstrate that Alb-Cre is expressed within the hepatoblasts using Rosa26 reporter expression as a readout, that DNA recombination of the Notch1 and Notch2 loci is equivalent in laser captured hilar and peripheral ducts, and that DNA recombination of the RBP locus is occurring as early as E14, I cannot speak to the latency of protein function and/or mRNA expression (Please refer to Appendix A). Therefore, it remains a possibility that hilar ducts, which develop first, are losing Notch expression after the initial requirement for hepatoblast specification and cholangiocyte remodeling. To date, the earliest published deletion of Notch signaling via FoxA3-Cre results in a quantitative reduction of bile ducts, but not complete absence (Zong et al., 2009). Therefore, with currently available mouse models, hilar bile ducts are able to form in the absence of Notch signaling. In support of different developmental mechanisms, I can demonstrate that activation of Notch signaling only increases peripheral, non-DBA-reacting, cholangiocytes (Figure 3.8). While loss-of-function studies depend on the half-life of mRNA and protein, gain-of-function studies can be correlated more directly with timing of locus recombination.

Notch signaling acts permissively within the hepatoblast population for cholangiocyte specification

Previous studies, in cultured hepatoblasts, have demonstrated that expression of the N1 intracellular domain (NICD) is sufficient to repress hepatocyte cell fate. Further, that NICD expression in hepatoblasts cultured in Martigel is able to induce the expression of cholangiocyte markers (Tanimizu and Miyajima, 2004). This *in vitro* data suggests that Notch is acting permissively, and additional factors are required to induce cholangiocyte cell fate. My data investigating the constitutive activation of the Notch pathway reveals that Notch promotes cholangiocyte differentiation, as observed by the excess cytokeratin-positive cells. However, these excess cells are zonal as early as P3 (Figure 3.5) and this zonation becomes more obvious at P120 (Figure 3.7). As not all hepatoblasts are fated to become cholangiocytes, I propose that Notch acts permissively *in vivo* to maintain a competence zone of hepatoblasts with the potential to respond to instructive cues to become cholangiocytes.

Notch signaling regulates the formation of peripheral branches

In this work, I've described a resin casting technique, which allows visualization of the intact 3D IHBD architecture (Figure 3.10). By reducing the amount of Notch signaling, I observe a progressive loss of peripheral branch density. While my results do not dispute that Notch2 is the predominant receptor in the liver, the resin casts highlight a previously unappreciated role for Notch1 in the absence of Notch2. Further, RBP KO resin casts demonstrate the most severe paucity of branches, and NICD resin casts show an excess of branches. Consistent with these results, AGS patient biopsies demonstrate peripheral defects with normal hilar regions (Libbrecht et al., 2005), thus further supporting that Notch signaling is differentially required for hilar and peripheral bile duct development.

Notch signaling modulations provide mouse models of cholestatic liver disease

The hallmark of cholestatic liver disease is an elevated alkaline phosphate (ALP) level in the serum. In this chapter, the mouse models with deficient Notch signaling (N2 KO, N1/N2 DKO and RBP KO) all have significantly elevated ALP levels as compared to control (Table 3.2). Surprisingly, the gain-of-function Notch signaling mutant, NICD also had significantly elevated ALP levels as compared to control (Table 3.2). Thus while alanine aminotransferase (ALT) and total bilirubin (TB) levels in NICD mice are lower than control, suggesting that these mice do not have damaged hepatocytes or hepatocyte function. An experimental model of cholestasis, which induces cholangiocyte proliferation, is administration of the compound α-Naphthylisothiocyanate (ANIT). ANIT is used to produce a distinctive form of cholestasis and of acute and chronic bile duct injury (Zimmerman, 1999). ANIT has been shown to induce cholangiocyte proliferation and increase the number of connected ducts in rat models (Masyuk et al., 2001). Thus morphologically, ANIT cholestasis resembles the phenotype in the genetic NICD manipulations. However, ANIT does not specifically damage cholangiocytes; ANIT treated animals have an increase in ALP as well as ALT and TB (Zimmerman, 1999). Thus in this chapter, I have described a unique model of cholestasis in NICD mice, as defined by elevated ALP levels, but without hepatocyte damage and general liver dysfunction.

CHAPTER IV

NOTCH SIGNALING IS REQUIRED TO MAINTAIN INTRAHEPATIC BILE DUCT COMMUNICATION IN ADULT MICE

Introduction

Alagille syndrome (AGS) is characterized primarily by a paucity of intrahepatic bile ducts (IHBDs). However, whether paucity of IHBDs is due to a developmental defect in bile duct morphogenesis, a lack of post-natal branching and elongation or an inability to maintain formed ducts remains unclear (Perrault, 1981; Hadchouel, 1992; Libbrecht et al., 2005). Interestingly, AGS patients have progressive paucity upon serial biopsy (Dahms et al., 1982), suggesting that, in addition to the developmental requirement of Notch signaling (Please refer to Chapter III), there maybe an additional requirement for Notch signaling in the post-natal maintenance of ductal structures.

To investigate the requirement of Notch signaling in bile duct maintenance, I used chronic alterations to reflect the changes in AGS patients, in which normal protein function is absent during development and in the adult. Activation of Notch signaling, via hepatoblast-specific expression of the Notch1 intracellular domain (NICD), and loss of Notch signaling, via hepatoblast-specific loss of RBP-J (RBP KO), were used to assess post-natal alterations of the IHBDs. To analyze IHBD changes, I have once again undertaken resin casting to resolve the global 3D architecture of the mouse IHBD systems. In this chapter, I have used resin casting in conjunction with microtomography (microCT) analysis to address the hypothesis that Notch signaling is required for the post-natal maintenance of intact IHBD structure.

IHBD resin casts were examined at P60, P90 and P120 in NICD and RBP KO mice. NICD resin casts demonstrate increased peripheral branches that were maintained with

age, however these data do not achieve statistical significance most likely due to the resolution limit of the microCT. Conversely, RBP KO resin casts resulted in an age-dependent loss of intact peripheral branches. Surprisingly, in 2D histological section, there were an initially reduced number of bile ducts per portal vein (BD/PV) and portal veins per millimeter (PV/mm), but no further reduction was observed at P120. Thus, chronic loss of Notch signaling in these mouse models does not mimic the 2D progressive paucity observed in AGS patients. Instead, I've defined a model that exhibits an acquired, post-natal disruption of the intact communicating IHBD system. I postulate that this model maybe used to understand a subset of AGS patients who fail biliary excretion tests, suggesting an obstruction. To my knowledge, this subset of patients has not been studied or well understood.

Results

Peripheral resin cast branches are modulated with age

To visualize the macro-structural effect of gain or loss of Notch signing on 3D IHBD architecture, resin casts were obtained from control, RBP KO and NICD mice at P60, P90 and P120 (Figure 4.1). Prior to P60, control mice are still rapidly growing (P30-P60 slope=8.43 vs. P60-P120 slope=3.98; Figure 4.2); therefore, I selected time points that allowed me to specifically assay the maintenance subsequent to the post-natal branching and elongation period. Stereoscopic images of left lobe resin casts from control mice showed no noticeable changes with age (Figure 4.1 A-C), whereas casts from RBP KO mice appeared to lose peripheral IHBDs (Figure 4.1 D-F). Conversely, casts from NICD mice have increased peripheral branches early in development, which are maintained with age (Figure 4.1 G-I).

To quantify changes in the structure of the IHBD system, I quantified the volume, thickness and number of branches in left lobe resin casts using microCT analysis. A representative reconstruction of a microCT scanned control resin cast is depicted in Figure 4.3 to demonstrate the level of resolution obtained by this approach (Figure 4.3A). Analysis of microCT scans was achieved by adapting trabecular bone analysis software from Scanco (Perrien et al., 2007). Left lobe casts of control, RBP KO and NICD mice were microCT scanned and analyzed at P60 (n=4, 5 and 3, respectively), P90 (n=4, 6 and 3, respectively) and P120 (n=4, 4 and 3, respectively). The same casts were analyzed throughout this chapter. As expected, based on growth curve analysis (Figure 4.2), the total volume of control IHBD casts did not change significantly with age (Figure 4.3B). However, the total volume of IHBD casts from RBP KO mice was reduced at P120, as compared to age-matched control mice ($P \leq 0.01$) and P60 RBP KO mice ($P \leq 0.05$) (Figure 4.3B). Conversely,

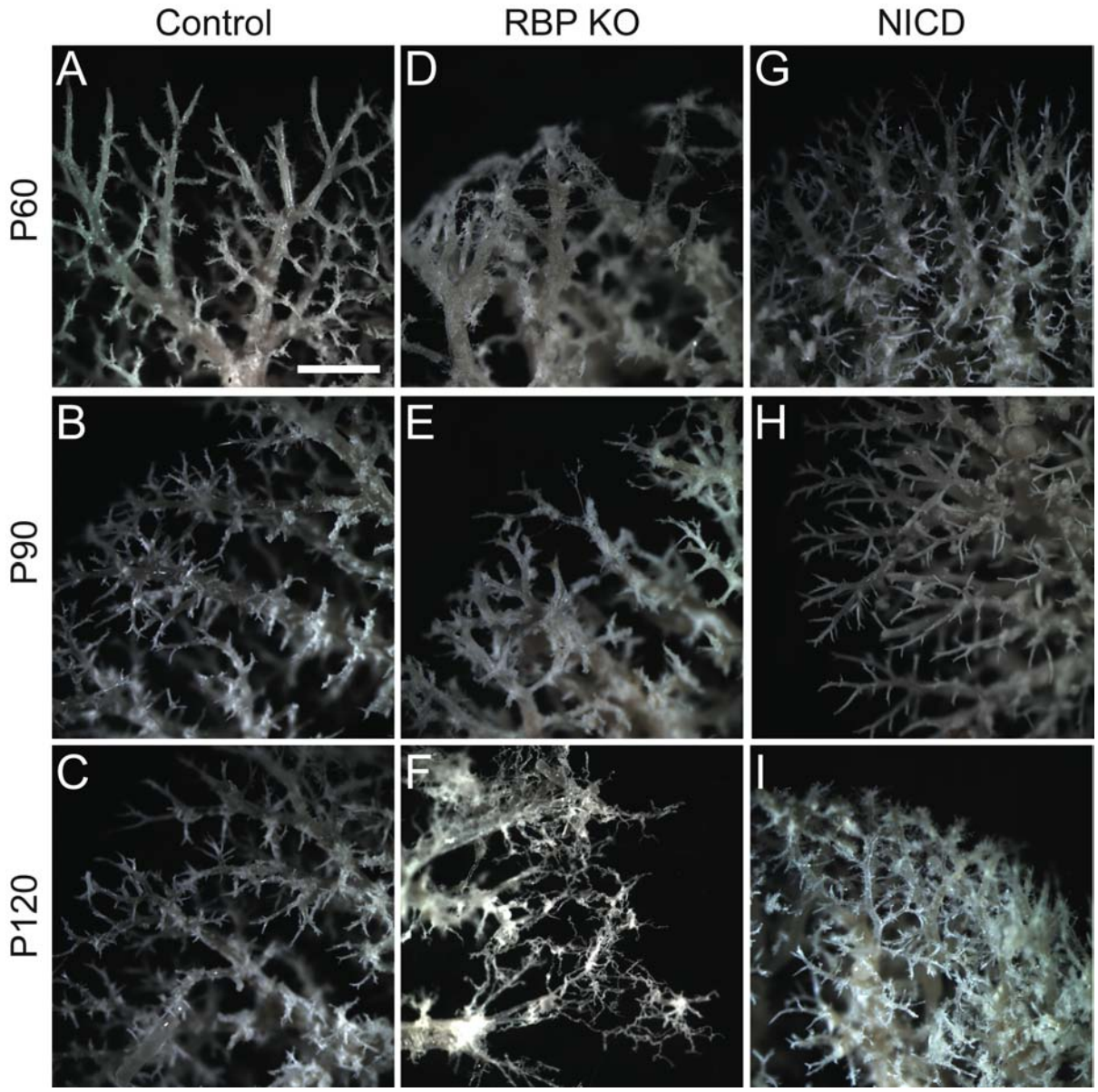

Figure 4.1 Resin casts of adult mice reveal IHBD changes upon altered Notch signaling. Resin casting was performed by manual, retrograde injection of a modified acrylic into the common bile duct, followed by tissue maceration. (A-F) Representative stereoscopic images of the peripheral branches of left lobe resin casts. Casts from control (A,B), RBP KO (C,D) and NICD (E,F) mice were obtained at P60 and P120. RBP KO IHBD casts were unable to maintain intact IHBD structure with age, whereas NICD IHBD casts maintain an excess of branches. Scale bar = 2 mm.

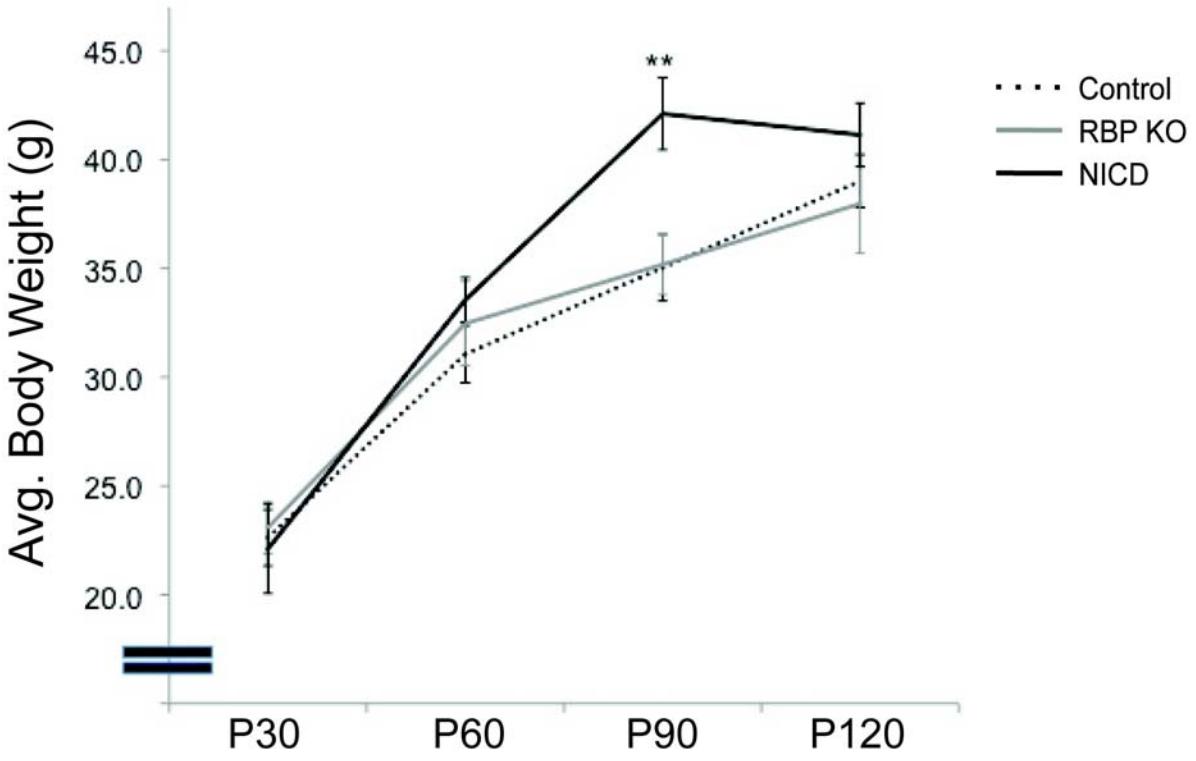

Figure 4.2 Alterations in Notch signaling do not affect body weight or growth. Average body weight from P30, P60, P90 and P120 control (n=18, 15, 15 and 15, respectively), RBP KO (n=6, 16, 10 and 15, respectively) and NICD (n=6, 9, 7 and 11, respectively). Average body weight for control and RBP KO mice continually increases with age, but is not significantly different. NICD mice demonstrate an increased body weight in line with control mice until P90 when there is a significant increase as compared to control mice. The reason for this increase is not understood. Error bars – standard error of the mean. **$p \leq 0.01$.

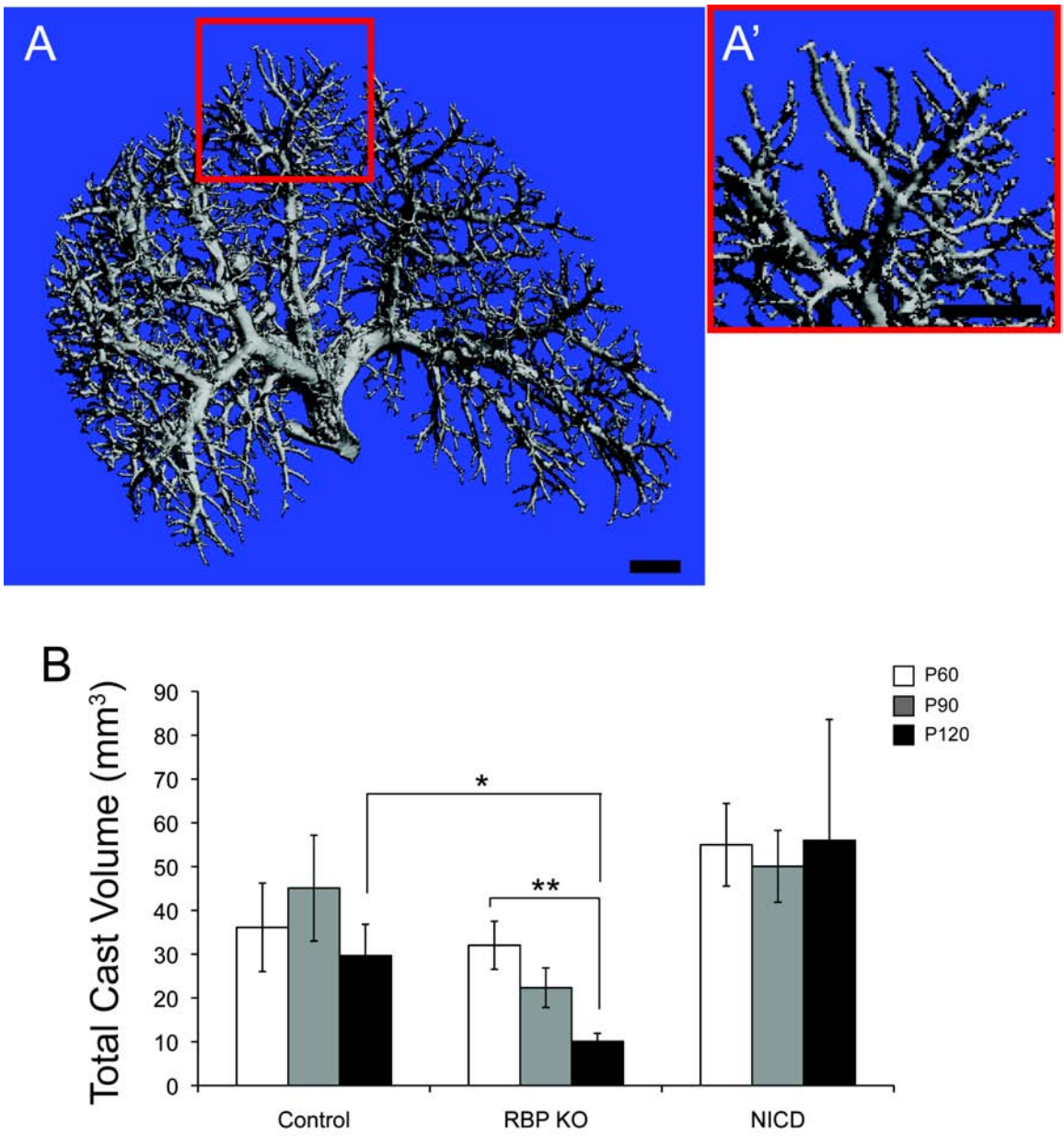

Figure 4.3 MicroCT analysis reveals that IHBD average volume is modulated with age upon deletion of RBP-J or activation of Notch1. Reconstruction of microCT scans provides a high-resolution global representation of resin casts. (A) Representative image from Scanco microCT 40 scanning of P120 control IHBD resin cast at 20 μm resolution. Red square demonstrates are in A'. (B) Total IHBD cast volume was calculated using software adapted from trabecular bone analysis. At P60, RBPK O cast volume is equivalent to control, however as age increases, the volume decreases when compared with control IHBD casts. This decrease is statistically significant at P120. The trend in NICD IHBD casts shows an increase in cast volume. For each genotype (control, RBP KO, NICD), casts at P60 (*n*=4, 5 and 3, respectively), P90 (*n*=4, 6 and 3, respectively) and P120 (*n*=4, 4 and 3, respectively) were scanned. Error bars – standard error of the mean. *$p \leq 0.05$, **$p \leq 0.01$. Scale bars = 1 mm.

NICD IHBD casts showed a consistent, but not significant, increase in cast volume with age compared with control (Figure 4.3B).

To further define the structural changes that are visually apparent in the resin casts, I calculated the distribution of branch thickness throughout the IHBD casts (Figures 4.4-4.6). Owing to variations in maximum thickness resulting from the imprecise method of individual lobe separation (i.e. separated manually), the analysis included only diameters less than 520 um, which consistently incorporates the main branches regardless of genotype. Small branches, as defined by a diameter of <15 um (Glaser et al., 2009), are not resolved by this method due to detection limitations imposed by cast size; however, I define intermediate (20-220 um) and main (240-520 um) branches for the purpose of this analysis. As demonstrated in Figure 4.4 C-E, branches with a diameter between 240 and 520 um highlight main branches, whereas branches with a diameter between 20 and 220 um compose intermediate branches. Control IHBD resin casts demonstrate a high frequency of intermediate branches, and this frequency changes very little with age (Figure 4.4 A). By contrast, RBP KO casts showed a significant decrease in intermediate branch frequency at P120 compared with control and RBP KO casts at P60 and P90 (Figure 4.4 A). Intermediate branch diameter frequency in NICD IHBD casts did not significantly change with age (Figure 4.4 A).

For all genotypes, the frequency of branches with a diameter of 240-520 um (main branches) was reduced compared with the frequency of intermediate branches (Figure 4.4 A-B). Main branch frequency remained consistent in control and NICD IHBD casts with age, but was reduced in RBP KO IHBD casts at P90 and P120 compared with control ($P \leq 0.05$ and $P \leq 0.01$, respectively), and at P120 compared with P60 RBP KO ($P \leq 0.001$) (Figure 4.4 B). Further dissection of the frequency of individual diameters revealed that 80 to 100 um diameters were the most frequent regardless of genotype or age (Figures 4.5-4.6 A-C). To visualize the relative contribution of each intermediate diameter branch to the total casts,

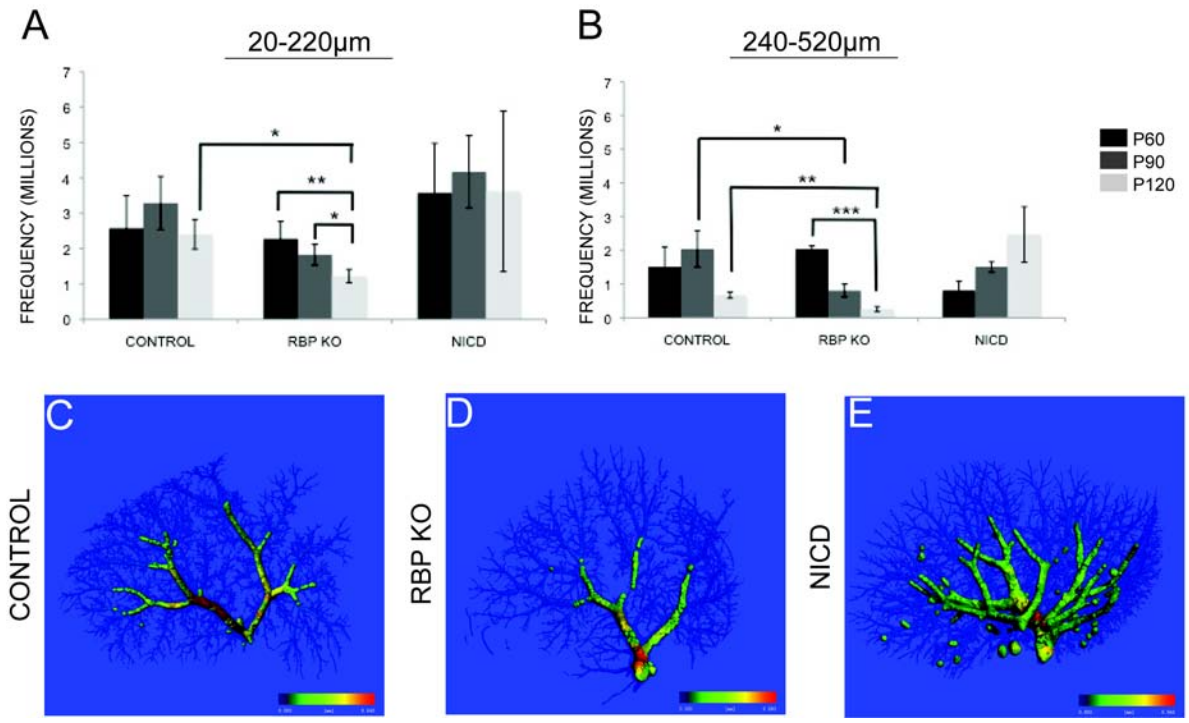

Figure 4.4 Alterations in Notch signaling affect the frequency of intermediate and main IHBD branches. (A,B) The frequency of intermediate branches (20-20 µm;A) and main branches (240-520µm;B) for each genotype are shown. The frequency of a diameter was 'counted' using the direct thickness determination model and summed for the indicated diameter range. (A) Control IHBD casts show a consistent frequency of intermediate branches with age. RBP KO IHBD casts demonstrate a significant reduction in intermediate branch frequency at P120 compared with control. Additionally, RBP KO cast demonstrate a progressive reduction in the frequency of intermediate branches within the genotype. NICD IHBD casts do not significantly change with this analysis. (B) Main branch frequency does not change significantly with age in control or NICD IHBD casts. However, there is a significant reduction in main branch frequency in RBP KO IHBD casts at P90 and P120 compared with control. (C-E) A representative scan from control (C), RBP KO (D) and NICD (E) IHBD casts, with branch thicknesses from 240 µm to 520 µm highlighted. I have defined this thickness range as sufficient to incorporate all main branches. Colored bars indicate heat map thickness range; blue = 20 µm to red = 520 µm. Error bars – standard error of the mean. *$p \leq 0.05$, **$p \leq 0.01$, ***$p \leq 0.001$.

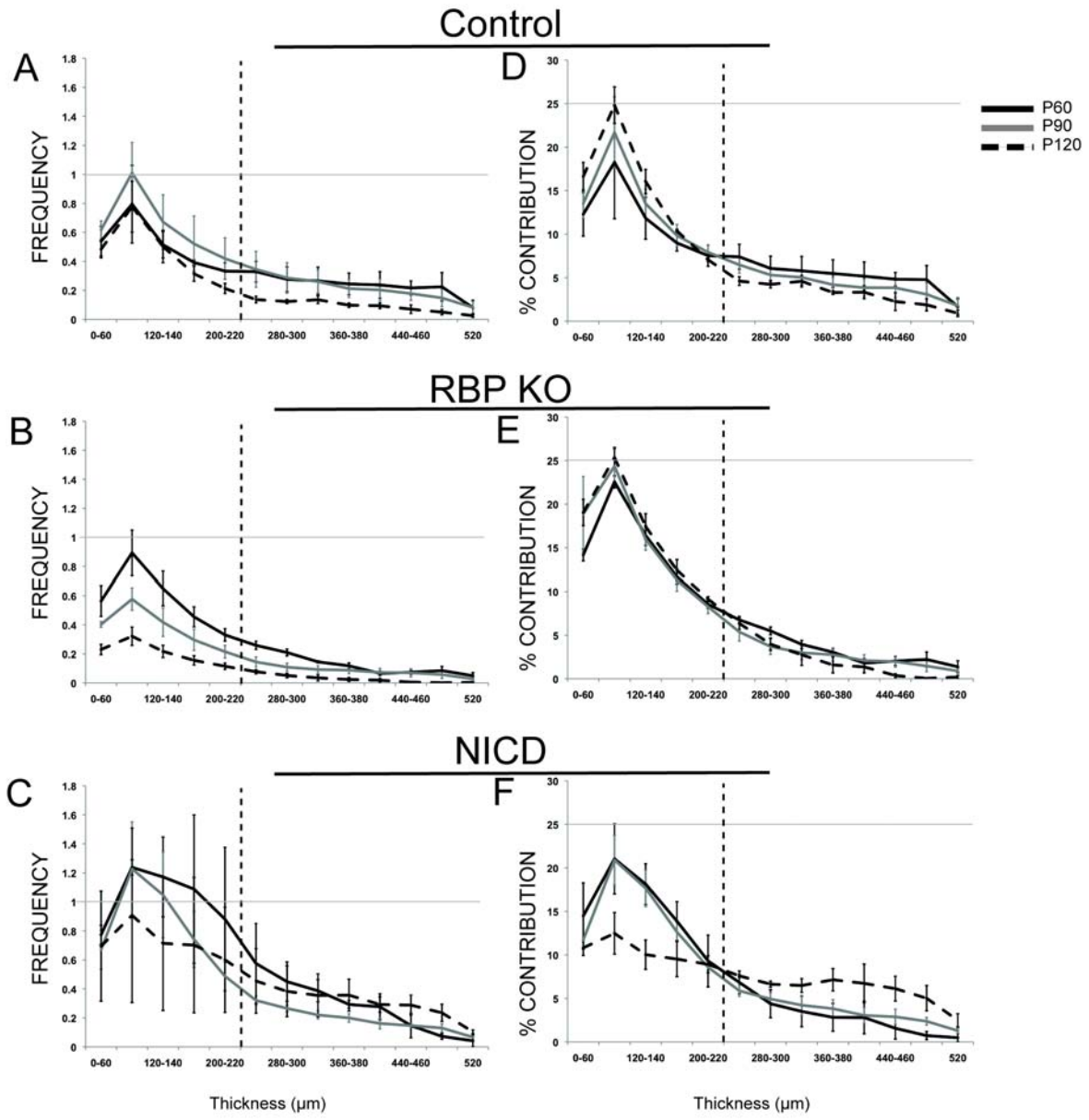

Figure 4.5 Notch signaling affects the frequency of different branch diameters in proportion to the original contribution. Individual diameter frequencies (A-C) represented as a percent contribution to the total structure (D-F). (A,D) In control IHBD casts, 80-100 µm branch diameters represent the greatest frequency and percent contribution. (B,E) RBP KO IHBD casts show decreased frequency of all diameters with age, but the percent contribution per branch diameter remains consistent with age. Therefore, all intermediate branches are lost in proportion to their original contribution. (C,F) NICD IHBD casts demonstrate consistent contribution of branch diameters at P60 and P90, however, at P120 there is a shift towards the main branch contribution. Vertical dotted lines represent division between intermediate and main branches. Horizontal grey line represents 1 million (A-C) and 25% (D-F). Error bars – standard error of the mean.

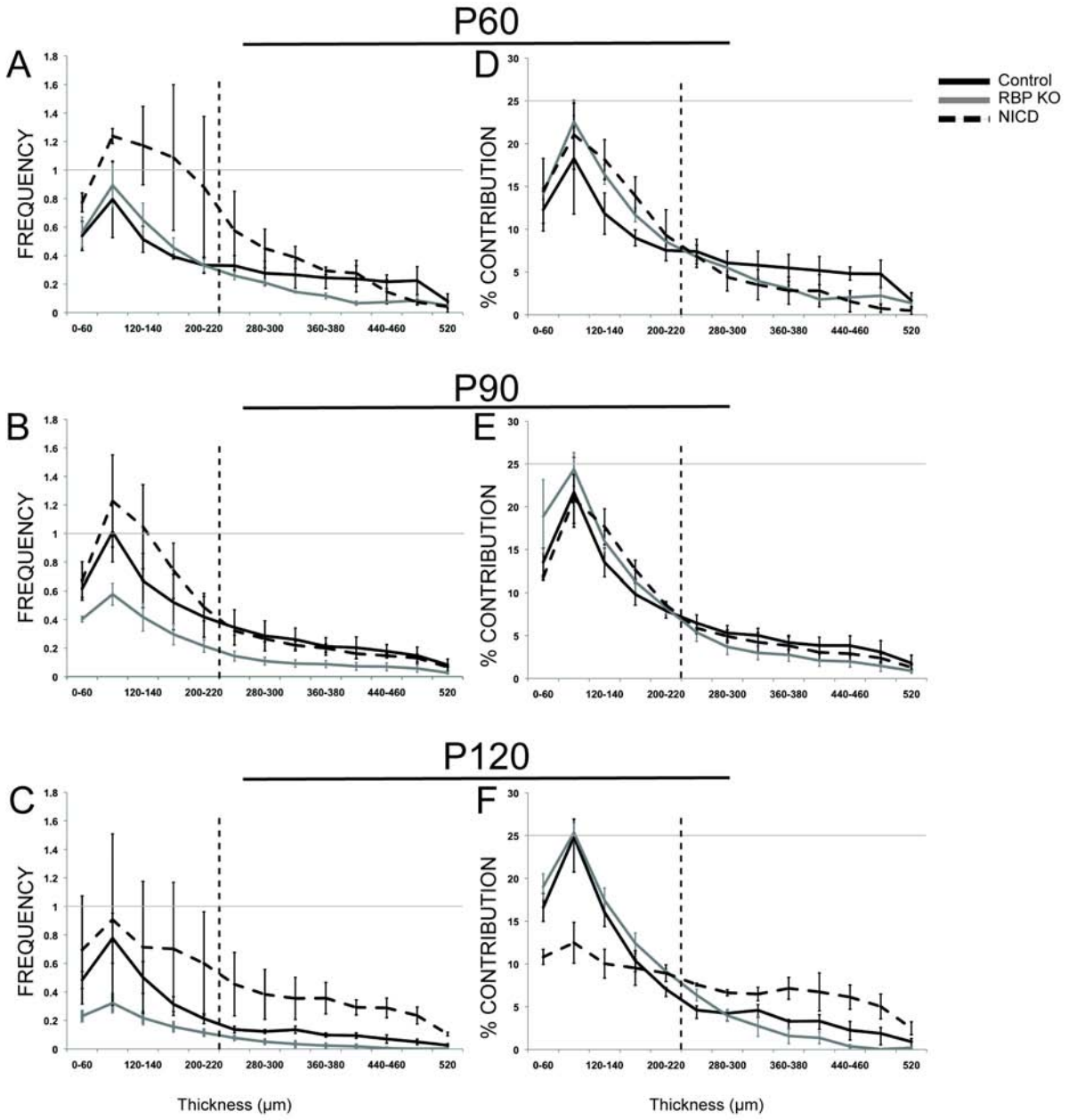

Figure 4.6 Notch signaling affects the frequency of different branch diameters in proportion to the original contribution. Data from Figure 4.5 graphed by age instead of genotype.

frequency was represented as a percentage of all diameters (Figures 4.5-4.6 D-F). Consistent with the raw data, the percent contribution of intermediate branches in control IHBD casts was the greatest of all the branch diameters and remained consistent with age (Figure 4.5 D). The percent contribution of each diameter in RBP KO IHBD casts did not change with age, indicating that RBP KO IHBD casts are losing intermediate and main branch diameters at the same rate (Figure 4.5 E). NICD IHBD casts demonstrated a shift in contribution towards main branches at P120, which could be attributed to the inability to resolve individual intermediate branches with increased cast density at later time points with the current scanning resolution (branch separation <20 um) (Figure 4.5 F).

For RBP KO IHBD casts, a reduction in the frequency of a specific diameter could be due to (1) branch shortening and/or (2) branch loss (Figure 4.7 A). In order to ascertain which possibility is more likely, I determined the total number of segments within the IHBD casts. A segment is defined as the portion between two branch points. The total number of segments in control IHBD casts was not significantly changed with age (Figure 4.7 B). In RBP KO IHBD casts, there was a significant reduction in segment number at P90 ($P \leq 0.05$) that was further reduced by P120 ($P \leq 0.05$) (Figure 4.7 B). NICD IHBD casts had a consistently, but not statistically significant increased number of segments compared to control (Figure 4.7 B). These data suggest that changes in branch diameter frequency in RBP KO are due, at least in part, to cast branch loss. However, we cannot rule out that branch loss is due to excessive branch shortening. Resin casting and microCT analysis demonstrated that intact intermediate and main branches were not maintained with age in RBP KO mice.

Reduction in 3D architecture is not due to structural loss of branches.

I hypothesize that Notch signaling might modulate maintenance of intact IHBD structure by (1) IHBD loss or gain, (2) functional blockage of the duct due to obstruction, or

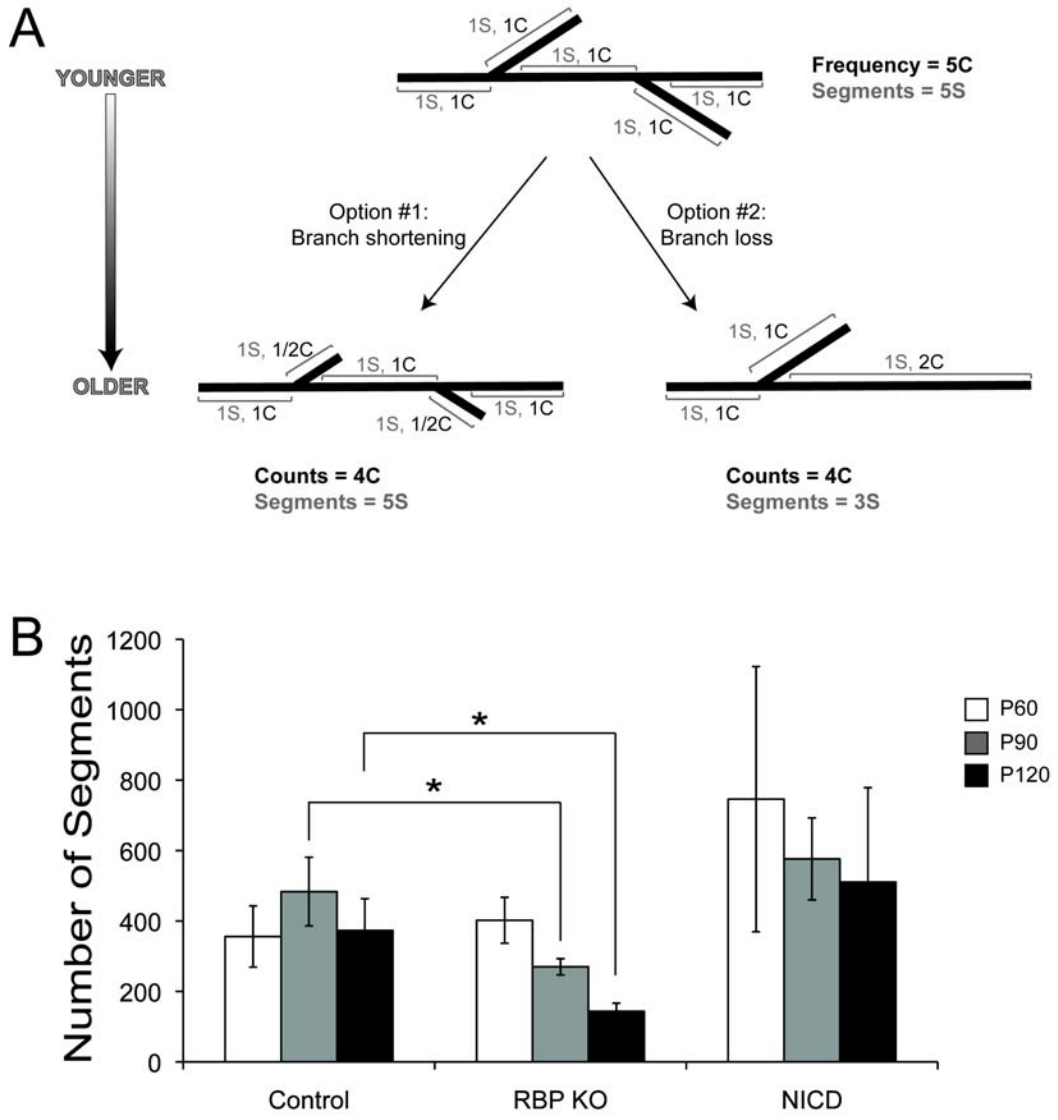

Figure 4.7 Loss of RBP-J results in a reduction of segments due to total branch loss with age. (A) Schematic illustrating a model of branch reduction in RBP KO IHBD casts. Upper panel represents a portion of the IHBD at a younger time point. This portion contains one originating branch with two side branches emanating from it. In this simplified example, the younger time point has five segments (S) and an initial frequency of a given diameter of five counts (C). A reduction in branch diameters as observed in RBP KO mice might be due to branch shortening (Option #1) and/or branch loss (Option #2). In either case, the frequency of branch diameter is reduced to 4C. To elucidate the difference between these two options, the number of segments must be taken into account. In the instance of branch shortening, the number of segments would not be affected (5S); however, in the instance of branch loss, there would be a reduction in the number of segments (3S). (B) The average number of segments, where a segment is defined as the portion between branch points, is consistent with age in control IHBD casts. In RBP KO casts, there is a progressive loss of segments compared to control. Conversely, NICD IHBD casts show a consistent, but not significant, increase in segments with age. Error bars – standard error of the mean. *$p \leq 0.05$.

(3) physical collapse of the IHBD structure. To address the underlying physiology leading to structural loss, I examined apoptosis and proliferation in the cytokeratin-positive cholangiocyte population. I found that cytokeratin-positive cells undergoing apoptosis are very rare regardless of genotype or age (Figure 4.8 C).

Cholangiocyte proliferation was assessed by BrdU administration for 4 days via the drinking water (Figure 4.8 A-B). In this analysis, peripheral branches refer collectively to the intermediate branches, as resolved by microCT, and small branches. In control mice, peripheral cytokeratin-positive cells show significantly reduced proliferation with age (P60 – 8.9%, P90 – 5.7% [$P \leq 0.05$ vs. P60] and P120 4.2% [$P \leq 0.01$ vs. P60]; Figure 4.8 A), which corresponds to the reduction in growth rate in these mice (Figure 4.2). There are no significant changes in the proliferation of hilar cholangiocytes composing main branches (Figure 4.8 B). In RBP KO mice, there is a significant increase in the proliferation of peripheral cytokeratin-positive cells at P90 and P120 (P60 – 12.7%, P90 – 14.6%, P120 – 13.1%) as compared to age-matched controls ($P \leq 0.05$ and $P \leq 0.01$, respectively) (Figure 4.8 A). RBP KO hilar cytokeratin-positive cells showed significantly increased proliferation as compared to control at P120 ($P \leq 0.01$) (Figure 4.8 B). Conversely, in NICD mice, there are no significant changes in proliferation rate at the hilum or the periphery as compared to control (Hilum/Periphery; P60 – 9.0%/5.5%, P90 – 12.5%/5.5%, P120 – 5.5%/4.6%; Figure 4.8 A-B).

It is important to note that there is no histological evidence of a ductular reaction (i.e. increased ductules (Roskams and Desmet, 1998)) in RBP KO mice, and all cytokeratin-positive cells were incorporated into a ductal structure (Please refer to Chapter III). However, to confirm this observation, I took an unbiased approach of ARIOL analysis. ARIOL is an automated platform, which allows for the imaging and quantification of immunohistochemical or immunofluorescent staining area (For full details, please refer to

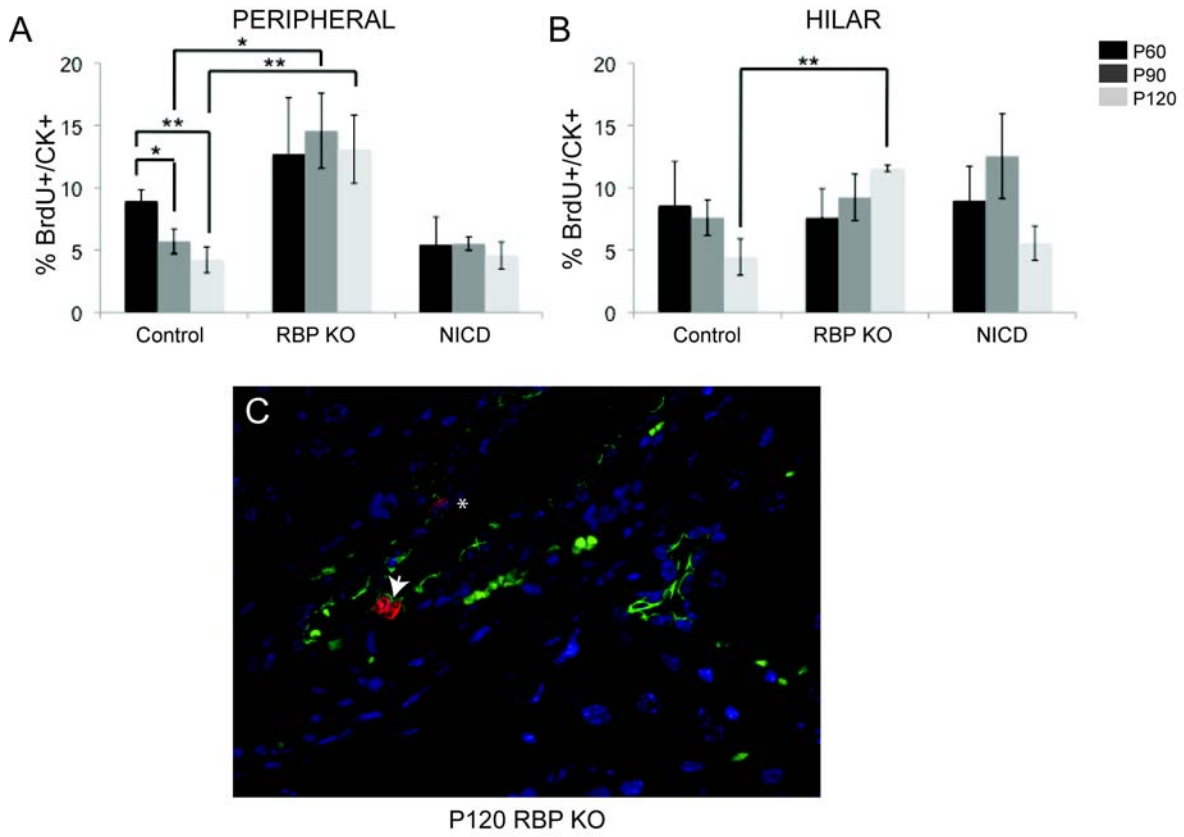

Figure 4.8 RBP KO mice have increased cholangiocyte proliferation without significant apoptosis. (A-B) Mice at the indicated age were labeled for 4 days with BrdU administered via drinking water. Paraffin sections were stained for pan-cytokeratin to mark cholangiocytes, BrdU to mark DNA replication and bis-benzamide to mark DNA. Pan-cytokeratin-positive and double pan-cytokeratin/BrdU-positive cells were counted from regions of the hilum and periphery. (A) In control mice, peripheral pan-cytokeratin-positive cells demonstrate a significant decrease in proliferation with age (*n*=4, 5 and 5 for P60, P90 and P120, respectively). RBP KO mice has significantly increased proliferation at P90 and P120 compared to control (*n*=4, 4 and 3 for P60, P90 and P120, respectively. NICD mice show no significant changes in proliferation (*n*=2, 3 and 4 for P60, P90 and P120, respectively). (B) Hilar pan-cytokeratin-positive cells in control and NICD mice have no significant changes in proliferation. RBP KO mice have an increased proliferation at P120 compared to control. (C) TUNEL-labeled cholangiocytes undergoing apoptosis in P120 RBP KO tissue (TUNEL – red, pan-cytokeratin – green, DNA – blue)). Cholangiocytes undergoing apoptosis are rare regardless of genotype or age. Error bars – standard error of the mean. *$p \leq 0.05$t, **$p \leq 0.01$.

Chapter II: *ARIOL analysis*). Using this approach, I assessed the cytokeratin-positive area in regions adjacent to portal veins, and was able to determine that there was no change in the total cytokeratin-positive between control and RBP KO tissue in hilar or peripheral regions at P15, P60 and P120 (Figure 4.9). To validate this approach, I also analyzed NICD mice and demonstrated a significant increase in cytokeratin-positive area as compared to control in the periphery at P15, P60 and P120 (Figure 4.9 B).

A further consequence of increased proliferation could be an expansion of liver size. However, analysis of the liver to body weight ratio of RBP KO mice, demonstrates that while this ratio is increased compared to control, it remains consistent at P60, P90 and P120 (Figure 4.10). An increased liver to body weight ratio at P30 in RBP KO mice is posited to be a result of compensatory growth, or expansion of the liver mass, in response to the hepatic necrosis observed at this time period (Please refer to Chapter III, Figure 3.4). Taken together, these results suggest that alterations in proliferation and/or apoptosis are not sufficient to explain the 3D structural loss with age.

Changes in the proliferation and/or apoptotic status of individual cholangiocytes do not preclude the possibility that full ductal structures are being lost, which results in the 3D structural loss with age. While the ARIOL analysis suggests we are maintaining cytokeratin area per portal vein, this could also be attributed to ductal or cellular hypertrophy. Therefore, I assessed the number of bile ducts per portal vein (BD/PV) in control and RBP KO mice at P60 and P120. For counting purposes, bile ducts were defined as cytokeratin-positive structures containing a lumen. As expected, there was a reduction in the number of bile ducts per portal vein in P60 and P120 RBP KO mice as compared with age-matched controls ($P \leq 0.0001$ and $P \leq 0.05$, respectively) (Figure 4.11 A). However, the number of BD/PV did not change between P60 and P120 in RBP KO mice (Figure 4.11 A). It remains a possibility that portal veins are lost, thus reducing the overall number of ducts without

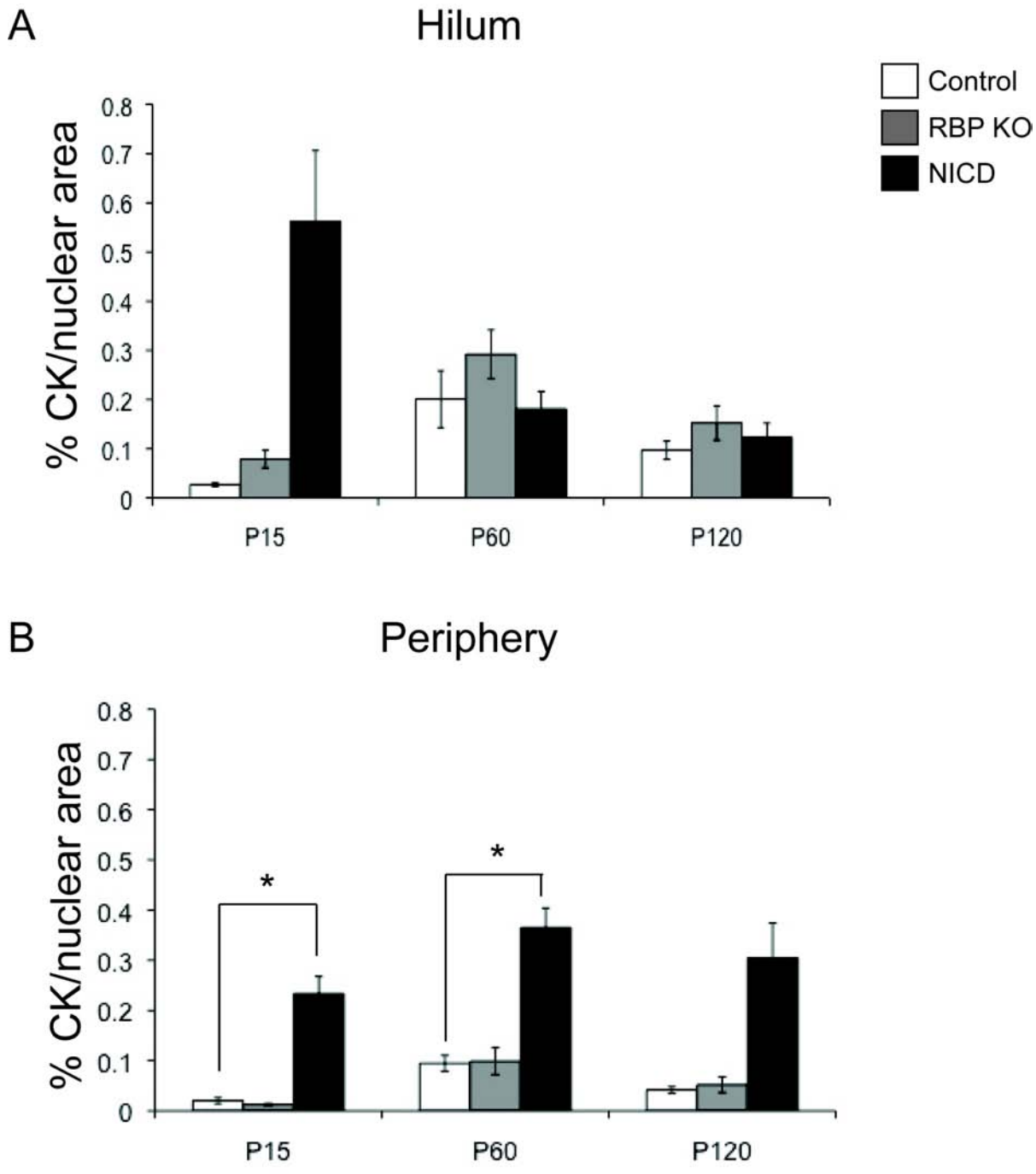

Figure 4.9 There is no change in cytokeratin19-positive area in RBP KO mice. Paraffin-embedded tissue was immunostained for cytokeratin19 and subjected to ARIOL analysis. Three different mice were analyzed from control, RBP KO and NICD at P15, P60 and P120. Total cytokeratin19-positive area in hilar (A) or peripheral (B) regions was normalized to total nuclear area. (A) The cytokeratin19-positive area at hilar regions is unchanged regardless of age of genotype. (B) The cytokeratin19-positive area at peripheral regions in NICD mice is significantly increased as compared to control at P15, P60 and P120. There are no differences in cytokeratin19-positive area in RBP KO as compared to control. Error bars – standard error of the mean. *$p \leq 0.05$.

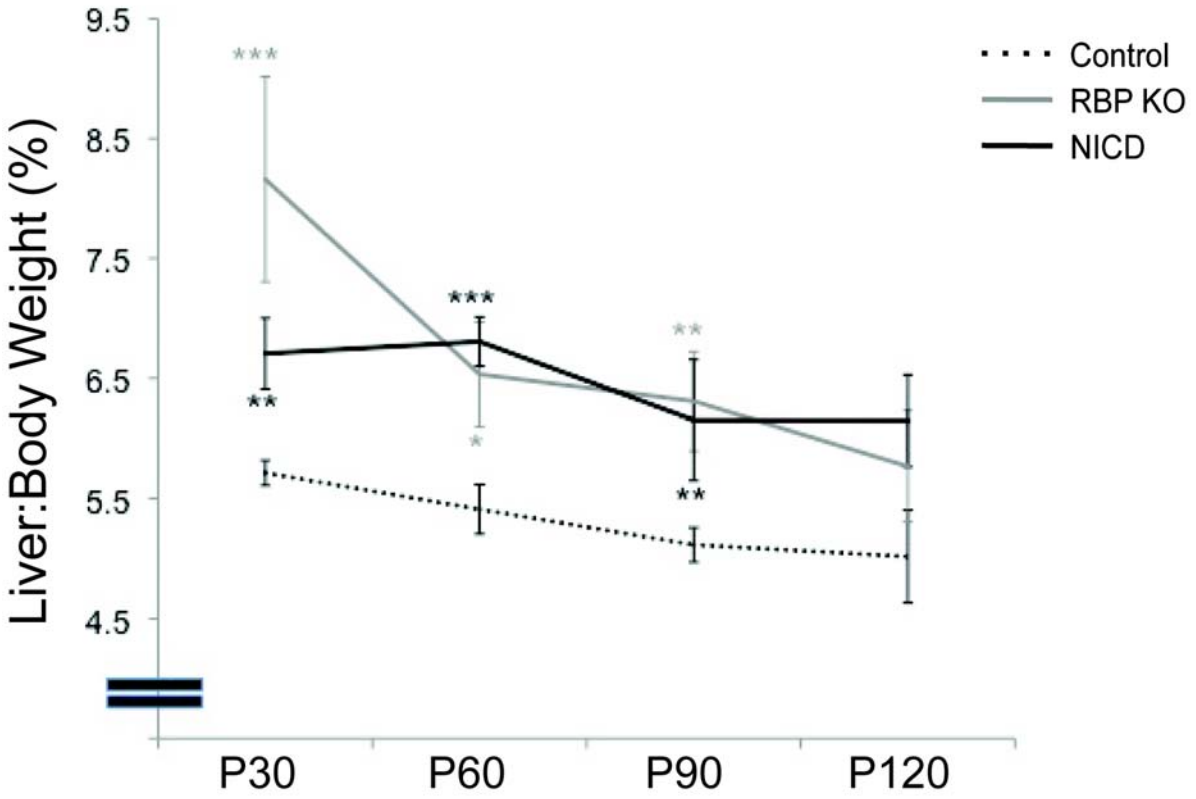

Figure 4.10 RBP KO and NICD mice demonstrate an elevated liver to body weight ratio compared to control. Liver to body weight ratios from P30, P60, P90 and P120 control (n=18, 15, 15 and 15, respectively), RBP KO (n=6, 16, 10 and 15, respectively) and NICD (n=6, 9, 7 and 11, respectively). Both RBP KO and NICD mice have an increased liver to body weight ratio as compared to control mice at P30, P60 and P90. Error bars – standard error of the mean. **$p \leq 0.01$, ***$p \leq 0.001$.

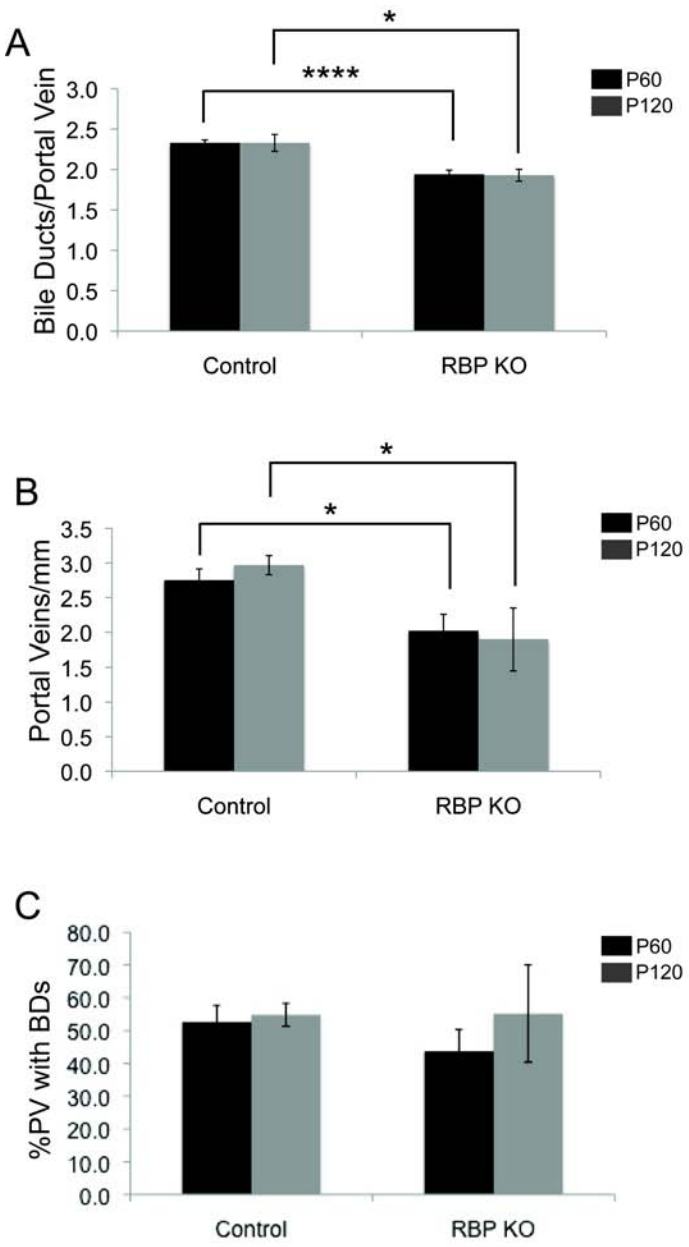

Figure 4.11 RBP KO mice have a reduction in bile ducts per portal vein and portal veins per area (mm) ratios at P60, which are not further reduced at P120. (A,B) Regions from the left or medial lobe were counted for peripheral bile ducts per portal vein and portal veins per mm. (A) RBP KO mice demonstrate significant reduction in bile ducts per portal vein at P60 (*n*=5) and P120 (*n*=4) compared with control (*n*=6 and 6, respectively). There is no difference in the number of bile ducts per portal vein in RBP KO mice at each age. (B) RBP KO mice demonstrate reduced portal veins per mm at P60 and P120 compared with age-matched controls. However, there is no difference in the number of portal veins per mm in RBP KO mice between P60 and P120. (C) A non-diffusible dye, CFDA, was injected into the portal vein to assess the number of portal veins with bile ducts associated. There is no significant difference in the number of portal veins with bile ducts associated at either time point (P60 or P120) between RBP KO and control. Error bars – standard error of the mean. *$p \leq 0.05$, ****$p \leq 0.0001$.

affecting the number of BD/PV. As there is a paucity of markers to distinguish portal from central veins, for this analysis, a portal vein was defined by having a bile duct associated. Consistent with the BD/PV analysis, there is an initially reduced number of PV/mm in P60 RBP KO compared with control, but no further reduction at P120 (Figure 4.11 B). The reduction in PV/mm in RBP KO mice is surprising, as this phenotype has not been previously described. Therefore to validate these findings and rule out the possibility that portal veins remain without any bile ducts associated, I assessed the number of portal veins by an additional method. I injected CFDA, a non-diffusible dye, which penetrates one cell layer deep and is irreversibly cleaved to fluoresce and inhibit transport out of the cell, into the portal vein. Thus marking the portal veins as those vessels marked by dye incorporation. Using this method, I stained with cytokeratin19 and counted the number of dye-labeled vessels with or with/out a bile duct associated. This analysis reveals that equivalent numbers of portal veins with bile ducts associated are indentified in control and RBP KO mice at P60 and P120 (Figure 4.11 C). This analysis identified a portal vein as any dye-incorporating area, thus only 50% of portal veins have bile ducts associated due to labeling of sinusoidal hepatocytes. Together, 3D and 2D analyses indicate that communicating branches are not maintained with age in RBP KO mice, however 2D ductal structures are maintained. Conversely, NICD mice maintain an excess of intermediate branches with age.

Discussion

Notch signaling regulates the three-dimensional architecture of IHBDs with age

Mechanistically, Notch signaling is linked to the regulation of cell fate, proliferation and/or death, and progenitor cell maintenance (Chiba, 2006). Previous studies have demonstrated a requirement of Notch signaling in the specification and morphogenesis of the IHBD (Geisler et al., 2008; Lozier et al., 2008; Zong et al., 2009), but the post-natal consequence of this improper development has not been studied. To date, many studies have evaluated "ductal cells" in 2D following chronic or acute genetic manipulations (Mishra, 2004), however these prior approaches have not revealed the 3D nature of the IHBD systems, which has limited our understanding of how intercellular and intracellular signals regulate the intact communicating IHBD structure. In this chapter, I describe the cell-autonomous requirement of chronic Notch signaling in liver epithelial cells to maintain an intact IHBD structure. My results establish that Notch signaling is required to maintain an intact IHBD structure, however subsequent to the initial establishment of the IHBD system, Notch is not required for the maintenance of the number of ductal structures per portal vein. Thus, this work reveals a previously unappreciated role for Notch signaling in the maintenance of an intact communicating IHBD network and describes a model of evolving cholestasis.

Resin casting and microCT anslysis have allowed us to define a role for Notch signaling in the maintenance of intact communicating IHBDs. In this chapter, I've shown that constitutive activation of Notch1 in hepatoblasts results in a slight overall increase in cast volume compared with control at all ages (Figure 4.3 B). I speculate that the changes in volume would be significantly greater should we have the ability to resolve small branches (<20 um) within the context of the whole left lobe resin cast. Furthermore, my data indicate a

consistent increase in intermediate braches (20-220 um) and main branches (240-520 um) within the IHBD resin casts, which was confirmed by individual branch diameter analysis at P60, P90 and P120 (Figures 4.4-4.6).

By contrast, loss of Notch signaling in the hepatoblasts resulted in a loss of cast volume in P120 resin casts (Figure 4.3 B), as a result of a reduced frequency of intermediate and main branches (Figures 4.4-4.6). Reduced frequency of intermediate branches in RBP KO resin casts was due in part to branch loss, as demonstrated by a reduction in the number of segments in P120 casts, but I cannot rule out the contribution of branch shortening to the phenotype (Figure 4.7). Conversely, the reduced frequency of main branches in RBP KO mice (Figure 4.4 B) was due to shortening without branch loss. I infer this because the stereotypical main branch structure did not change in RBP KO resin casts compared with control (Figure 4.12). In summary, RBP KO resin casts demonstrate progressive reduction of peripheral branches with age, and thus an inability to maintain an intact IHBD network.

Loss of the three-dimensional IHBD structure is not due to changes in proliferation, apoptosis or cytokeratin19-positive area.

To determine the underlying physiology of 3D branch loss and reduction in diameter, I first analyzed the potential contribution of proliferation and apoptosis (Figure 4.8). Peripheral RBP KO cholangiocytes have increased proliferation as compared to control at P90 and P120 (Figure 4.8 A), and hilar RBP KO cholangiocytes have increased proliferation at P120 as compared to control (Figure 4.8 B). The increased proliferation is due to a reduction in control proliferation levels, but maintenance of higher proliferation in RBP KO mice. I am unable to detect significant apoptosis within these cells (Figure 4.8 C). As no ductular reaction is observed, one possible explanation is an increase in the total ductal

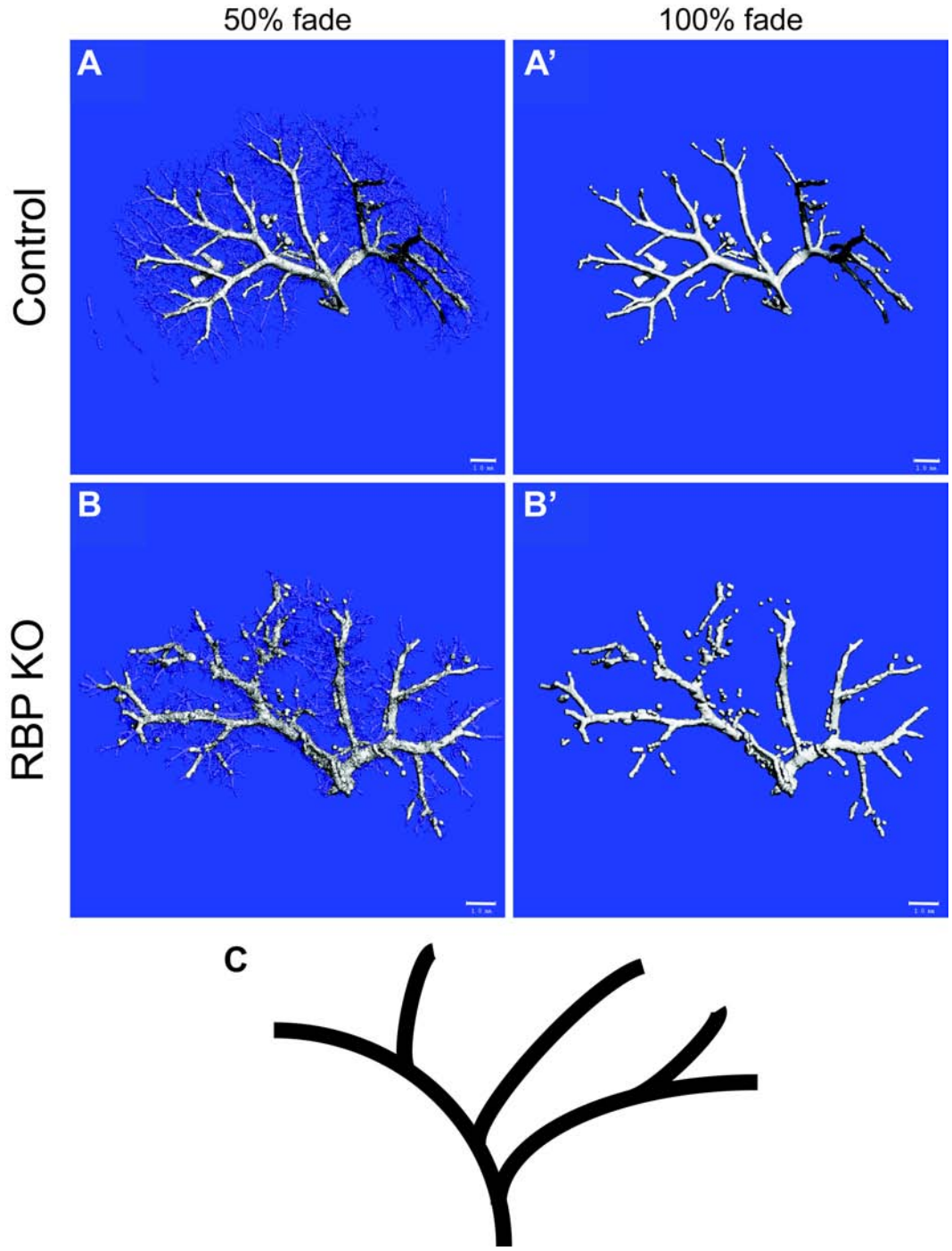

Figure 4.12 A stereotypical main branch structure is maintained in RBP KO mice. Main branch determination was made by computerized removal of peripheral branches, and comparison of control casts at all ages (P60, P90 and P120). (A,A') Representative image of a P120 control casts with peripheral branches faded to 50% transparency (A) and 100% transparency (A'). (B,B') Representative image of a P120 RBP KO casts with peripheral branches faded to 50% transparency (B) and 100% transparency (B'). (C) Analysis of main branch patterning defined a stereotypical pattern, which is maintained in RBP KO mice. Scale bar = 1 mm.

area. To address this possibility, I used ARIOL analysis to determine the cytokeratin-positive area, specifically adjacent to portal veins. This analysis detected no difference in cytokeratin-positive area between control and RBP KO in peripheral or hilar regions at P15, P60 or P120 (Figure 4.9). Analysis of liver to body weight ratios suggests, that while the liver to body weight percentages are significantly higher in RBP KO mice than age-matched controls, the ratio does not increase in RBP KO mice with age (Figure 4.10), nor is there a difference in overall growth rate (Figure 4.2). Together, these data indicate that RBP KO cholangiocytes are maintaining a higher level of proliferation without affect the cytokeratin-positive area. While I am not able to detect apoptosis within the cholangiocytes, it has been hypothesized that when cholangiocytes initiate an apoptotic program, they are extruded from the duct and shed into the lumen (Strazzabosco et al., 2000). Thus I postulate RBP KO cholangiocytes increase their turnover with age, however these results are not sufficient to explain the 3D structural changes observed in the resins.

While the total cytokeratin-positive area, as assessed by ARIOL analysis, is unchanged in RBP KO mice compared to control (Figure 4.9), this study was limited to cytokeratin-positive areas adjacent to portal veins and does not account for the number or size of ducts. Therefore these results do not preclude the possibility that entire ducts are being lost and consequently I analyzed the number of BD/PV. I found that the number of BD/PV was reduced in RBP KO mice at P60 compared with control, but there was no further reduction at P120 (Figure 4.11 A). The initial reduction in BD/PV can be attributed to the reduced number of ductal cells specified early in development, as described in Chapter III (Please refer to Chapter III, Figure 3.5). Thus, duct loss cannot explain the loss of 3D structural in RBP KO resin casts from P60 to P120. However, these results do not preclude that loss of entire portal veins could contribute to the 3D phenotype. Yet I have demonstrated that this is not the case as the number of PV/mm is maintained from P60 to P120 in RBP KO mice (Figure 4.11 B). An initial reduction in PV/mm in RBP KO mice at P60

and P120 was observed compared with age-matched controls (Figure 4.11 B). In the PV/mm analysis, a portal vein was defined as having a bile duct associated. However, it is possible that the portal vein remained intact, but no longer had a bile duct associated. The lack of markers to distinguish portal and central veins necessitated that I use an alternative approach; I injected a non-diffusible dye, CFDA, into the portal vein to mark these vessels specifically. Analysis of the number of portal veins, as marked by dye incorporation, with bile ducts associated is unchanged between control and RBP KO at P60 or P120 (Figure 4.11 C). Together these results describe a mouse model in which there is a reduction in the number of portal veins per millimeter of tissue.

To my knowledge, a defect in portal vein number has not been described in AGS patient biopsies or in any mouse model. The reduction in PV/mm could be due to a feedback requirement of the biliary system from proper venous development, portal vein destruction, or an inability of the portal vein to expand with post-natal growth. As a wave of necrosis is observed in RBP KO mice at P30 (Please refer to Chapter III, Figure 4C), and the consequence of this necrosis is not understood, it is possible that portal tracts containing portal veins are lost during this period. However, at P15, an age that precedes the necrotic period, the increased liver to body weight ratio and reduction in PV/mm was already observed in peripheral tissue (Figure 4.13). Thus these results suggest the reduction in PV/mm in peripheral tissue is not due to destruction of portal veins nor an inability to expand with post-natal growth. Instead, these results suggest a developmental defect, however, the mechanism of this reduction remains to be understood. Together, my 3D and 2D results demonstrate a failure to maintain an intact 3D biliary system without concomitant loss of ductal structures.

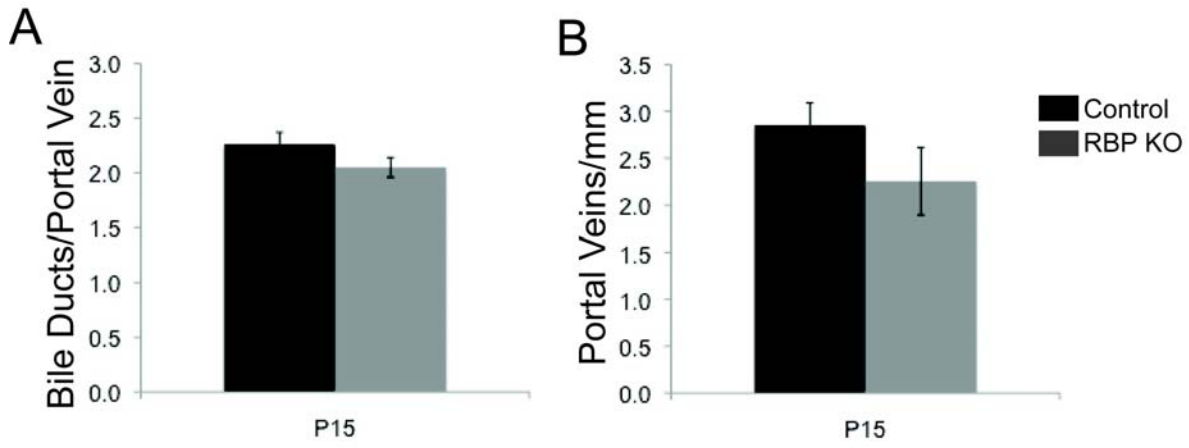

Figure 4.13 RBP KO mice have a reduction in bile ducts per portal vein and portal veins per area (mm) ratios at P15. (A,B) Regions from the left or medial lobe were counted for peripheral bile ducts per portal vein and portal veins per mm. (A) RBP KO mice demonstrate a reduction in bile ducts per portal vein at P15 (*n*=3) compared with control (*n*=2). (B) RBP KO mice demonstrate reduced portal veins per mm at P15 compared with age-matched controls. Error bars – standard error of the mean.

Loss of three-dimensional architecture without concomitant ductal loss suggests progressive IHBD obstruction in RBP KO mice.

A reduction of intact structure with age in RBP KO mice without 2D ductal loss suggests an obstruction or physical collapse within the IHBD. In the periphery of RBP KO casts, the resin changes from a completely filled structure to fine tenuous branches (Figure 4.1 F). I postulate that this fill pattern is indicative of a blockage at the point of transition between complete structure and tenuous branches, where the resin can only pass in fine, high velocity streams. An alternative explanation for the apparently contradictory 2D and 3D observations is non-productive compensatory sprouting. This phenomenon has been noted in tumor angiogenesis after Delta-like-4, a Notch ligand, blockade resulting in reduced Notch signaling (Noguera-Troise et al., 2006). If this were the case, we would expect to see an increase in ductal structures with progressive 3D loss; however, in our model the number of BD/PV was unchanged with age. Therefore, this model is not as likely to explain my results. Instead, I hypothesize that loss of intact structure is due to a progressive obstruction of the intact IHBD, which prevents resin from completely filling the distal tips. This hypothesis will be investigated further in Chapter V.

CHAPTER V

LOSS OF HEPATIC NOTCH SIGNALING LEADS TO INTRALUMINAL OBSTRUCTION OF THE INTRAHEPATIC BILE DUCT SYSTEM

Introduction

Alagille syndrome (AGS) is a pleiotropic developmental disorder that is highly associated with Notch pathway mutations (McDaniell et al., 2006; Warthen et al., 2006). AGS is characterized, in the majority of cases, by neonatal jaundice, cholestasis and paucity of intrahepatic bile ducts (IHBDs). However, there is a lack of understanding how specific mutations correlate with the severity and pleiotropy of the disease, suggesting environmental or other genetic factors are involved (Kamath et al., 2003). A study assessing the outcome of 163 children diagnosed with AGS, revealed that cholestasis usually worsens until school age, and then in some children will improve (Lykavieris et al., 2001). However, there are no known radiological or genetic markers to predict which children will progress to liver failure and which will improve.

Studies into the role of Notch signaling in bile duct development have been well described (McCright et al., 2002; Loomes et al., 2007; Geisler et al., 2008; Zong et al., 2009), however the long-term consequence of improper development is not well understood. In the previous chapter, I described a mouse model in which loss of Notch signaling results in an acquired post-natal obstruction of the IHBD. This is particularly intriguing as a subset of AGS patients demonstrate an inability to transport bile, based on failure to excrete biliary tracer upon hepatobiliary scintigraphy, suggesting an obstruction of the IHBD (Emerick et al., 1999). Unfortunately, these patients are often misdiagnosed as biliary atresia patients as a result of these tests and undergo a Kasai procedure, which replaces the extrahepatic bile duct with a portion of the intestine in an attempt to alleviate extrahepatic biliary obstruction.

AGS patients who undergo a Kasai procedure due to misdiagnosis are highly likely to proceed to liver failure and require transplant (Kaye et al., 2010). While Kaye et al. suggest that the Kasai procedure itself leads to increased mortality by interfering with liver function in AGS patients, it is not clear whether these patients had an IHBD obstruction due to irresolvable cholestasis which correlated with the severity of disease.

In this chapter, I investigate the underlying mechanism of IHBD obstruction in RBP KO mice, and assess the role of Notch signaling in the maintenance of proper liver function in the adult. My results provide evidence that obstruction is due to inspissated material accumulation within the ductal lumen. However, this obstruction cannot be attributed to alterations in the bile acid content or dysregulation of bile acid metabolism within the liver, gallbladder or intestine. Further, my preliminary results suggest that the acquired post-natal defects are independent of Notch signaling, and support a model in which post-natal defects are secondary to ductal malformations. Current models of cholestasis are achieved by acute surgical or chemical obstruction, therefore this model would provide a non-surgical, non-chemical model to study the progression of cholestatic liver disease.

Results

Intrahepatic bile duct blockage is due to intraluminal obstruction

In Chapter IV, I demonstrated that loss of Notch signaling within the hepatoblast population (*Alb-Cre;RBP-J*$^{flox/flox}$ [RBP KO]) results in an age-dependent loss of intact IHBD structure without concomitant loss of ductal structures. Three possible models can substantiate these findings; the first model is that at focal points within the ductal structure, the bile ducts are constricted and do not allow resin to pass, one possible cause for this is benign stricturing of the duct. A second model provides that focal cellular loss results in disconnection of the communicating structure. A third, and final model, suggests that intraluminal obstruction prevents the resin from completely filling the distal branches of the IHBD.

Benign biliary stricturing as a result of excessive inflammation and subsequent fibrosis has been described previously in a dog model of biliary trauma (Geng et al., 2005). As RBP KO mice have inflammation at hilar ducts (Please refer to Chapter III, Figure 3.6H,K). I assessed the levels of collagen deposition by Sirius Red staining in RBP KO mice. I qualitatively observed that there was no substantial difference in the amount of fibrosis in hilar regions P120 RBP KO mice compared to control (Figure 5.1).

To isolate the point of obstruction and narrow down the possible models, I added a fluorescent dye, Nile Red, to the methyl methacrylate resin for casting. Surface images of Nile Red resin injected P120 control and RBP KO liver lobes confirmed that the resin is not filling distal structures in RBP KO mice (Figure 5.2). Specifically, control resin casts demonstrate fluorescent resin filling the surface vessels (Figure 5.2 A), whereas RBP KO resin casts demonstrate surface vessels void of fluorescent resin (Figure 5.2 B). As demonstrated by the surface images of fluoresecently-labeled resin injections, visualization below the cell surface with conventional microscopy is not feasible. Therefore,

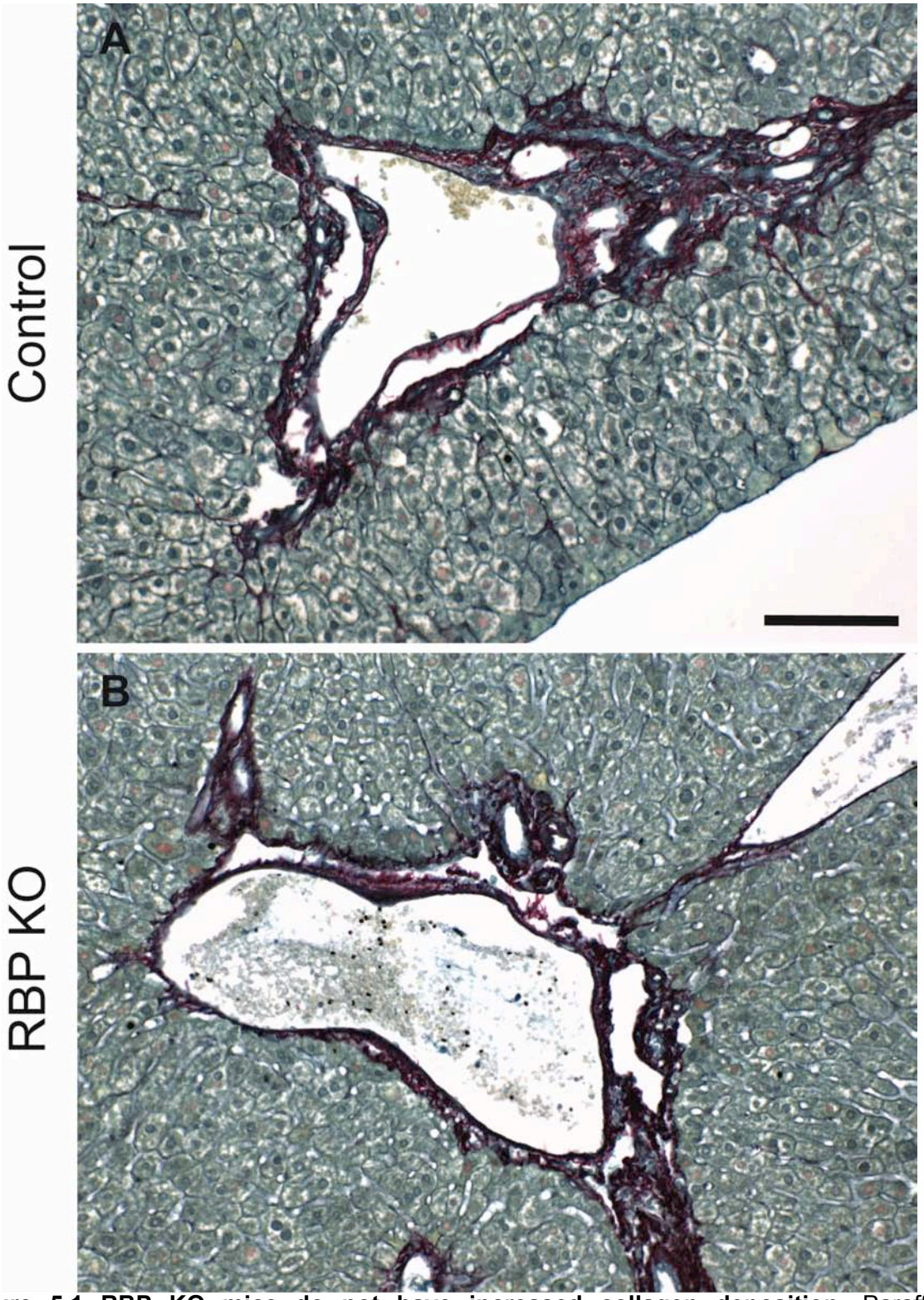

Figure 5.1 RBP KO mice do not have increased collagen deposition. Paraffin-embedded tissue was stained for Collagen with Sirius Red. Analysis of collagen deposition at hilar ducts in control (A) and RBP KO (B) mice at P120 reveals no obvious defects. Scale bar = 50 μm.

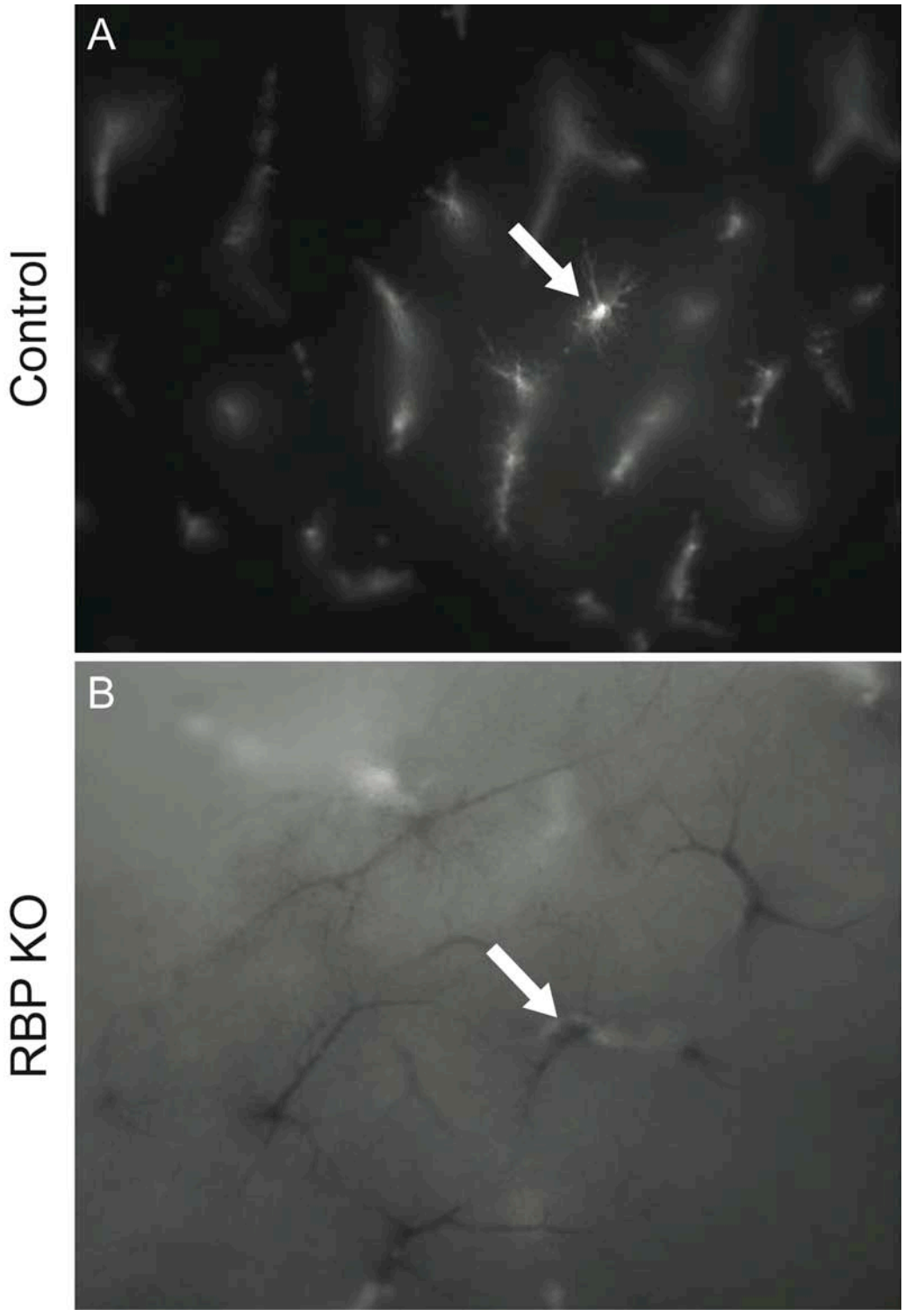

Figure 5.2 Fluorescently-labeled resin does not reach the liver surface in RBP KO mice. Nile red was added to the methyl methacrylate resin to a final concentration of 0.05 mg/ml, and injected in p120 control (A) and RBP KO (B) mice. Surface images of whole liver from (A) control mice, demonstrate that the fluorescent resin is visible at the surface of the liver lobe. (B) RBP KO mice demonstrate no fluorescent resin visible at the surface of the liver lobe, though vessels remain identifiable. Arrows – surface vessels.

in order to isolate the blockage, liver lobes were cleared with benzyl alcohol/benzyl benzoate (BABB) (Figure 5.3 A-B), and then sliced into 1mm sections (Figure 5.3 C-D). RBP KO slices were screened for those that incorporated the transition from completely filled resin to the fine tenuous structures (please refer to Discussion Chapter IV: *Loss of three-dimensional architecture without concomitant ductal loss suggests progressive IHBD obstruction in RBP KO mice*). These slices were then paraffin processed and serial sectioned. Sections were counterstained with hematoxylin (Figure 5.4) and examined for the point where fluorescent resin was no longer visible within the bile duct. In control resin casts, the fluorescent resin completely fills the bile duct and can be traced indefinitely through the tissue (Figure 5.4 A). Conversely, in the RBP KO mice, the resin initially completely fills the bile ducts in hilar regions (Figure 5.4 B), but progressively disappears as the sections proceed peripherally into the tissue (Figure 5.4 C-E). These data support a model of intraluminal obstruction (Figure 5.5). Indeed, at the point where the resin stopped filling the bile duct, inspissated material is observed in the lumen (Figure 5.5 B).

RBP KO mice do not have a leaky epithelium

In the Nile Red resin cast sections, I observed resin in the periportal space and while this was mild in control mice, the periportal resin was quite prevalent in RBP KO mice (Figure 5.4). This extra-ductular resin could be due to two different reasons; first, that the RBP KO mice have a leaky biliary epithelium or second, the pressure of the resin after encountering the blockages breaks apart the epithelium. To investigate the possibility of a leaky epithelium, I injected into the common bile duct, CFDA, a non-diffusible dye that incorporates into a cell and is irreversibly cleaved to fluoresce and render itself unable to be exported from the cell. Thus, if RBP KO mice had a leaky epithelium, I would expect to see dye incorporation into the cell layer next to the epithelium. However, this is not the case as the only cells incorporating CFDA are either bile duct epithelia or hepatocytes at the canals

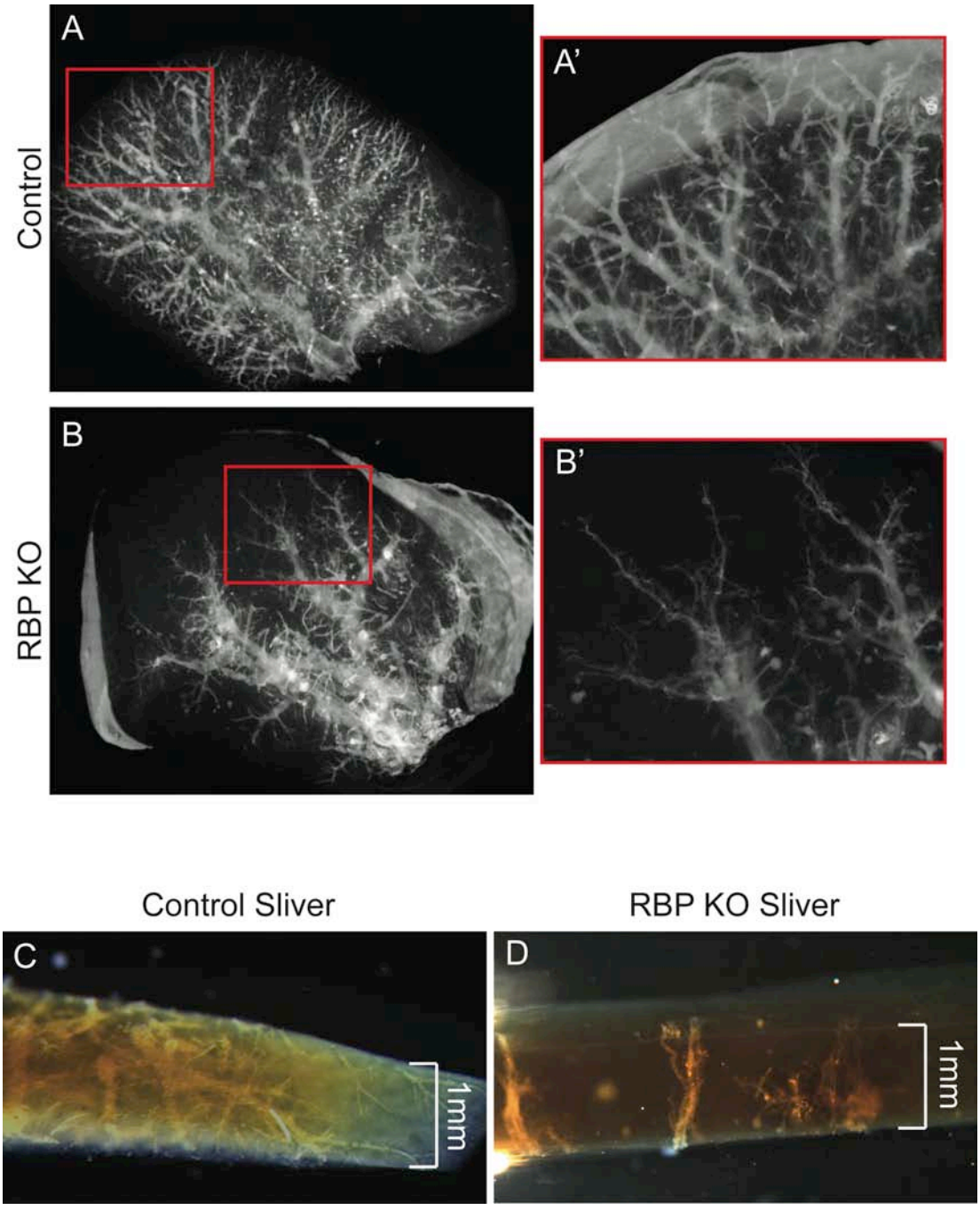

Figure 5.3 Fluorescently-labeled resin in conjunction with clearing the tissue allows visualization of cast structure and isolation of obstruction. (A-B) Nile red was added to the methyl methacrylate resin to a final concentration of 0.05 mg/ml, and injected into P120 control (A) and RBP KO (B) mice. Tissue was cleared using Benzyl-Alcohol/Benzyl-Benzoate (BABB). Red boxes indicate regions in A' and B'. (C-D) After injection, left liver lobes were sliced into 1 mm segments and screened for blockage. (C) A 1 mm slice from a control resin cast demonstrates resin filled to the periphery. (D) A 1 mm slice from a RBP KO resin cast demonstrates a potential obstruction, as defined by the transition from filled structure to fine tenuous branches.

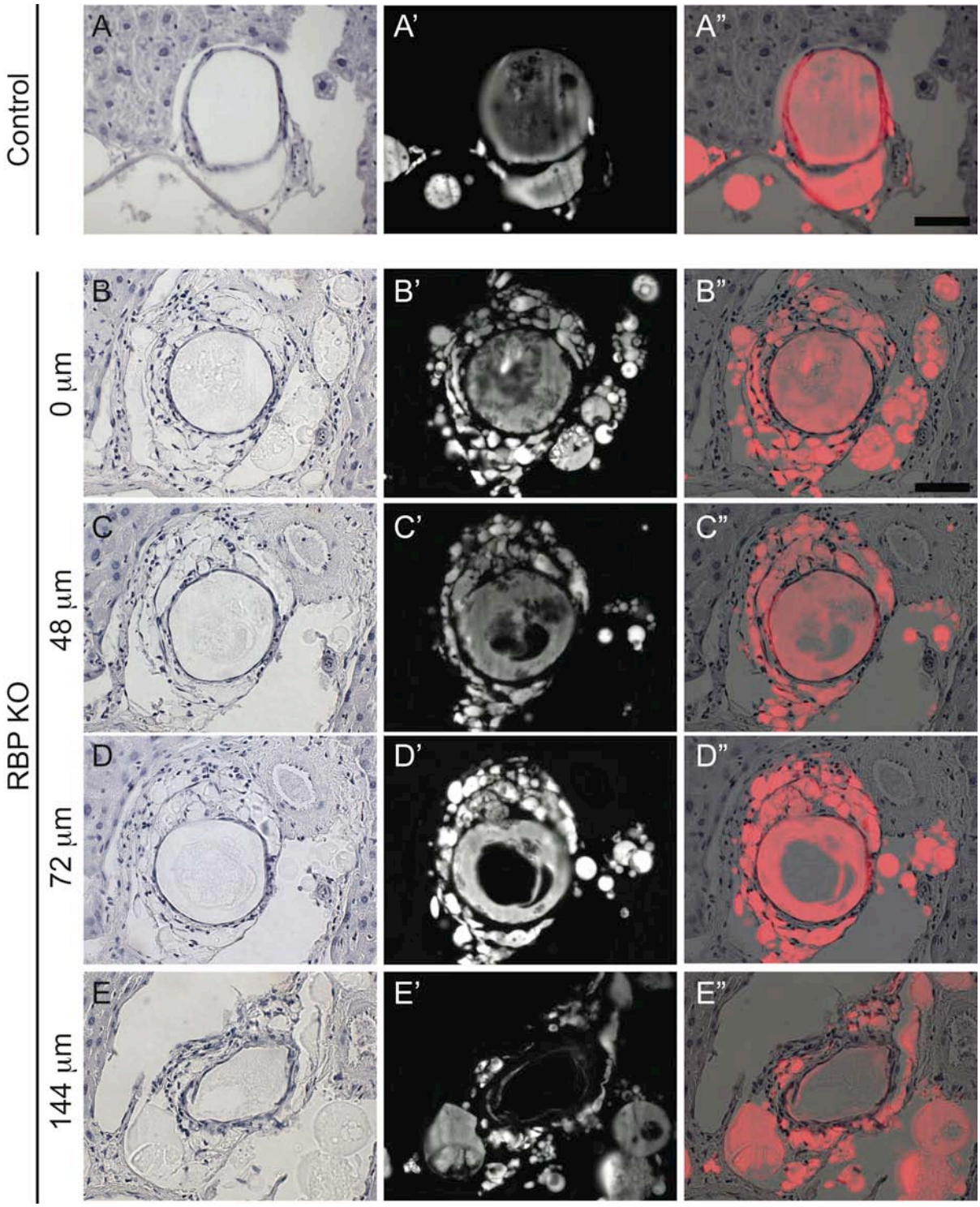
Control
RBP KO
0 µm
48 µm
72 µm
144 µm
A
A'
A"
B
B'
B"
C
C'
C"
D
D'
D"
E
E'
E"

Figure 5.4 Serial sections of fluorescently-labeled resin injection reveals nature of obstruction in RBP KO mice. Nile red was added to the methyl methacrylate resin to a final concentration of 0.05 mg/ml, and injected into P120 control and RBP KO mice. Tissue was sliced into 1 mm segments, cleared with BABB and screened for obstruction. Paraffin-embedded slices were serial sectioned, counterstained with Mayer's hematoxylin and screened for the resin to vacate the bile duct. (A-E) Mayer's hematoxylin counterstain. (A'-E') Flourescent resin. (A"-E") Overlay of Mayer's hematoxylin and fluorescent resin. (A-A") Control resin casts demonstrate complete fill of the ductal structure with minimal resin observed outside of the duct. (B-B") In RBP KO resin casts, at an arbitrary distance of 0 μm, the resin completely fills the ductal structure. Extra-ductal resin is observable at this distance. (C-C") At 48 μm after the initial image, the resin still mostly fills the ductal structure, but regions void of resin start to be observed. (D-D") At 72 μm after the initial image, the resin is filling only the outer edges of the bile duct. (E-E") At 144 μm after the initial image, the resin is completely absent from the ductal structure, however the extra-ductal resin becomes even more apparent at this point. An intraluminal obstruction is the reason for a reduction in the intact communicating IHBD in RBP KO mice. Scale bar = 100 μm.

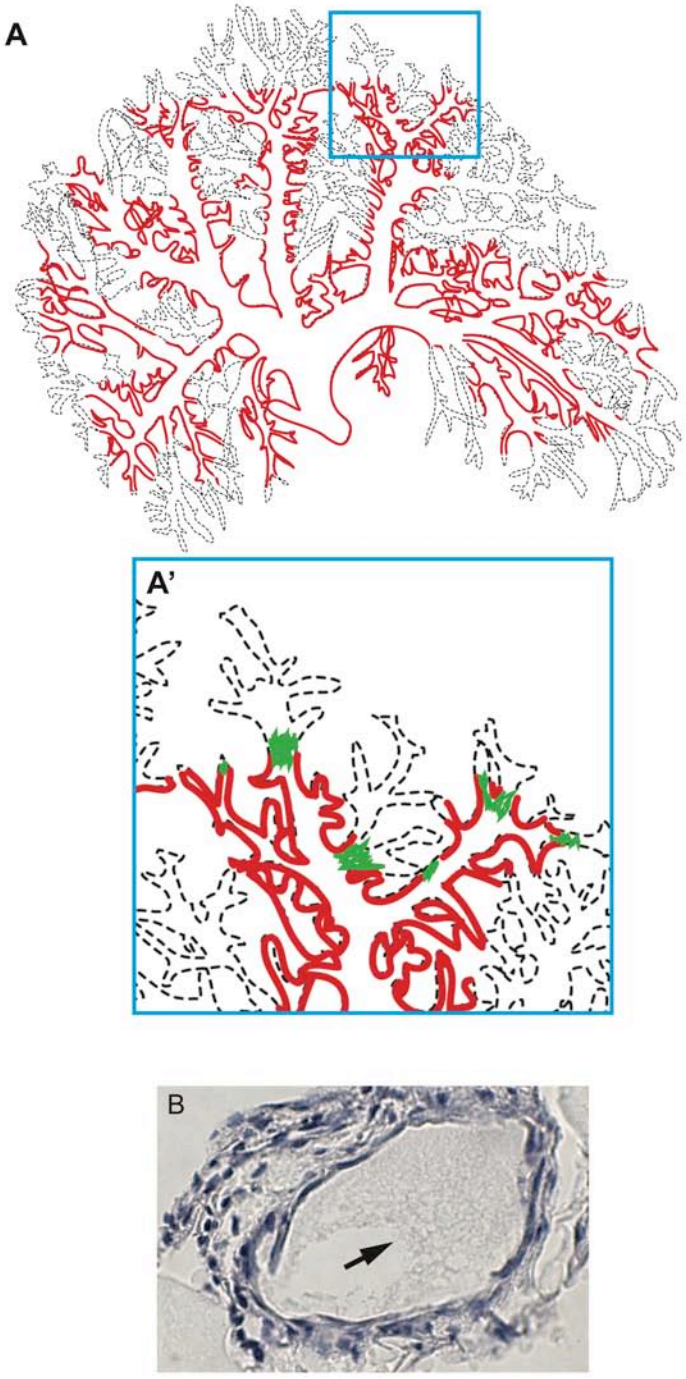

Figure 5.5 Model of IHBD obstruction in RBP KO mice. Isolation of the obstruction in RBP KO mice via fluorescent resin tracing revealed an intraluminal obstruction as the source. (A) Dotted black line indicates the ductal structure, as observed in section. Red line indicates where resin fills. Blue box indicates region in A'. (A') At the point where the resin stops filling the IHBD system, a blockage is observed (green). The source of this blockage remains to be defined. (C) Inspissated material is observable within the duct of RBP KO mice at the point of obstruction (arrow).

of Herring (Figure 5.6). Surprisingly, even the most distal bile ducts in RBP KO mice incorporate CFDA, suggesting that a less viscous liquid is able to pass the biliary obstruction.

CFDA incorporation suggests that epithelial integrity is not compromised when it comes to passive diffusion, however cell junctions may not be well-established in RBP KO mice. To further assess the integrity of the epithelium, I looked for membrane localization of beta-catenin in bile ducts. Consistent with the CFDA results, beta-catenin is properly localized at cell junctions in both control (Figure 5.7 A-D) and RPB KO mice (Figure 5.7 M-P) at P30 and P120. To confirm broadly that modulations in Notch signaling do not affect beta-catenin localization, P30 and P120 N2 KO (Figure 5.7 E-H), N1/N2 DKO (Figure 5.7 I-L) and NICD (Figure 5.7 Q-T) liver tissue was analyzed. As expected, beta-catenin is properly localized, although the epithelium looks qualitatively different, regardless of the levels of Notch signaling. Therefore, my results suggest that the resin leakage observed in RBP KO mice is not due to epithelial integrity problems, but rather a result of increased pressure due to luminal obstruction.

Biliary obstruction is not due to changes in bile composition.

To identify the source of obstruction in RBP KO mice, I investigated the hypothesis that improper bile formation leads to obstruction. First, it is important to note that Hall's Bilirubin Stain, which detects bilirubin, the pigment of bile, in RBP KO tissue did not identify any bile plugs or bile lakes within the tissue. However, to my knowledge, no study has described bile plugs in mice, thus this maybe a phenomenon specific to human liver.

To investigate the hypothesis that bile composition is altered, I analyzed the concentration of bile acids, the major component of bile, from four different sources: the liver, gallbladder, serum and feces using UPLC-MS/MS. During normal bile acid

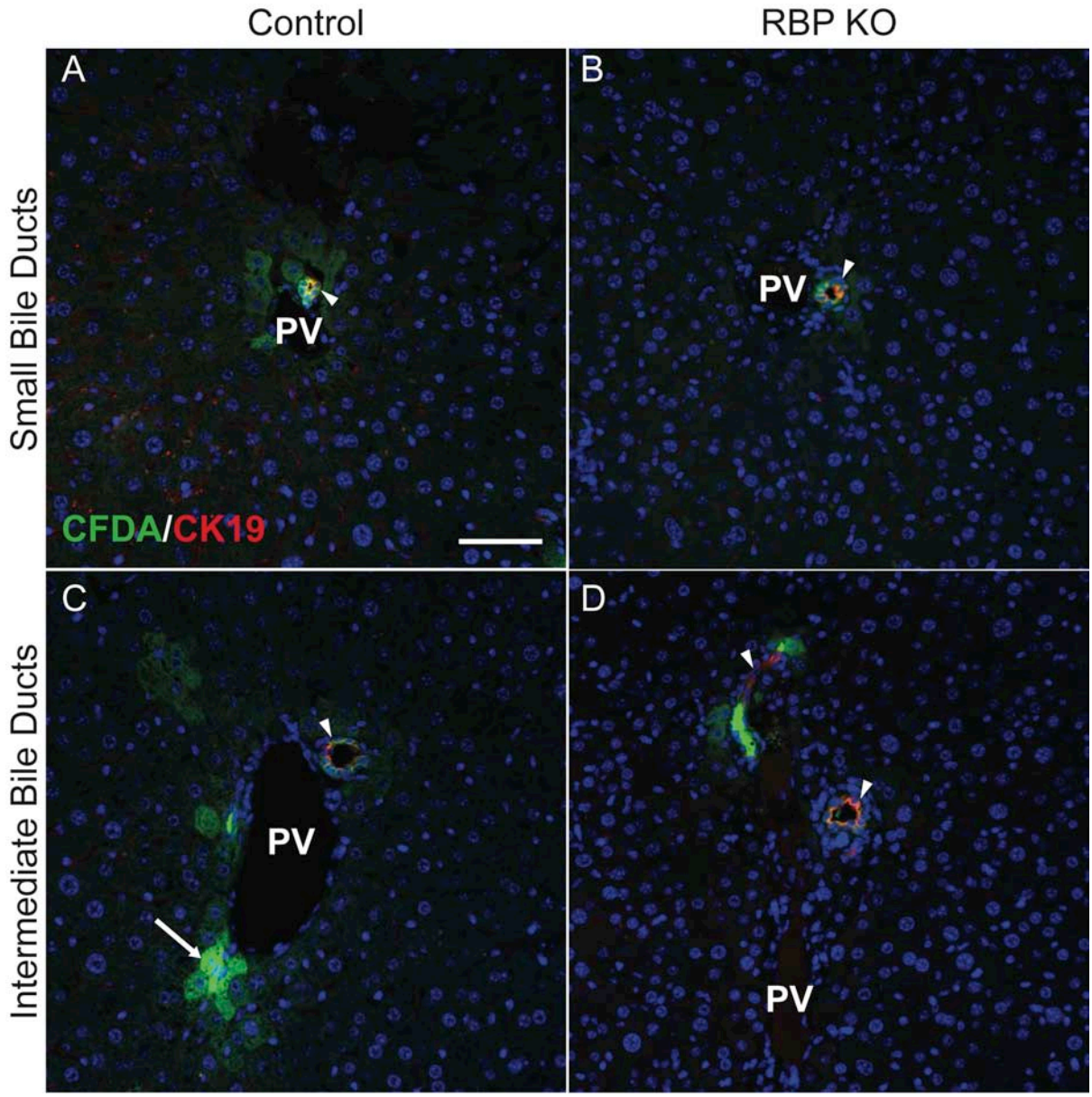

Figure 5.6 RBP KO mice do not have leaky epithelium. A non-diffusible dye, CFDA, was injected into the common bile duct of P120 control (A,C) and RBP KO (B,D) mice. Dye was allowed to incorporate for 1-hour before fixation and paraffin embedding. Sections were stained for cytokeratin19 to mark cholangiocytes. (A-B) Small bile ducts demonstrate cytokeratin19-positivity (Red) and CFDA incorporation (Green). (C-D) Intermediate ducts also demonstrate cytokeratin19-positivity and CFDA incorporation. A leaky epithelium would result in hepatocytes around ducts incorporating CFDA, however that is not observed. In some instances, hepatocytes surrounding the canals of Hering do incorporate dye (Arrow). Arrowheads – double-positive ducts. Scale bar = 50 μm.

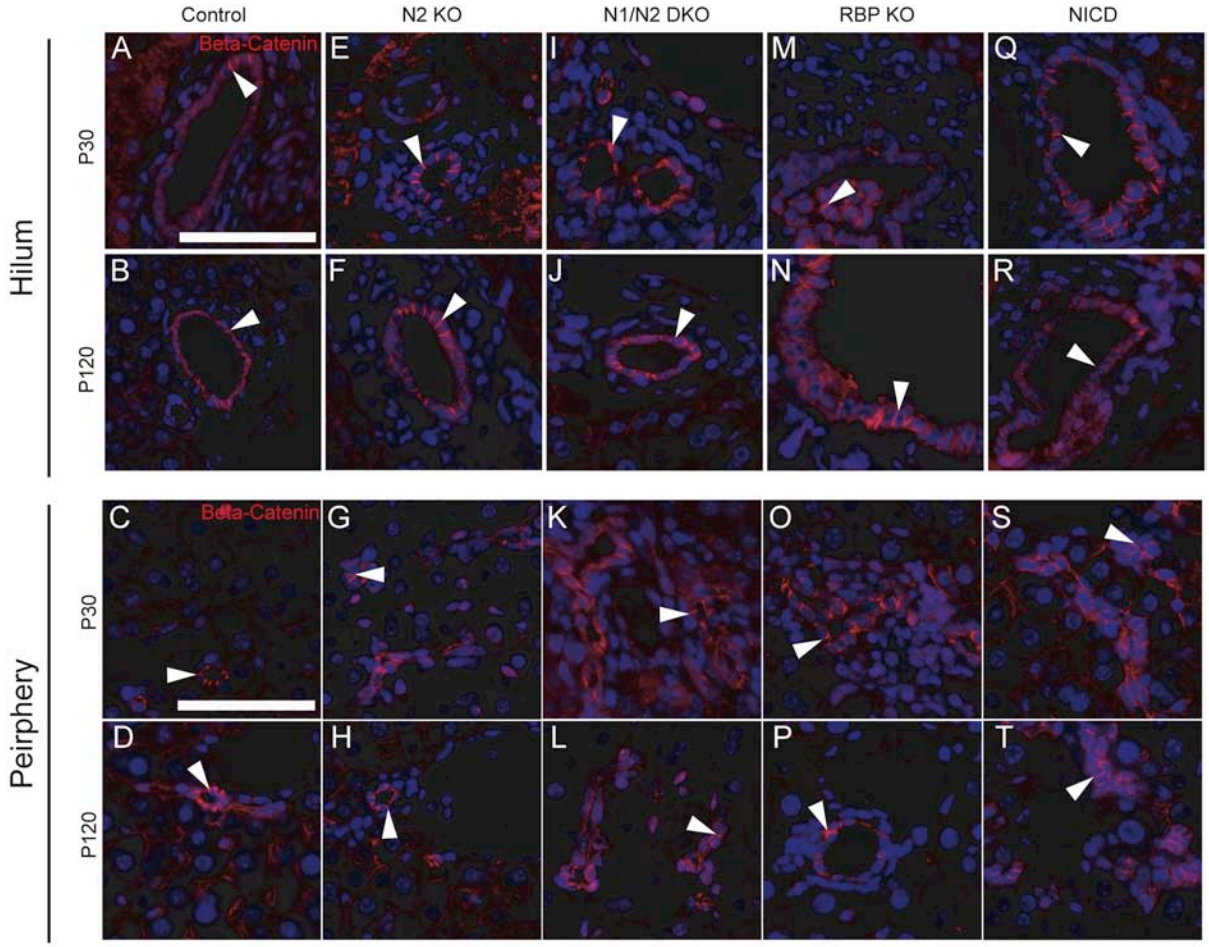

Figure 5.7 Beta-catenin is properly localized to cell junctions at P30 and P120 in all modulations of Notch signaling. An additional assessment of epithelial integrity is the proper localization of cell adhesion proteins. Paraffin-embedded sections from control, N2 KO, N1/N2 DKO, RBP KO and NICD mice at P30 and P120 were stained for beta-catenin. Hilar (A,B,E,F,I,J,M,N,Q,R) and peripheral (C,D,G,H,K,L,O,P,S,T) regions were analyzed. (A-D) Control tissue at P30 and P120 demonstrate normal localizations of beta-catenin in hilar and peripheral regions. (E-H) N2 KO tissue demonstrates proper localization of beta-catenin, even in un-remodeled cells, the cell contacts localized beta-catenin. (I-L) N1/N2 KO tissue also demonstrates proper localization of beta-catenin. (M-P) RBP KO tissue has proper localization of beta-catenin in hilar and peripheral ducts at P30 and P120. (Q-T) NICD mice demonstrate that the excess ductal cells properly localize beta-catenin. Scale bar = 100 μm.

metabolism, bile is produced within the liver, stored in the gallbladder, and excreted via the feces. Bile acids within the circulation are a result of the enterohepatic circulation recycling bile acids back to the liver. Thus analysis of bile acids within these pools lends insight into the potential misregulation of the bile acid metabolism pathway and of bile transporters or proteins involved in cholesterol metabolism. UPLC-MS/MS analysis was performed in collaboration with Dr. Grace Guo, an expert in bile acid metabolism, at the University of Kansas Medical Center. Interestingly, there is no change in the concentration of un-conjugated, taurine-conjugated, glycine-conjugated or total bile acids in liver, gallbladder or feces at P120 between control and RPB KO samples (Figures 5.8-5.10). However, in the serum analysis, all types of bile acids were increased in RBP KO samples compared to control (Figure 5.11 A), suggesting a failure of the enterohepatic circulation.

A failure of the enterohepatic circulation, and thus elevated serum bile acids, can be the result of defects in hepatocyte function or defects in hepatic sinusoids. To investigate if a failure of the enterohepatic circulation in RBP KO mice is due to hepatocyte defects, I took a candidate approach to analyze the mRNA expression of different components of the bile acid metabolism pathway. Specifically, I analyzed two nuclear receptors, Liver X Receptor (LxR) and Farnesoid X Receptor (FxR), which act as receptors for bile acids and regulate bile acid metabolism at a transcriptional level. At P120, both nuclear receptors were elevated, however only FxR transcript levels achieved statistical significance (Figure 5.12). A downstream target of FxR is the bile salt exporter protein (BSEP), which also has significantly increased transcript levels compared to control (Figure 5.12). Increases in these components would correlate with a cholestatic phenotype by decreasing bile acid production and increasing bile acid export. However, I also analyzed other transporters, specifically the multi-drug resistance-2 (MDR2), multi-drug resistance protein-2 (MRP2), multi-drug resistance protein-3 (MRP3) and organic anion transporting polypeptide-1 (OatP1). MDR2

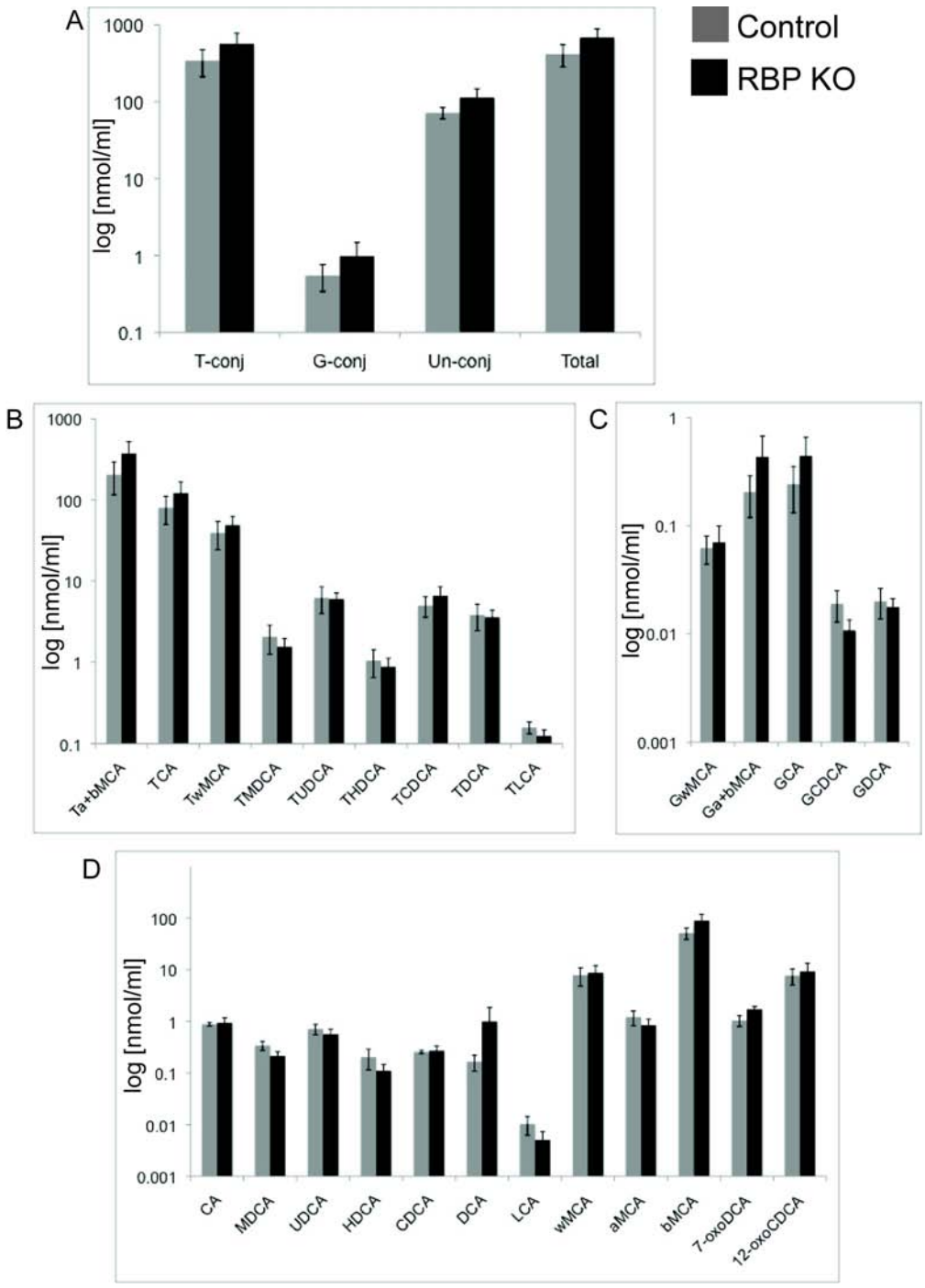

Figure 5.8 Liver bile acids are unchanged in P120 RBP KO mice. Bile acids were isolated from liver and analyzed by UPLC/MS. (A) Total levels of Taurine-conjugated (T-conj), Glycine-conjugated (G-conj), Un-conjugated (Un-Conj) and total bile acids are unchanged between control and RBP KO. (B) Individual Taurine-conjugated bile acids demonstrate no difference between control and RBP KO. (C) Individual Glycine-conjugated bile acids demonstrate no difference between control and RBP KO. (D) Un-conjugated bile acids demonstrate no difference between control and RBP KO. Error bars – standard error of the mean.

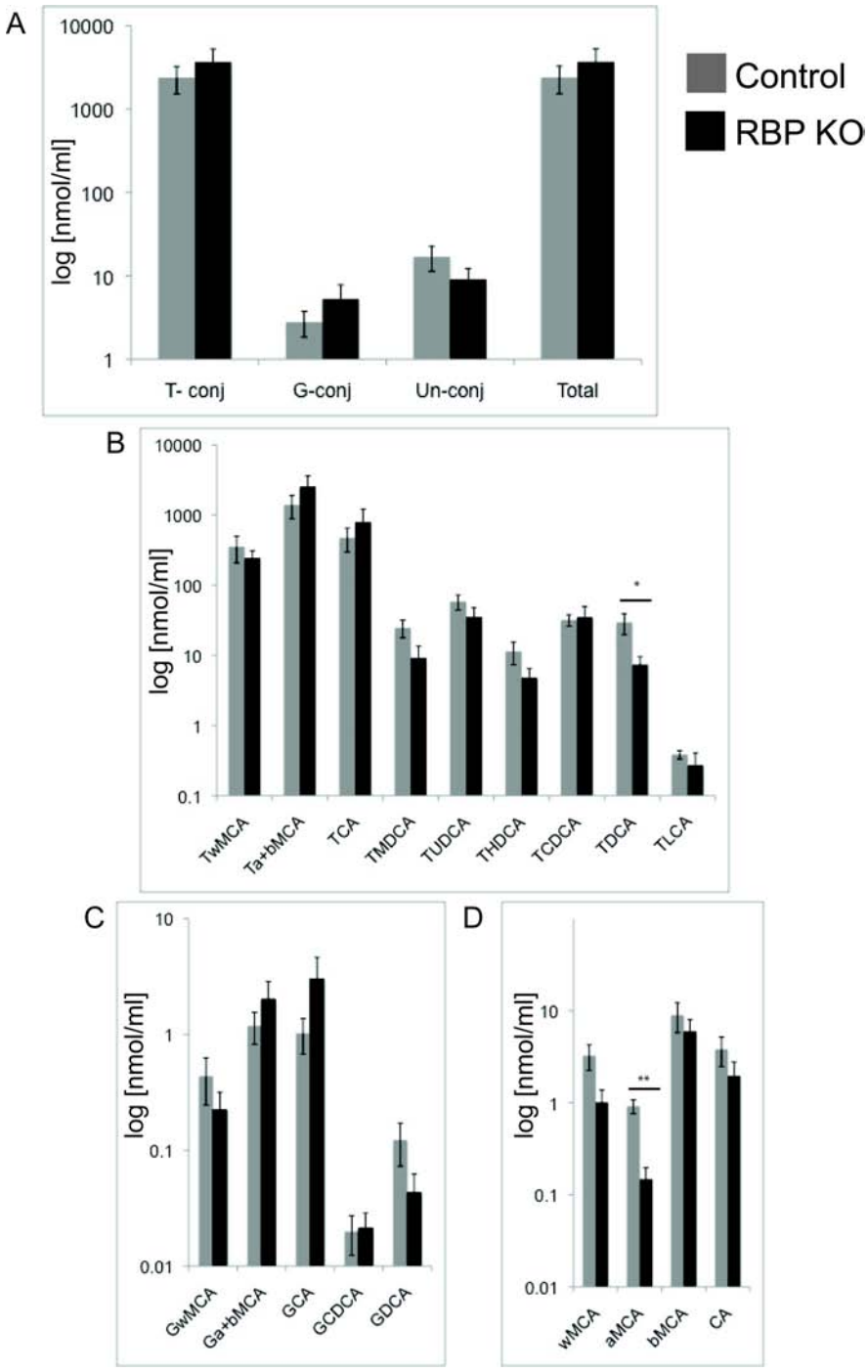

Figure 5.9 Gallbladder bile acids are unchanged in P120 RBP KO mice. Bile acids were isolated from the gallbladder and analyzed by UPLC/MS. (A) Total levels of Taurine-conjugated (T-conj), Glycine-conjugated (G-conj), Un-conjugated (Un-Conj) and total bile acids are unchanged between control and RBP KO. (B) Individual Taurine-conjugated bile acids demonstrate a significant reduction in only TDCA in RBP KO compared to control. (C) Individual Glycine-conjugated bile acids demonstrate no difference between control and RBP KO. (D) Un-conjugated bile acids demonstrate a significant reduction in aMCA in RBP KO compared to control. Error bars – standard error of the mean. *$p \leq 0.05$, **$p \leq 0.01$.

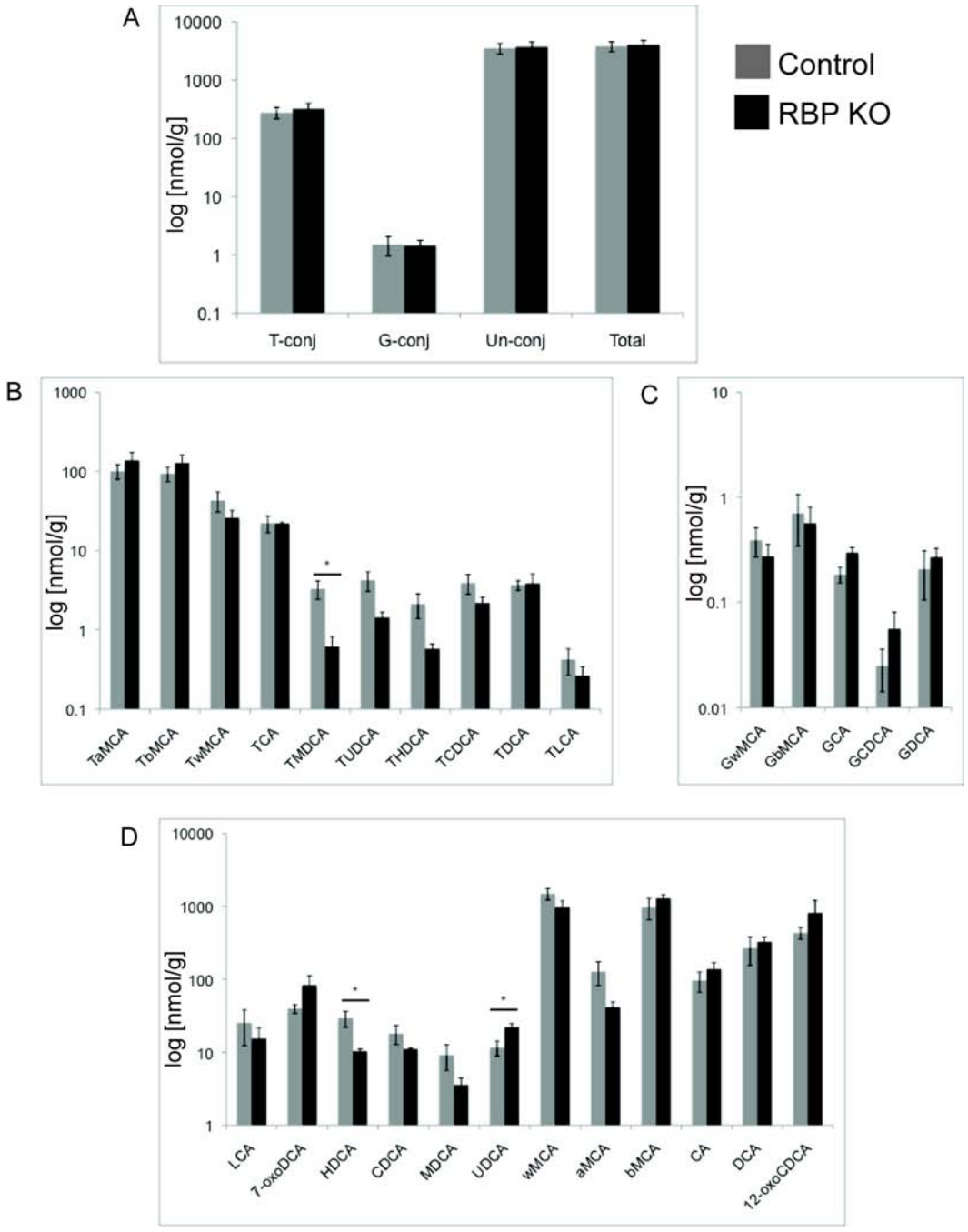

Figure 5.10 Fecal bile acids are unchanged in P120 RBP KO mice. Bile acids were isolated from feces and analyzed by UPLC/MS. (A) Total levels of Taurine-conjugated (T-conj), Glycine-conjugated (G-conj), Un-conjugated (Un-Conj) and total bile acids are unchanged between control and RBP KO. (B) Individual Taurine-conjugated bile acids demonstrate a significant reduction in only TMDCA in RBP KO compared to control. (C) Individual Glycine-conjugated bile acids demonstrate no difference between control and RBP KO. (D) Un-conjugated bile acids demonstrate a significant reduction in HDCA and an increase in UDCA in RBP KO compared to control. Error bars – standard error of the mean. *$p \leq 0.05$.

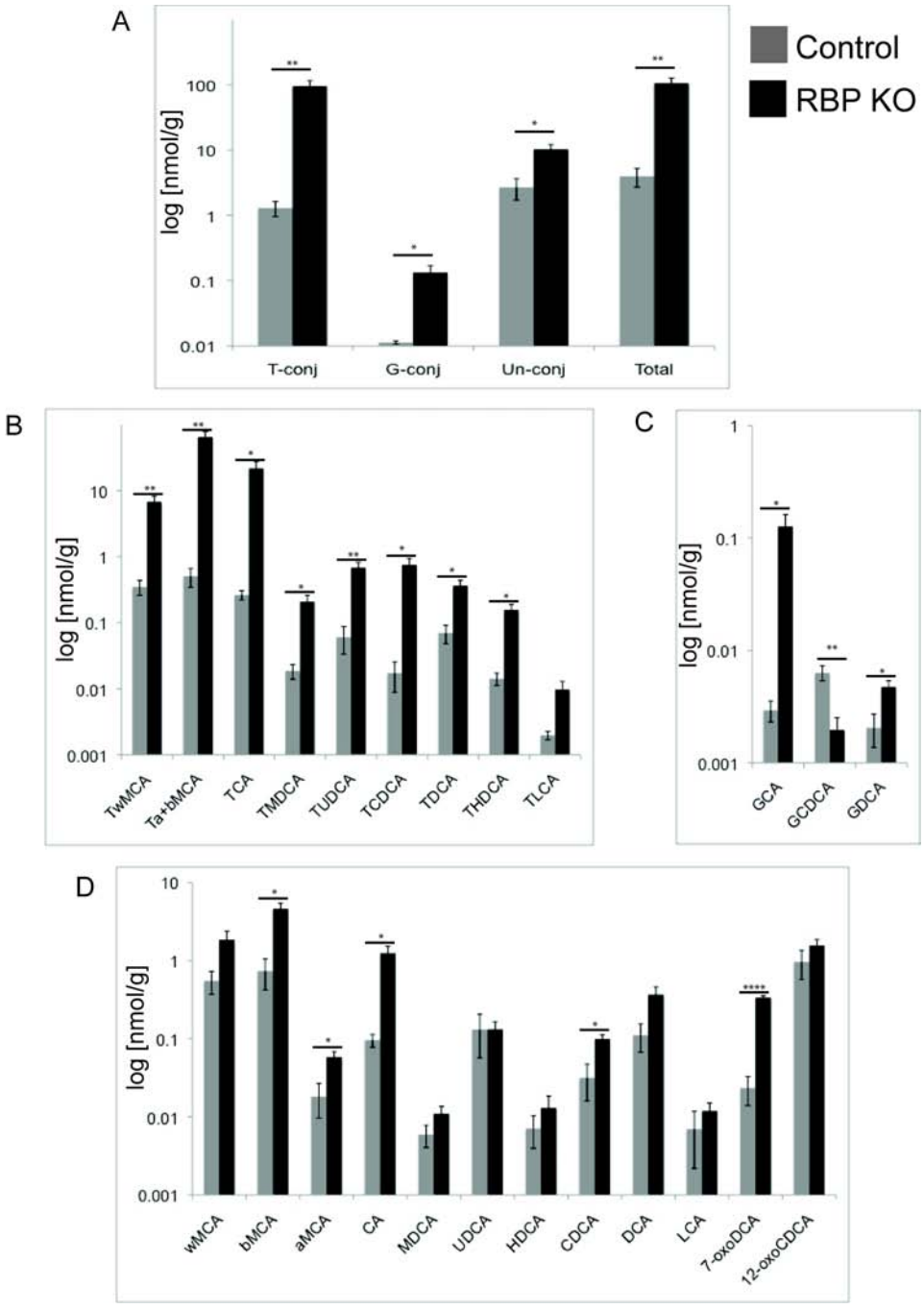

Figure 5.11 Conjugated and unconjugated bile acids are elevated in the serum of P120 RBP KO mice. Bile acids were isolated from serum and analyzed by UPLC/MS. (A) Total levels of Taurine-conjugated (T-conj), Glycine-conjugated (G-conj), Un-conjugated (Un-Conj) and total bile acids are significantly increased in RBP KO mice compared to control. (B) Individual Taurine-conjugated bile acids demonstrate a significant increase in all analyzed, except TLCA in RBP KO compared to control. (C) Individual Glycine-conjugated bile acids demonstrate a significant increase in all analyzed in RBP KO compared to control. (D) Un-conjugated bile acids demonstrate a significant in bMCA, aMCA, CA, CDCA, and 7-oxoDCA in RBP KO compared to control. Error bars – standard error of the mean. *$p \leq 0.05$, **$p \leq 0.01$, ****$p \leq 0.0001$.

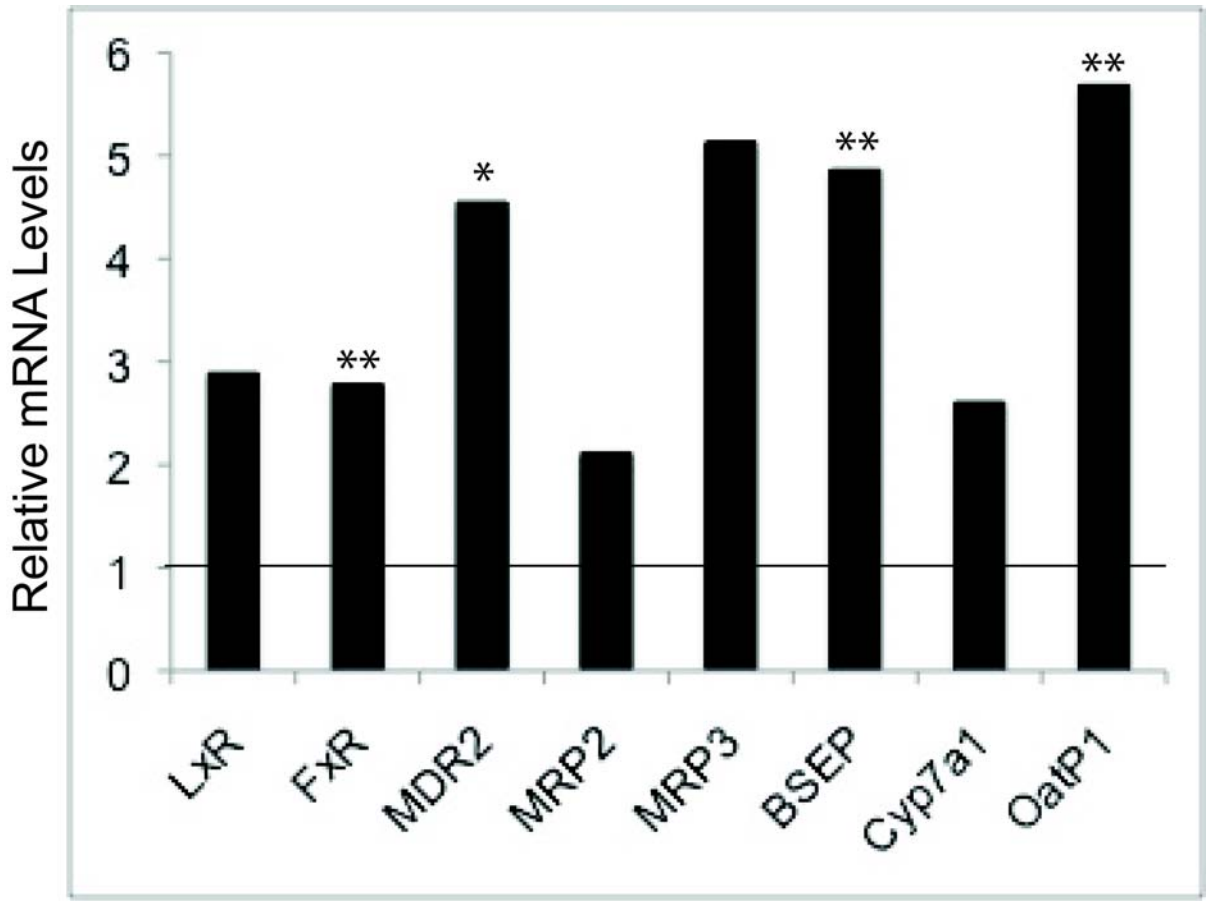

Figure 5.12 Bile acid metabolism components mRNA expression increase in P120 RBP KO total liver as compared to control. The relative expression ratio of bile acid metabolism components was calculated using real-time PCR efficiency and the deviation in cycle threshold (Ct) of RBP KO versus control samples, expressed in comparison to GAPDH mRNA levels. At P120, FxR, MDR2, BSEP and OatP1 are elevated in RBP KO compared to control. Horizontal line represents control value. *$p \leq 0.05$, **$p \leq 0.01$.

and OatP1 transcript levels were significantly increased in RBP KO mice at P120 (Figure 5.12). Increases in OatP1 would not necessarily correlate with a cholestatic phenotype, as increased OatP1 would result in increased bile acid uptake. MDR2 is involved in broad substrate export, and is not specific to bile acid regulation. Interestingly, these results suggest that a failure of enterohepatic circulation in RBP KO mice is not due to hepatocytes defects. Further, these results correlate with the bile acid analysis and demonstrate a general increase in bile acid production, both uptake and export, which would result in an increase in both conjugated and un-conjugated bile acids. Taken together, these results suggest a failure of the enterohepatic circulation, but are not indicative of hepatocyte defects.

RBP KO mice have an increase in mucin-producing peribiliary glands

Another documented, although rare, source of biliary obstruction has been attributed to mucinous masses (Smith and Matzen, 1985). During homeostasis, cytokeratin-positive peribiliary glands, preferentially located around hilar bile ducts, produce mucus. Mucus secretion is proposed to play a dual role; both in the protection of the epithelium from toxic bile and in the defense against infection by enterogeous micro-organisms (Nakanuma et al., 1994b). However, during liver injury, peribiliary glands have been documented to increase mucosal secretion as a non-specific reactive process. Seromucinous hypersecretion can lead to retardation of bile flow, alteration of bile composition and/or increased bile viscosity (Nakanuma et al., 1994a). Therefore, I stained P60 and P120, control and RBP KO tissue with Alcian Blue at pH 1.0 and pH 2.5, to detect sulfated acid and acid mucins respectively. Nakanuma et al. had described peribiliary glands to only secrete neutral and acid mucins (Nakanuma et al., 1994b); consistent with this, I observed no ducts regardless of age or genotype, which expressed sulfated acid mucins. In contrast, I detected a significant increase in the number of acid mucin-producing ducts in P120 RBP KO compared to P120

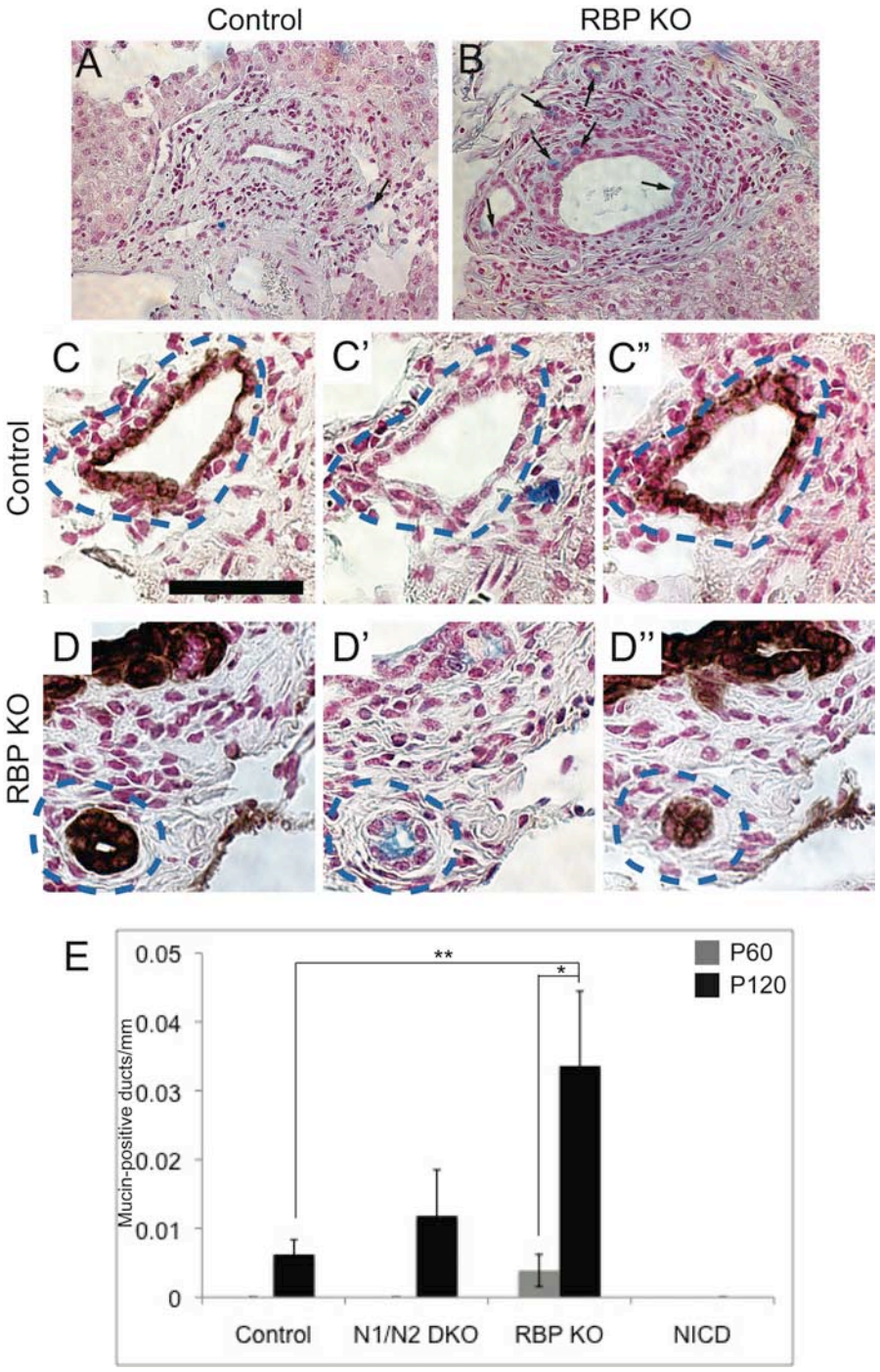

Figure 5.13 RBP KO mice have an increase in mucinous ducts at P120. (A-B) Alcian blue pH 2.5 staining in control and RBP KO tissue demonstrates an increase in acid mucin-producing ducts in RBP KO. (C-D) Serial sections stained with cytokeratin19, alcian blue pH 2.5 and cytokeratin19 confirms the localization of mucin to ductal structures. (E) Quantification of the number of ducts containing mucinous cells in control, N1/N2 DKO, RBP KO and NICD mice. RBP KO mice have an increase in mucinous ducts at P120 compared to P120 control and P60 RBP KO. Error bars – standard error of the mean. *$p \leq 0.05$, **$p \leq 0.01$.

control and P60 RBP KO (Figure 5.13 E). Mucin-producing ducts were only observed in small bile ducts associated with hilar ducts or hilar ducts themselves, consistent with the location of peribiliary glands (Figure 5.13 A-B). Further, I confirmed that mucin-producing cells were cytokeratin-positive by staining serial sections (Fig 13 C-D). Interestingly, this phenomenon is specific to the RPB KO mice, as N1N2 DKO and NICD mice do not have an increase in mucin-producing ducts (Figure 5.13 E). Therefore, it remains a possibility that excess mucin production by peribiliary glands results in biliary obstruction.

RBP KO mice have longer cilia

In addition to the possibility that mucous production alters bile content, cholangiocyte regulation of bile composition may also contribute to an obstructive phenotype. It has been established that cholangiocytes have a primary cilium radiating from their apical surface that acts as a mechano- and chemo-sensory organelle to detect and regulate bile composition and flow (Masyuk et al., 2008). As ductal defects have been described within the RBP KO mouse model (Please refer to Chapters III and IV), it remains possible that the cholangiocytes are unable to properly regulate bile composition and flow, thus contributing to an obstruction of the IHBD. Interestingly, in P120 RBP KO cholangiocytes, the cilia, as identified by Arl13b staining, appear longer (Figure 5.14). Thus alterations in bile consistency and/or flow as a result of irregular cholangiocyte cilia remain a possible source of obstruction.

Post-natal cholangiocyte function may not require Notch signaling

An additional question that remains is the role of Notch signaling in adult phenotype. The progressive obstruction observed in mice with a chronic loss of Notch signaling (RBP KO) can be attributed to one of three models: 1. There is an additional requirement of Notch signaling for the adult function of cholangiocytes, 2. Notch signaling is required

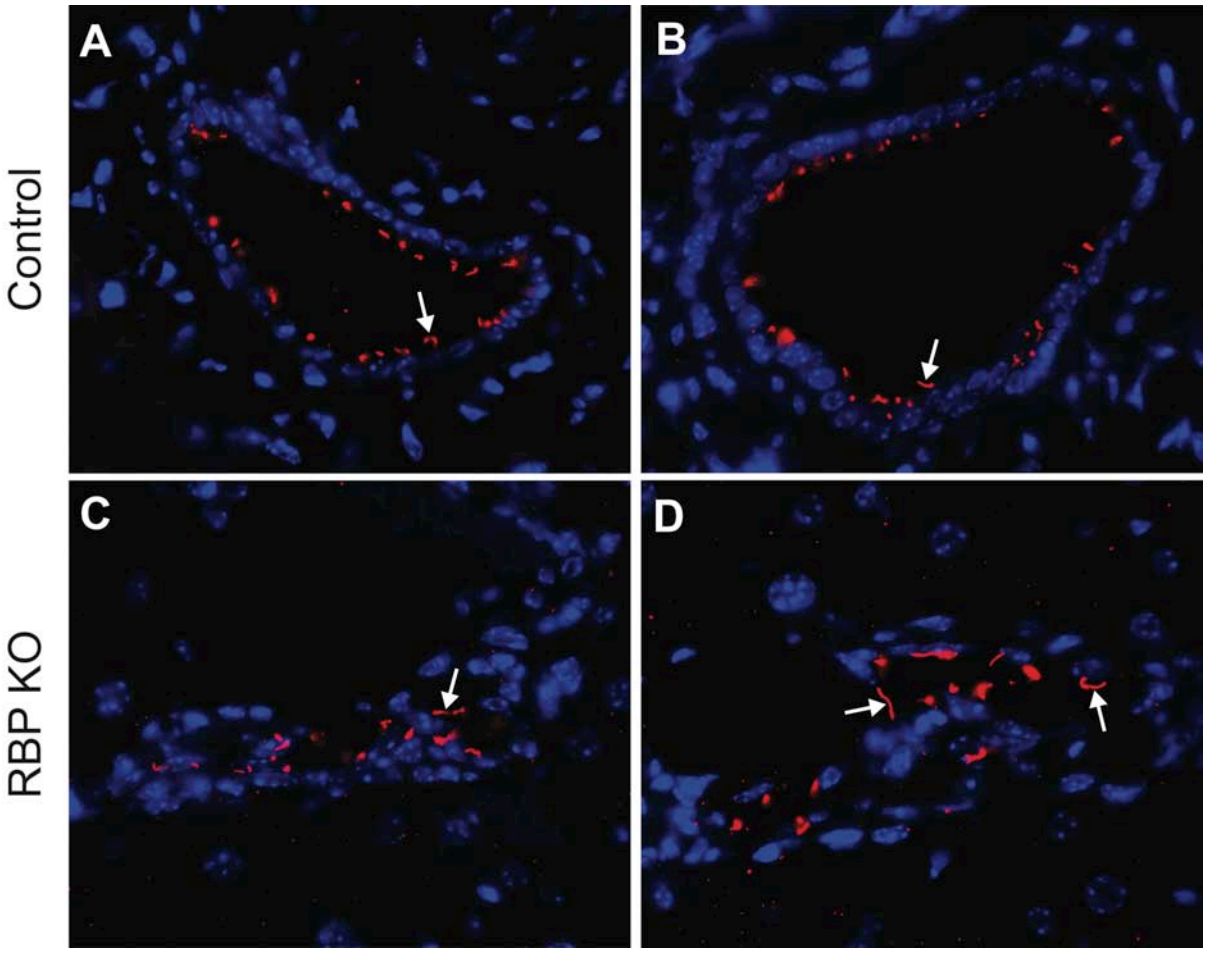

Figure 5.14 RBP KO mice appear to have longer cholangiocyte cilia at P120 compared to control. Paraffin-embedded tissue was immunostained for Arl13b to mark cilia. (A-B) Control sections demonstrate small cilia, with the longest indicated by the arrow. (C-D) In contrast, RBP KO sections demonstrate long cilia, as indicated by the arrow.

developmentally for the lineage restriction of properly functioning cholangiocytes, or 3. Post-natal obstruction defects are secondary to the ductular malformations resulting from loss of Notch signaling. To investigate the requirement of Notch signaling in adult cholangiocytes, I utilized a mouse model which allows spatial and temporal deletion of RBP-J via a Cytokeratin19-CreERT2 (*K19-CreERT2;RBP-J$^{flox/flox}$* [RBPΔK19]) (Means et al., 2008). While the Cytokeratin19-CreERT2 is expressed in a multitude of tissues as assessed by ROSA26 Reporter (R26R) expression, within the liver it is specifically expressed in cholangiocytes (data courtesy of Teagan Walter). To address the effects of deleting RBP-J in the adult mouse, Tamoxifen was administered every other day for 4 days at 4mg per injection to P30 or P60 mice. This approach achieves <50% recombination as assessed by R26R expression (data courtesy of Teagan Walter).

At three months post-injection, RBPΔK19 mice were analyzed to determine if similar defects to RBP KO mice were observed. Initial analysis of liver function tests suggests no difference in ALT, TB or ALP levels between control (Tamoxifen-treated) and RBPΔK19 mice (Table 5.1). Histological analysis of mice administered Tamoxifen at P30 and sacrificed at P120, revealed no overt ductal deformation or architectural defects (Figure 5.15). However, as noted in RBP KO mice, intra-luminal blockage may not be apparent in histological section, and the definitive experiment is resin casting. At three months post-Tamoxifen, with injections beginning at P60, resin casts from P150 RBPΔK19 mice are visually normal as compared to Tamoxifen injected littermate controls (Figure 5.16), however quantitative microCT analysis has not been performed, therefore subtle defects cannot be discounted. Unfortunately at 3 months post-Tamoxifen injection, RBPΔK19 mice develop keratinous cysts in the muzzle, paws and tail, and must be euthanized. Thus, this mouse model can only demonstrate that within three-months at approximately 50% recombination, there are no obvious ductal differences noted in RBPΔK19 mice.

Genotype	n	ALT	n	TB	n	ALP
Control (+TAM)	2	79.0 ± 12.3	1	0.429	1	5.6
RBPΔK19 (+TAM)	3	64.0 ± 19.3	3	0.418 ± 0.08	3	4.2 ± 2.6

Table 5.1 Serum chemistry analysis. Serum was obtained from control (Tamoxifen-injected) and RBPΔK19 (Tamoxifen-injected) mice and analyzed for alanine aminotransferase (ALT), total bilirubin (TB), and alkaline phosphatase (ALP). Values are mean (IU/L) ± standard error of the mean. P values are calculated by a student *t*-test.

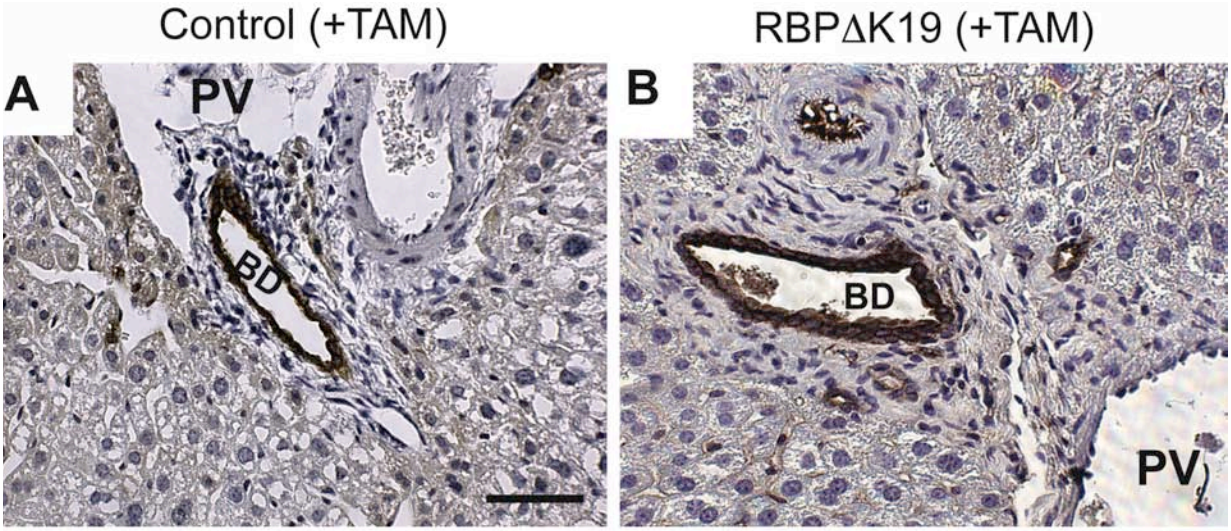

Figure 5.15 RBPΔK19 mice have normal bile duct morphology. Control and RBPΔK19 mice were administered Tamoxifen (TAM), 4 x 4 mg, every other day at P30, and analyzed at P120. Paraffin-embedded tissue was immunostained for cytokeratin19 to mark ductal cells. (A) The administration of TAM to control mice did not alter bile duct morphology. (B) The deletion of RBP-J within the adult cholangiocyte has no effect on bile duct morphology. PV – portal vein, BD – bile duct. Scale bar = 50 μm.

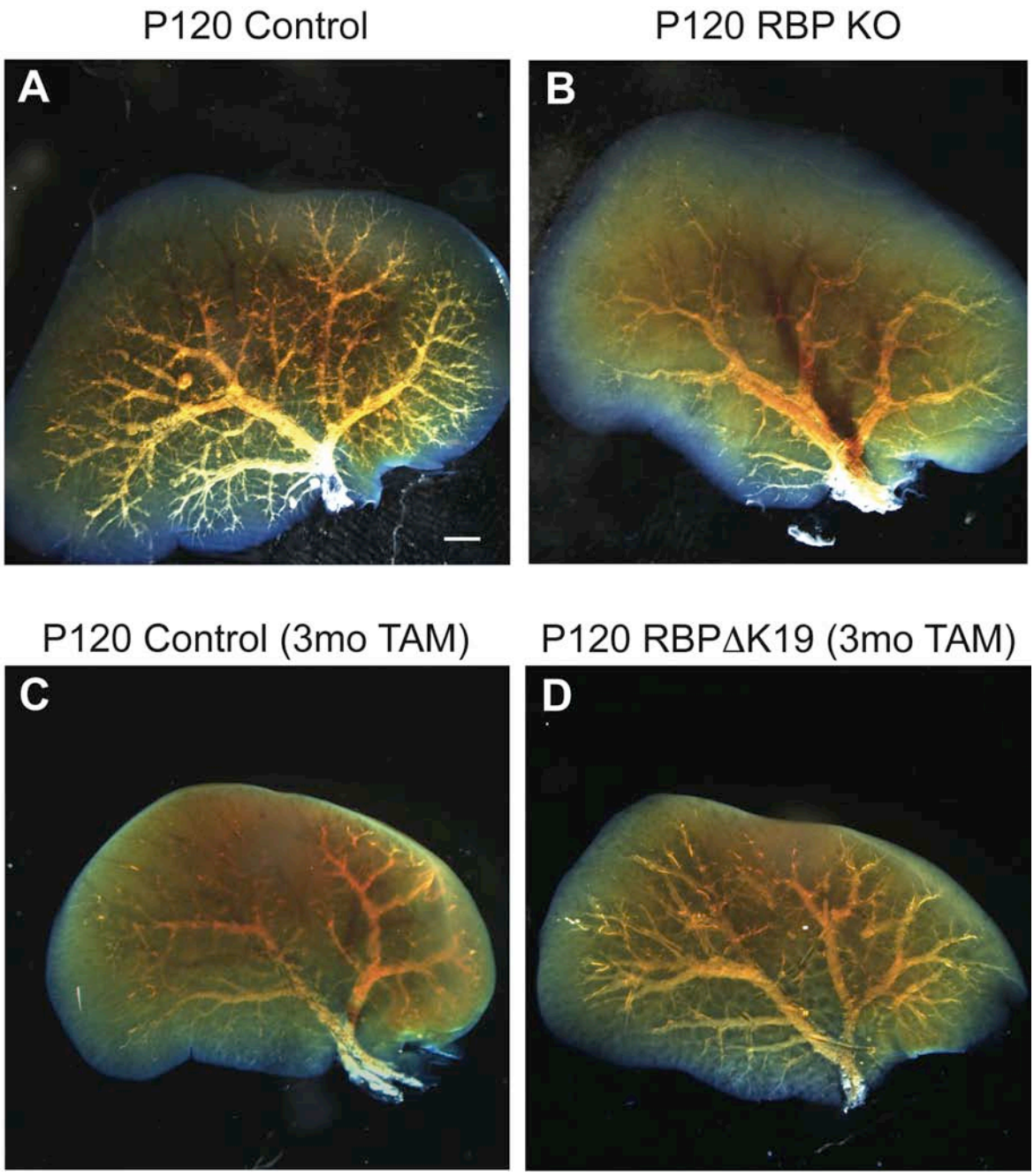

Figure 5.16 RBPΔK19 mice have no gross defects in IHBD architecture. Resin casts were BABB cleared and imaged. (A) P120 control resin casts demonstrate normal biliary architecture. (B) P120 RBP KO resin casts demonstrate the extreme paucity as described previously. (C-D) Control and RBPΔK19 mice were administered Tamoxifen (TAM), 4 x 4 mg, every other day at P60, and analyzed at P150. (C) The administration of TAM to control mice does not appear to affect the gross IHBD structure. (D) RBPΔK19 do not demonstrate structural defects, as observed in RBP KO mice. Scale bar = 2 mm.

RBPΔK19 data suggests that Notch is not required for adult cholangiocyte function, however it does not distinguish between the other models as to the developmental requirement of Notch signaling. Therefore, I investigated the possibility that Notch signaling is required for cholangiocyte lineage restriction and thus required to specify functional cholangiocytes. Utilizing the same candidate approach for components of the bile acid metabolism pathway mentioned earlier in this chapter (Figure 5.12), I investigated the mRNA expression in P15 control and RBP KO mice. Interestingly, there is no detectable difference in gene expression between control and RBP KO mice at P15 (Figure 5.17). This data suggests that the components of the bile acid metabolism pathway that are dysregulated in RBP KO mice at P120 are not due to improper lineage restriction. Together these data suggest a model in which an acquired post-natal obstruction is secondary to the ductular defects resulting from loss of Notch signaling.

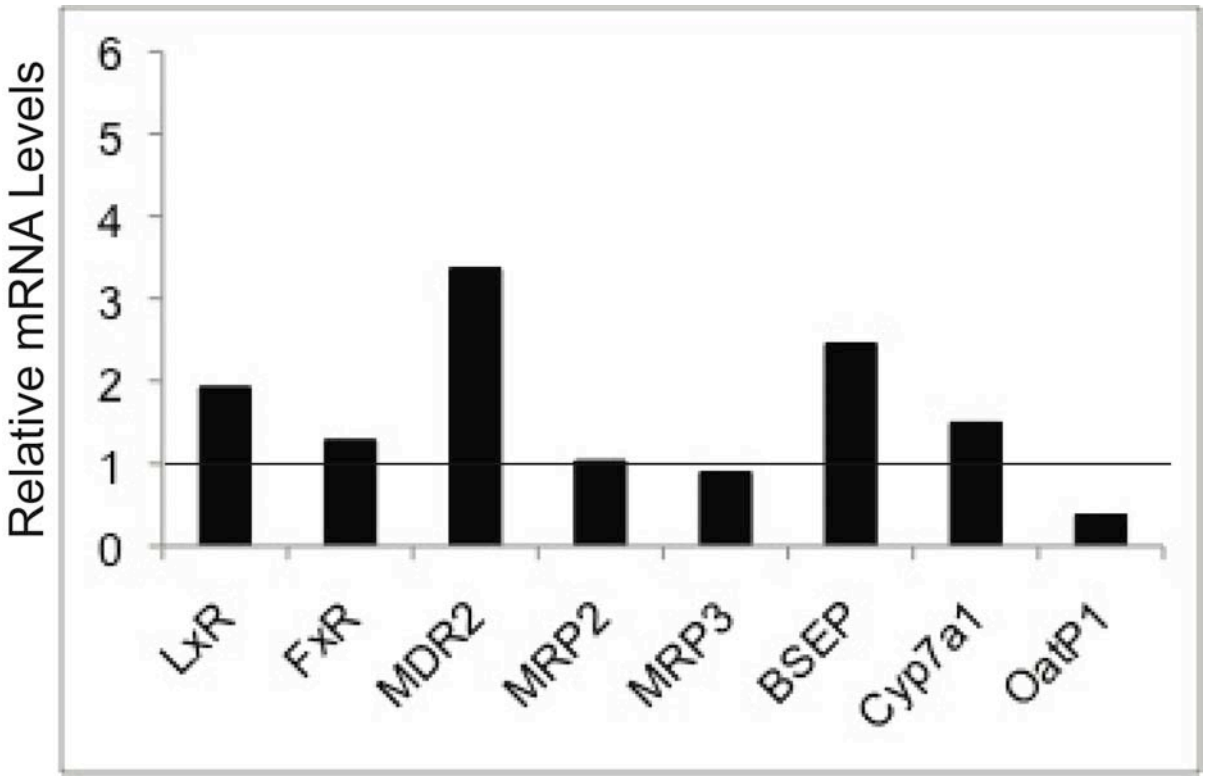

Figure 5.17 Bile acid metabolism components mRNA expression is unchanged at P15 in RBP KO total liver as compared to control. The relative expression ratio of bile acid metabolism components was calculated using real-time PCR efficiency and the deviation in cycle threshold (Ct) of RBP KO versus control samples, expressed in comparison to GAPDH mRNA levels. At P15, none of the bile acid metabolism components are elevated in RBP KO compared to control. Horizontal line represents control value.

Discussion

Developmental loss of Notch signaling results in progressive obstructive cholestasis

A progressive obstructive phenotype, as observed in RBP KO mice can be explained by one of three models: 1. At focal points within the ductal structure, the bile ducts are constricted and do not allow resin to pass, potentially due to fibrotic constriction, 2. Focal cellular loss results in disconnection of the communicating structure or 3. Intraluminal obstruction prevents the resin from completely filling the distal branches of the IHBD. Analysis of collagen deposition in P120 RBP KO mice suggests that ductal constriction due to fibrosis is not a likely scenario (Figure 5.1). Therefore to identify what is occurring at the site of obstruction, I undertook a method of tracing flourescent resin through the tissue. Using this approach, I was able to provide evidence that the progressive obstruction of IHBD structure observed in RBP KO mice is due to an intraluminal impediment as observed by inspissated material accumulation at the point of cessation of luminal resin (Figure 5.4).

It is surprising to note that the absence of resin is initially observed in the center of the duct, suggesting that the obstruction is more tightly associated with itself than the epithelium. This indicates that the obstructive material is likely not due solely to mucinous accumulation (Figure 5.13), which I would expect to be more closely associated with the biliary epithelium than itself. Further, a less viscous liquid, such as the dye CFDA, which is diluted in PBS, is able to pass the obstruction, suggesting this is not an impassable blockage depending on the viscosity of the liquid (Figure 5.6). While this analysis has lent insight into the character of the obstruction, the source remains to be determined.

Improper bile acid metabolism is not the source of obstruction.

Bile acid analysis suggests that the composition of bile within the liver and gallbladder remain in the normal range. Further confirmation of this finding is observed with mRNA expression of bile acid metabolism components. Interestingly, components that increase both the uptake and export of bile acids are increased in RRB KO livers, suggesting an upregulation of genes to generally increase hepatocyte function.

I was intrigued to note a general increase of bile acids, conjugated and un-conjugated within the serum (Figure 5.11). A failure of the hepatocytes to uptake bile acids from the enterohepatic circulation would result in increased serum bile acids, which is consistent with no changes in other routes of excretion. However, it is surprising that the increase in total bile acids is due to increase in both conjugated and un-conjugated bile acids. If the increased bile acids were due to defects in hepatocyte function, either impaired uptake or release of bile acids, I would expect to see either conjugated or un-conjugated bile acids increase. I propose that one or two different mechanism may contribute to the increase in both conjugated and un-conjugated bile acids within the serum. The first contributing factor may be that RBP KO mice have a reduced number of portal veins per millimeter (Please Refer to Chapter IV, Figure 4.11 B), therefore I speculate that the reduction of portal veins results in a decreased enterohepatic circulation. A second contributing factor maybe defects in the sinusoids or bile canaliculi, which would allow bile acids to leak back into the circulation instead of being transported to the biliary tree. These data support the hypothesis that a reduction in the enterohepatic circulation accounts for the increased serum bile acids observed in the RBP KO mice, and I postulate that this is due to a two-fold process: reduction in portal veins and damage to sinusoids and/or canaliculi.

Analysis of bile acid levels does not preclude the possibility that bile is the source of obstruction. It remains feasible that the regulation of other bile components and/or regulation of bile flow contributes to the obstructive phenotype. In light of this, I observe an increase in

mucinous ducts (Figure 5.13), as well as longer cholangiocyte cilia in P120 RBP KO mice (Figure 5.13). As mentioned earlier in this discussion, mucous production alone is not sufficient to explain the obstructive phenotype, however it may contribute in the context of other defects. One of the other defects that may contribute is abnormal cilium (Figure 5.14).

An alternative hypothesis is that the luminal obstruction is due to cellular debris. As documented in Chapter IV, RBP KO cholangiocytes have increased turnover at P120 compared with control cholangiocyte (Please refer to Chapter IV, Figure 4.8). Since the accepted idea within the field is that apoptotic cells are shed into the lumen (Strazzabosco et al., 2000), I posit that an increase in cellular debris can also lead to the obstructive phenotype observed in RBP KO mice. However the exact nature of luminal obstruction in RBP KO mice remains to be determined.

Notch signaling may not be required for adult cholangiocyte function

The requirement of chronic Notch signaling for the progressive obstruction observed adult RBP KO mice could be attributed to one of three models. The first model suggests there is a requirement of Notch signaling for the function of cholangiocytes in the adult. The second model posits that Notch signaling is required developmentally for the lineage restriction of properly functioning cholangiocytes and thus affects adult function. Finally, the third model suggests that post-natal obstruction defects are secondary to the ductular defects but independent of Notch signaling.

To investigate the first model, that Notch signaling is required in the adult cholangiocyte for proper function, I used a mouse model that allowed temporal deletion within the adult cytokeratin19-positive population. Examination of ductal morphology at 3 months post-Tamoxifen injection, revealed no obvious ductal defects by cytokeratin19 immunohistochemical analysis and resin casting (Figure 5.15-5.16). However, I cannot rule out that observation over a longer time course would result in loss of the communicating

ductal structure. Unfortunately, this mouse model has limitations due to the formation of keratinous cysts on the muzzle, paws and tail, independent of a liver phenotype. Further Cre recombination efficiency is poor in the adult, presumably due to the quiescent nature of cholangiocytes (Please refer to Chapter IV, Figure 4.8). Therefore, while the definitive role of Notch signaling in the adult cholangiocytes remains to be fully defined, at this juncture, my results indicate that Notch signaling is dispensable for adult cholangiocyte function.

The second model of how Notch contributes to the adult phenotype is in the initial lineage restriction of cholangiocytes. This model suggests that loss of Notch signaling results in immature, improperly functioning cholangiocytes. To investigate this possibility, I examined the mRNA expression of the bile acid metabolism genes, which are up-regulated in the adult RBP KO liver (Figure 5.12). Interestingly, there are no detectable differences in gene expression at P15, suggesting that improper liver function is a product of an acquired defect, not improper lineage decision (Figure 5.17). However, it is important to note that the components of the bile acid metabolism pathway analyzed here are restricted to hepatocytes. At this time, I have not defined specific molecular defects within cholangiocytes, therefore I cannot directly assess defects associated with improper lineage restriction within the cholangiocyte population. These data make the assumption that if cholangiocyte defects result in liver dysfunction, and the cholangiocyte defects are due to improper lineage restriction, that at P15 the liver dysfunction would be observable. However, without definitive results as to the mechanism of biliary obstruction, it is difficult to fully define the requirement of Notch signaling in the adult obstructive phenotype.

Within this chapter, I have begun to investigate the underlying mechanism of biliary obstruction as described in Chapter IV. This investigation is two-fold; first in the discovery of the source of obstruction, and second into the precise requirement of Notch signaling in this phenotype. While at this juncture, I am unable to make irrefutable conclusions; I have outlined my future directions to further refine these conclusions in Chapter VI.

CHAPTER VI

SUMMARY AND FUTURE DIRECTIONS

Hepatobiliary disease and in particular cholangiopathies are a prevalent health concern in the United States. While a variety of insults, both genetic and exogenous, can result in cholangiopathies, a common pathology is associated with all cholangiopathies. These pathologies include inflammation, cholestasis, fibrosis, and apoptosis (Strazzabosco et al., 2005). In particular, cholestasis, or the reduction in bile flow, is a very important clinical consideration. Cholestasis can result from impaired bile formation at the level of the hepatocytes, or defects in bile regulation or flow at the level of the cholangiocytes. As the diagnosis of cholangiopathies is the number one predictor of pediatric liver transplant and the number three predictor of adult liver transplant (Bogert and LaRusso, 2007), understanding the pathogenesis of the disease is critical for future therapeutics.

In particular, one genetic cholangiopathy to which much effort has been devoted is Alagille syndrome (AGS). Mutations in the Notch pathway are causative of AGS, thus providing a tool to study how bile duct morphogenesis is regulated. The bulk of my studies have been focused on defining the role of Notch signaling in the development and maintenance of biliary formation and structure.

Initially, I defined the cell-autonomous requirement of Notch signaling within the liver progenitor hepatoblast population for bile duct development and the formation of the biliary architecture. These results revealed the three-dimensional (3D) effect of genetic modulations in Notch signaling and demonstrated that the level of Notch signaling correlates with a dose-dependent reduction in peripheral branch density in IHBD resin casts. The underlying two-dimensional (2D) morphology suggests a threshold requirement for Notch signaling in cholangiocyte specification and bile duct formation; in the absence of all Notch

signaling, fewer cholangiocytes are specified, however when limited levels of Notch signaling remain, cholangiocytes are specified but cannot remodel. Together these results indicate that the level of Notch signaling contributes to the variable clinical severity of AGS patients.

To investigate the post-natal consequence of improper bile duct development, my studies transitioned into the examination of the adult phenotype as a result of chronic loss or gain of Notch signaling. The first observation of note was a reduction in the intact IHBD architecture with age in the complete absence of Notch signaling. These results were consistent with a progressive paucity described in AGS patients (Dahms et al., 1982), however I was surprised to determine that the loss of intact structure was not due to ductopenia. Instead, I have identified a progressive obstructive phenotype with the complete loss of Notch signaling. The source of this obstruction and the source of dysregulated signaling are the focus of my future investigations as discussed below.

Overall, the clinical outcome of AGS patients into adulthood has not been well described. Thus understanding the post-natal consequence of improper bile duct development is critical to predict the outcome of adult AGS patients. Further, my results suggest that the progressive obstructive phenotype is independent of a direct requirement for Notch signaling. Thus, I have defined a general model of acquired cholestasis that can be utilized to identify new therapeutics and test the effectiveness of current therapeutics. Currently, the most common model to study obstructive cholestasis is the bile duct ligation (BDL) model. This model is generated by the surgical constriction of the common bile duct, thus mechanically disrupting bile flow out of the liver. As this model utilizes a physically imposed constriction, it cannot be used to identify new therapeutics, as the obstruction could not be relieved by a therapeutic. Thus, the further characterization of the progressive obstructive mouse model is critical to define a non-surgical model of general cholestasis.

Future Directions

Identification of Obstructive Material

The future directions of this work include first and foremost the identification of the source of obstruction. As outlined in Chapter V, I hypothesize that the obstructive material is either improperly formed bile or cellular debris. I have ruled out the possibility that hepatocyte defects contribute to improper bile formation. However, it remains possible that the cholangiocytes are unable to generate an osmotic gradient and control the water content of the bile. As this regulation is intimately tied to the presence and proper function of cholangiocyte cilia, I will examine the mutant cholangiocytes for cilia defects. This approach will be two fold; first I will quantitate the number and length of cholangiocyte cilia in control and RBP KO mice. Second, a collaborator in Australia, Alessandra Warren, is performing scanning electron microscopy (SEM) on control and RBP KO liver tissue. I anticipate being able to characterize any cilia defects by the coordinated effort of these two approaches.

The other potential source of obstructive material is cellular debris as a result of increased cholangiocyte turnover. To investigate this possibility, I plan to collect bile by fasting mice for four hours and collecting the bile accumulating in the gallbladder. I will then cytospin the bile and stain for DNA content. While bile collection by this method is not ideal, as I have no evidence that cellular debris would enter the gallbladder, the other method by which to collect bile requires a non-survival surgery, in which animals are under anesthesia for extended periods of time with a catheter attached to the common bile duct to collect bile, which we are not approved to perform at this time.

Together, I anticipate these experiments will reveal the source of the biliary obstruction. However, a third option is to perform imaging mass spectrometry on the obstruction as identified by tracing the fluorescent resin. Unfortunately due to the harsh

nature by which the tissue is treated to identify the obstruction, and the size of the obstruction, I am unsure how much information this approach will be able to provide.

Acute Requirement of Notch Signaling

The second immediate future direction is to further define the role of Notch signaling within the adult cholangiocyte. My attempt to address this question *in vivo* by cholangiocyte-specific deletion of RBP-J in the adult was disappointing due to off-target skin defects. Thus, to further refine the acute role of Notch signaling *in vivo*, I have undertaken the analysis of a mouse model that both activates and removes Notch signaling within the hepatoblast. By both activating and removing Notch signaling, this allows cholangiocytes to be specified and remodeled, but subsequently cannot utilize Notch signaling. My initial characterizations of this model are described in Appendix C. At this junction, I can confirm that bile ducts are formed, but in depth analysis remains to be completed.

To supplement the rather unconventional *in vivo* approach, I will also address the requirement of Notch signaling *in vitro* in cultured cholangiocytes. I have successfully implemented a cholangiocyte isolation technique in our laboratory (Please refer to Appendix F). This isolation technique allows me to culture, not only single cells, but also intrahepatic bile duct units (IHBUs) (Cho et al., 2001). I will culture adult $RBP^{flox/flox}$ cholangiocytes and IHBUs with or without exogenous Cre. An alternative approach is to culture isolated RBPΔK19 cholangiocytes with or without 4-Hydroxytestosterone (4-OHT) to induce recombination. In single cell cultures, I will analyze proliferation and apoptosis to determine the role of RBP-J in adult cholangiocyte turnover. In IHBU cultures, I will analyze the ability of cholangiocytes to respond to exogenous secretin; the response will be monitored by the luminal expansion after treatment as previously described (Cho et al., 2001). This approach assumes a functional defect in the ability of RBP KO cholangiocytes to regulate the aqueous content of the bile.

Lastly, I plan to use these isolations to define global changes in gene expression within cholangiocytes. I will isolate cholangiocytes from P60 and P120 control and RBP KO mice, isolate the mRNA and perform RNA sequencing on the samples. This experiment will allow me to identify gene expression changes between control and RBP KO cholangiocytes, as well as any changes that may occur as the cholestatic phenotype progresses in RBP KO mice. I will also be able to use RNA sequencing to assess the gene expression changes in cultured adult cholangiocytes in which RBP-J has been acutely removed. The use of RNA sequencing allows characterization of all transcripts and avoids the limitations imposed by microarray technology which only asseses a subset of transcripts. Comparison of the expression profiles of P120 RBP KO cholangiocytes and P120 cultured cholangiocytes with acute loss of RBP-J will allow me to identify the acute changes in gene expression in cholangiocytes upon loss of Notch signaling. As mentioned in Chapter V, it remains possible that the progressive cholestatic phenotype due to chronic loss of Notch signaling results in improper lineage restriction of cholangiocytes. Thus RNA sequencing will allow me to globally address some of questions as to cholangiocyte identity and the acute requirement of Notch signaling by analyzing specific transcripts that are over- or under-represented in RBP KO cholangiocytes as compared to control. A caveat of this approach is that the heterogeneity of the cholangiocyte population, both in terms of hilar and peripheral cells as well as potential intra-ductal heterogeneity, is lost in this pooled analysis. Therefore, I may isolate cholangiocytes based on size or DBA-positivity to determine the difference in RNA profile within the heterogeneous population.

The coordination of these three approaches will allow me to determine the acute requirement of Notch signaling within adult cholangiocytes. If my preliminary results are correct, and the progressive obstruction is not due to an adult requirement of Notch signaling within cholangiocytes, then I will have defined a non-surgical model of progressive obstructive cholestasis.

Inflammatory-mediated Cholangiopathies

Another predominant finding in cholangiopathies is inflammation. In RBP KO mice, I observe hilar inflammation beginning at P15 and persisting throughout the life of the mice (Please refer to Appendix B). The inflammation is perplexing, as it is only observed at hilar ducts, which are completely formed, although tortuous (based on 2D analysis of cytokeratin19 expression), and patterned normally (based on 3D analysis of IHBD resin casts) in P120 RBP KO mice. Therefore, I am interested in pursuing the question of how inflammation contributes to cholestatic liver disease. Two future directions exist within this project; first to define the origin and identity of the inflammatory cells, and second to define the physiological consequence of inflammation.

The origin and identity of the inflammatory cells has been the subject of some investigation by myself. As inflammation is observed early and persists, the source of the immune cells could be attributed to improper maintenance of a hematopoietic stem/progenitor cell niche or persistent homing of immune cells in response to cholestasis. To address the possibility that RBP KO mice improperly maintain a hematopoietic stem/progenitor cell niche, I isolated non-parenchymal cells and assessed their ability to form colonies in methylcellulose cultures. Colony formation in methylcellulose cultures indicates the presence of a myeloid stem/progenitor cell. In RBP KO methylcellulose cultures of non-parenchymal cells, there was no statistical difference in the number of colonies formed compared to control. This suggests that the observed inflammatory cells in tissue section are not due to the maintenance of a hematopoietic stem/progenitor cell niche. Thus, my results suggest that inflammatory cells observed in RBP KO mice are due to a homing of immune cells into the liver as a result of liver injury. To confirm this possibility, I have undertaken bone marrow transplants of GFP-labeled bone marrow cells into sub-lethal irradiated RBP KO mice. I will assess the ability of GFP-positive immune cells to home to the liver at 1 week and 4 weeks post-transplant.

The effect of inflammation on the progression of cholestatic liver disease has been minimally documented. For example, one study determined that inflammatory cells modulate the expression of hepatocyte transporters leading to improper bile formation and subsequent obstruction in a mouse model of biliary atresia (Yang et al., 2009). In this study, transporters were down-regulated as a consequence of inflammation. In contrast, RBP KO up-regulate hepatocyte transporter expression, suggesting the potential for an alternative influence of inflammation in cholestasis.

To further address the role of inflammation in the RBP KO cholestatic phenotype, I plan to assess the levels of common inflammatory cytokines (i.e. TNF-alpha, IL6) in whole liver mRNA from control and RBP KO mice. Upon determination of the increase in an inflammatory cytokine, I will exogenously add that cytokine to cultures of wild-type cholangiocytes and assess the effects on proliferation, apoptosis, and secretion. Additionally, I will attempt to co-culture wild-type cholangiocytes with isolated wild-type or RBP KO non-parenchymal cells and assess the effects on proliferation, apoptosis and secretion.

At this juncture, the specific identity of immune cells, whether macrophages, monocytes, etc., is unknown. I have examined markers of individual hematopoietic cell fates by immunohistochemistry, however the staining was either negative or did not work for technical reasons. Thus another future direction is to define the specific cell type, isolate by fluorescence-activated cell sorting (FACS) and co-culture specific immune cell types with the isolated cholangiocytes. Unfortunately a caveat of this study is that the majority of antibodies that recognize subsets of hematopoietic cells specifically recognize cells from the C57/B6 strain background mice, and our mice are on a CD1 outbred strain background. Therefore identification of specific cell types requires back-crossing onto a C57/B6 strain background. I have performed cytospins of non-parenchymal liver cells and determined a general increase in all cell types based on morphology, however immunofluorescent confirmation of this has

been limited due to the specificity of antibodies. Therefore a future direction, and future project, is to define the role of inflammation in the RBP KO model of obstructive cholestasis.

Therapeutic Screens

The RBP KO model provides many interesting future directions in terms of developing therapeutics. As mentioned in the introduction, the most prevalent treatment for cholestasis is the administration of bile acid binding resin or secondary bile acids. Therefore, an important next step is to administer cholestyramine (a bile acid binding resin) or UDCA (a secondary bile acid) to RBP KO mice and assess by resin casting whether these therapeutics relieve the obstruction. Interestingly, the mechanisms by which cholestyramine and UDCA alleviate cholestasis are not well understood. Thus a well-characterized model of progressive obstructive cholestatic liver disease such as the RBP KO will be useful not only to identify how current therapeutics are mediating therapeutic benefits, but also to identify similar or completely different drugs that may be used to alleviate biliary obstruction.

APPENDIX A

TIMING AND EXTENT OF GENE DELETION BY THE ALBUMIN-CRE TRANSGENE

Introduction

As discussed in the Introduction, there is a deficiency of Cre lines that mediate specific recombination of loxP sites within the liver (Please refer to Introduction: Molecular Cue for Bile Duct Development, *Notch Signaling in Cholangiocyte Development: the Signal-Receiving Cell*). Thus the issue of timing and extent of gene deletion is very important for the interpretation of experimental results. I have made use of the *Albumin-Cre* (*Alb-Cre*) transgene to generate mice with chronic deletion or activation of Notch signaling. Alb-Cre was originally designed to facilitate gene recombination within the adult hepatocytes (Postic et al., 1999). The initial report investigating recombination of the glucokinase locus, revealed by Southern Blot analysis, to quantify gene recombination, that full recombination (90%) did not occur until 6 weeks of age, with 40% recombination at P1 (Postic and Magnuson, 2000). However as this analysis was performed on whole liver genomic DNA from C57/Bl6 strain background mice, it is impossible to determine the level of recombination specifically in the liver epithelial lineage. Thus my further characterization of this Cre line is discussed within this appendix.

Results

Timing and extent of deletion mediated by *Alb-Cre* was first assessed using the ROSA26-LacZ reporter (R26R). In this mouse model, the beta-galactosidase gene preceded by a floxed STOP cassette is knocked-in to the ROSA26 locus (Soriano, 1999). Upon Cre expression, the STOP cassette is deleted by permanent recombination of the genetic locus, and beta-galactosidase is expressed. This technique permanently labels cells expressing the Cre and their progeny. Using this approach, *Alb-Cre* is expressed in the majority of hepatoblasts at E16.5 (Figure A.1 A). To further confirm the expression within hepatoblasts, I analyzed P30 tissue, and identified lineage labeled cells within the bile duct (Figure A.1 B). As Albumin is not expressed in cholangiocytes, recombination must have occurred in the hepatoblast for expression in the adult cholangiocytes. These results are in contrast to the original characterization that suggests gene recombination is occurring only in the hepatocyte.

While R26R expression serves as an indicator for the timing of Cre expression, the LacZ reporter expression is not necessarily directly correlative to other genetic loci. Therefore, I first analyzed the recombination of the Notch1 and Notch2 loci in P120 control and N1/N2 DKO cholangiocytes. I used laser capture microdissection (LCM) to capture hilar and peripheral ducts as identified by morphology (Figure A.2 A-D). DNA was isolated from the captured tissue and analyzed for the amplification product resulting from the recombined Notch1 or Notch2 genomic loci (quantitative PCR analysis performed by Kari Huppert). This analysis revealed that significantly more recombination of both the Notch1 and Notch2 loci in both hilar and peripheral regions as compared to control (Figure A.2 E-F). These data further support the expression of the *Alb-Cre* transgene in the hepatoblast population prior to the bi-potential decision to differentiate into cholangiocytes or hepatocytes.

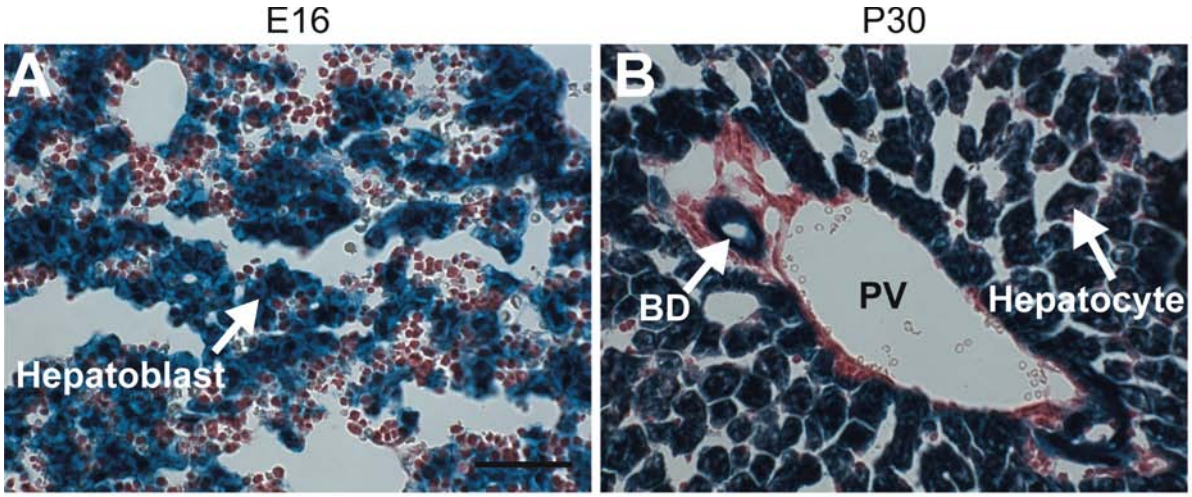

Figure A.1 Alb-Cre-mediated recombination results in hepatoblast-specific recombination. Panels demonstrate X-gal detection of Cre-inducted recombination of the ROSA26-LacZ reporter allele in frozen sections with a nuclear fast red counterstain. (A) At E16, hepatoblasts (arrow) stain blue indicating recombination of the reporter. Cells that are not X-gal positive are hematopoietic cells, as the liver is the major site of hematopoiesis at this age. (B) At P30, the two derivatives of the hepatoblast lineage, hepatocytes (arrow) and cholangiocytes (indicated as BD), are X-gal positive. Cells that are not X-gal positive are non-hepatoblast-derived, forming hepatic arteries, portal veins, mesenchymal cells surrounding the portal triad or the endothelial and stellate cells in the parenchyma. PV – portal vein, BD – bile duct. Scale bars = 50 μm.

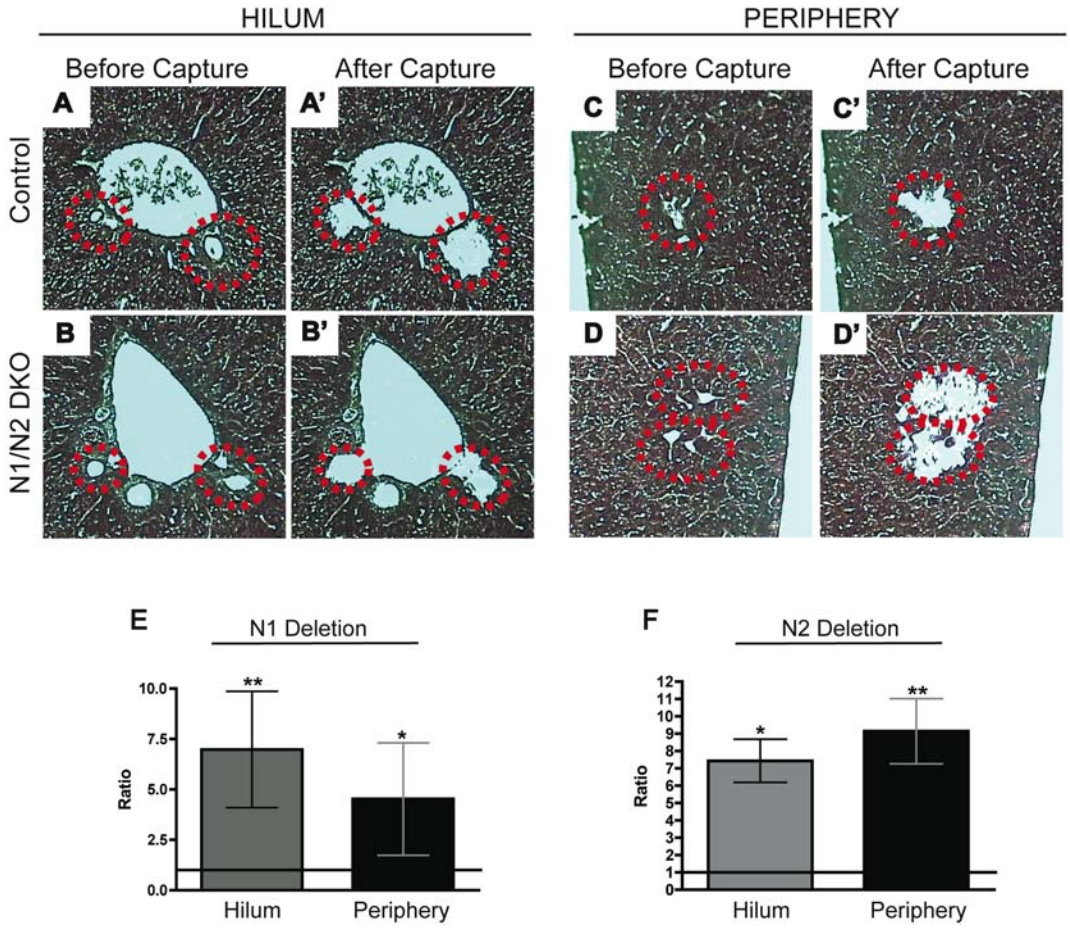

Figure A.2 Laser capture microdissection of P120 liver. Paraffin sections from the left lobe of control (Notch1$^{flox/flox}$;Notch2$^{flox/flox}$, A,C) and N1/N2 DKO (Alb-Cre;Notch1$^{flox/flox}$;Notch2$^{flox/flox}$, B,D) were rehydrated, hematoxylin and eosin stained, and dehydrated. Bile ducts, identified by morphology from hilum (A-B) and periphery (C-D) were dissected. (A-D) Representative tissue regions before and (A'-D') after capture. Dotted lines indicated specific region of capture. DNA was isolated from capture tissue using the Picopure kit. Three slides of two mice per genotype were captured. (E-F) Quantiative genomic PCR results of Notch1 (E) and Notch2 (F) deletion at the hilum and periphery demonstrate significant deletion at both regions. Statistical analysis was performed using a one-way ANOVE with Tukey's Multiple Comparison test. Error bars – standard error of the mean. *$p \leq 0.05$, **$p \leq 0.01$.

LCM analysis could not be used to assess the recombination of the RBP-J locus, as peripheral ducts are too few. Instead, genomic recombination of the RBP-J was assessed by whole liver analysis. Genomic DNA was isolated from at least three different mice per genotype (control [*RBP-J*$^{flox/flox}$] and RBP KO [*Alb-Cre;RBP-J*$^{flox/flox}$]) at E14, E15, and E16. Quantitiative PCR analysis was used to determine the amount of genomic recombination at the RBP-J locus compared to control (Figure A.3 A). Surprisingly, as early as E14, I can detect a significant level of recombination. The amount of recombination is progressively increased with age, however as this analysis was performed on whole liver DNA, the increase in recombination with age could be attributed to an decreased ratio of non-epithelial cells in the liver. However, these results suggest that Albumin promoter-driven Cre is expressed even earlier than previously supposed.

To assess whether the adult cholangiocytes that compose patent bile ducts in RBP KO mice have experienced Cre expression, I crossed the RBP KO mice to the R26R-YFP reporter mice (Srinivas et al., 2001), and examined reporter expression at P60 and P120 (Figure A.3 B-E). The lineage-traced YFP expression is observed in peripheral ducts at P60 and P120 (Figure A.3 B,D). Interestingly in hilar ducts, a few cells have escaped recombination, however these cells are found at P60 and P120, and do not appear to preferentially expand with age (Figure A.3 B',D'). Thus these results suggest that cells, which have expressed Cre in their lineage, compose the majority of adult cholangiocytes both in the peripheral and hilar ducts.

For NICD mice, the Notch1 intracellular domain preceded by a floxed STOP cassette and followed by an internal ribosomal entry site (IRES) GFP was knocked into the ROSA26 locus (Murtaugh et al., 2003). Monitoring the expression of the Notch1 intracellular domain in NICD mice was achieved by analyzing expression of the IRES-GFP. In NICD mice, GFP expression is observed at E16.5 at various levels in the majority of hepatoblasts (Figure A.4 C). At P3, the expression of GFP can be detected in both ductal and parenchymal cells,

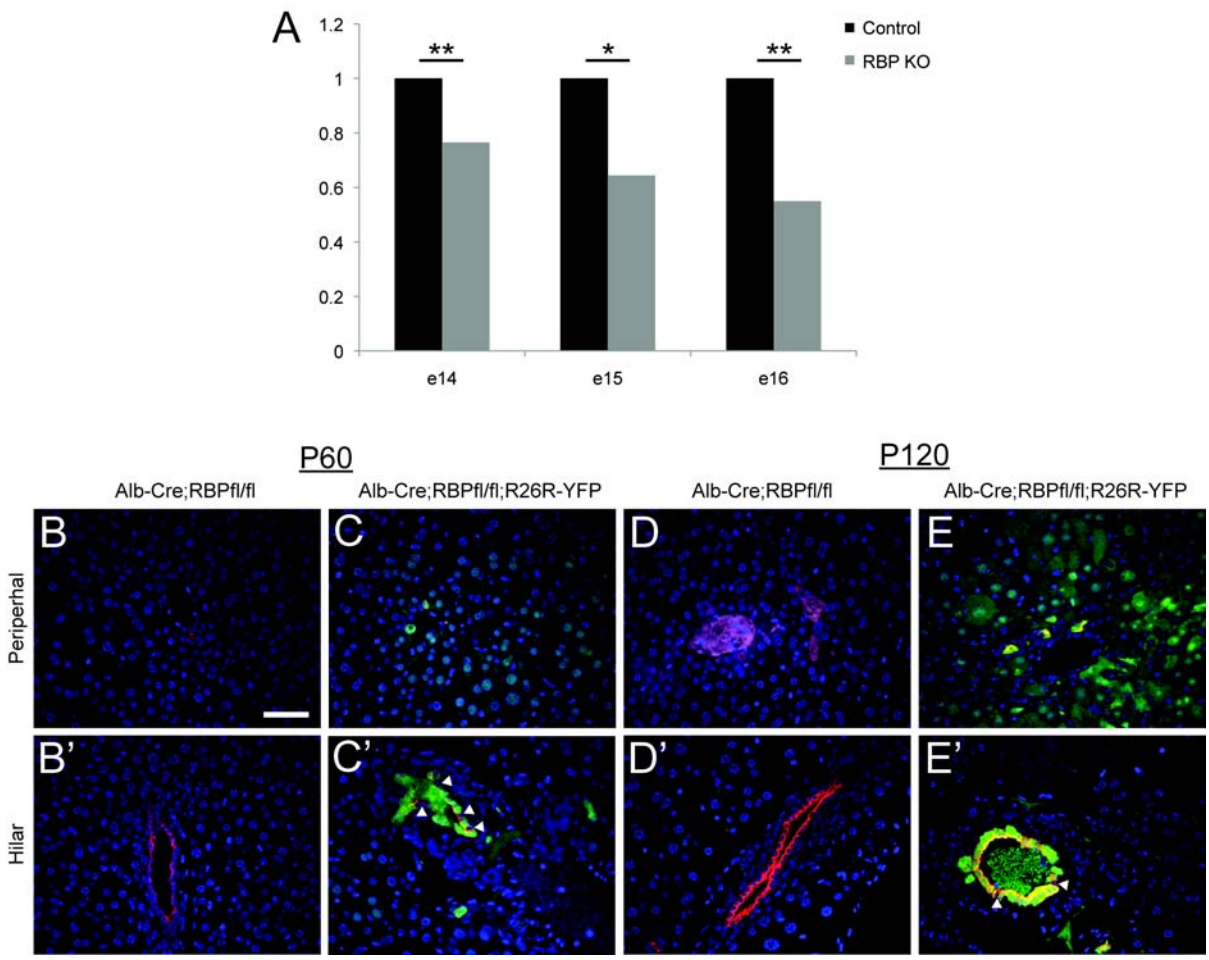

Figure A.3 Alb-Cre-mediated recombination of the RBP-J conditional allele. (A) Quantitative PCR analysis of genomic DNA isolated from whole liver at E14, E15 and E16. Whole liver analysis demonstrates that Cre-mediated recombination of the RBP-J locus begins at E14. (B-E) Co-immunfluorescence for GFP and cytokeratin19 in P60 and P120 livers. (B,D) RBP KO mice without R26R-YFP reporter activity demonstrate no reactivity with the GFP antibody. (C,E) RBP KO mice with R26R-YFP demonstrate reporter expression in peripheral and hilar ducts. At P60 and P120, a small number of cells do not express reporter in hilar ducts, suggesting that these cells have escaped recombination (arrowhead). Non-GFP-positive cells have not been observed in peripheral cytokeratin19-positive ductal calls. Scale bar = 50 μm. *$p \leq 0.05$, **$p \leq 0.01$.

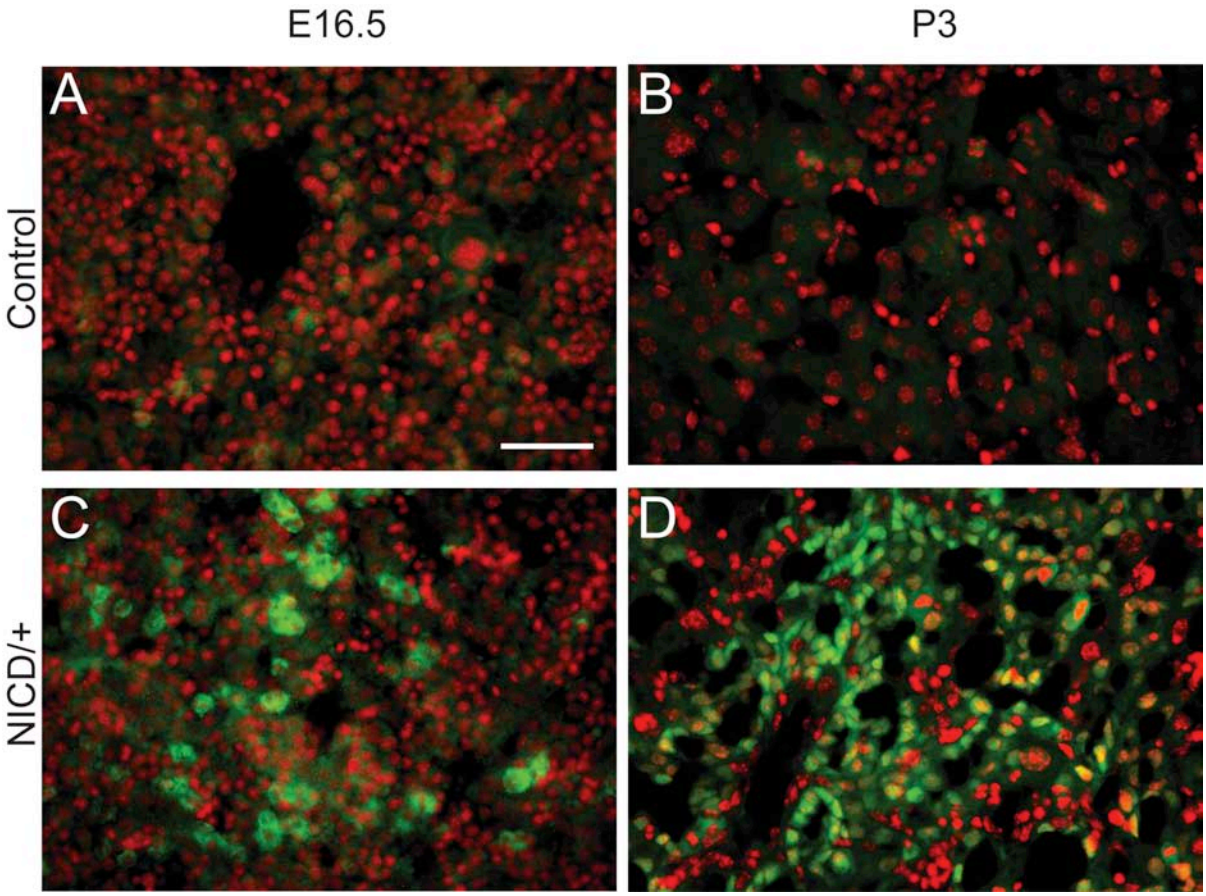

Figure A.4 Alb-Cre-mediated recombination of the ROSA26^{Notch1} conditional allele. Immunofluorescent staining for GFP expression expressed from the ROSA26^{Notch1} internal ribosomal entry site. (A) E16.5 and (B) P3 control liver tissue demonstrates no GFP expression. (C) E16.5 and (D) P3 NICD liver tissue shows expression of GFP. Scale bar = 100 μm.

based on morphology (Figure A.4 D). Thus, in NICD mice, GFP-expression can be extrapolated to infer NICD expression by Alb-Cre-mediated recombination of the ROSA26 locus, and can be identified as early as E16.5.

Discussion

Analysis of both reporter expression and specific loci recombination by *Alb-Cre* suggests efficient recombination by E16.5. Thus timing of genomic recombination can be determined by these approaches. Unfortunately, I have not been able to examine the extent of specific recombination at early time points. Further, while I can demonstrate genomic recombination of the RBP-J locus as early as E14, the half-life of RBP-J messenger RNA and protein is currently unknown. The lack of antibodies for immunohistochemical analysis has hindered my ability to identify protein expression in the RBP KO mice. Therefore, the timing at which RBP-J protein is no longer present is currently unknown.

An additional caveat of these results is contribution of non-epithelial liver cells, which have not recombined the genetic loci, to expression levels. While LCM allowed me to focus more specifically on ductal regions, I cannot obtain single cell resolution due to the limits of the LCM equipment and the highly fibrous nature of the liver. Thus, I made various attempts to use fluorescence activated cell sorting (FACS) to isolate cholangiocytes. Unfortunately, a poor cholangiocyte cell yield (<0.3% in control) and poor cell quality after sorting has made FACS unfeasible. I have recently learned a cholangiocyte cell isolation technique based on magnetic cell sorting, which allows for a good cell yield and the ability to culture after isolation (Please refer to Appendix F). For future experiments, I plan to isolate ductal cells and analyze both the recombination of the genetic loci as well as culture and troubleshoot antibodies.

Materials and Methods

Beta-Galactosidase Activity and Immunofluorescence

Liver tissue was fixed for 4 to 6 hours at 4ºC in 4% formaldehyde. To detect ROSA26-LacZ reporter activity, tissue was washed in PBS, equilibrated in 30% sucrose, and embedded in optimal cutting temperature (OCT) compound. Frozen, 10 µm sections were incubated with 2 mM $MgCl_2$, 5 mM potassium ferricyanide, 5 mM potassium ferrocyanide, 0.1% Triton-X 100, and 1 mg/ml X-gal in PBS, and color development was monitored. Sections were post-fixed and counterstained with nuclear fast red.

For the detection of the ROSA26-YFP reporter in RBP KO mice, tissue was fixed at 4ºC overnight in 4% paraformaldehyde. Paraffin-embedded tissue was sectioned at 6 µm, and subjected to antigen retrieval with 100 mM Tris, pH 10 at 60ºC overnight. Slides were incubated overnight at 4ºC with rat-anti-cytokeratin19 (1:250; DSHB) and rabbit-anti-GFP (1:500; Novus) in a 1% BSA, 0.2% nonfat dry milk, and 0.3% Triton-X 100 in PBS. Slides were incubated overnight in the appropriate secondaries and incubated in bis-benzamide to label DNA.

For the detection of the IRES GFP expression in NICD mice, tissue was fixed at 4ºC overnight in 4% formaldehyde, equilibrated in 30% sucrose and embedded in OCT. Frozen, 10 µm sections were incubated overnight at 4ºC in chicken-anti-GFP (1:500; Abcam) in 1% BSA. Slides were then incubated overnight at 4ºC in anti-chicken-biotin secondary (1:500; Jackson Immunoresearch), followed by a 1 hour incubation with avidin-Cy3 (1:500; Jackson Immuno). Bis-benzamide was used to label DNA. Images were acquired using a Zeiss Axioplan2 microscope and QImaging RETIGA EXi camera.

Laser Capture Microdissection

Paraffin sections from the left lobe of control (*Notch1*$^{flox/flox}$*;Notch2*$^{flox/flox}$) and N1/N2 DKO (*Alb-Cre;Notch1*$^{flox/flox}$*;Notch2*$^{flox/flox}$) mice were sectioned, placed on non-charged glass slides and allowed to air dry overnight. Slides were hematoxylin and eosin (H&E) stained; slides were rehydrated (2 x 5' xylene, 2 x 5' 100% ethanol, 1 x 5' 95% ethanol), stained (3 quick washes in distilled water, 5 dips in hematoxylin, 3 quick washes in distilled water, 5 dips in eosin), and dehydrated (1 x 5' 95% ethanol, 2 x 5' 100% ethanol, 2 x 5' xylene). Slides were placed in a vacuum bell jar until capture. An average of 84 hilar and 164 peripheral regions were captured per mouse and pooled for quantitative PCR analysis. Average capture area was 33.3 μm and 36.2 μm for hilum and periphery, respectively.

Quantitative PCR analysis

For laser capture microdissection (LCM; Veritas Microdissection System, CapSure Macro LCM Cap) hilar and peripheral ducts were dissected from three slides per mouse and two mice per genotype. DNA was isolated using the Picopure kit (Arcturus). For detection of RBP-J deletion, I isolated genomic DNA from whole liver. 25ng of total DNA was used for quantitative PCR analysis using ABI Prism 7900. Primers used to detect deletion are identified in Table A.1.

Statistical Analysis

Genomic recombination in the N1/N2 DKO mice was subjected to a one-way ANOVA with Tukey's Multiple Comparison Test. Genomic recombination in the RBP KO mice was subjected a Students *t*-test. In both instances, a *P*-value of $\leq$0.05 was considered significant.

Primer	Forward (5' to 3')	Reverse (5' to 3')
Notch1 Del	TGG CCT GCC TGT CTG GAA CAA CAG TTC AGG	ACC CTT GCC TCA GTT CAA ACA CAA GAT ACG
Notch2 Del	TCA TCA CGC TCA GCT AGA GTG TTG TTC TTC	ATA ACG CTA AAC GTG CAC TGG AG
RBP-J Del	GAG ATA GAC CTT GGT TTG TTG	CCA CTG TTG TGA ACT GGC GT
RBP-J Ref	GCC ACT CCA TGT CCA AAA GA	GCA AGT TAT AGC TCA GAA CAG CAA
Beta-actin	TTC CTT CTT GGG TAT GGA AT	GAG CAA TGA TCT TGA TCT TC

Table A.1 Primers for quantitative genomic PCR. Primers used within this appendix are described.

APPENDIX B

CHARACTERIZATION OF THE IMMUNE RESPONSE IN RBP KO MICE

Introduction

The liver can be considered an important component of the immune system, as it hosts the largest population of tissue macrophages (Kupffer cells), dendritic cells, T lymphocytes, natural killer and natural killer T cells in the body (Szabo et al., 2007). All of these components, with the exception of T lymphocytes, are components of the innate immune system, and recognize invading pathogens. In cholangiopathies, a primary pathology and indicator for the progression of cholestasis is the presence of inflammation.

Understanding how inflammation contributes to the progression of cholestasis is an area of much study. The majority of work to determine the contribution of inflammation to cholestasis has focused on models with defective hepatocellular transport mechanisms or biliary atresia (Yang et al., 2009; Kosters and Karpen, 2010). Specifically, it has been well defined in both types of cholangiopathies that inflammation leads to the down-regulation of hepatocyte-specific bile acid metabolism pathway components, and subsequently a reduction in bile formation (Yang et al., 2009; Kosters and Karpen, 2010). Despite these recent advances, the effect of inflammation on cholangiocytes has not been investigated.

In the instance of chronic loss of Notch signaling (RBP KO), I observe an inflammatory response beginning at P15 and persisting through the lifespan of the mice. Interestingly, this inflammation is concentrated around hilar ducts, which have no significant alterations in IHBD patterning (Please refer to Chapter IV, Figure 4.12). Thus in this Appendix, I will describe my attempts to characterize the inflammatory response and consequence in RBP KO mice.

Results

RBP KO mice demonstrate an increase in non-hepatocyte, non-ductal cells at hilar portal triads visible at P15 and persisting until P120 (Figure B.1). At P15, the extra cells in RBP KO mice are concentrated within the confines of the portal triad (Figure B.1 B), yet by P120, they have also extended out into the parenchyma (Figure B.1 D). The identity of these cells could be either mesenchymal or immune in nature.

To investigate the possibility that these cells are an expansion of the mesenchymal cell compartment, I stained control and RBP KO tissue at P15 and P30 for desmin (Figure B.2). In the liver, desmin has been demonstrated to label three populations of fetal mesenchymal cells: hepatic stellate cells in the parenchyma, perivascular mesenchymal cells and submesothelial cells (Asahina et al., 2009). In control tissue, I can detect perivascular desmin-positive cells, however parenchymal hepatic stellate cells are only weakly visualized (Figure B.2 A-B). In RBP KO tissue, there is an increase in desmin-positive cells, however they are still concentrated periportally and reveal an increase in hepatic artery formation at P30 (Figure B.2 C-D). Therefore, an increase in the mesenchymal cell compartment is not sufficient to account for the increased non-hepatocyte, non-ductal cells in RBP KO mice. This result is consistent with the observation that RBP KO mice do not demonstrate an increase in fibrosis compared to control (Please refer to Chapter V, Figure 5.1).

To investigate the hypothesis that the increased non-hepatocyte, non-ductal cells in RBP KO mice are due to immune cells, I stained P15 control and RBP KO mice tissue with for CD45 (Figure B.3). CD45 is a protein tyrosine kinase found in all nucleated hematopoietic cells, therefore, not erythrocytes or platelets. In control tissue at P15, there are a few CD45-positive cells adjacent to the hilar bile ducts (Figure B.3 A) as expected due to the liver's general role in immunity. In contrast, in P15 RBP KO tissue, there is an

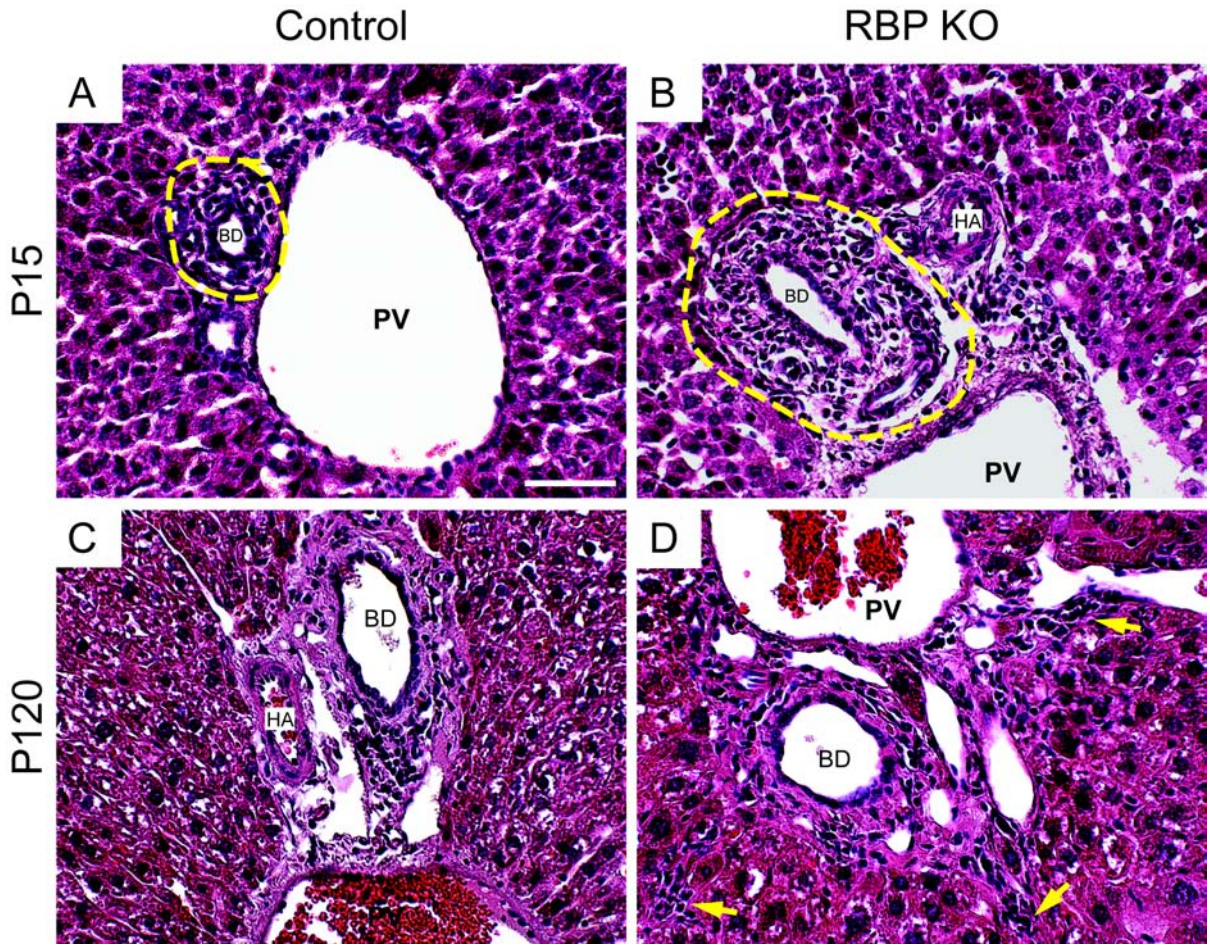

Figure B.1 RBP KO mice have an increase in cells with a high nucleo-cytoplasmic ratio at the portal vein visible at P15 and persisting until P120. Paraffin-embedded tissue from control and RPB KO mice at P15 and P120 was hematoxylin and eosin stained. (A-B) At P15, control tissue demonstrates a small amount of non-hepatocyte, non-ductal cells within the mesenchymal space. Conversely, RBP KO mice demonstrate an expansion of these cells. Area denoted by yellow dotted line. (C-D) at P120, there is still minimal non-hepatocyte, non-ductal cells within the control tissue, however these cells have persisted in RBP KO mice and now extend into the parenchyma (Arrows). PV – portal vein, BD – bile duct, HA – hepatic artery. Scale bar = 50 μm.

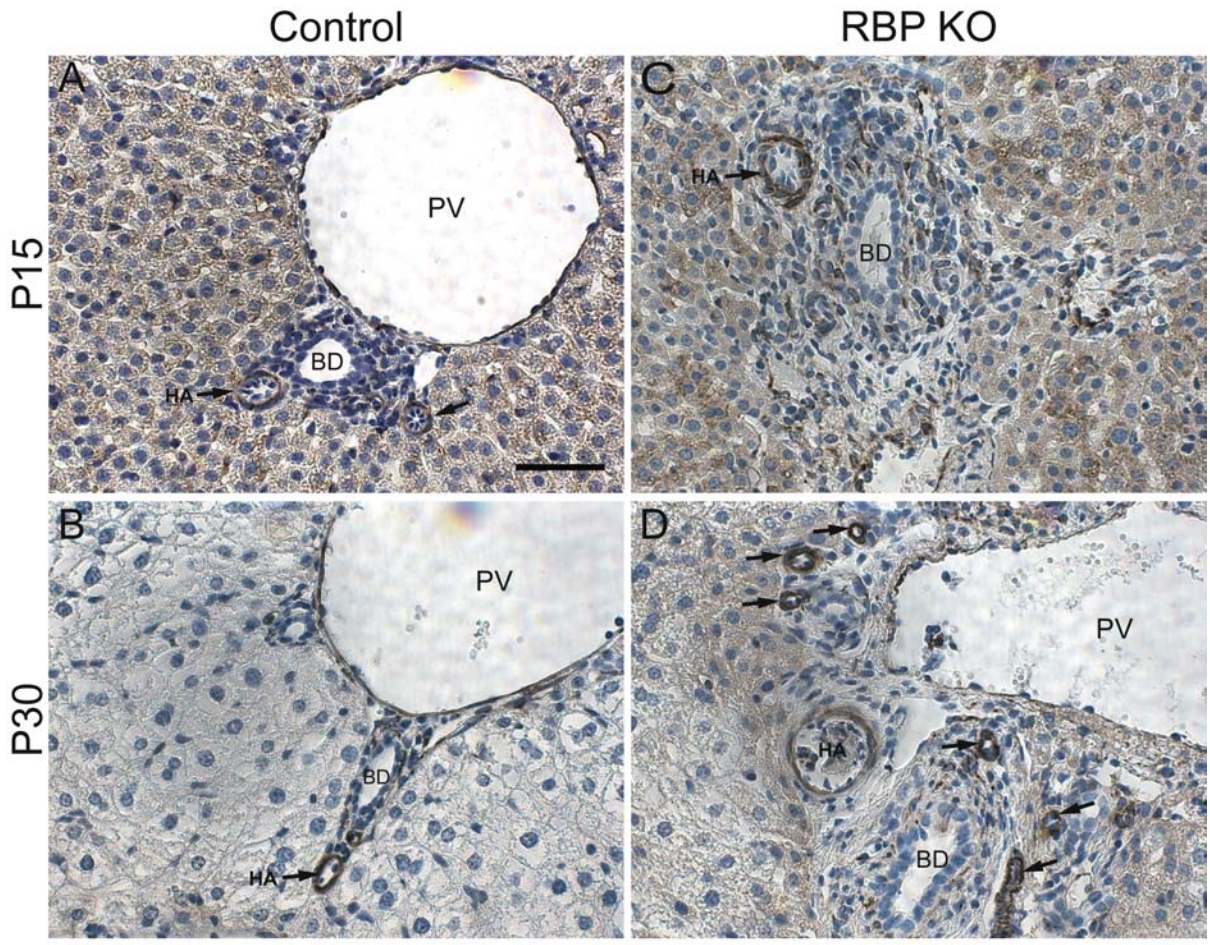

Figure B.2 Increased cells with a high nucleo-cytoplasmic ratio in RBP KO mice are not due to an expansion of mesenchymal cells. Paraffin-embedded tissue from control and RBP KO mice at P15 and P30 was immunostained for desmin to mark mesenchymal cells. (A-B) Desmin-positive cells, brown, in control at P15 and P30 specifically surround the hepatic artery (HA). (C-D) In RBP KO mice, despite the expansion of non-hepatocyte, non-ductal cells, there is not an increase in desmin-positive cells. PV – portal vein, BD – bile duct, HA – hepatic artery. Arrows – desmin-positive cells surrounding hepatic arteries. Scale bar = 50 μm.

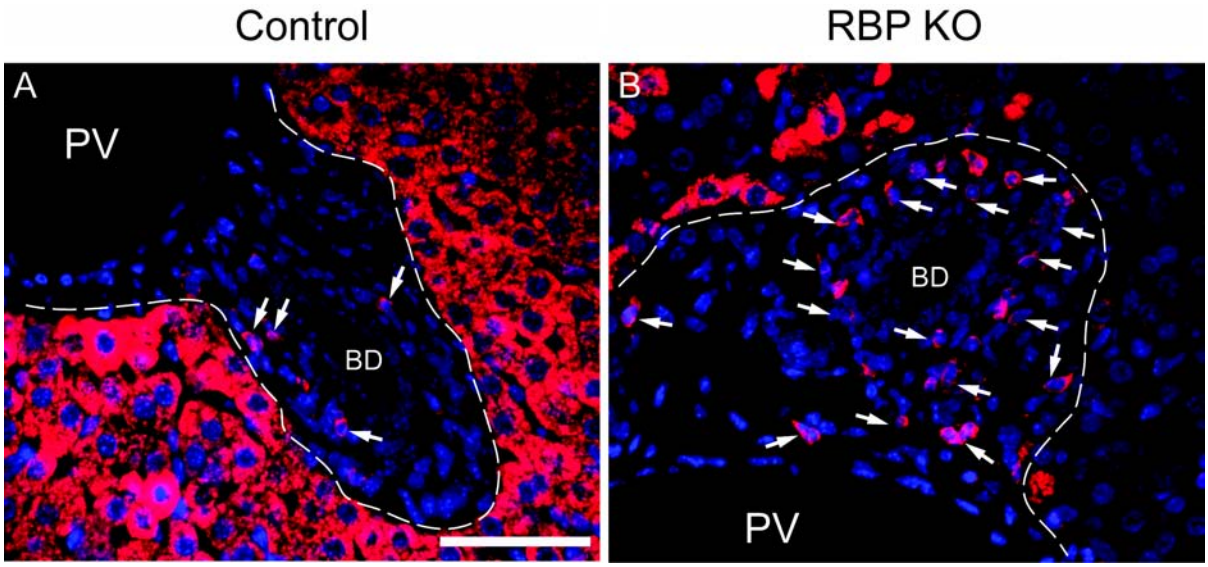

Figure B.3 Increased cells with a high nucleo-cytoplasmic ratio in RBP KO mice are due to immune cells. Paraffin-embedded tissue from control and RBP KO mice at P15 was immunostained for CD45 to generally mark cells from the hematopoietic lineage. (A) Control tissue demonstrates a few immune cells. (B) RBP KO tissue demonstrates a significant expansion in CD45-positive cells. PV – portal vein, BD – bile duct. Arrows – CD45-positive cells. Scale bar = 50 μm.

qualitative increase in the number of CD45-positive cells in the regions adjacent to hilar bile ducts (Figure B.3 B). These results suggest the increase in non-hepatocyte, non-ductal cells at the hilum in RBP KO mice is due to immune cells.

To characterize the immune response as innate or adaptive immunity, I undertook a series of approaches. First, I attempted to identify the specific type of immune cells by immunofluorescent techniques. I stained P30 control and RBP KO tissue with B220 to identify B cells, a component of adaptive immunity (Figure B.4). While B220-positive cells were readily identifiable in both control and RBP KO livers, there was no apparent increase in the number of B220-positive cells in RBP KO mice. Thus an increase in B cells is not sufficient to explain the increase in immune cells. In an attempt to further identify the immune cells with immunofluescence, I stained for markers of T-cells (CD4), monocytes (CD11b) and macrophages (F4/80). Unfortunately, I have been unable to work out staining conditions for these antibodies. A caveat of this approach is that most antibodies that have been raised against hematopoietic cells from C57/B6 strain background mice and may not cross-react with CD1 strain background mice.

A different approach that I used to identify the type of immune cells was to isolate cells <70 μm in size, cytospin and count the cells based on morphology (Figure B.5). Using this approach I can identify lymphocytes, neutrophils, eosinophils, monocytes, macrophages and promonocytes. Analysis of P9 control (*n*=2) and RBP KO (*n*=2) mice revealed that there was no change in the contribution of each cell type (Figure B.5 A), but instead there was an overall increase in the number of immune cells identified (Figure B.5 B). These results suggest that the immune infiltrate is composed of cells types from all lineages. A caveat of this approach is that I preformed analysis on P9 mice, and the immune response is more obvious later in development.

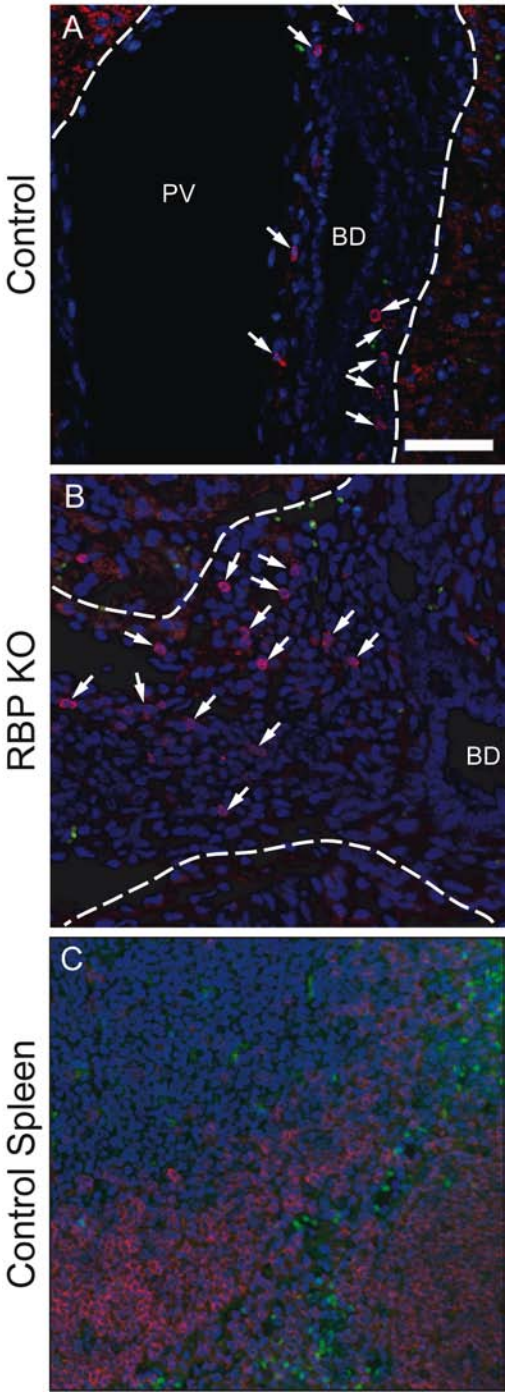

Figure B.4 RBP KO immune infiltration is not due to increased B cells. Paraffin-embedded tissue from control and RBP KO mice at P30 was immunostained for B220 to mark B cells. (A) Control liver tissue demonstrates a few B220-positive cells (Red). (B) RBP KO mice demonstrate a few B220-positive cells, but not enough to account for the total increase in immune cells. (C) Spleen was stained for B220 as a positive control (Red – B220, Green – red blood cell autofluorescence). PV – portal vein, BD – bile duct. Dotted line – boundary of non-hepatocyte tissue. Arrows – B220-positive cells. Scale bar = 50 μm.

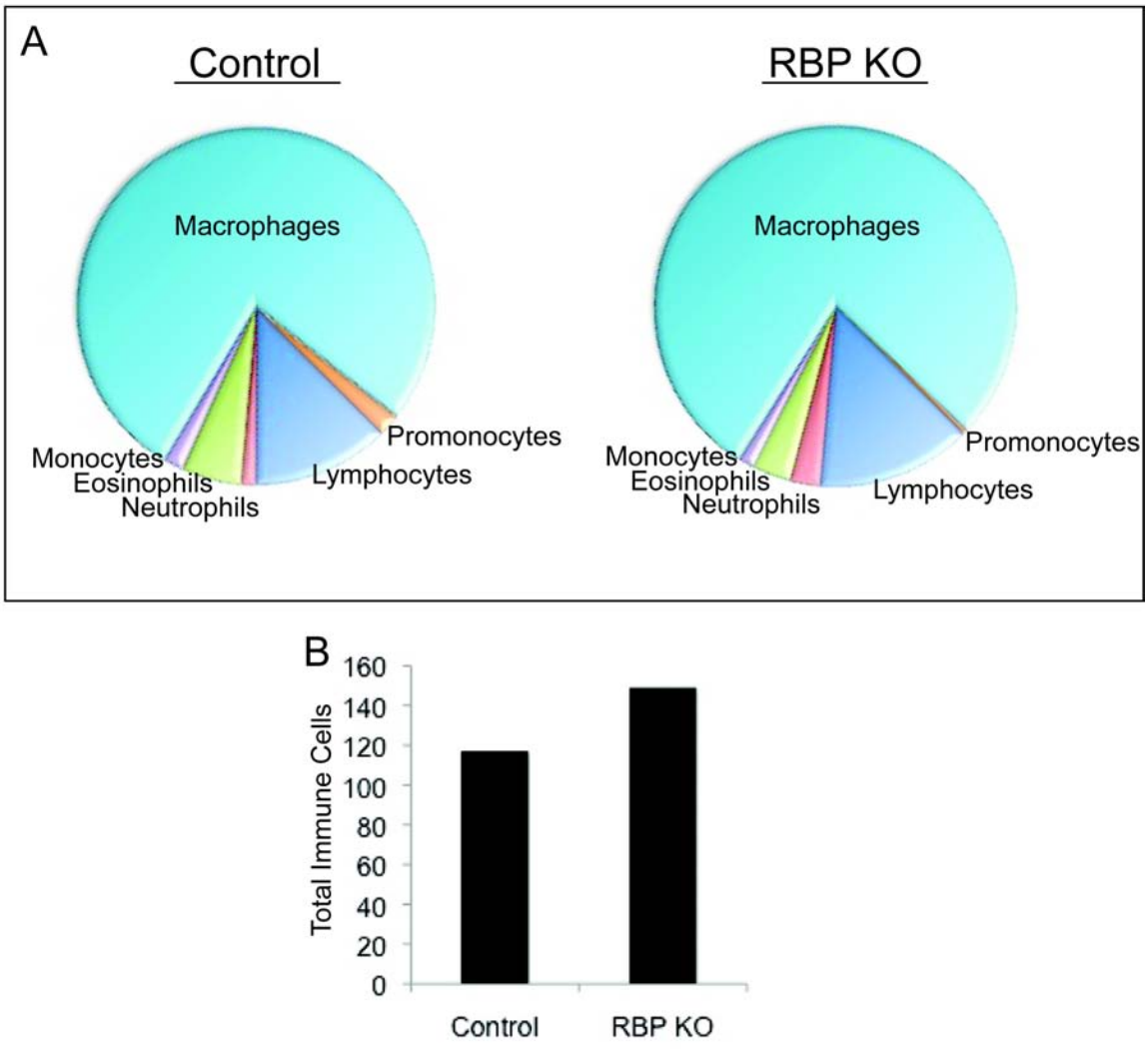

Figure B.5 Cytospin analysis of P9 RBP KO mice reveals a general increase in immune cells. Non-parenchymal cells were isolated from P9 control and RBP KO livers, cytospun and analyzed for morphology. (A) This technique allows identification of macrophages, monocytes, eosinophils, neutrophils, lymphocytes and promonocytes. The distribution of cells between control and RBP KO mice was not altered drastically. (B) The total number of immune cells was increased in RBP KO mice compared to control.

While it was originally presumed that the excess cells in RBP KO mice were a consequence of homing of immune cells to the liver, it remains possible that these cells are the result of improper maintenance of a hematopoietic stem/progenitor cell niche in the liver. The cytospin results suggesting a general increase in all types of immune cells supported this hypothesis. Therefore, to investigate the possibility that the immune cells are due to improper maintenance of a hematopoietic stem/progenitor cell niche, I isolated cells <70 μm in size from P15 control (*n*=5) and RBP KO (*n*=7) mice, and cultured the cells in methylcellulose to promote colony formation (Figure B.6). Using this approach, there was no significant difference in the number of colonies formed between control and RBP KO mice, thus suggesting the immune cells observed in RBP KO mice are not due to improper maintenance of a hematopoietic stem/progenitor cell niche.

Finally, I wanted to address whether the immune response was local or systemic. A systemic immune response would be identifiable by peripheral blood analysis. Therefore, I analyzed peripheral blood from P120 control (*n*= 9) and RBP KO (*n*=9) mice (Figure B.7). At P120, there is no difference in the amount of white blood cells (WBCs), suggesting that RBP KO mice do not have a systemic response. Lack of a systemic response, confirms localized inflammation, and an absence of infection.

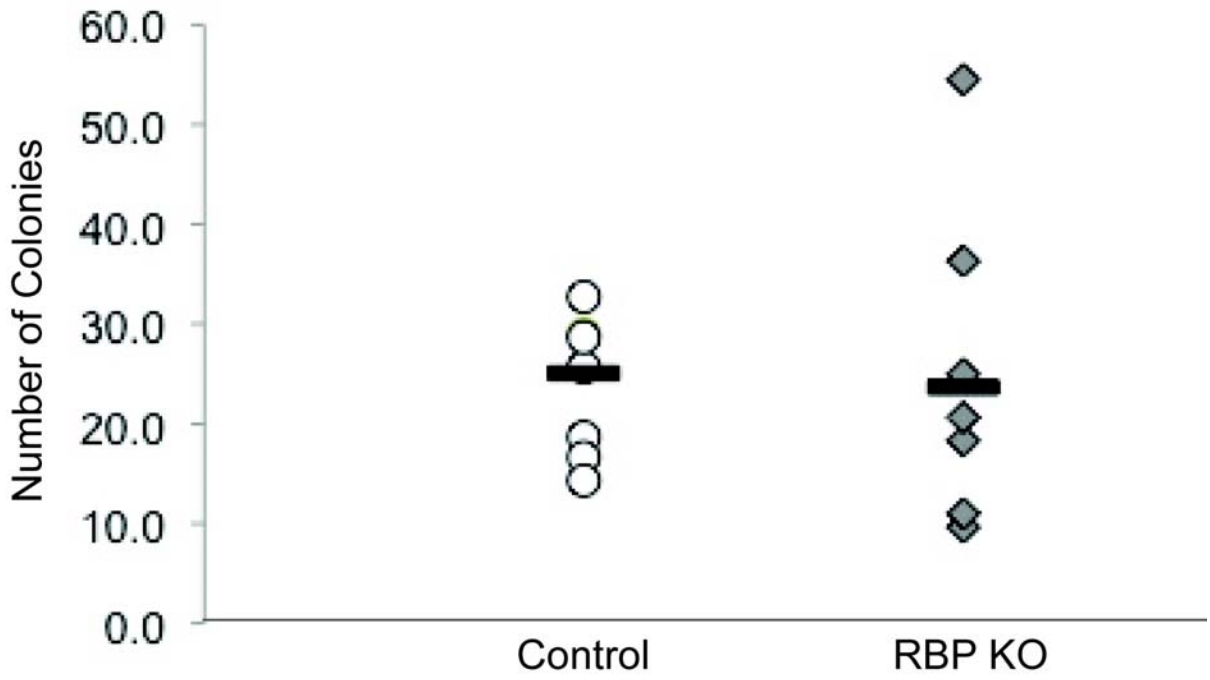

Figure B.6 RBP KO immune cells are not hematopoietic stem/progenitor cells. Non-parenchymal cells were isolated from P15 control and RBP KO livers and cultured in methylcellulose to promote colony formation. Analysis of the number of colonies after 13 days of culture reveals no difference in the number of colonies formed. Horizonal black line – average number of colonies.

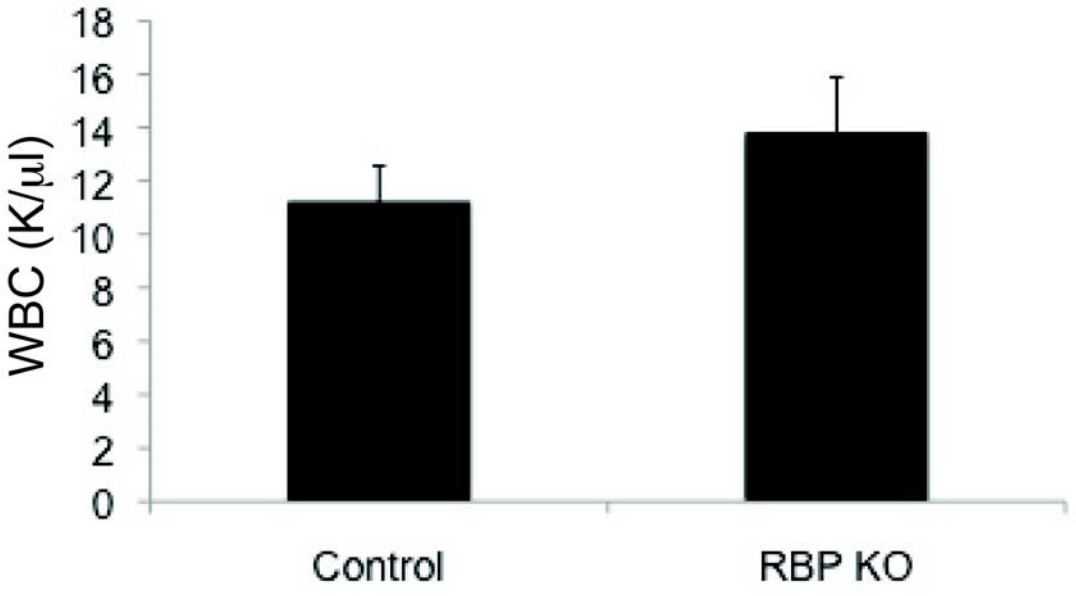

Figure B.7 The increased inflammatory cells in RBP KO mice do not result in a systemic response. Complete blood count (CBC) analysis of peripheral blood from P120 control and RBP KO mice reveals no difference in the number of while blood cells (WBC).

Discussion

At this juncture, I have determined that the increased non-hepatocyte, non-ductal cells in RBP KO mice are due to the presence of immune cells. In investigating the identity of these immune cells, I have determined that there is an increase in CD45-positive hematopoietic cells, but not due to improper maintenance of hematopoietic stem/progenitor cells. Interestingly, in cytospin analysis, it appears that all types of immune cells are increased in RBP KO mice compared with control (Figure B.5), however it is important to note that this analysis was done at P9 and merits being done again at later time points. Antibody identification of specific types of immune cells has proven difficult, as the antibodies are more often used for flow cytometry, and raised against C57/Bl6 strain background mice.

To determine if cells are continually homing to the liver in response to injury, I have performed bone marrow transplants of GFP-labeled bone marrow into sub-lethal irradiated P120 RBP KO mice. The results of this experiment are pending, but will reveal the nature of the immune response, whether a continual homing from the bone marrow, or a tissue-specific response. Further, chronic inflammation usually results in the transition from innate immune to adaptive immune responses (i.e. B and T cells) and the simultaneous destruction and healing of the offending tissue. Interestingly, I cannot observe the shift to adaptive immune, as assessed by the presence of B cells, and the consequence of inflammation on the ductal cells is not clear. I have, previously in this dissertation, suggested that RBP KO cholangiocytes increase their turnover with age (Please refer to Chapter IV, Figure 4.8), and I hypothesize that inflammation contributes to this phenotype. Therefore, in the future, I will analyze the inflammatory response and consequence on ductal cells in depth (Please refer to Chapter VI, Future Directions: *Inflammatory-mediated Cholangiopathies*).

Materials and Methods

Histology, Immunohistochemistry and Immunofluorescence

Liver tissue was fixed in 4% paraformaldehyde overnight at 4ºC. Paraffin-embedded tissue was sectioned at 6 µm. Hematoxylin and eosin staining was performed by standard histotechnology techniques (Carson, 1990).

For Desmin antibody staining, slides were subjected to antigen retrieval with 100 mM Tris, pH 10, overnight at 60ºC. Sections were incubated in primary antibody, goat-anti-desmin (1:100; Santa Cruz Biotechnology) overnight at 4ºC. Sections were incubated at room temperature for 4 hours in anti-goat-biotin secondary (1:1000; Jackson Immunoresearch), followed by incubation in Vectashield ABC reagent and developed with DAB substrate.

For CD45 antibody staining, freshly cut slides were subjected to antigen retrieval with 10 mM sodium citrate, pH 6 for 20 min in a rice cooker. Slides were incubated in primary antibody, anti-CD45-biotin (1:200; Biolegend) overnight at 4ºC. Slides were incubated at room temperature for 4 hours in streptavidin-Cy3 (1:300; Jackson Immunoresearch), followed by incubated in bis-benzamide.

For B220 antibody staining, freshly cut slides were incubated in primary antibody, anti-B220-biotin (1:50; aliquot courtesy of Dr. Sandra Zinkel) at room temperature for 1 hour. Slides were incubated at room temperature for 4 hours in streptavidin-Cy3, and then incubated in bis-benzamide.

Cytospins

For cytospin analysis, livers were removed from P9 mice and chopped coarsely in PBS with a razor blade. Livers were subsequently passed 6 times through a 21-gauge needle, and filtered through 70 µm cell strainers. Dissociated liver was placed in a 1.7 ml

Eppendorf tube and centrifuged for 5 min at 12000 rpm to pellet cells. Supernatant was discarded and cells were resuspended in 1 ml of red blood cell lysis buffer (Qiagen EL Buffer). After 5 min, total volume was brought up to 15 ml with water, and samples centrifuged at 12000 rpm for 5 min. Approximately 25,000 cells were resuspended in 1 ml of water and loaded into cytospin chambers. Cells were spun at 800 rpm for 5 mins. Slides were stained using a Hema3 Stat Pack (Fisher), and counted using the Atlas of Mouse Hematopathology as a reference guide (Fredrickson and Harris, 2000).

Methylcellulose Cultures

Non-parenchymal cells were isolated as described for cytospins. After counting, cells were resuspended in Dulbecco's Modified Eagle Medium (DMEM). Cells were mixed with 1.5 ml of methylcellulose optimized for the detection and quantification of erythroid progenitors, granulocyte-monocyte progenitors, and multi-potent granulocyte, erythroid, macrophage, megakaryocyte progenitors (MethoCult GF Stem Cell Technologies), and plated in triplicate. Colonies were counted at 13 day after beginning culture, and a colony was considered to be greater than 32 cells.

Complete Blood Count (CBC)

Blood was collected postmortem using a cardiac stick method. Whole blood was placed in tubes containing EDTA to prevent coagulation (Microtainer Tubes, Becton Dickinson). Samples were loaded into a Hemavet 950 CBC machine for complete blood analysis.

APPENDIX C

CHARACTERIZATION OF MICE WITH CHRONIC ACTIVATION AND DELETION OF NOTCH SIGNALING

Introduction

To address the requirement of Notch signaling subsequent to bile duct specification and remodeling, I analyzed a Cre line that allowed for gene recombination within the adult cholangiocytes (RBPΔK19). Unfortunately, analysis of this mouse line was limited due to the development of keratinous cysts (Please refer to Chapter V: *Post-natal cholangiocyte function does not require Notch signaling*).

An alternative approach to analyze the requirement of Notch signaling subsequent to the initial developmental requirement is to use the developmental *Alb-Cre* to both activate and delete Notch signaling (NICD/RBP). This mouse model was recently described in a model of osteogenesis, where it was used to determine that the effects of activating Notch signaling were solely dependent on RBP-J-mediated gene transcription (Tao et al., 2010). As *Alb-Cre* mediates deletion after the initial cholangiocyte specification and remodeling at the hilum, this provides a time period during which the Notch1 intracellular domain (NICD) is expressed and latent messenger RNA (mRNA) and protein expression of RBP-J allow for Notch signaling to be propagated (Figure C.1). When RBP-J transcript and protein turnover is complete, the ability for the NICD to signal via the canonical pathway is removed. Thus subsequent to the initial specification and remodeling of bile ducts, Notch signaling is removed.

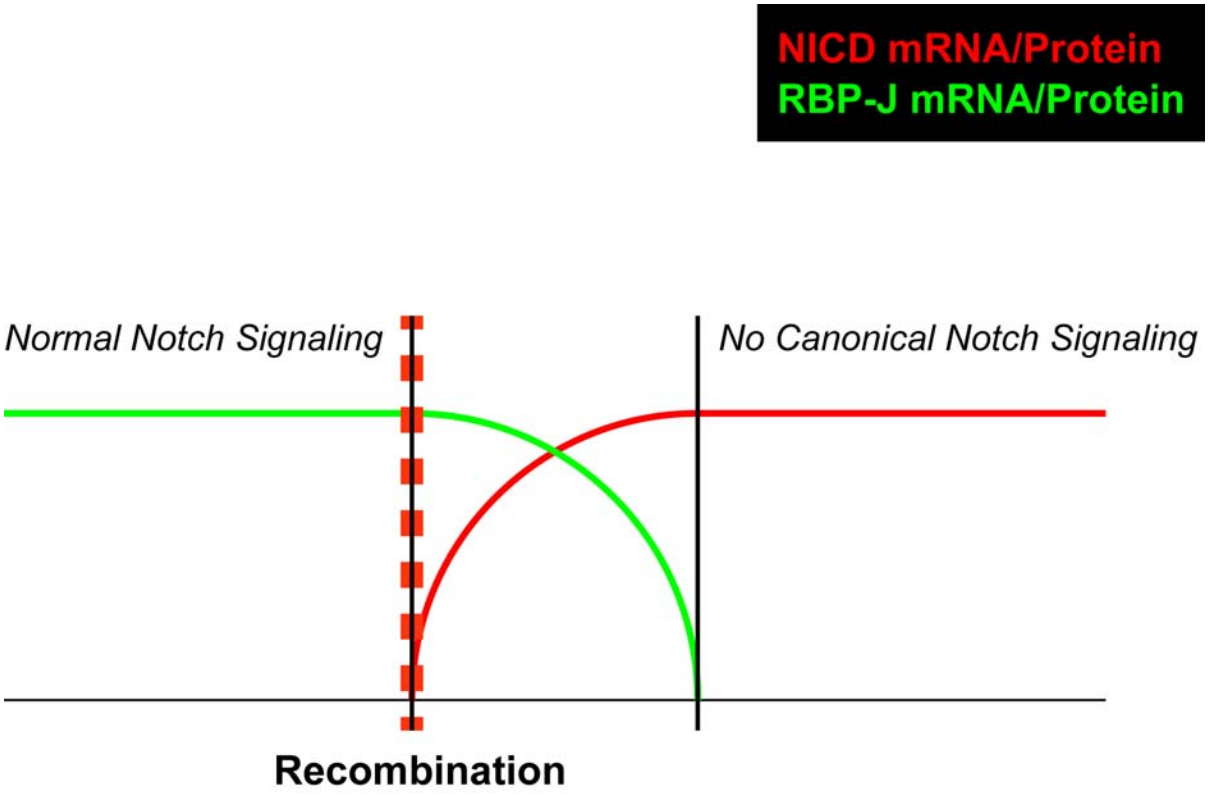

Figure C.1 NICD/RBP mice experience a period of Notch activation followed by an inability to signal. This schematic represents the predicted expression period of mRNA/protein in NICD/RBP mice. As Alb-Cre mediates gene recombination after the initial cell fate decisions, the hepatoblasts will experience *Normal Notch Signaling* until the Cre is expressed. After Cre expression (vertical red dotted line), the RBP-J mRNA and protein levels will slowly taper off (green line), dependent on the half-life of the transcript and protein. Conversely, at the time of recombination, the NICD mRNA and protein levels wills slowly increase as the gene is expressed (red line). Thus for a period of time, the NICD/RBP mice have an increase in Notch signaling, followed by an inability to signal once the RBP-J transcript and protein levels cease, *No Canonical Notch Signaling*.

Results

To assess the effects of both activating and deleting Notch signaling within the hepatoblasts, I analyzed the alterations in morphology of cytokeratin19-positive cells in NICD/RBP mice at P15, P30, P60 and P120 (Figure C.2-C.3). At P15 there is an increase in the number of cytokeratin-positive cells at the periphery (Figure C.2 E), however the excess cells are limited as compared to NICD tissue (Please refer to Chapter III, Figure 3.5). Interestingly, the excess ductal cells are maintained at P30, P60 and P120 and form luminal structures (Figure C.2 F-H). Conversely, at all ages hilar ducts demonstrate little change compared to control, with a few excess cytokeratin-positive cells noted (Figure C.3), but again significantly less than in NICD tissue (Please refer to Chapter III, Figure 3.6). While the excess of cholangiocytes does not change with age in the NICD/RBP mice, I have not performed quantitative analysis, either ductal counts or cytokeratin19-positive area by ARIOL analysis, to fully confirm this observation.

Of note, is a significant level of focal inflammation in the periphery of NICD/RBP mice at P60 (Figure C.2 G-inset). The origin and consequence of this inflammation is not understood at this time. Also, it is not clear whether the inflammation is occurring at portal or central veins. Inflammation is usually noted at portal veins, however the lack of bile ducts in the region of inflammation suggests either central vein inflammation or immune-mediated destruction of bile ducts. Therefore further analysis is required to define this model.

Interestingly, liver function tests from 2-month to 4-month old mice reveal that NICD/RBP mice have a statistically significant increase in ALT and ALP levels as compared to control (Table C.1). However, it is important to note that the levels of ALT in the NICD/RBP mice are significantly lower than those in RBP KO ($P \leq 0.01$), further supporting a reduced severity of phenotype. As more cholangiocytes are specified and bile ducts formed in the NICD/RBP mice as compared to RBP KO mice, the increased ALT levels in

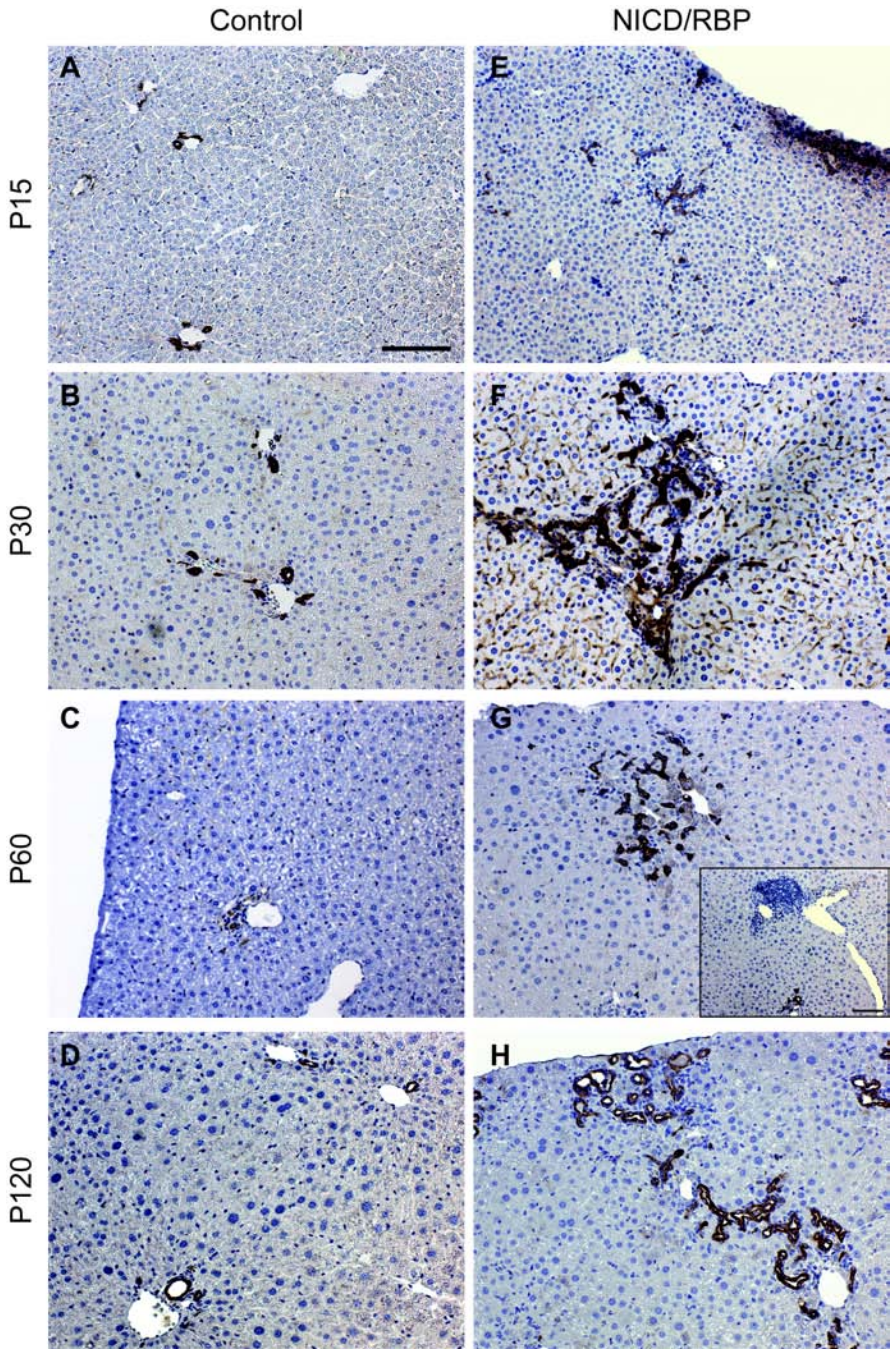

Figure C.2 Morphological defects in cytokeratin19-positive cells in peripheral liver tissue with hepatoblast-specific deletion of RBP-J and activation of Notch1. Paraffin-embedded sections from control (A-D) and NICD/RBP (E-H) tissue over a developmental time course was immunostained for cytokeratin19 to mark cholangiocytes and counterstained with Mayer's hematoxylin. (A,E) At P15, NICD/RBP peripheral cholangiocytes are scattered within the parenchyma, and extra cells are observed. (B,F) At P30, there is an even more apparent increase in peripheral ductal cells, limited to regions directly surrounding the portal vein. (C,G) At P60, the excess ducts are maintained, however areas of severe inflammation are observed (G, inset). (D,H) At P120, the extra ducts are also maintained, but appear cystic and dilated. Scale bar = 50 μm.

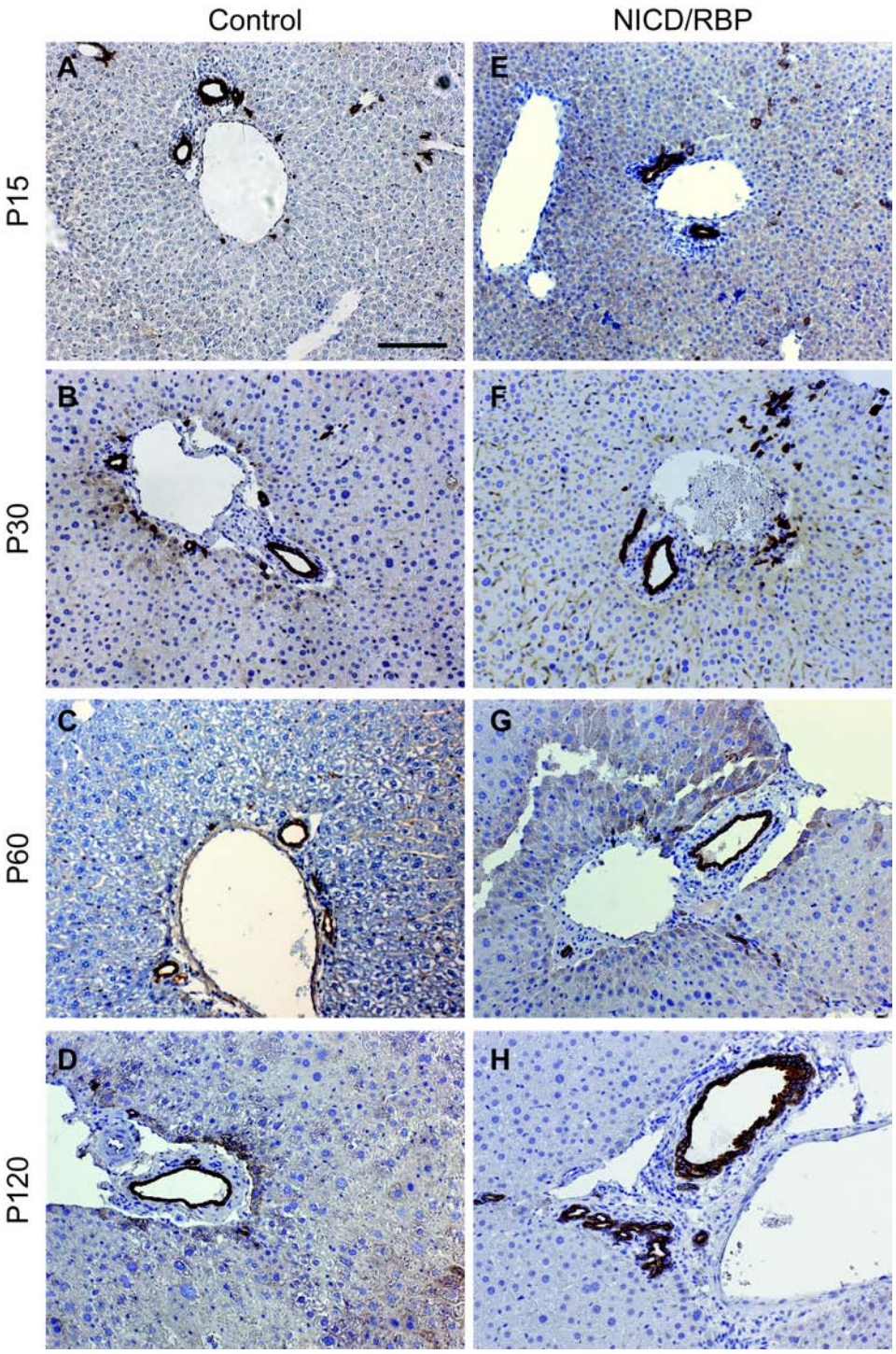

Figure C.3 Morphological defects in cytokeratin19-positive cells in hilar liver tissue with hepatoblast-specific deletion of RBP-J and activation of Notch1. Paraffin-embedded sections from control (A-D) and NICD/RBP (E-H) tissue over a developmental time course was immunostained for cytokeratin19 to mark cholangiocytes and counterstained with Mayer's hematoxylin. (A,E) At P15, NICD/RBP hilar cholangiocytes are all incorporated into a ductal structure. (B,F) At P30, there a few excess cytokeratin19-positive cells are observed in hilar regions. (C,G) At P60, the few excess cells are maintained. (D,H) At P120, the few extra ducts are maintained. Scale bar = 50 μm.

Genotype	n	ALT	n	TB	n	ALP
Control	40	57.5 ± 5.5	37	1.2 ± 0.1	29	8.421±1.197
NICD/RBP	20	86.07 ± 9.1 **	16	0.6 ± 0.1	16	17.30 ± 4.8 *

Table C.1 Serum chemistry analysis. Serum was obtained from control and NICD/RBP mice between 2-months and 4-months, and analyzed for alanine aminotransferase (ALT), total bilirubin (TB), and alkaline phosphatase (ALP). Values are mean (IU/L) ± standard error of the mean. P values are calculated by a student *t*-test. *$p \leq 0.05$, **$p \leq 0.01$.

NICD/RBP mice suggest a requirement for Notch signaling subsequent to the initial development.

To determine the effects on three-dimensional structure, and whether a progressive obstruction, as defined in the RBP KO mice, is also observed in NICD/RBP mice, I analyzed resin casts from P60 and P120 control and NICD/RBP mice (Figure C.4). At P60, NICD/RBP resin casts are reminiscent of NICD casts with an excess of branches (Figure C.4 A-C). Interestingly, the NICD/RBP casts do appear to lose branches at P120 (Figure C.4 D-F), however these resin casts have not been quantified by microCT.

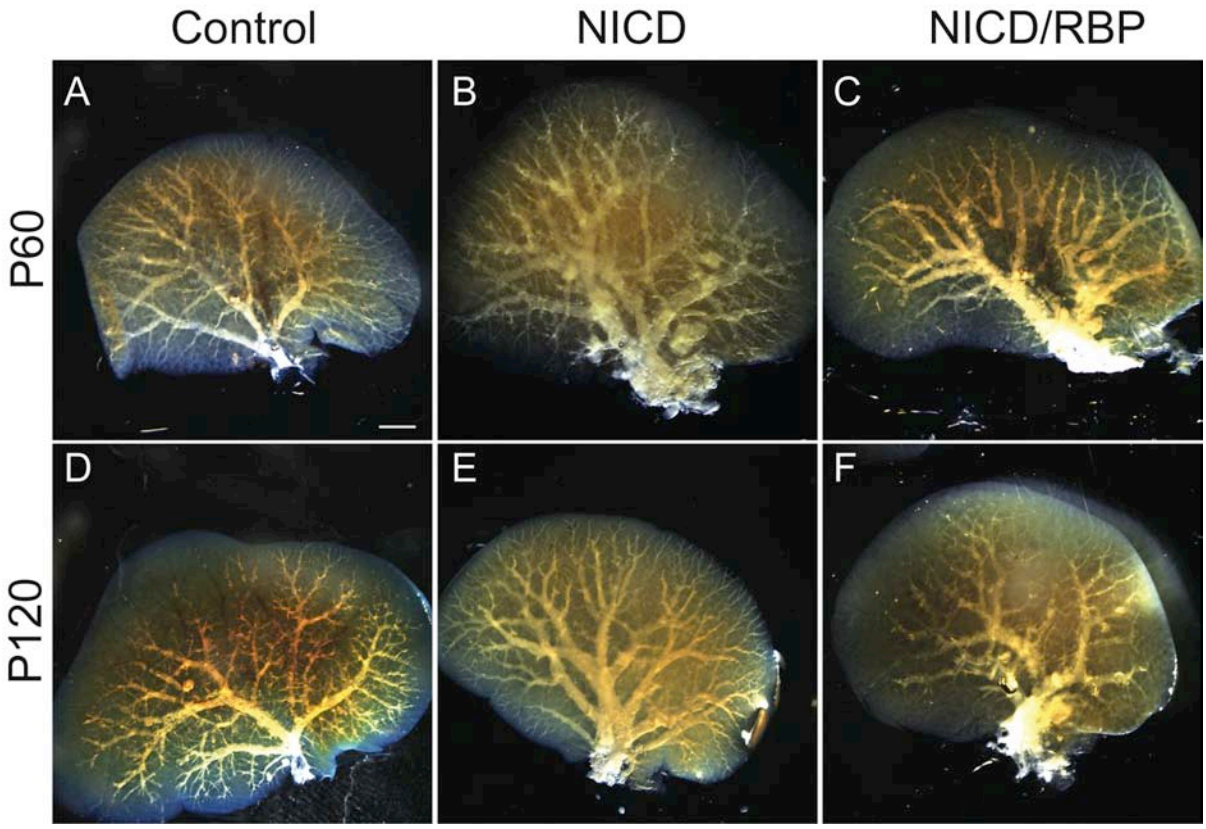

Figure C.4 Three-dimensional resin casting of the biliary system reveals a role for Notch signaling to maintain the intact communicating IHBD (A-F) Representative images of the ventral surface of left lobe resin casts are shown at P60 and P120. (A,D) Control resin casts (*n*=2 and 7). (B,E) NICD resin casts demonstrate a duplication of the main branches and a general increase in branches (*n*=6 and 5). (C,F) NICD/RBP mice demontrate a duplication of the main branches and a general increase in branches at P60 (*n*=1), however the branches are attenuated at P120 (*n*=2), suggesting an acute requirement for Notch signaling in the maintenance of IHBD structure. Scale bar = 2 mm.

Discussion

Initial characterization of the NICD/RBP mice reveals ductal morphology consistent with a window of Notch signaling in which specification and remodeling occur, albeit to a lesser extent than the NICD alone mice (Figure C.2-C.3). Excess ductal structures are limited to peripheral tissue, and do not visually alter morphology with age (Figure C.2-C.3). Thus two-dimensional analysis doesn't reveal any alterations after the initial specification and remodeling of the ductal system.

Conversely, an increase in ALT and ALP levels in NICD/RBP mice suggest that despite having formed ducts NICD/RBP mice have liver damage (Table C.1). As ALP levels are increased in NICD alone mice, this particular readout of liver function does not suggest much. In contrast, the increase in ALT, albeit less than in the RBP KO, suggests that despite the formation of ductal structures, liver damage is still occurring without acute Notch signaling in the adult. Further, three-dimensional analysis revealed an initially expanded structure, similar to the NICD, which appeared to lose branches with age (Figure C.3). Together, these results suggest that the progressive obstructive phenotype, as observed in RBP KO mice, is due, in part to an acute post-natal requirement of Notch signaling. However, more careful analysis of this model is required for definite conclusions. While this approach is unconventional and remains to be validated, it will augment the finding in cultured cholangiocytes (See Appendix F).

Materials and Methods

Mouse Lines

CD1 mice carrying the *Albumin-Cre* (*Alb-Cre*) were crossed with the conditional deletion allele for RBP-J and the conditional activation allele for Notch1 (*Alb-Cre;RBP-J$^{flox/flox}$;ROSA^{Notch1}*). Genotyping was performed by polymerase chain reaction (PCR) analysis using previously published primer pairs.

Immunohistochemistry, resin casting and serum chemistry was performed as described in Chapter II, Materials and Methods.

APPENDIX D

ANALYSIS OF RBP FLOX/NULL MICE

Introduction

As discussed, gene deletion by *Alb-Cre* occurs around E16.5 (Please refer to Appendix A), thus in an attempt to facilitate deletion, we generated an *Alb-Cre;RBP-J*$^{flox/null}$ (RBP fl/null) mouse line. We anticipated a more severe ductal phenotype than the RBP KO, as Cre was only required to mediate deletion of one allele, as all cells are null for RBP-J at the other allele. Interestingly, the phenotype of the RBP fl/null mice has been quite perplexing, and appears to be a hybrid between the RBP KO and the N1/N2 DKO mice. Further, the previous characterization of the role of RBP-J in ductal specification used RBP fl/null mice, which developmentally appear identical to RBP KO mice, however the authors did not analyze the post-natal phenotype (Zong et al., 2009). The initial characterization of the post-natal phenotype is described within this Appendix.

Results

RBP fl/null tissue at P15, P30, P60 and P120 was analyzed for cytokeratin19-positive expression to assess the morphological changes (Figure D.1-D.2). At P15 in RBP fl/null mice, there are un-remodeled cytokeratin-positive cells within the peripheral liver tissue (Figure D.1 E). Surprisingly, these un-remodeled cells are resolved at P30, and form tortuous ducts (Figure D.1 F), which are then further reduced with age, at P60 and P120 (Figure D.1 G-H). Consistent with the observation in N1/N2 DKO and RBP KO mice at P30, necrosis is detectable in RBP fl/null mice (Figure D.1 F-inset). In contrast, hilar ducts appear normal, with mild inflammation at all ages (Figure D.2 E-G) and expansion of large cystic structures with age (Figure D.2 H). The cysts are not cytokeratin positive, suggesting they are not due to ductal expansion. I postulate that these cysts are lymphatic in origin, but the nature of these cysts is not understood at this point. These results suggest that RBP fl/null mice have un-remodeled peripheral ducts in early post-natal periods, but are unable to maintain them.

Assessment of the three-dimensional architecture of the IHBD revealed mild defects in biliary structure at P60 (Figure D.3 C). At P120, RBP fl/null resin casts appear to have a reduction in the intact communicating IHBD (Figure D.3 F), similar to that observed in the RBP KO mice. Thus, the acquired post-natal defects observed in RBP KO mice, appear to occur similarly in RBP fl/null mice.

To further address the severity of the RBP fl/null phenotype, I assessed liver function in 2-month to 4-month old RBP fl/null mice (Table D.1). RBP fl/null mice have elevated ALT and ALP levels as compared to control, however the values are not statistically significantly different than the RBP KO mice. Thus together these data suggest that while the underlying histology in RBP fl/null mice is quite different from RBP KO mice, the effects on liver function and IHBD architectural defects are equivalent.

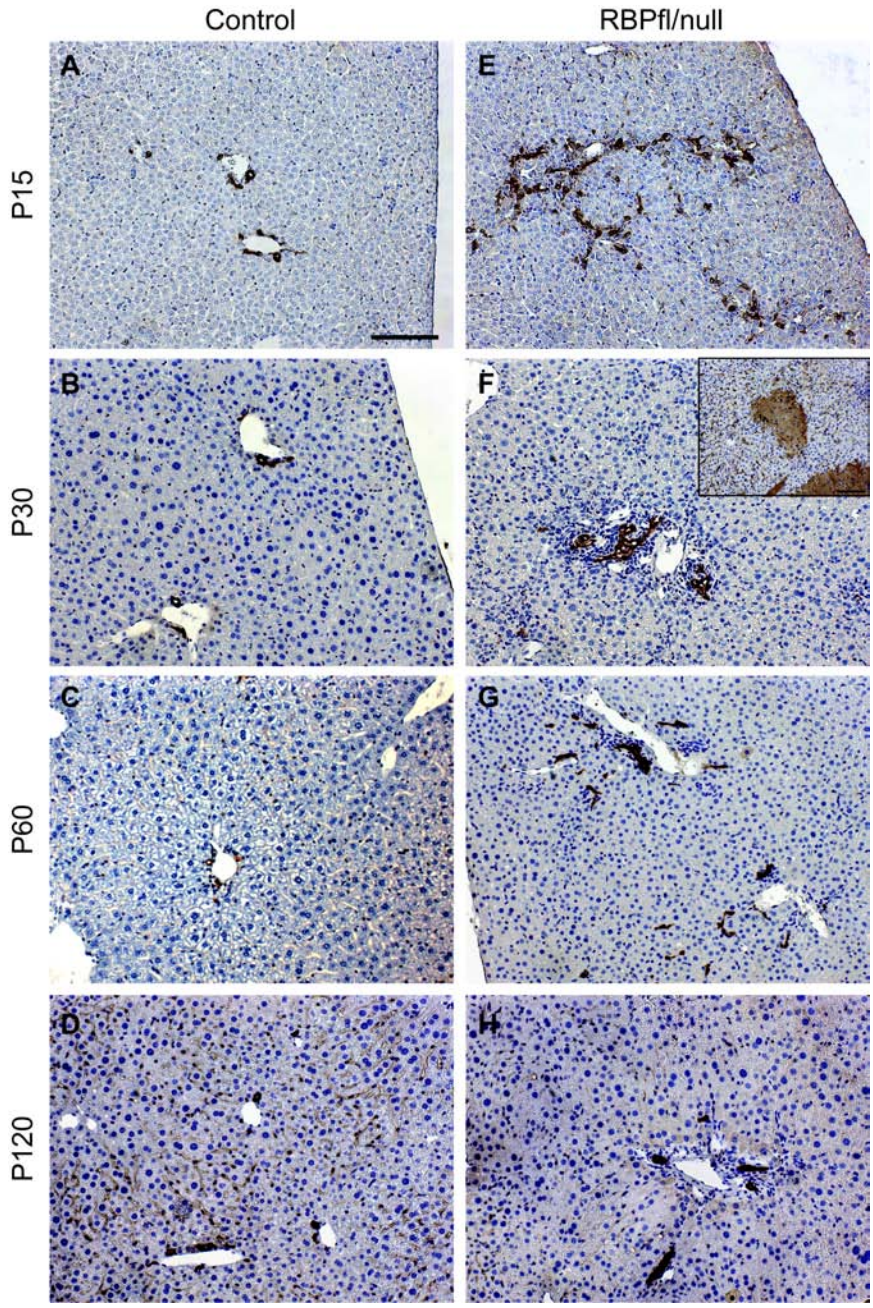

Figure D.1 Morphological defects in cytokeratin19-positive cells in peripheral liver tissue with hepatoblast-specific deletion of one allele of RBP-J and global inactivation of the other allele. Paraffin-embedded sections from control (A-D) and RBP fl/null (E-H) tissue over a developmental time course was immunostained for cytokeratin19 to mark cholangiocytes and counterstained with Mayer's hematoxylin. (A,E) At P15, RBP fl/null peripheral cholangiocytes are un-remodeled and resemble the N1/N2 DKO. (B,F) At P30, the un-remodeled cells are resolved into tortuous ductal structures. As with other mouse models in which Notch signaling is removed, RBP fl/null mice demonstrate hepatic necrosis at P30. (C,G) At P60, the peripheral ducts appear grossly normal. (D,H) At P120, the early phenotype of RBP fl/null is completely resolved. Scale bar = 50 μm.

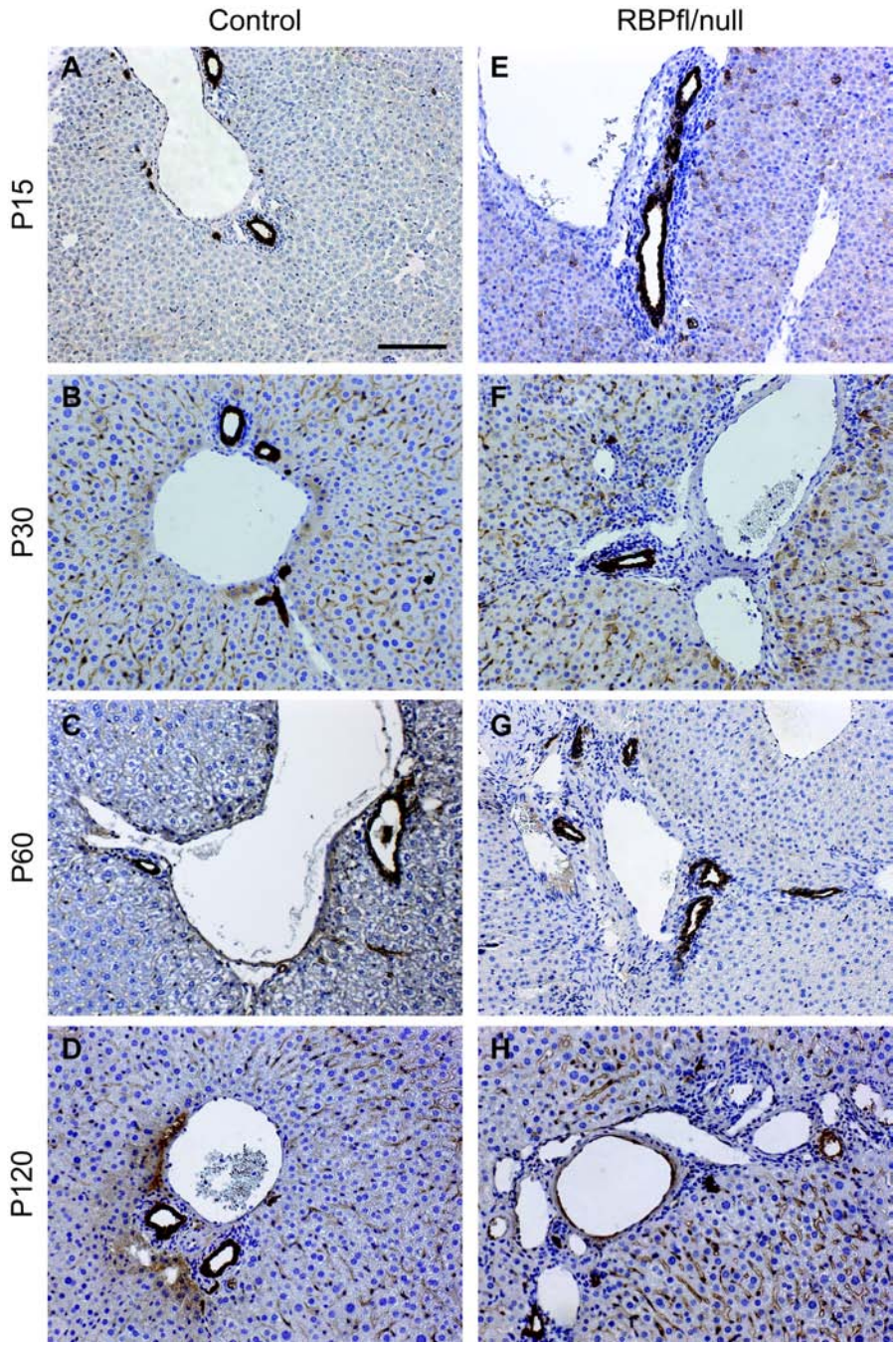

Figure D.2 Morphological defects in cytokeratin19-positive cells in hilar liver tissue with hepatoblast-specific deletion of one allele of RBP-J and global inactivation of the other allele. Paraffin-embedded sections from control (A-D) and RBP fl/null (E-H) tissue over a developmental time course was immunostained for cytokeratin19 to mark cholangiocytes and counterstained with Mayer's hematoxylin. (A,E) At P15, RBP fl/null hilar ducts are well formed, with mild inflammation. (B,F) At P30, the hilar ducts are unaltered in RBP fl/null mice. (C,G) At P60, the hilar ducts are unaltered compared to P15 and P30. (D,H) At P120, the hilar ducts in RBP fl/null mice are grossly normal, however large cystic dilations become evident at this age. Scale bar = 50 μm.

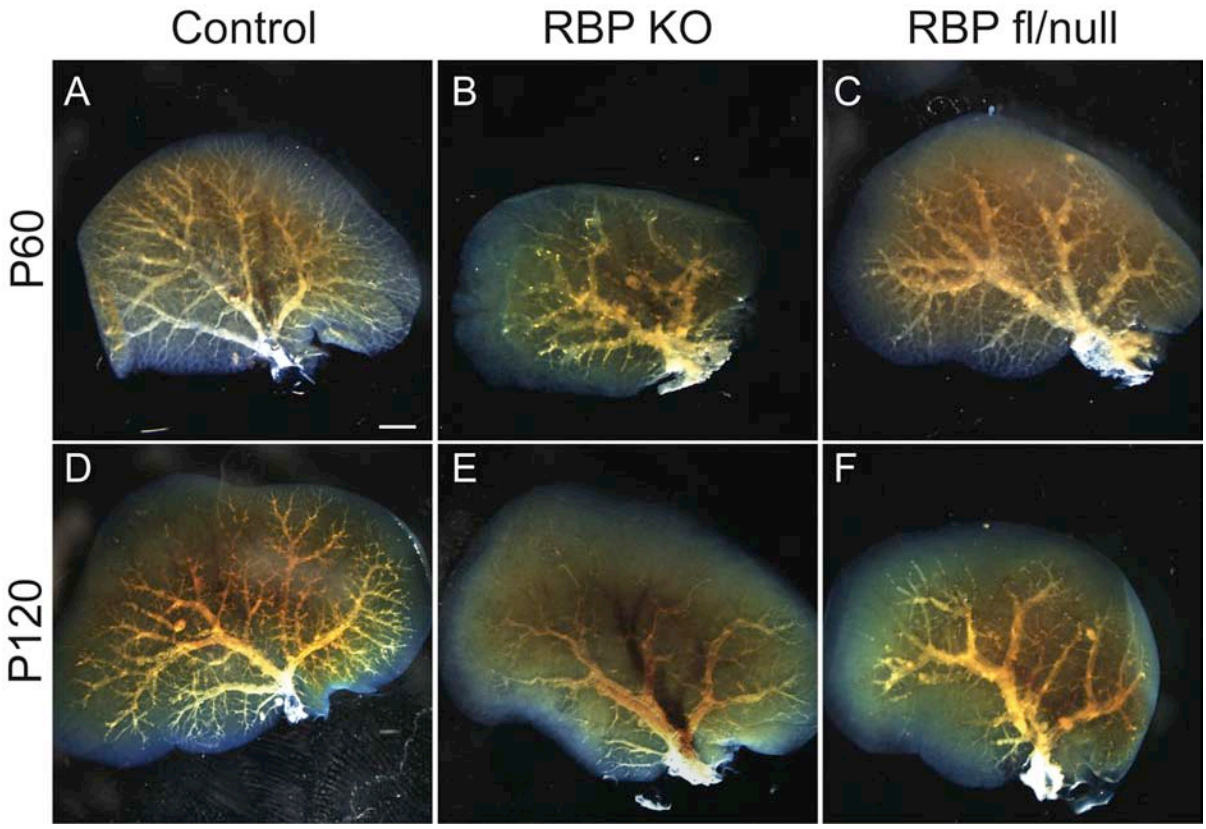

Figure D.3 Three-dimensional resin casts of the RBP fl/null biliary system are grossly indistinguishable from RBP KO casts. (A-F) Representative images of the ventral surface of left lobe resin casts are shown at P60 and P120. (A,D) Control resin casts (*n*=2 and 7). (B,E) RBP KO resin casts demonstrate the loss of branches from P60 (*n*=6) to P120 (*n*=5), as previously quantified. (C,F) RBP fl/null mice also demonstrate a progressive paucity of IHBD architecture with age (*n*=3 and 4). Scale bar = 2 mm

Genotype	n	ALT	n	TB	n	ALP
Control	40	57.5 ± 5.5	37	1.2 ± 0.1	29	8.42 ± 1.1
RBPfl/null	19	105.0 ± 8.7 ***	16	0.7 ± 0.1	19	29.21 ± 4.6 ***

Table D.1 Serum chemistry analysis. Serum was obtained from control and RBP fl/null mice between 2-months and 4-months, and analyzed for alanine aminotransferase (ALT), total bilirubin (TB), and alkaline phosphatase (ALP). RBP fl/null values are not statistically significantly different than RBP KO values. Values are mean (IU/L) ± standard error of the mean. P values are calculated by a student *t*-test. ***p≤0.001.

Discussion

While we originally set out to utilize the RBP fl/null mouse as the most severe loss of Notch signaling, the analysis of this model has been quite confusing. Specifically, the two-dimensional ductal morphology appears less severe at the periphery in early post-natal time points (P15, Figure D.1 E) resembling a N2 KO or N1/N2 DKO instead of the RBP KO. Subsequently RBP fl/null mice undergo a period of ductal hypertrophy (P30, Figure D.1 F), and become visually equivalent to the RBP KO at later post-natal time points (P60 and P120, Figure D.1 G-H). Thus, RBP fl/null mice are unable to maintain the un-remodeled cytokeratin19-positive cells in the periphery. The mechanism of differential histology in RBP KO and RBP fl/null mice is currently not understood. One approach we have undertaken to further characterize the severity of the RBP fl/null, is to cross it into the background of the activated Notch, thus producing *Alb-Cre;RBP-J*$^{flox/null}$*;ROSA26*^{Notch1} mice. We anticipate that these mice will help to address the question of severity in this model.

Materials and Methods

Mouse Models

Alb-Cre and *RBP-J*$^{flox/flox}$ have been described in Chapter II: Materials and Methods. RBP null mice (Oka et al., 1995), which are heterozygous viable, were crossed into the RBP KO line. Genotyping was performed by PCR analysis using previously described primers.

Immunohistochemistry, resin casting and serum chemistry was performed as described in Chapter II, Materials and Methods.

APPENDIX E

INTRAHEPATIC BILE DUCT STRUCTURAL ALTERATIONS DURING LIVER REGENERATION

Introduction

Liver regeneration is generally divided into two types: proliferation of normally quiescent hepatocytes and activation of a liver progenitor cell. Thus, regeneration studies have mainly focused on the role of hepatocytes or progenitors respectively, with little focus on the response of cholangiocytes. To study regeneration due to the proliferation of normally quiescent hepatocytes, the common experimental approach is the 70% partial hepatectomy (PHx). A common method to study liver progenitors in mice is the administration of 3,5-diethoxycarbonyl-1,4-dihydrocollidine (DDC) to induce a progenitor “oval cell” response. In this Appendix, I use both PHx and DDC feeding, in conjunction with resin casting to address the structural changes in the intrahepatic bile duct (IHBD) network during liver regeneration.

Results

To address the alterations in IHBD architecture after 70% PHx, I resin cast mice at 3, 7, 10 and 14 days post-PHx (Figure E.1). PHx surgeries were performed at Washington University St. Louis School of Medicine, in the laboratory of Dr. David Rudnick. It is important to note that the liver to body weight ratio is not fully recovered until 14 days post-PHx (Figure E.2). Analysis of biliary resin casts after PHx reveal that the IHBD structure expands in concert with the growing size of the regenerating lobes. While further analysis is required to determine how proliferation and/or cell elongation plays into the expansion of the ductal system, I have demonstrated that the IHBD maintains a normal distribution throughout regeneration. It remains possible that earlier than 3 days post-PHx, the IHBD will not have expanded with the lobes, but this remains to be determined.

To address the alterations in the IHBD ductal architecture during progenitor cell-mediated regeneration, I administered DDC to P120 control mice for 10 days and then resin cast (Figure E.3). The administration of DDC is considered to induce cholestais, due to IHBD obstruction by porphyrin plaque accumulation. Therefore, I hypothesized that DDC administration would lead to an obstruction of the IHBD reminiscent of obstruction observed in RBP KO mice. Instead, analysis of resin casts after 10 days of feeding DDC reveals no alterations in IHBD architecture (Figure E.3 A). Further I assessed the effect of feeding DDC on the IHBD structure in P120 RBP KO and NICD mice (Figure E.3 B-C). Surprisingly, no obvious defects are detected in these genetic backgrounds either. Analysis of mice who have been fed DDC longer is currently in progress, however these results suggest minimal alterations to the biliary structure during early progenitor cell-mediated injury responses.

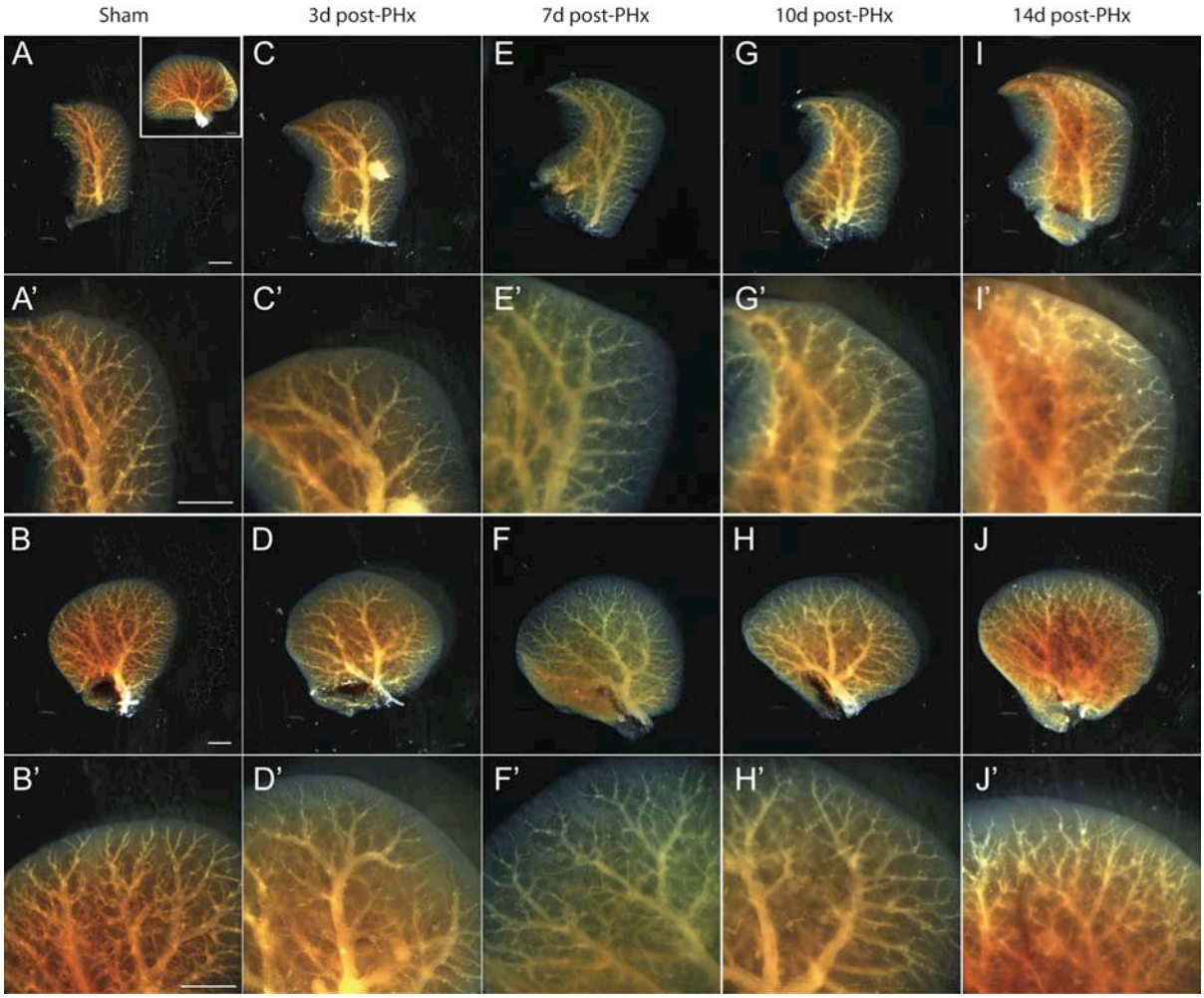

Figure E.1 Three-dimensional resin casting of control mice after 70% partial hepatectomy. Representative images of right lobe resin casts at 3, 7, 10 and 14 days post-partial hepatectomy (PHx) on a CD1 strain background. (A-B) Sham operated mice demonstrate the normal IHBD structure in the two left lobes (*n*=8). (C-D) Resin casts at 3 days post-PHx (*n*=5). (E-F) Resin casts at 7 days post-PHx (*n*=5). (G-H) Resin casts at 10 days post-PHx (*n*=5). (I-J) Resin casts at 14 days post-PHx (*n*=5). Resin casts after PHx reveal no obvious alterations in structure and suggest a general expansion of the IHBD coincident with the growth of the lobe. Scale bar = 2 mm.

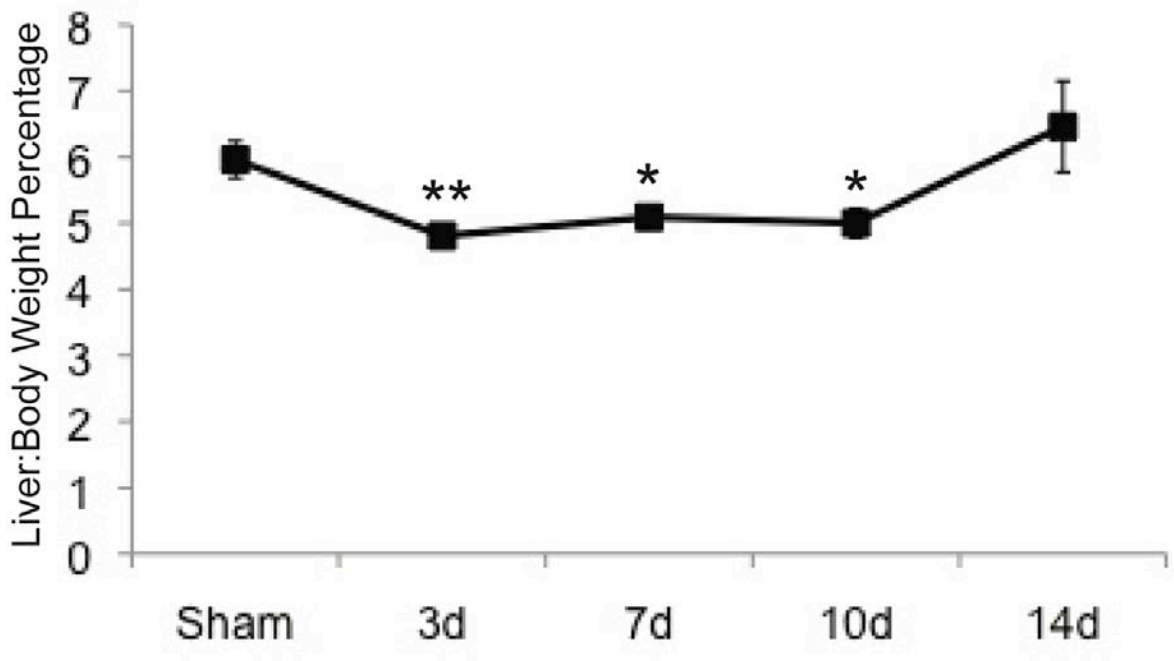

Figure E.2 The liver to body weight ratio in CD1 strain background mice is recovered at 14 days post-partial hepatectomy. Liver to body weight ratios from sham (n=8), 3 days post-PHx (n=5), 7 days post-PHx (n=5), 10 days post-PHx (n=5) and 14 days post-PHx (n=5) were calculated. Mice demonstrate a liver to body weight recovery to sham levels at 14 days post-PHx. Error bars – standard error of the mean. **$p \leq 0.01$, ***$p \leq 0.001$.

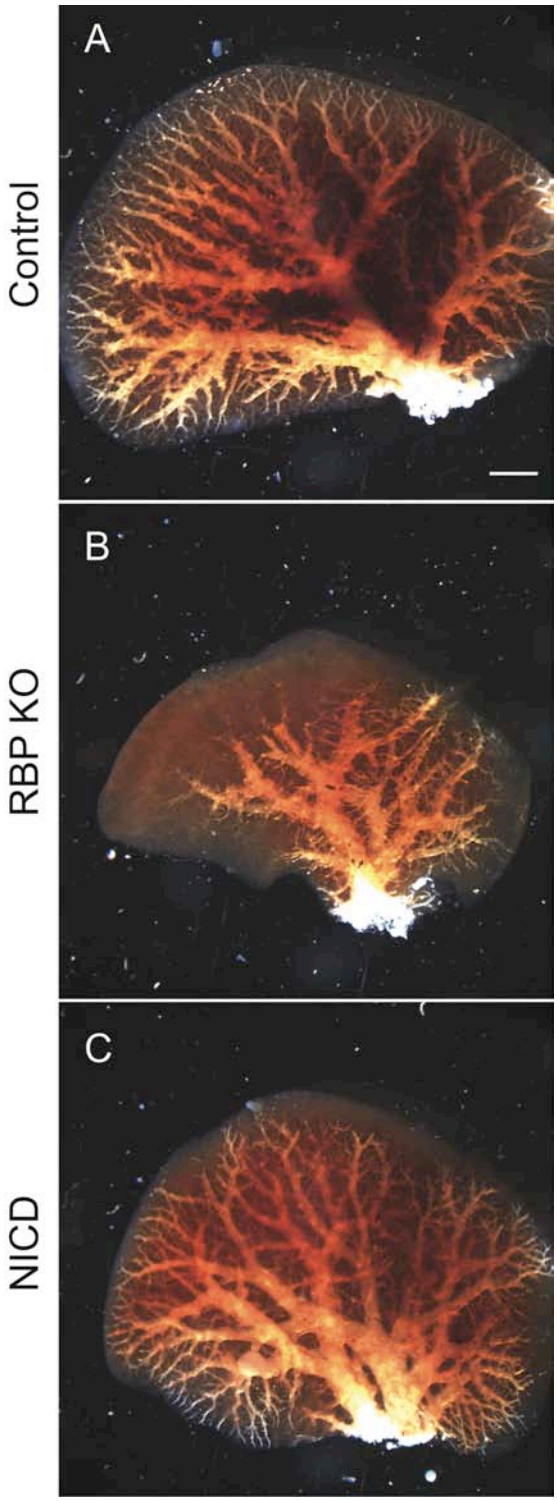

Figure E.3 Three-dimensional resin casting of control, RBP KO and NICD mice during oval cell activation. Control, RBP KO and NICD mice were administered a diet of 0.1% DDC for 10 days prior to resin injection. (A-C) Representative images of left lobe resin casts. (A) Control (*n*=4), (B) RBP KO (*n*=4) and (C) NICD (*n*=5) mice demonstrate no obvious changes to the IHBD structure after 10 days of DDC. Scale bar = 2 mm.

Discussion

Thus far, analysis of IHBD structural changes during liver regeneration has not revealed striking qualitative changes. Instead, in the 70% PHx model, the IHBD appears to gradually expand with the regenerating lobes (Figure E.1). Further, in the DDC oval cell model, no structural affects on the IHBD are evident after 10 days of feeding DDC (Figure E.3). Further examination of the two-dimensional ductal cholangiocyte changes are required to fully interpret this data.

Materials and Methods

Partial Hepatectomy

Partial hepatectomy procedures were completed at Washington University St. Louis School of Medicine in Dr. David Rudnick's laboratory. In brief, mice were anesthetized, and an incision was made in the abdomen. Medial and left lobes were tied off at the hilum and excised. Mice were sutured and allowed to come out of anesthesia.

DDC Injury

Mice were fed a diet containing 0.1% 3,5-diethoxycarbonyl-1,4-dihydrocollidine (DDC) for 10 days prior to resin casting.

Resin casting was performed as described in Chapter II, Materials and Methods.

APPENDIX F

CHOLANGIOCYTE ISOLATION

Introduction

The isolation and culturing of cholangiocytes to assess function *in vitro* is critical to overcome the deficiencies of the *in vivo* analysis, and to augment the mouse genetic analysis. Further, the establishment of cholangiocyte cultures will allow me to use molecular analysis in a pure cholangiocyte population to answer questions such as the acute requirement of Notch signaling for cholangiocyte function, and the role of immune-mediate destruction in the phenotypes observed in RBP KO mice (Please refer to Chapter VI, Future Directions for a full description of experiments). Thus, I recently traveled to Yale University to the laboratory of Dr. Mario Strazzabosco to learn a cholangiocyte cell isolation technique. The isolation technique is outlined within this Appendix and the initial cholangiocyte images are displayed.

Results

The successful isolation of cholangiocytes is demonstrated by cytokeratin19-positive staining (Figure F.1). Epithelial cell adhesion molecule (EpCAM), a cholangiocyte-specific marker within the liver was used for Immuno-magnetic isolation. EpCAM isolated cells demonstrate a specific isolation of cytokeratin19-positive cells (Figure F.1 A-B), which was confirmed by a no-primary control (Figure F.1 C). However, plating and staining of cells that were not pulled-down with the magnet reveals that the efficiency of isolation is poor (Figure F.1 D).

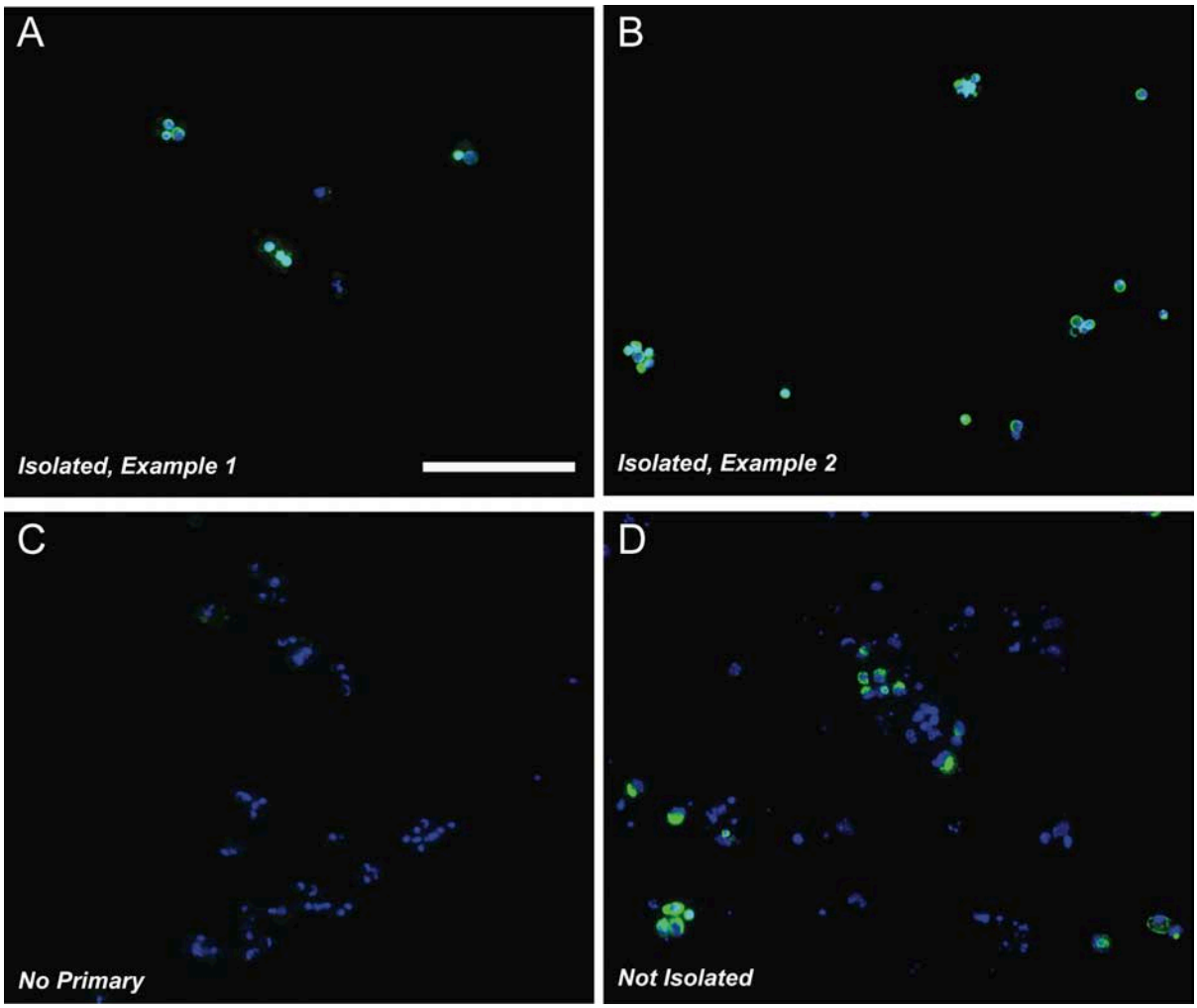

Figure F.1 Cholangiocyte cultures. Representative images of immuno-magnetic EpCAM-positive isolated cholangiocytes, stained with cytokeratin19 (green). (A-B) Successful isolation of cytokeratin19-positive cells. (C) No primary (cytokeratin19) control demonstrates cytokeratin19-positivity. (D) Cells not isolated by immuno-magnetic selection, reveals an inefficient isolation. Scale bar = 50 μm.

Discussion

The isolation and culture of cholangiocytes will be used for many aspects of my future research. While initial indications suggest that cholangiocyte isolation and culture is feasible, optimization of the protocol remains to be completed. Increasing the concentration of primary antibody will be the first step in this optimization. The amount of secondary conjugated beads is currently in excess, and the suitable amount for the isolation of 2.5 million cells, which is far greater than the expected number of cholangiocytes to be isolated by this method.

Materials and Methods

Immunomagnetic Isolation of Cholangiocytes

Hanks A and Hanks B buffers were prepared fresh and incubated at 37ºC in 5% CO_2 for one half hour prior to use. Per mouse, 30 ml of each solution was prepared. To the Hanks B buffer, 25mg of Collagenase XI (Sigma) was added per 30 ml.

Mice were sacrificed by CO_2 asphyxiation and the portal vein was cannulated with polyethylene (PE) 50 tubes and secured with a ligature of 5.0 silk. The inferior vena cava was cut to release blood and perfusate. Mice were perfused by hand with 30 ml of Hanks A followed by 30 ml of Hanks B with collagenase. Livers were incubated for 5-10 mins until the liver became malleable.

Livers were removed from the body, placed in L15 media and the capsule was manually removed using forceps. Livers were shaken to release the majority of hepatocytes. The remaining structure was placed in a solution containing Pronase (50ml alpha-MEM, 1 ml Penicillin/Streptomycin, 1.5 ml fetal bovine serum, 1% bovine serum albumin, 0.06% Collagenase IV, 0.06% DNase and 0.33% Pronase [Sigma]). The structure was manually shredded using scissors, then allowed to shake at 37ºC for 30 min. Digested cells were filtered sequentially through a 100 μm and 30 μm filter. Cells that did not pass through the filters were subsequently incubated in a solution containing Hyaluronidase (50ml alpha-MEM, 1 ml Penicillin/Streptomycin, 1.5 ml fetal bovine serum, 1% bovine serum albumin, 0.06% Collagenase IV, 0.06% DNase and 0.33% Hyaluronidase [Sigma]) at 37ºC for 30 min, shaking. Cells were filtered through a 30 μm filter and cells <30 μm in size were combined, and centrifuged at 1600 rpm for 10 min, resuspended in 6% DNase in RPMI.

Cells were resuspended in primary antibody (rat-anti-EpCAM, 1:50; DSHB) and incubated on ice for 30 min. Cells were centrifuged at 1600 rpm for 10 min, and

resuspended in secondary-conjugated magnetic beads (anti-rat IgG, 25 µl per 2,500,000 target cells, Invitrogen) to incubate for 30 min on ice. After incubation, tubes were placed on the magnet (Dynamag-Spin, Invitrogen) for 1 min. Non-magnetized cells were removed and plated to determine efficiency of isolation. Cells were washed using the magnet, 10 times for 1 min each. Cells were resuspended in 100 µ l of fetal bovine serum and plated on coverslips.

Cells were allowed to attach for 5 hours, then fixed in 100% methanol for 10 min at -20ºC. Cells were incubated in primary antibody (rat-anti-CK19, 1:100; DSHB) overnight at 4ºC. The following day, cells were incubated in secondary antibody (anti-rat-Alexa488, 1:300; Invitrogen), and mounted using a DAPI mounting media (Prolong Gold with DAPI; Invitrogen).

Abramoff, M., Magelhaes, P. and Ram, S. (2004). Image Processing with ImageJ. *Biophotonics International* **11**, 36-42.

Alagille, D. (1996). Alagille syndrome today. *Clin Invest Med* **19**, 325-330.

Alpini, G., McGill, J. M. and Larusso, N. F. (2002). The pathobiology of biliary epithelia. *Hepatology* **35**, 1256-1268.

Antoniou, A., Raynaud, P., Cordi, S., Zong, Y., Tronche, F., Stanger, B. Z., Jacquemin, P., Pierreux, C. E., Clotman, F. and Lemaigre, F. P. (2009). Intrahepatic bile ducts develop according to a new mode of tubulogenesis regulated by the transcription factor SOX9. *Gastroenterology* **136**, 2325-2333.

Asahina, K., Tsai, S. Y., Li, P., Ishii, M., Maxson, R. E., Jr., Sucov, H. M. and Tsukamoto, H. (2009). Mesenchymal origin of hepatic stellate cells, submesothelial cells, and perivascular mesenchymal cells during mouse liver development. *Hepatology* **49**, 998-1011.

Bogert, P. T. and LaRusso, N. F. (2007). Cholangiocyte biology. *Curr Opin Gastroenterol* **23**, 299-305.

Bozkulak, E. C. and Weinmaster, G. (2009). Selective use of ADAM10 and ADAM17 in activation of Notch1 signaling. *Mol Cell Biol* **29**, 5679-5695.

Bucher, N. L. (1963). Regeneration of Mammalian Liver. *Int Rev Cytol* **15**, 245-300.

Bucher, N. L. (1967). Experimental aspects of hepatic regeneration. *N Engl J Med* **277**, 738-746 concl.

Bucher, N. L. and Glinos, A. D. (1950). The effect of age on regeneration of rat liver. *Cancer Res* **10**, 324-332.

Bucher, N. L., Scott, J. F. and Aub, J. C. (1951). Regeneration of the liver in parabiotic rats. *Cancer Res* **11**, 457-465.

Bucher, N. L., Schrock, T. R. and Moolten, F. L. (1969). An experimental view of hepatic regeneration. *Johns Hopkins Med J* **125**, 250-257.

Bucher, N. L., Patel, U. and Cohen, S. (1977). Hormonal factors concerned with liver regeneration. *Ciba Found Symp*, 95-107.

Carson, F. L. (1990). Histotechnology : a self instructional text. Chicago: ASCP Press.

Carton, J., Daly, R. and Ramani, P. (2007). Clinical pathology. In *Oxford core texts*, pp. xxviii, 598 p. Oxford: Oxford University Press.

Cassiman, D., Barlow, A., Vander Borght, S., Libbrecht, L. and Pachnis, V. (2006). Hepatic stellate cells do not derive from the neural crest. *J Hepatol* **44**, 1098-1104.

Chari, S., Umetsu, S. E. and Winandy, S. (2010). Notch target gene deregulation and maintenance of the leukemogenic phenotype do not require RBP-J kappa in Ikaros null mice. *J Immunol* **185**, 410-417.

Chiba, S. (2006). Notch signaling in stem cell systems. *Stem Cells* **24**, 2437-2447.

Cho, W. K., Mennone, A. and Boyer, J. L. (2001). Isolation of functional polarized bile duct units from mouse liver. *Am J Physiol Gastrointest Liver Physiol* **280**, G241-246.

Christensen, J. L., Wright, D. E., Wagers, A. J. and Weissman, I. L. (2004). Circulation and chemotaxis of fetal hematopoietic stem cells. *PLoS Biol* **2**, E75.

Clotman, F., Libbrecht, L., Gresh, L., Yaniv, M., Roskams, T., Rousseau, G. G. and Lemaigre, F. P. (2003). Hepatic artery malformations associated with a primary defect in intrahepatic bile duct development. *J Hepatol* **39**, 686-692.

Clotman, F., Lannoy, V. J., Reber, M., Cereghini, S., Cassiman, D., Jacquemin, P., Roskams, T., Rousseau, G. G. and Lemaigre, F. P. (2002). The onecut transcription factor HNF6 is required for normal development of the biliary tract. *Development* **129**, 1819-1828.

Clotman, F., Jacquemin, P., Plumb-Rudewiez, N., Pierreux, C. E., Van der Smissen, P., Dietz, H. C., Courtoy, P. J., Rousseau, G. G. and Lemaigre, F. P. (2005). Control of liver cell fate decision by a gradient of TGF beta signaling modulated by Onecut transcription factors. *Genes Dev* **19**, 1849-1854.

Coffinier, C., Gresh, L., Fiette, L., Tronche, F., Schutz, G., Babinet, C., Pontoglio, M., Yaniv, M. and Barra, J. (2002). Bile system morphogenesis defects and liver dysfunction upon targeted deletion of HNF1beta. *Development* **129**, 1829-1838.

Conlon, R. A., Reaume, A. G. and Rossant, J. (1995). Notch1 is required for the coordinate segmentation of somites. *Development* **121**, 1533-1545.

Crawford, J. M. (2002). Development of the intrahepatic biliary tree. *Semin Liver Dis* **22**, 213-226.

Dahms, B. B., Petrelli, M., Wyllie, R., Henoch, M. S., Halpin, T. C., Morrison, S., Park, M. C. and Tavill, A. S. (1982). Arteriohepatic dysplasia in infancy and childhood: a longitudinal study of six patients. *Hepatology* **2**, 350-358.

De Strooper, B., Annaert, W., Cupers, P., Saftig, P., Craessaerts, K., Mumm, J. S., Schroeter, E. H., Schrijvers, V., Wolfe, M. S., Ray, W. J. et al. (1999). A presenilin-1-dependent gamma-secretase-like protease mediates release of Notch intracellular domain. *Nature* **398**, 518-522.

Ema, H. and Nakauchi, H. (2000). Expansion of hematopoietic stem cells in the developing liver of a mouse embryo. *Blood* **95**, 2284-2288.

Emerick, K. M., Rand, E. B., Goldmuntz, E., Krantz, I. D., Spinner, N. B. and Piccoli, D. A. (1999). Features of Alagille syndrome in 92 patients: frequency and relation to prognosis. *Hepatology* **29**, 822-829.

Fabris, L., Cadamuro, M., Libbrecht, L., Raynaud, P., Spirli, C., Fiorotto, R., Okolicsanyi, L., Lemaigre, F., Strazzabosco, M. and Roskams, T. (2008). Epithelial expression of angiogenic growth factors modulate arterial vasculogenesis in human liver development. *Hepatology* **47**, 719-728.

Farber, E. (1956). Similarities in the sequence of early histological changes induced in the liver of the rat by ethionine, 2-acetylamino-fluorene, and 3'-methyl-4-dimethylaminoazobenzene. *Cancer Res* **16**, 142-148.

Fredrickson, T. N. and Harris, A. W. (2000). Atlas of mouse hematopathology. Amsterdam, Netherlands: Harwood Academic Publishers.

Friedman, S. L. (2008). Hepatic stellate cells: protean, multifunctional, and enigmatic cells of the liver. *Physiol Rev* **88**, 125-172.

Geerts, A. (2001). History, heterogeneity, developmental biology, and functions of quiescent hepatic stellate cells. *Semin Liver Dis* **21**, 311-335.

Geisler, F., Nagl, F., Mazur, P. K., Lee, M., Zimber-Strobl, U., Strobl, L. J., Radtke, F., Schmid, R. M. and Siveke, J. T. (2008). Liver-specific inactivation of Notch2, but not Notch1, compromises intrahepatic bile duct development in mice. *Hepatology* **48**, 607-616.

Geng, Z. M., Yao, Y. M., Liu, Q. G., Niu, X. J. and Liu, X. G. (2005). Mechanism of benign biliary stricture: a morphological and immunohistochemical study. *World J Gastroenterol* **11**, 293-295.

Germain, L., Noel, M., Gourdeau, H. and Marceau, N. (1988). Promotion of growth and differentiation of rat ductular oval cells in primary culture. *Cancer Res* **48**, 368-378.

Glaser, S. S., Francis, H., Marzioni, M., Taffetani, S., Phyinizy, J. L., LeSage, G. and Alpini, G. (2004). Functional Heterogeneity of the Intrahepatic Biliary Epithelium. In *The Pathophysiology of Biliary Epithelia* (eds G. Alpini D. Alvaro M. Marzioni G. LeSage and N. LaRusso), pp. 245-254. Georgetown, TX: Landes Bioscience.

Glaser, S. S., Gaudio, E., Rao, A., Pierce, L. M., Onori, P., Franchitto, A., Francis, H. L., Dostal, D. E., Venter, J. K., DeMorrow, S. et al. (2009). Morphological and functional heterogeneity of the mouse intrahepatic biliary epithelium. *Lab Invest* **89**, 456-469.

Grisham, J. W. (1962). A morphologic study of deoxyribonucleic acid synthesis and cell proliferation in regenerating rat liver; autoradiography with thymidine-H3. *Cancer Res* **22**, 842-849.

Grisham, J. W. (1963). Ciliated Epithelial Cells in Normal Murine Intrahepatic Bile Ducts. *Proc Soc Exp Biol Med* **114**, 318-320.

Grompe, M., al-Dhalimy, M., Finegold, M., Ou, C. N., Burlingame, T., Kennaway, N. G. and Soriano, P. (1993). Loss of fumarylacetoacetate hydrolase is responsible for the neonatal hepatic dysfunction phenotype of lethal albino mice. *Genes Dev* **7**, 2298-2307.

Grompe, M., Lindstedt, S., al-Dhalimy, M., Kennaway, N. G., Papaconstantinou, J., Torres-Ramos, C. A., Ou, C. N. and Finegold, M. (1995). Pharmacological correction of neonatal lethal hepatic dysfunction in a murine model of hereditary tyrosinaemia type I. *Nat Genet* **10**, 453-460.

Hadchouel, M. (1992). Paucity of interlobular bile ducts. *Semin Diagn Pathol* **9**, 24-30.

Hamada, Y., Kadokawa, Y., Okabe, M., Ikawa, M., Coleman, J. R. and Tsujimoto, Y. (1999). Mutation in ankyrin repeats of the mouse Notch2 gene induces early embryonic lethality. *Development* **126**, 3415-3424.

Han, H., Tanigaki, K., Yamamoto, N., Kuroda, K., Yoshimoto, M., Nakahata, T., Ikuta, K. and Honjo, T. (2002). Inducible gene knockout of transcription factor recombination signal binding protein-J reveals its essential role in T versus B lineage decision. *Int Immunol* **14**, 637-645.

Hendriks, H. F., Verhoofstad, W. A., Brouwer, A., de Leeuw, A. M. and Knook, D. L. (1985). Perisinusoidal fat-storing cells are the main vitamin A storage sites in rat liver. *Exp Cell Res* **160**, 138-149.

Hildebrand, T. and Rüegsegger, P. (1997). A new method for the model-independent assessment of thickness in three-dimensional images. *Journal of Microscopy* **185**, 67-75.

Hofmann, J. J., Zovein, A. C., Koh, H., Radtke, F., Weinmaster, G. and Iruela-Arispe, M. L. (2010). Jagged1 in the portal vein mesenchyme regulates intrahepatic bile duct development: insights into Alagille syndrome. *Development* **137**, 4061-4072.

Hori, K., Cholewa-Waclaw, J., Nakada, Y., Glasgow, S. M., Masui, T., Henke, R. M., Wildner, H., Martarelli, B., Beres, T. M., Epstein, J. A. et al. (2008). A nonclassical bHLH Rbpj transcription factor complex is required for specification of GABAergic neurons independent of Notch signaling. *Genes Dev* **22**, 166-178.

Huang, B. Q., Masyuk, T. V., Muff, M. A., Tietz, P. S., Masyuk, A. I. and Larusso, N. F. (2006). Isolation and characterization of cholangiocyte primary cilia. *Am J Physiol Gastrointest Liver Physiol* **291**, G500-509.

Isfort, R. J., Cody, D. B., Stuard, S. B., Randall, C. J., Miller, C., Ridder, G. M., Doersen, C. J., Richards, W. G., Yoder, B. K., Wilkinson, J. E. et al. (1997). The combination of epidermal growth factor and transforming growth factor-beta induces novel phenotypic changes in mouse liver stem cell lines. *J Cell Sci* **110 (Pt 24)**, 3117-3129.

Kamath, B. M., Schwarz, K. B. and Hadzic, N. (2010). Alagille syndrome and liver transplantation. *J Pediatr Gastroenterol Nutr* **50**, 11-15.

Kamath, B. M., Bason, L., Piccoli, D. A., Krantz, I. D. and Spinner, N. B. (2003). Consequences of JAG1 mutations. *J Med Genet* **40**, 891-895.

Kamath, B. M., Thiel, B. D., Gai, X., Conlin, L. K., Munoz, P. S., Glessner, J., Clark, D., Warthen, D. M., Shaikh, T. H., Mihci, E. et al. (2009). SNP array mapping of chromosome 20p deletions: genotypes, phenotypes, and copy number variation. *Hum Mutat* **30**, 371-378.

Kanno, N., LeSage, G., Glaser, S., Alvaro, D. and Alpini, G. (2000). Functional heterogeneity of the intrahepatic biliary epithelium. *Hepatology* **31**, 555-561.

Kaye, A. J., Rand, E. B., Munoz, P. S., Spinner, N. B., Flake, A. W. and Kamath, B. M. (2010). Effect of Kasai procedure on hepatic outcome in Alagille syndrome. *J Pediatr Gastroenterol Nutr* **51**, 319-321.

Kellendonk, C., Opherk, C., Anlag, K., Schutz, G. and Tronche, F. (2000). Hepatocyte-specific expression of Cre recombinase. *Genesis* **26**, 151-153.

Kosters, A. and Karpen, S. J. (2010). The role of inflammation in cholestasis: clinical and basic aspects. *Semin Liver Dis* **30**, 186-194.

Krantz, I. D., Colliton, R. P., Genin, A., Rand, E. B., Li, L., Piccoli, D. A. and Spinner, N. B. (1998). Spectrum and frequency of jagged1 (JAG1) mutations in Alagille syndrome patients and their families. *Am J Hum Genet* **62**, 1361-1369.

Krebs, L. T., Xue, Y., Norton, C. R., Sundberg, J. P., Beatus, P., Lendahl, U., Joutel, A. and Gridley, T. (2003). Characterization of Notch3-deficient mice: normal embryonic development and absence of genetic interactions with a Notch1 mutation. *Genesis* **37**, 139-143.

Krebs, L. T., Xue, Y., Norton, C. R., Shutter, J. R., Maguire, M., Sundberg, J. P., Gallahan, D., Closson, V., Kitajewski, J., Callahan, R. et al. (2000). Notch signaling is essential for vascular morphogenesis in mice. *Genes Dev* **14**, 1343-1352.

Kuwahara, R., Kofman, A. V., Landis, C. S., Swenson, E. S., Barendswaard, E. and Theise, N. D. (2008). The hepatic stem cell niche: identification by label-retaining cell assay. *Hepatology* **47**, 1994-2002.

Lazaro, C. A., Rhim, J. A., Yamada, Y. and Fausto, N. (1998). Generation of hepatocytes from oval cell precursors in culture. *Cancer Res* **58**, 5514-5522.

Lee, C. S., Sund, N. J., Behr, R., Herrera, P. L. and Kaestner, K. H. (2005). Foxa2 is required for the differentiation of pancreatic alpha-cells. *Dev Biol* **278**, 484-495.

Libbrecht, L., Cassiman, D., Desmet, V. and Roskams, T. (2002). The correlation between portal myofibroblasts and development of intrahepatic bile ducts and arterial branches in human liver. *Liver* **22**, 252-258.

Libbrecht, L., Spinner, N. B., Moore, E. C., Cassiman, D., Van Damme-Lombaerts, R. and Roskams, T. (2005). Peripheral bile duct paucity and cholestasis in the liver of a patient with Alagille syndrome: further evidence supporting a lack of postnatal bile duct branching and elongation. *Am J Surg Pathol* **29**, 820-826.

Lindor, K. D. and Talwalker, J. A. (2008). Cholestatic liver disease. Totowa, N.J.: Humana.

Loomes, K. M., Russo, P., Ryan, M., Nelson, A., Underkoffler, L., Glover, C., Fu, H., Gridley, T., Kaestner, K. H. and Oakey, R. J. (2007). Bile duct proliferation in liver-specific Jag1 conditional knockout mice: effects of gene dosage. *Hepatology* **45**, 323-330.

Lozier, J., McCright, B. and Gridley, T. (2008). Notch signaling regulates bile duct morphogenesis in mice. *PLoS ONE* **3**, e1851.

Lykavieris, P., Hadchouel, M., Chardot, C. and Bernard, O. (2001). Outcome of liver disease in children with Alagille syndrome: a study of 163 patients. *Gut* **49**, 431-435.

Maher, J. J. (2001). Interactions between hepatic stellate cells and the immune system. *Semin Liver Dis* **21**, 417-426.

Martin, M. A. and Bhatia, M. (2005). Analysis of the human fetal liver hematopoietic microenvironment. *Stem Cells Dev* **14**, 493-504.

Massague, J. and Gomis, R. R. (2006). The logic of TGFbeta signaling. *FEBS Lett* **580**, 2811-2820.

Masyuk, A. I., Masyuk, T. V. and LaRusso, N. F. (2008). Cholangiocyte primary cilia in liver health and disease. *Dev Dyn* **237**, 2007-2012.

Masyuk, T. V., Ritman, E. L. and LaRusso, N. F. (2001). Quantitative assessment of the rat intrahepatic biliary system by three-dimensional reconstruction. *Am J Pathol* **158**, 2079-2088.

Masyuk, T. V., Ritman, E. L. and LaRusso, N. F. (2003). Hepatic artery and portal vein remodeling in rat liver: vascular response to selective cholangiocyte proliferation. *Am J Pathol* **162**, 1175-1182.

McCright, B., Lozier, J. and Gridley, T. (2002). A mouse model of Alagille syndrome: Notch2 as a genetic modifier of Jag1 haploinsufficiency. *Development* **129**, 1075-1082.

McCright, B., Lozier, J. and Gridley, T. (2006). Generation of new Notch2 mutant alleles. *Genesis* **44**, 29-33.

McCright, B., Gao, X., Shen, L., Lozier, J., Lan, Y., Maguire, M., Herzlinger, D., Weinmaster, G., Jiang, R. and Gridley, T. (2001). Defects in development of the kidney, heart and eye vasculature in mice homozygous for a hypomorphic Notch2 mutation. *Development* **128**, 491-502.

McDaniell, R., Warthen, D. M., Sanchez-Lara, P. A., Pai, A., Krantz, I. D., Piccoli, D. A. and Spinner, N. B. (2006). NOTCH2 mutations cause Alagille syndrome, a heterogeneous disorder of the notch signaling pathway. *Am J Hum Genet* **79**, 169-173.

Means, A. L., Xu, Y., Zhao, A., Ray, K. C. and Gu, G. (2008). A CK19(CreERT) knockin mouse line allows for conditional DNA recombination in epithelial cells in multiple endodermal organs. *Genesis* **46**, 318-323.

Meier-Stiegen, F., Schwanbeck, R., Bernoth, K., Martini, S., Hieronymus, T., Ruau, D., Zenke, M. and Just, U. (2010). Activated Notch1 target genes during embryonic cell differentiation depend on the cellular context and include lineage determinants and inhibitors. *PLoS One* **5**, e11481.

Michalopoulos, G. K. (2007). Liver regeneration. *J Cell Physiol* **213**, 286-300.

Michalopoulos, G. K. and DeFrances, M. C. (1997). Liver regeneration. *Science* **276**, 60-66.

Miliutina, N. A. (1989). [A cell population analysis of the initial period of hepatocyte proliferation in the regenerating mouse liver]. *Biull Eksp Biol Med* **108**, 359-361.

Mishra, L. (2004). Mouse Knockout Models of Biliary Epithelial Cell Formation and Disease. In *The Pathophysiology of Biliary Epithelia* (eds G. Alpini D. Alvaro M. Marzioni G. LeSage and N. LaRusso). Georgetown, TX: Landes Bioscience.

Moore, M. A. and Metcalf, D. (1970). Ontogeny of the haemopoietic system: yolk sac origin of in vivo and in vitro colony forming cells in the developing mouse embryo. *Br J Haematol* **18**, 279-296.

Muller, R. (2009). Hierarchical microimaging of bone structure and function. *Nat Rev Rheumatol* **5**, 373-381.

Murtaugh, L. C., Stanger, B. Z., Kwan, K. M. and Melton, D. A. (2003). Notch signaling controls multiple steps of pancreatic differentiation. *Proc Natl Acad Sci U S A* **100**, 14920-14925.

Mushtaq, I., Logan, S., Morris, M., Johnson, A. W., Wade, A. M., Kelly, D. and Clayton, P. T. (1999). Screening of newborn infants for cholestatic hepatobiliary disease with tandem mass spectrometry. *BMJ* **319**, 471-477.

Nakanuma, Y., Sasaki, M., Terada, T. and Harada, K. (1994a). Intrahepatic peribiliary glands of humans. II. Pathological spectrum. *J Gastroenterol Hepatol* **9**, 80-86.

Nakanuma, Y., Katayanagi, K., Terada, T. and Saito, K. (1994b). Intrahepatic peribiliary glands of humans. I. Anatomy, development and presumed functions. *J Gastroenterol Hepatol* **9**, 75-79.

Nathanson, M. H. and Boyer, J. L. (1991). Mechanisms and regulation of bile secretion. *Hepatology* **14**, 551-566.

Nguyen, D. L., Juran, B. D. and Lazaridis, K. N. (2010). Primary biliary cirrhosis. *Best Pract Res Clin Gastroenterol* **24**, 647-654.

Noguera-Troise, I., Daly, C., Papadopoulos, N. J., Coetzee, S., Boland, P., Gale, N. W., Lin, H. C., Yancopoulos, G. D. and Thurston, G. (2006). Blockade of Dll4 inhibits tumour growth by promoting non-productive angiogenesis. *Nature* **444**, 1032-1037.

Obata, J., Yano, M., Mimura, H., Goto, T., Nakayama, R., Mibu, Y., Oka, C. and Kawaichi, M. (2001). p48 subunit of mouse PTF1 binds to RBP-Jkappa/CBF-1, the intracellular mediator of Notch signalling, and is expressed in the neural tube of early stage embryos. *Genes Cells* **6**, 345-360.

Oka, C., Nakano, T., Wakeham, A., de la Pompa, J. L., Mori, C., Sakai, T., Okazaki, S., Kawaichi, M., Shiota, K., Mak, T. W. et al. (1995). Disruption of the mouse RBP-J kappa gene results in early embryonic death. *Development* **121**, 3291-3301.

Olave, I., Reinberg, D. and Vales, L. D. (1998). The mammalian transcriptional repressor RBP (CBF1) targets TFIID and TFIIA to prevent activated transcription. *Genes Dev* **12**, 1621-1637.

Overturf, K., al-Dhalimy, M., Ou, C. N., Finegold, M. and Grompe, M. (1997). Serial transplantation reveals the stem-cell-like regenerative potential of adult mouse hepatocytes. *Am J Pathol* **151**, 1273-1280.

Pan, Y., Lin, M. H., Tian, X., Cheng, H. T., Gridley, T., Shen, J. and Kopan, R. (2004). gamma-secretase functions through Notch signaling to maintain skin appendages but is not required for their patterning or initial morphogenesis. *Dev Cell* **7**, 731-743.

Parfitt, A. M., Mathews, C. H., Villanueva, A. R., Kleerekoper, M., Frame, B. and Rao, D. S. (1983). Relationships between surface, volume, and thickness of iliac trabecular bone in aging and in osteoporosis. Implications for the microanatomic and cellular mechanisms of bone loss. *J Clin Invest* **72**, 1396-1409.

Perrault, J. (1981). Paucity of interlobular bile ducts: getting to know it better. *Dig Dis Sci* **26**, 481-484.

Perrien, D. S., Akel, N. S., Edwards, P. K., Carver, A. A., Bendre, M. S., Swain, F. L., Skinner, R. A., Hogue, W. R., Nicks, K. M., Pierson, T. M. et al. (2007). Inhibin A is an endocrine stimulator of bone mass and strength. *Endocrinology* **148**, 1654-1665.

Plumb-Rudewiez, N., Clotman, F., Strick-Marchand, H., Pierreux, C. E., Weiss, M. C., Rousseau, G. G. and Lemaigre, F. P. (2004). Transcription factor HNF-6/OC-1 inhibits the stimulation of the HNF-3alpha/Foxa1 gene by TGF-beta in mouse liver. *Hepatology* **40**, 1266-1274.

Postic, C. and Magnuson, M. A. (2000). DNA excision in liver by an albumin-Cre transgene occurs progressively with age. *Genesis* **26**, 149-150.

Postic, C., Shiota, M., Niswender, K. D., Jetton, T. L., Chen, Y., Moates, J. M., Shelton, K. D., Lindner, J., Cherrington, A. D. and Magnuson, M. A. (1999). Dual roles for glucokinase in glucose homeostasis as determined by liver and pancreatic beta cell-specific gene knock-outs using Cre recombinase. *J Biol Chem* **274**, 305-315.

Riehle, K. J., Dan, Y. Y., Campbell, J. S. and Fausto, N. (2011). New concepts in liver regeneration. *J Gastroenterol Hepatol* **26 Suppl 1**, 203-212.

Roberts, S. K., Yano, M., Ueno, Y., Pham, L., Alpini, G., Agre, P. and LaRusso, N. F. (1994). Cholangiocytes express the aquaporin CHIP and transport water via a channel-mediated mechanism. *Proc Natl Acad Sci U S A* **91**, 13009-13013.

Roskams, T. and Desmet, V. (1998). Ductular reaction and its diagnostic significance. *Semin Diagn Pathol* **15**, 259-269.

Shiojiri, N. and Nagai, Y. (1992). Preferential differentiation of the bile ducts along the portal vein in the development of mouse liver. *Anat Embryol (Berl)* **185**, 17-24.

Si-Tayeb, K., Lemaigre, F. P. and Duncan, S. A. (2010). Organogenesis and Development of the Liver. *Dev Cell* **18**, 175-189.

Smith, E. and Matzen, P. (1985). Mucus-producing tumors with mucinous biliary obstruction causing jaundice: diagnosed and treated endoscopically. *Am J Gastroenterol* **80**, 287-289.

Soriano, P. (1999). Generalized lacZ expression with the ROSA26 Cre reporter strain. *Nat Genet* **21**, 70-71.

Sparks, E. E., Huppert, K. A., Brown, M. A., Washington, M. K. and Huppert, S. S. (2010). Notch signaling regulates formation of the three-dimensional architecture of intrahepatic bile ducts in mice. *Hepatology* **51**, 1391-1400.

Srinivas, S., Watanabe, T., Lin, C. S., William, C. M., Tanabe, Y., Jessell, T. M. and Costantini, F. (2001). Cre reporter strains produced by targeted insertion of EYFP and ECFP into the ROSA26 locus. *BMC Dev Biol* **1**, 4.

Stocker, E. and Heine, W. D. (1971). Regeneration of liver parenchyma under normal and pathological conditions. *Beitr Pathol* **144**, 400-408.

Stocker, E., Wullstein, H. K. and Brau, G. (1973). [Capacity of regeneration in liver epithelia of juvenile, repeated partially hepatectomized rats. Autoradiographic studies after continous infusion of 3H-thymidine (author's transl)]. *Virchows Arch B Cell Pathol* **14**, 93-103.

Strazzabosco, M. (1997). Transport systems in cholangiocytes: their role in bile formation and cholestasis. *Yale J Biol Med* **70**, 427-434.

Strazzabosco, M., Spirli, C. and Okolicsanyi, L. (2000). Pathophysiology of the intrahepatic biliary epithelium. *J Gastroenterol Hepatol* **15**, 244-253.

Strazzabosco, M., Fabris, L. and Spirli, C. (2005). Pathophysiology of cholangiopathies. *J Clin Gastroenterol* **39**, S90-S102.

Swiatek, P. J., Lindsell, C. E., del Amo, F. F., Weinmaster, G. and Gridley, T. (1994). Notch1 is essential for postimplantation development in mice. *Genes Dev* **8**, 707-719.

Szabo, G., Mandrekar, P. and Dolganiuc, A. (2007). Innate immune response and hepatic inflammation. *Semin Liver Dis* **27**, 339-350.

Tanigaki, K. and Honjo, T. (2010). Two opposing roles of RBP-J in Notch signaling. *Curr Top Dev Biol* **92**, 231-252.

Tanimizu, N. and Miyajima, A. (2004). Notch signaling controls hepatoblast differentiation by altering the expression of liver-enriched transcription factors. *J Cell Sci* **117**, 3165-3174.

Tanimizu, N., Miyajima, A. and Mostov, K. E. (2009). Liver progenitor cells fold up a cell monolayer into a double-layered structure during tubular morphogenesis. *Mol Biol Cell* **20**, 2486-2494.

Tao, J., Chen, S., Yang, T., Dawson, B., Munivez, E., Bertin, T. and Lee, B. (2010). Osteosclerosis owing to Notch gain of function is solely Rbpj-dependent. *J Bone Miner Res* **25**, 2175-2183.

Tchorz, J. S., Kinter, J., Muller, M., Tornillo, L., Heim, M. H. and Bettler, B. (2009). Notch2 signaling promotes biliary epithelial cell fate specification and tubulogenesis during bile duct development in mice. *Hepatology* **50**, 871-879.

Terada, T. and Nakanuma, Y. (1995). Detection of apoptosis and expression of apoptosis-related proteins during human intrahepatic bile duct development. *Am J Pathol* **146**, 67-74.

Trauner, M., Wagner, M., Fickert, P. and Zollner, G. (2005). Molecular regulation of hepatobiliary transport systems: clinical implications for understanding and treating cholestasis. *J Clin Gastroenterol* **39**, S111-124.

Tremblay, K. D. (2010). Inducing the liver: Understanding the signals that promote murine liver budding. *J Cell Physiol*.

van Tetering, G., van Diest, P., Verlaan, I., van der Wall, E., Kopan, R. and Vooijs, M. (2009). Metalloprotease ADAM10 is required for Notch1 site 2 cleavage. *J Biol Chem* **284**, 31018-31027.

Visintine, R. E., Michaels, G. D., Fukayama, G., Conklin, J. and Kinsell, L. W. (1961). Xanthomatous biliary cirrhosis treated with cholestyramine. A bile-acid-adsorbing resin. *Lancet* **2**, 341-343.

Wang, X., Foster, M., Al-Dhalimy, M., Lagasse, E., Finegold, M. and Grompe, M. (2003). The origin and liver repopulating capacity of murine oval cells. *Proc Natl Acad Sci U S A* **100 Suppl 1**, 11881-11888.

Warthen, D. M., Moore, E. C., Kamath, B. M., Morrissette, J. J., Sanchez, P., Piccoli, D. A., Krantz, I. D. and Spinner, N. B. (2006). Jagged1 (JAG1) mutations in Alagille syndrome: increasing the mutation detection rate. *Hum Mutat* **27**, 436-443.

Xue, Y., Gao, X., Lindsell, C. E., Norton, C. R., Chang, B., Hicks, C., Gendron-Maguire, M., Rand, E. B., Weinmaster, G. and Gridley, T. (1999). Embryonic lethality and vascular defects in mice lacking the Notch ligand Jagged1. *Hum Mol Genet* **8**, 723-730.

Yang, H., Plosch, T., Lisman, T., Gouw, A. S., Porte, R. J., Verkade, H. J. and Hulscher, J. B. (2009). Inflammation mediated down-regulation of hepatobiliary transporters contributes to intrahepatic cholestasis and liver damage in murine biliary atresia. *Pediatr Res* **66**, 380-385.

Zhang, Y. and Klaassen, C. D. (2010). Effects of feeding bile acids and a bile acid sequestrant on hepatic bile acid composition in mice. *J Lipid Res* **51**, 3230-3242.

Zimmerman, H. J. (1999). Hepatotoxicity : the adverse effects of drugs and other chemicals on the liver. Philadelphia: Lippincott Williams & Wilkins.

Zong, Y., Panikkar, A., Xu, J., Antoniou, A., Raynaud, P., Lemaigre, F. and Stanger, B. Z. (2009). Notch signaling controls liver development by regulating biliary differentiation. *Development* **136**, 1727-1739.